THE ROLE OF TROPOMYOSIN AND CARDIAC MYOSIN BINDING PROTEIN-C IN MODULATING THIN FILAMENT ACTIVITY

by Alessio Vincenzo Inchingolo

A thesis submitted to the University of Kent for the degree of

Doctor of Philosophy in Biochemistry

School of Biosciences, February 2019

“Sometimes, data vary” – anonymous, 2018

Dedicated to my family and my wife, Yuhan

No part of this thesis has been submitted in support of an application for any degree or other qualification of the University of Kent, or any other University or Institution of learning

INDEX

Abstract i

List of Figures iii

CHAPTER 1: INTRODUCTION 1

1.1 – The muscle and its smallest contractile unit: the sarcomere 1

1.2 – The thin filament 4

1.2.1 – Actin 4

1.2.2 – Tropomyosin 9

1.2.3 – Troponin 11

1.3 – The thick filament and Myosin II 15

1.4 – The cross-bridge cycle 18

1.5 – Myosin Binding Protein-C 23

1.6 – Hypertrophic Cardiomyopathy 28

1.6.1 – Physiological effects 28

1.6.2 – Notable mutations and where to find them 30

1.7 – Experimental techniques used for the study of muscle 38

1.8 – Project objectives 44

CHAPTER 2: EXPERIMENTAL METHODS 46

2.1 – Myosin purification 46

2.1.1 – Extraction of myosin from chicken pectoralis 46

2.1.2 – Papain digestion of myosin head 48

2.2 – Acetone powder preparation and actin purification 50

2.3 – Obtaining Tropomyosin and its E180G mutant 52

2.3.1 – Molecular biology of the plasmids 52

2.3.2 – Bacterial expression and purification 52

2.4 – Expression and purification of the troponin complex 54

2.5 – Fluorescent labelling of S1 with GFP 56

2.5.1 – Switching the 6xHis-tag from the N-terminal to the C-terminal end of the RLC-GFP 56

2.5.2 – Expression and purification of the RLC-GFP-6xHis 59

2.5.3 – Labelling of S1 with RLC-GFP-6xHis and final purification 60

2.6 – Myosin Binding Protein-C (MyBP-C) N-terminal fragments purification and labelling 62

2.7 – Reconstitution and labelling of actin thin filaments 63

2.8 – The *in-vitro* motility assay 64

2.8.1 – Experimental procedure 64

2.8.2 – Data analysis 66

2.9 – The thin filament tightropes assay 68

2.9.1 – Experimental procedure 68

2.9.2 – The Oblique Angle Fluorescence microscope (OAFM) 70

2.9.3 – Imaging thin filament tightropes 73

2.9.3 – Data analysis 75

CHAPTER 3: INVESTIGATING THE EFFECTS OF THE HYPERTROPHIC CARDIOMYOPATHY α-TROPOMYOSIN E180G MUTATION ON THIN FILAMENT ACTIVATION 77

3.1 – Introduction 77

3.2 – Results 78

3.2.1 – The α-tropomyosin E180G mutation increases thin filament calcium sensitivity in the motility assay 78

3.2.2 – Studying the effects of the α-tropomyosin E180G mutation on S1-GFP binding to regulated thin filaments 81

3.3 – Discussion 96

CHAPTER 4: THE CATASTROPHIC COLLAPSE OF ACTIVE REGIONS OF MYOSIN BOUND TO THE THIN FILAMENT AS A MECHANISM FOR MUSCLE RELAXATION 102

4.1 – Introduction 102

4.2 – Results 103

4.2.1 - Sub-maximal thin filament activation promotes local clusters of S1 103

4.2.2 – De-convoluting kymographs into transition matrices 106

4.2.3 – Modelling the transition probability within an active region 109

4.3 – Discussion 112

CHAPTER 5: CHARACTERIZING THE CONSEQUENCES OF N-TERMINAL MYOSIN BINDING PROTEIN-C FRAGMENTS INTERACTIONS WITH ACTIN 116

5.1 – Introduction 116

5.2 – Results 117

5.2.1 – Investigating the effects of cMYBP-C N-terminal fragments on myosin binding to thin filaments 117

5.2.2 – Visualising cMyBP-C N-terminal fragments binding to actin 120

5.2.3 – Dynamics of cMyBP-C N-terminal fragments on RTFs 128

5.3 – Discussion 132

5.3.1 – The whole N-terminus of cMyBP-C is responsible for thin filament activation 132

5.3.2 – cMyBP-C possesses a weak binding state to actin 134

5.3.3 – Inhibition of myosin binding is due to cooperative proximal binding of cMyBP-C to thin filaments 137

CHAPTER 6: DISCUSSION 139

APPENDIX 148

A.1 – Sequencing results of the 6xHis-RlC-GFP 148

A.2 – Sequencing results of the RlC-GFP-6xHis 151

A.3 – Matlab script for the extraction of intensity data 153

A.4 – Calculating the relative ratios of A_{CL} and A_M used in the kinetic model 155

A.5 – Calculating the second order ATP binding rate constant 156

A.6 – The Reversible Jump Markov-Chain Monte Carlo (RJMCMC) and generation of transition matrices 157

A.7 – Determination of the number of Gaussian distributions for the fitting of the C0C3 intensity histogram 160

BIBLIOGRAPHY 162

ACKNOWLEDGEMENTS 200

Abstract

Muscle contraction is a finely tuned mechanism involving cyclical interactions between actin and myosin, regulated by calcium through troponin and tropomyosin and modulated by myosin binding protein-C. Genetic mutations of the proteins involved in such complex mechanism can thus lead to potential life threatening diseases, such as Hypertrophic Cardiomyopathy (HCM). Although being mostly asymptomatic, HCM affects 1 in 500 people, ultimately leading to poor prognosis and sudden death, thought to occur through the impairment of relaxation during diastole.

In this thesis I present the experiments conducted to improve our current understanding of the molecular mechanism behind HCM, specifically on the role of tropomyosin and myosin binding protein-C in modulating thin filament activation and relaxation. Using a single molecule approach, we first visualised fluorescent myosin binding to reconstituted thin filaments and examined their dynamics in the presence of the tropomyosin HCM causing E180G mutation, demonstrating a shift of the thin filament activation state towards the closed state, facilitating myosin binding at low calcium, and a reduction of the thin filament regulatory unit.

We then looked at the dynamics of very highly concentrated clusters of myosin, showing how the sudden collapse of these active regions cannot be explained by normal relaxation mechanisms, thus suggesting an alternative mechanistic role for tropomyosin and how its mutations could lead to impaired relaxation in HCM.

Finally, we turned our focus on N-terminal fragments of cardiac myosin binding protein-C (cMyBP-C) and study their role in thin filament activation, by looking at how

they affect acto-myosin interactions. We found that only the presence of the whole cMyBP-C N-terminus was able to promote acto-myosin interactions at low Ca^{2+} or repressing them at high Ca^{2+}. Moreover, by looking at the dynamics of the fragments, we were able to determine that cMyBP-C possesses a two steps binding mechanism to actin, leading us to define its mechanism by which it activates the thin filament.

List of Figures

Figure 1.1: The hierarchy of muscle

Figure 1.2: The bands structure of the sarcomere

Figure 1.3: The two different forms of Actin

Figure 1.4: Actin treadmilling

Figure 1.5: The coiled-coil structure of tropomyosin

Figure 1.6: The troponin complex substructure

Figure 1.7: The crystal structure of troponin C

Figure 1.8: The structure of myosin II and the thick filament

Figure 1.9: Diagram of the three states of the thin filament

Figure 1.10: The effect of regulatory proteins on the acto-S1 ATPase

Figure 1.11: Cardiac MyBP-C and its subdomains in relation with the thick and thin filaments

Figure 1.12: The effects of C0C2 on myosin ATPase

Figure 1.13: The effects of hypertrophic cardiomyopathy on the heart

Figure 1.14: HCM mutations and their effect

Figure 1.15: The motility assay

Figure 1.16: The three beads assay

Figure 1.17: The tightropes assay

Figure 1.18: Analysing myosin cooperativity through fluorescence intensity histograms

Figure 2.1: 10% SDS-PAGE gel of the myosin purification protocol

Figure 2.2: From full-length myosin to S1, digestion and purification

Figure 2.3: 10% SDS-PAGE gels of the actin purification protocol

Figure 2.4: The tropomyosin purification protocol

Figure 2.5: Purification of the troponin complex

Figure 2.6: Switching the 6xHis-tag

Figure 2.7: Purification of the RLC-GFP-6xHis.

Figure 2.8: Purification of the S1-GFP

Figure 2.9: Analysing the motility assay data

Figure 2.10: The tightrope assay set-up

Figure 2.11: Determining the beads density

Figure 2.12: The Oblique Angle Fluorescence Microscope set-up

Figure 2.13: Selecting good tightropes

Figure 2.14: Calibrating the pixel size of the microscope camera

Figure 3.1: The motility properties of E180G-RTFs

Figure 3.2: Visualising the interactions between S1-GFP and E180G-RTFs

Figure 3.3: Histograms of the extrapolated intensity values

Figure 3.4: Quantifying the binding of S1-GFP to E180G-RTFs

Figure 3.5: Determination of a single S1-GFP fluorescence intensity

Figure 3.6: Histograms of the # of myosin (S1-GFP) binding to E180G-RTFs at increasing [Ca^{2+}]

Figure 3.7: Histograms of the # of myosin (S1-GFP) binding to E180G-RTFs at increasing [S1-GFP]

Figure 3.8: Probability histograms of S1-GFP binding to E180G-RTFs

Figure 3.9: The effect of E180G on thin filament activation

Figure 4.1: Highlighting locally active regions in a kymograph

Figure 4.2: Experimental transition matrices of myosin patches

Figure 4.3: Calculated transition matrix of S1-GFP on thin filaments

Figure 5.1: Effects of cMyBP-C N-terminal fragments on acto-myosin interactions

Figure 5.2: Quantifying cMyBP-C N-terminal fragments effect on S1-GFP binding to thin filaments

Figure 5.3: Imaging fluorescent C0C3

Figure 5.4: Imaging fluorescent C0C1f and C0C1

Figure 5.5: Calculating the fluorescent intensity of a single binder

Figure 5.6: The distribution of cMyBP-C fragment molecules per cluster

Figure 5.7: Comparing the dynamics of cMyBP-C fragments on actin and thin filaments

Figure A.1: Extracting the fluorescence intensity from a kymograph

Figure A.2: Calculating the second order ATP binding rate constant

Figure A.3: Selecting the number of Gaussian distributions

CHAPTER 1

INTRODUCTION

1.1 – The muscle and its smallest contractile unit: the sarcomere

Muscles can be classified based on their appearance and function. There are three main types of muscle, skeletal, cardiac and smooth. Smooth muscle is found in the oesophagus, blood vessels and trachea, skeletal muscle is the one responsible for the motion of limbs and cardiac muscle is found in the heart. Smooth and cardiac muscles are also termed involuntary, as their contraction or relaxation cannot be controlled. Moreover, skeletal and cardiac muscle are called striated because of their appearance under the microscope, being organised in a highly hierarchical and repetitive structure. Figure 1.1 shows a drawing of this structure, where it can be seen that each muscle is a fasciculus made of myofibres, each one subsequently composed of a network of myofibrils, in turn made of thousands of smaller repetitive units called sarcomeres. Shown in figure 1.2, a sarcomere is the smallest contractile unit of a muscle, its length varying from about 1-3 µm during contraction-relaxation (Gordon *et al.*, 1966; Walker and Schrodt, 1974; Cutts, 1988).

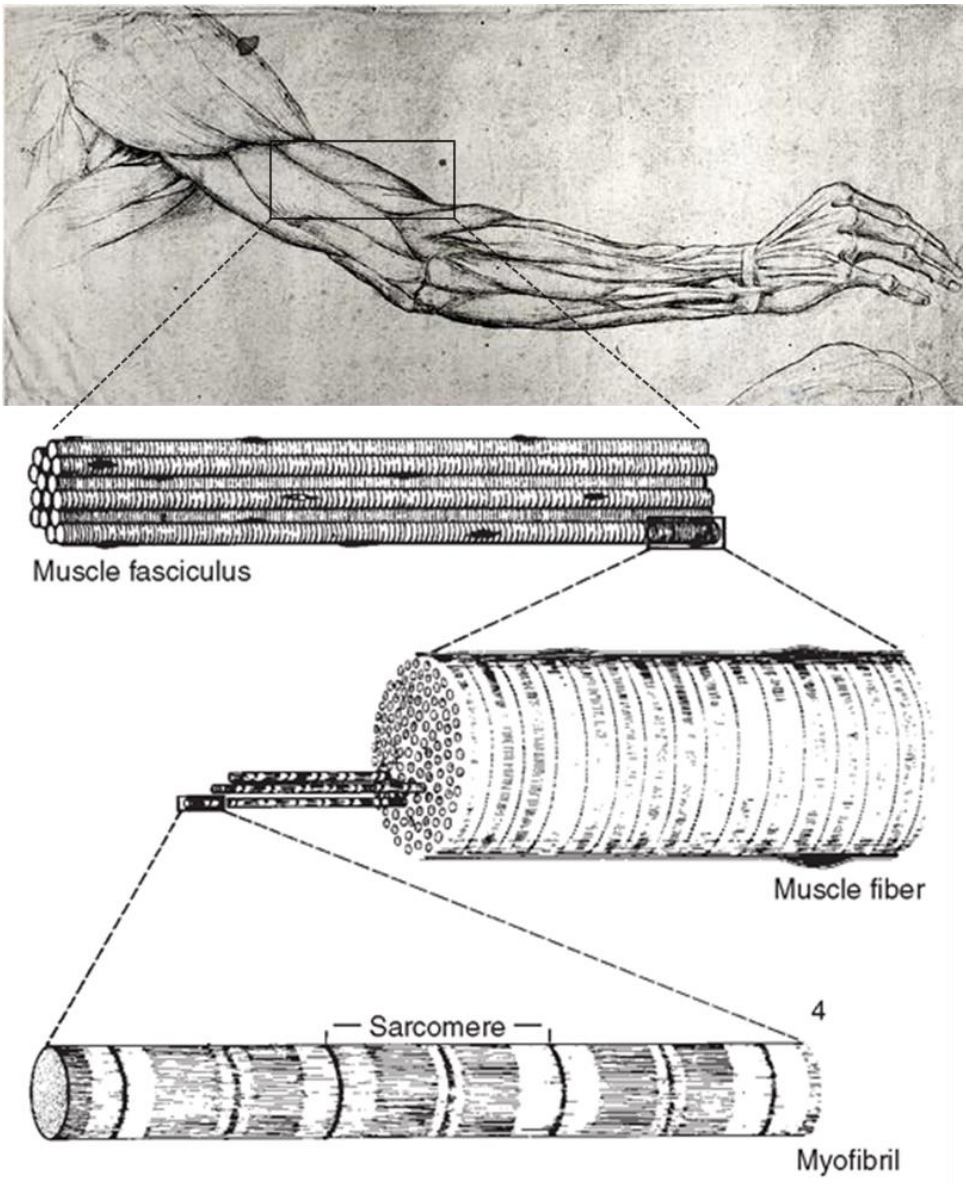

Figure 1.1: **The hierarchy of muscle.** Drawing of the hierarchical structure of striated muscle, down to its smallest contractile unit, the sarcomere. Adapted from *Study of Arms*, Leonardo da Vinci and *Histology and Cell Biology*, Douglas Paulsen, McGraw Hill, 5th Edition.

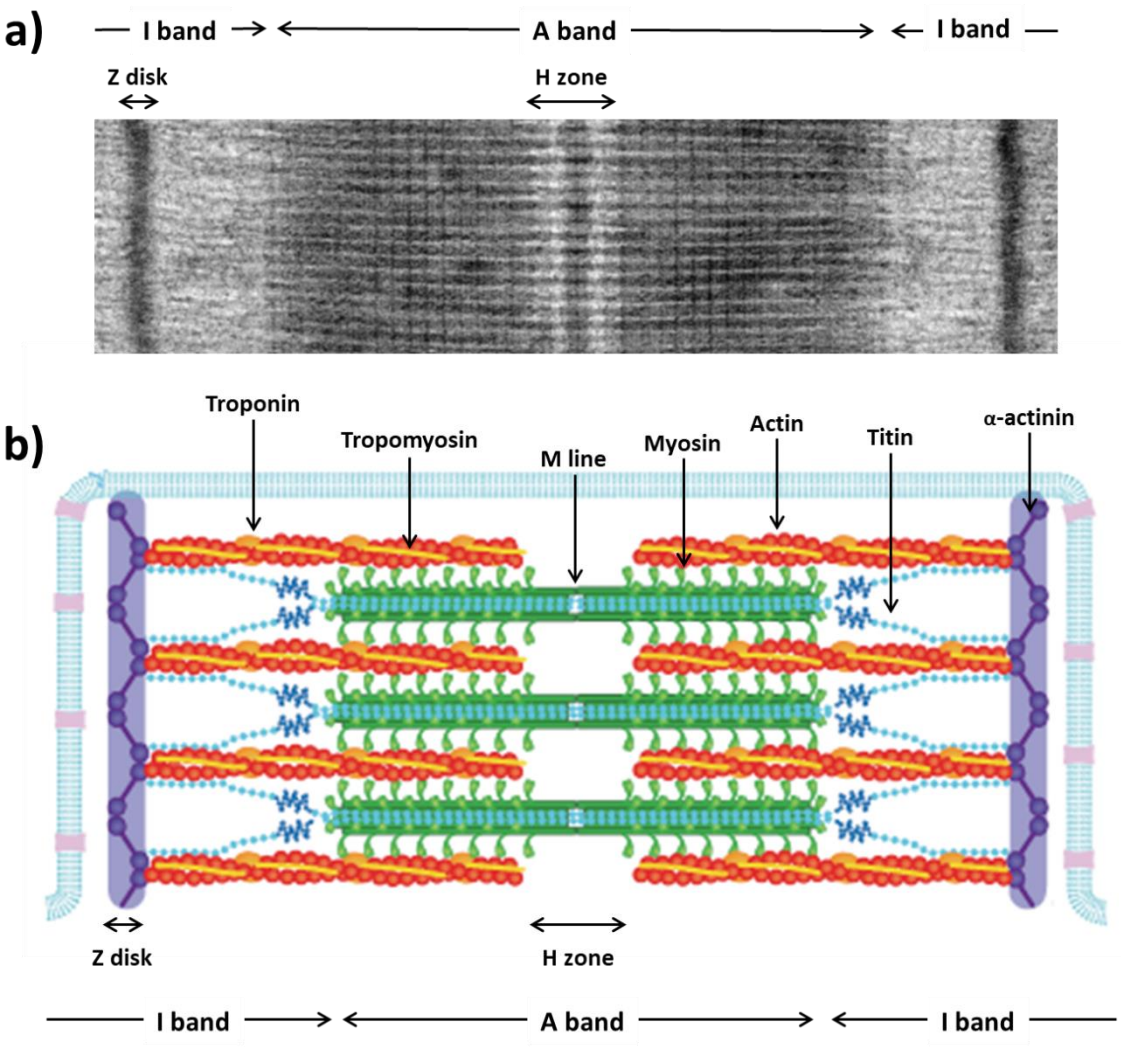

Figure 1.2: **The bands structure of the sarcomere.** a) electron micrograph of a sarcomere, adapted from (Luther and Craig, 2011) and b) schematic of a sarcomere with the main proteins involved in muscle contraction, adapted from (Kobirumaki-Shimozawa *et al.*, 2012).

Under optical illumination, the sarcomere appears as an alternation of dark and white patches, with the two major ones named the A (anisotropic) and I (isotropic) bands (figure 1.2a). Although reports that showed how contraction is caused by the interaction between two main proteins found in muscle purifications, myosin and actin, date back to the late 1930s (for a review of the history of the biochemistry of muscle contraction see (Szent-Györgyi, 2004)), it was the work of (Huxley and Niedergerke,

1954) and (Huxley and Hanson, 1954) that correlated the bands to the actin containing thin filament and the myosin containing thick filaments, giving birth to the sliding filament theory. More specifically, the A band corresponds to the region where both the thin and thick filaments are found, while, in the I band and the H zone, only the thin filament or the thick filament are present, respectively (figure 1.2).

The sarcomere structural integrity is kept together by two other proteins, α-actinin and titin, with the former being responsible for crosslinking antiparallel actin filaments, forming the Z-disk, with titin, which in turns acts as a molecular ruler and scaffold, connecting the Z disk to the M line and to which the myosin binds to form the thick filament (Sjöblom *et al.*, 2008; Luther, 2009; Gautel, 2011; Ribeiro *et al.*, 2014).

In the next sections, I will describe the main players involved in muscle contraction and their role, as well as highlighting some of the structural properties that can be of help to better understand the data reported in the following chapters.

1.2 – The thin filament

1.2.1 – Actin

Discovered by Straub in 1942 (Straub, 1943), actin is one of the most common protein in eukaryotic cells and the main constituent protein of the thin filament (Hanson and Huxley, 1953), and it has been extensively reviewed (Tobacman, 1996; Dominguez and Holmes, 2011). Actin can be either monomeric (G-actin) or filamentous (F-actin), where the polymerisation of G-actin gives rise to a double helix with a 36 nm pitch (Holmes *et al.*, 1990), forming the backbone of the thin filament.

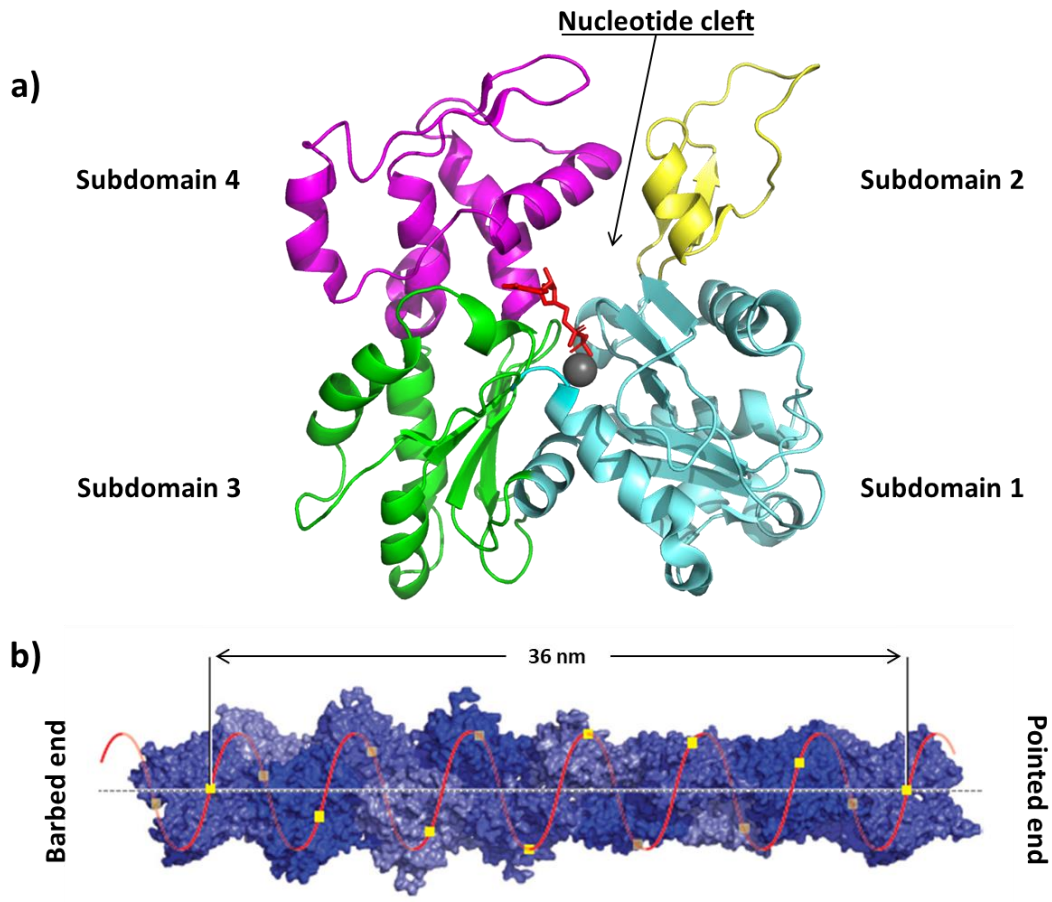

Figure 1.3: **The two different forms of Actin.** a) structure of G-actin (adapted from PDB-2ZWH (Oda et al., 2009)) in the ADP (in red) bound state and coordinated by Ca^{2+} and colour coded to highlight the different subdomains; b) structure of F-actin, depicting the two different ends and highlighting its 36 nm periodicity, followed by the red curve (adapted from (Dominguez and Holmes, 2011)).

The structure of G-actin, shown in figure 1.3a, has been resolved in numerous studies, mostly using small molecules to prevent polymerisation (Kabsch *et al.*, 1990; McLaughlin *et al.*, 1993; Schutt *et al.*, 1993; Wang *et al.*, 2010). It appears as a globular protein (55 x 55 x 35 Å) structured into four subdomains separated by a central cleft (Kabsch et al., 1990). In the cleft is a binding site for ATP, which hydrolysis functions as a modulator of G-actin polymerisation (Cooke, 1975; Carlier *et al.*, 1984). Throughout the subdomains there are also multiple binding sites for divalent ions such as Ca^{2+} and

Mg^{2+}, with the most important one being just next to the ATP binding site and termed catalytic, for its role in coordinating water molecules which are thought to promote the ATPase mechanism (Carlier *et al.*, 1986; Otterbein *et al.*, 2001; Wang *et al.*, 2010).

G-actin assembles into filaments with a period of 13 monomers every six left-handed turns, corresponding to a genetic right-handed helix with a period of about 36 nm, as shown in figure 1.3b (Holmes *et al.*, 1990; Lorenz *et al.*, 1993; Lorenz *et al.*, 1995; Fujii *et al.*, 2010). When G-actin polymerises into F-actin, structural changes in the subdomains occur, most notably domain 2 twists by 20° towards the outside of the F-actin filament while domain 4 twists by 7° towards the centre of the filament, making the G-actin monomer in the F-actin state flatter than free G-actin (Oda et al., 2009). With this reconfiguration, the nucleotide cleft opens up, resulting in residue Gln137 moving closer to the γ-phosphate of ATP and promoting hydrolysis, starting the polymerisation process (Iwasa *et al.*, 2008; Fujii *et al.*, 2010). In the filamentous state, all actin monomers points towards the same direction, making the thin filament a polar structure with two different ends, termed barbed (or plus (+)) end and pointed (or (-)) end.

Actin polymerization occurs in a process known as “treadmilling” or “head –to-tail polymerization” (figure 1.4), where the two ends of the filament have different growth rates (Pollard and Mooseker, 1981): the fast end is the barbed end while the slow one is the pointed end. Defining the critical concentration C^0 as the concentration at which the dissociation and association process of monomers at one end are in equilibrium, (Wegner and Isenbergt, 1983) found that under physiological conditions, C^0 is about 12 fold higher at the pointed end (C_-^0 = 1.5 µM for the pointed end vs. C_+^0 = 0.12 µM

for the barbed end, see figure 1.4). Above the critical concentration the growth will be net at both ends but still going at a faster rate for the barbed end.

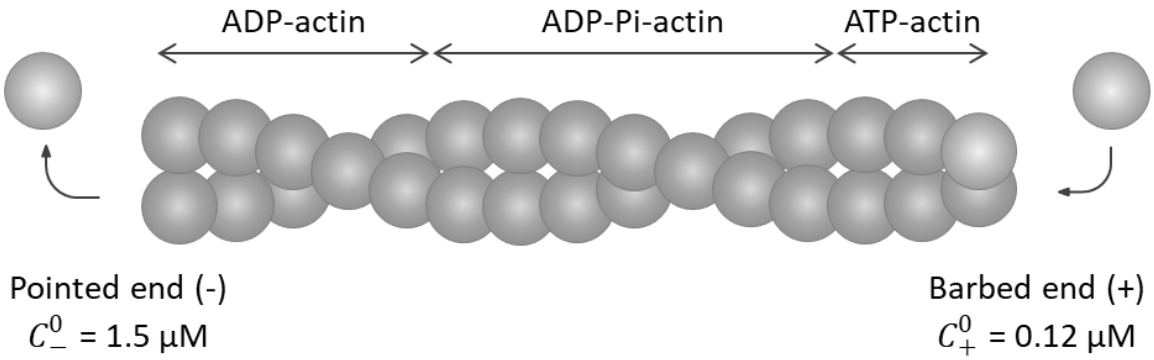

Figure 1.4: **Actin treadmilling.** Cartoon of the F-actin polymerisation/depolymerisation dynamics, highlighting its dependence on the nucleotide state within each actin monomer.

Actin treadmilling can be altered by several molecules or proteins, most notably formin, profilin and cofilin, and completely stopped by end capping proteins CapZ and tropomodulin. In particular, formin stabilises actin nuclei and enhances actin polymerisation by processive capping, where it binds to the barbed end of the actin filaments and provides a template to which G-actin binds (Goode and Eck, 2007; Sherer *et al.*, 2018), activity that has been linked to the assembly and maintenance of myofibrils (Iskratsch and Ehler, 2011; Fenix *et al.*, 2018). Profilin can instead both hamper and accelerate actin polymerisation, by either binding to G-actin in solution, sequestering actin monomers, or by increasing the rate of nucleotide exchange, respectively (Krishnan and Moens, 2009). Finally, cofilin works to depolymerise actin, either by increasing the detachment rate of ADP-actin monomers from the filaments or by severing parts of the ADP-actin filaments, to increase the amount of depolymerising ends (Carlier *et al.*, 1997; Ichetovkin *et al.*, 2000).

End capping proteins CapZ and tropomodulin binds at the (+) and (-) end of F-actin respectively, preventing both actin assembly and disassembly. CapZ can be found at the Z-disk of the sarcomere and is composed of two α and β subunits very similar in sequence. It has been shown that its capping properties come from the last 30 amino acids on the C-terminal region of each subunit (also referred to as "tentacles"), which bind to hydrophobic regions of multiple actin subunits and can independently block polymerisation (Casellas and Torres, 1994; Wear *et al.*, 2003; Yamashita *et al.*, 2003). CapZ has also demonstrated a functional role in the myocytes, with its capping dynamics being dependent on exercise (Lin *et al.*, 2013), hypertrophy (Lin *et al.*, 2016) or cardiac arrest (Yang and Pyle, 2011). Tropomodulin capping function is instead achieved by its binding to three actin monomers and to the two tropomyosin chains on either side of the filament at the same time through several low affinity interactions (Rao *et al.*, 2014). Tropomodulin does not completely inhibit actin monomer dissociation but functions instead as a leaky cap, controlling the thin filament length through the alteration of G-actin depolymerisation dynamics (Littlefield *et al.*, 2001; Yamashiro *et al.*, 2012; Gokhin *et al.*, 2015).

A mention as an actin assembly modifier should also go to phalloidin (Estes *et al.*, 1981). Originating from the poisonous mushroom Amanita Phalloides (Wieland and Heinz, 1995), phalloidin binds actin in its cleft region and it has been proven to stabilise F-actin and prevent depolymerisation or denaturation when in stoichiometric concentrations as low as 1:2 phalloidin:actin (Vandekerckhove *et al.*, 1985; Miyamoto *et al.*, 1986; De La Cruz and Pollard, 1994). This stabilisation has proven to not affect the contractile properties of myosin binding to actin and cross bridge formation (VanBuren *et al.*, 1998), therefore this molecule is nowadays commonly used in a

variety of assays to fluorescently label actin filaments, including the experiments in this thesis.

1.2.2 – Tropomyosin

Tropomyosin is 40 nm long protein dimer, forming a α-helical coiled-coil wrapped around actin. In striated muscle, it can be found in two different isoforms, α and β, which can assemble into αα homodimers or αβ heterodimer, with percentages in cardiac muscle varying between species and age, but the αα being predominant (Lehrer and Qian, 1990; Boussouf *et al.*, 2007). Due to its coiled-coil structure, it is arranged in a-b-c-d-e-f-g pseudo-heptad repeats, as seen in figure 1.5a and b, where a and d are non-polar amino acids, and e and g are charged. Within the coiled-coil, the two monomers are in contact through hydrophobic interactions between amino acids a-a' and d-d' and through electrostatic forces between e-g' and g-e'. Finally, a salt bridge between residues e and g confers stability to the whole structure (McLachlan and Stewart, 1976).

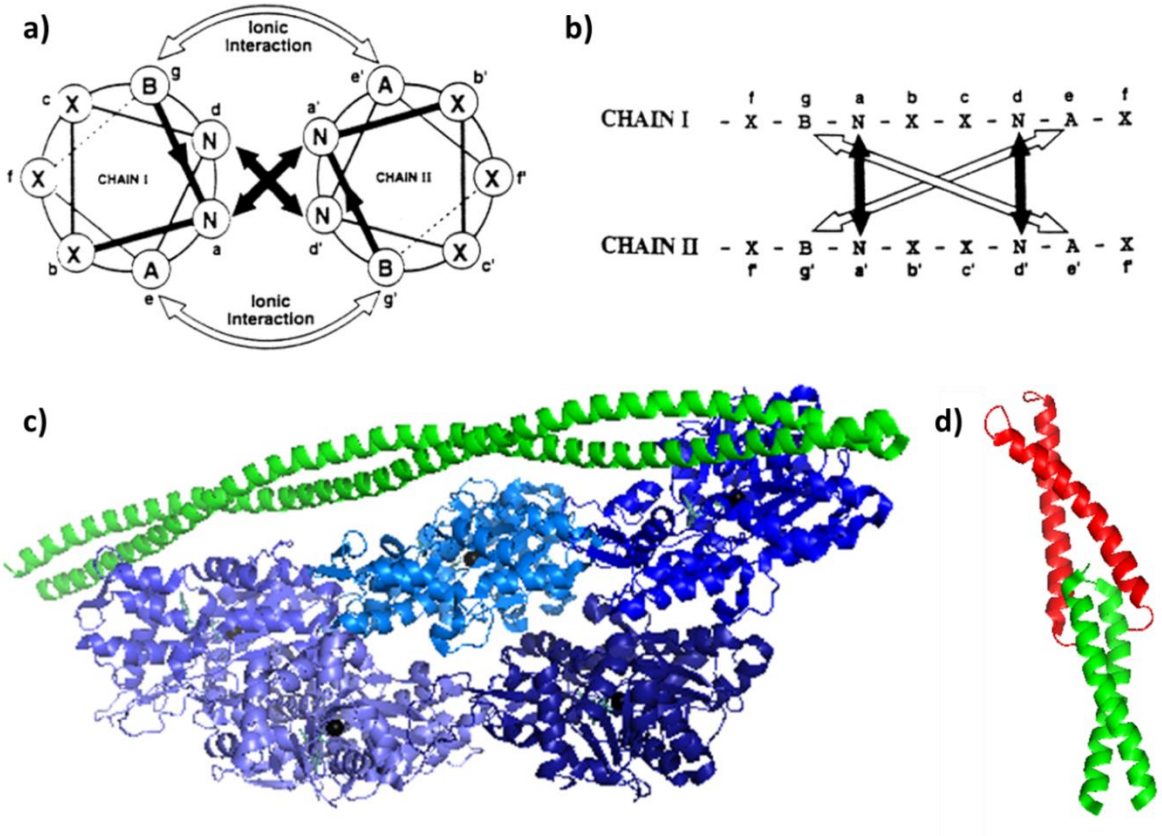

Figure 1.5 : **The coiled-coil structure of tropomyosin.** The heptad repeat of tropomyosin visualised in a) section and b) linearly, where amino acids denoted as N are non-polar, A are acidic, B are basic and X are polar; c) Structural view of one of the coiled coil tropomyosin filaments as bound to F-actin. Adapted from (Perry, 2001) and PDB structures 5JLF from (von der Ecken *et al.*, 2015) and 2G9J from (Greenfield *et al.*, 2006).

Tropomyosin polymerizes on actin, spanning along seven actin monomers (a shortened version is visualised in figure 1.5c), in a head to tail fashion, in which the N-terminus is positioned between the two previous C-terminal α-helices (also called knob-into-hole configuration), forming a four α-helices superstructure called the overlap region (figure 1.5d). This configuration is caused by a water molecule that disrupts the C-terminus of tropomyosin, breaking the local 2-fold symmetry and causing its splaying to accommodate the N-terminus (Murakami *et al.*, 2008). Although the stability of the whole region is decreased, this configuration allows the binding of another thin

filament protein, troponin, as will be discussed in the next section, which overall creates a stable structure (Li *et al.*, 2002; Palm *et al.*, 2003). The overlap region is also highly dynamic and is partly responsible for tropomyosin elasticity and flexibility and it acts as a swivel as it transitions and moves across the actin filament (Greenfield *et al.*, 2006; Murakami *et al.*, 2008). The length of the overlap region varies between isoforms, from 9 residues of skeletal tropomyosin to the 15 residues necessary in smooth muscle (Frye *et al.*, 2010). Furthermore, the surface of tropomyosin is mostly negatively charged therefore on the thin filament it tends to occupy a positively charged groove on the actin surface, at ~40 Å from the centre of F-Actin (von der Ecken *et al.*, 2015). This position is also responsible for stabilising and increasing the stiffness of the actin filament, by strengthening interactions between adjacent actin monomers (Kojima *et al.*, 1994; Isambert *et al.*, 1995; Khaitlina *et al.*, 2017).

Native tropomyosin is acetylated on its N-terminus, which provides extra stability and greatly improves tropomyosin binding to actin. In fact, it has been shown that unacetylated tropomyosin expressed in *E.coli* is not capable of binding actin and does not show head to tail polymerisation (Hitchcock-DeGregori and Heald, 1987). However, substitutes for acetylation have been engineered, such as the addition of an alanine followed by a serine at its N-terminus, capable of fully recovering tropomyosin function (Monteiro *et al.*, 1994; Urbancikova and Hitchcock-DeGregori, 1994).

1.2.3 – Troponin

Troponin is a complex of three proteins, Troponin T (TnT), Troponin I (TnI) and Troponin C (TnC). Each of these subunits has a specific role in muscle contraction, reflected in their names: TnT is responsible for holding together each of the other

subunits on the thin filament, having binding sites for both actin and tropomyosin, TnI is the inhibitory part of troponin, since it binds actin and inhibits myosin ATPase while TnC can bind calcium, starting the whole process of thin filament activation.

Troponin T can be cleaved by chymotrypsin into two different subunits, TnT1 (the N-terminal region, 1-158 amino acids) and TnT2 (the C-terminal region), which possess two different functions. TnT1 binds to the overlap region of tropomyosin, specifically within residues 258-284 of its C-terminus, as inferred by (Li et al., 2002) by looking at the crystal structure of the overlap region and at conserved residues within species. TnT2 can bind to TnI (together sharing a coiled coil (Stefancsik *et al.*, 1998)), TnC and Tm. It extends from TnT1 to tropomyosin, reaching in the region around its residue 190 (Chong and Hodges, 1982; Morris and Lehrer, 1984) and possibly stabilising its position on actin in the absence of calcium while, in the presence of Ca^{2+}, this interaction is weakened for a more stable binding to TnC (Pearlstone and Smillie, 1982). In particular, deletion of the last 14 amino acids of TnT2 have been seen causing an increase in myosin-S1 ATPase, further suggesting that the C-terminus is partly responsible for holding tropomyosin in the blocked position on actin (Franklin et al., 2012). However, in (Pearlstone and Smillie, 1982) TnT showed this behaviour only with skeletal and not aorta tropomyosin. Furthermore, (Dahiya et al., 1994) have shown that cardiac Tn-Tm complex affinity to actin is greater in skeletal muscle compared to cardiac muscle, suggesting that these calcium dependences might be caused by small changes in the amino acids structures between different isoforms.

Troponin I is the inhibitory subunit of troponin and is composed of several regions, as shown in figure 1.6, each one with a specific function.

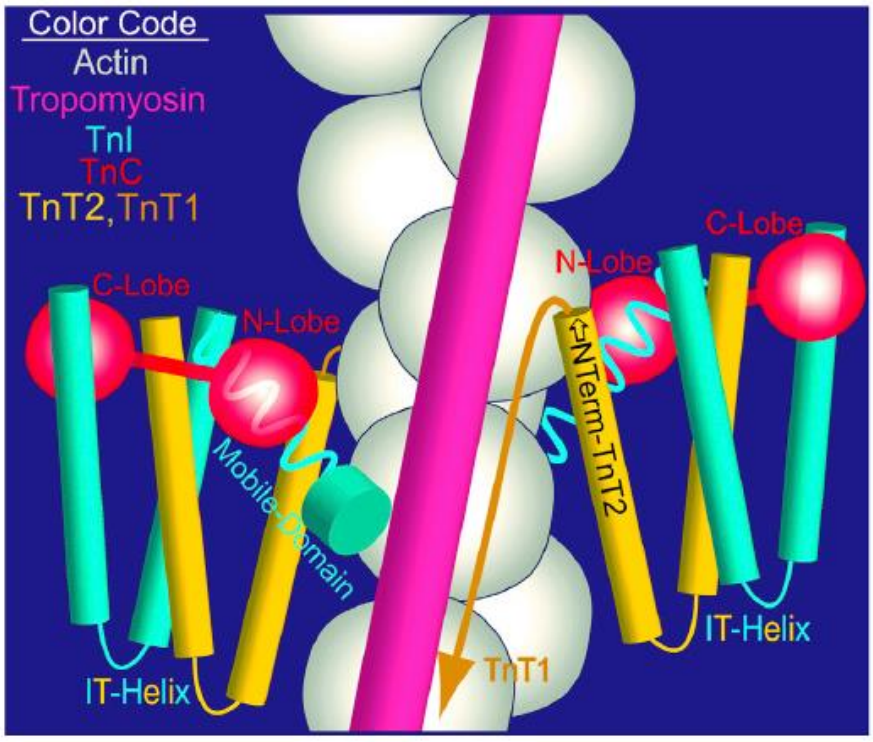

Figure 1.6: **The troponin complex substructure.** Cartoon of the troponin complex bound to tropomyosin and actin, color coded for TnI (cyan), TnC (red), TnT (yellow and orange), actin (white) and tropomyosin (pink), adapted from (Yang *et al.*, 2014).

Its first 30 N-terminal residues are present only in its cardiac isoform and interacts with the N-terminus of TnC. Phosphorylation of two sites present in this region weakens interaction with TnC, decreasing calcium sensitivity, as well as increasing relaxation and cross-bridge cycling (Howarth et al., 2007). Following this region, a pair of α-helices are connected by a small linker which, together with TnT, form a W-shape called the IT arm. This region of TnI is mainly structural and its primary role is to orientate TnI and communicate the motion and structural changes within troponin itself, upon calcium binding. In particular, of these two helices, the first one (H1) binds to TnC while the second one (H2) forms a coiled-coil with one of the α-helices of TnT (Takeda *et al.*, 2003; Yang *et al.*, 2014).

After the IT arm is the inhibitory region, which is known to bind to actin in a 1:1 stoichiometry ratio on its own and in a 1:7 ratio in the presence of tropomyosin (Potter & Gergely, 1974; Syska et al., 1976). This peptide also shows differences between cardiac TnI and skeletal TnI; specifically, in cTnI this peptide tends to be less ordered than in sTnI, making it generally difficult to crystallize (Vinogradova *et al.*, 2005).

The last section of TnI is the switch peptide, fundamental for thin filament activation, since it has a strong affinity for the N-terminal of TnC in the presence of calcium. When the switch peptide is bound to TnC, it promotes a conformational change in the entire troponin complex, resulting in the release of its inhibitory domain from actin and in the subsequent movement of tropomyosin in the closed position, favouring myosin binding (Jayasundar *et al.*, 2014; Yang *et al.*, 2014).

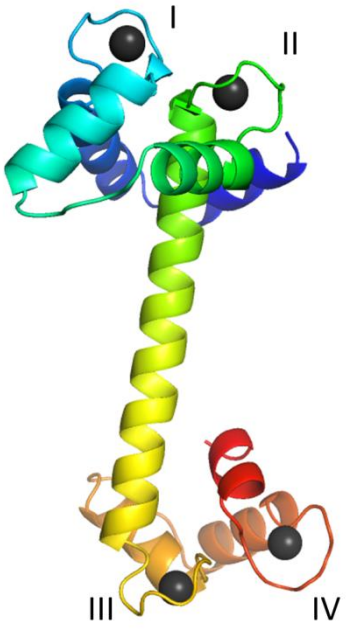

Figure 1.7: **The crystal structure of troponin C.** Cartoon of the crystal structure of skeletal TroponinC, showing the four coordination sites (I-IV), adapted from PDB 2TN4.

The last subdomain of troponin, troponin C, consists of two globular domains separated by a α-helix (figure 1.7) (Houdusse et al., 1997) and is the calcium sensor of the thin filament. The short and rigid α-helix connecting the N- and C-terminals is thought to function as a mediator between the two, with thermodynamic studies finding an inverse dependence of each other's stability in the presence of calcium (De Oliveira *et al.*, 2013).

Each globular domain is able to accommodate two Mg^{2+} or Ca^{2+} ions, however there are differences between the two. In particular, the C-terminal binding domains have a similar affinity to either Mg^{2+} and Ca^{2+} (about 10^7 M^{-1}), the former

being mostly bound when the muscle is in relaxed conditions, while the N-terminal domain is highly specific to calcium, its affinity for it being of about 10^5 M^{-1}. The C-terminal sites are also considered to be structural, since they promote TnC to TnI and TnT binding (Zot and Potter, 1982; Ingraham and Swenson, 1984) and FRET experiments performed by (Badr et al., 2016) have evidenced conformational changes upon either Mg^{2+} or Ca^{2+} binding to site III or IV. Moreover, in cardiac muscle, due to small changes in the amino acid sequence, the N-terminus of TnC can only host one Ca^{2+} ion (van Eerd and Takahashi, 1975). In the N-terminus domain is also a hydrophobic pocket which possesses the fundamental role of transmitting the Ca^{2+} signal to the rest of the thin filament. Upon Ca^{2+} binding to this region, the interaction between TnC and TnI is also favoured, leading to the detachment of TnI from actin and the release of tropomyosin (Takeda et al., 2003).

1.3 – The thick filament and Myosin II

Myosin II (termed myosin from now on) is the main protein in the thick filament and the molecular motor that drives muscle contraction. It is a complex of two heavy chains and four light chains (two Essential Light Chains (ELC) and two Regulatory Light Chains (RLC)), about 500 kDa in total.

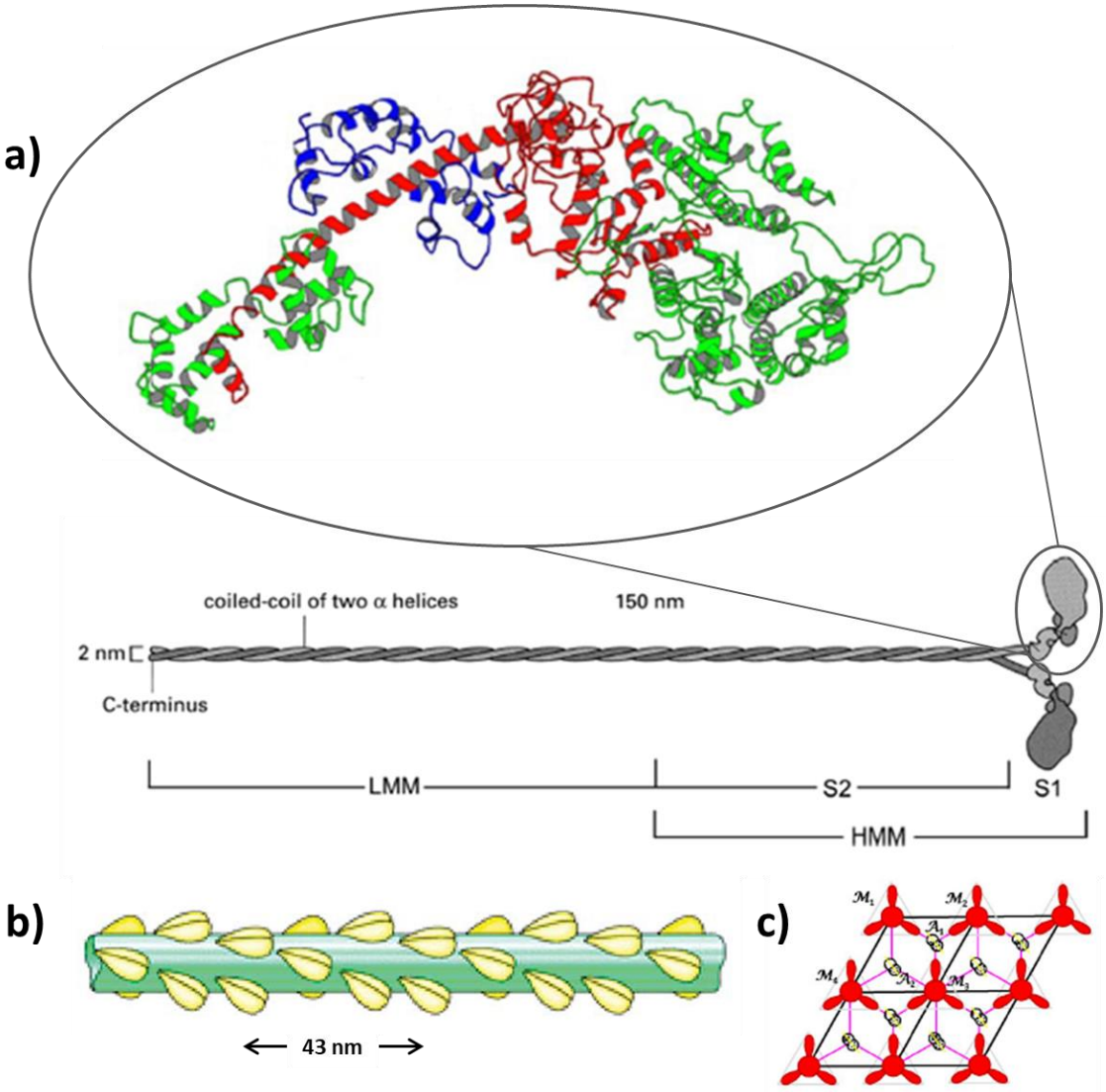

Figure 1.8: **The structure of myosin II and the thick filament.** a) diagram of myosin II, showing the tail (LMM and S2), neck and head region (S1) and its crystal structure (adapted from (Squire, 2009)) highlighting its lever arm section (red) and motor domain (green); b) cartoon of the thick filament, showing the three-stranded helical pattern and the crowns periodicity of 43 nm, adapted from (Al-Khayat, 2013); c) cross section of the A band of the sarcomere, showing the hexagonal arrangement of thick and thin filaments (taken from (Mijailovich *et al.*, 2016)).

As shown in figure 1.8a, each myosin heavy chain is composed of a tail, a neck region and a head. The two heavy chains are bound together through their tails, which form a coiled-coil up until the neck region. The tails of several myosin complexes can then assemble into the thick filament through electrostatic interactions, forming a structure

in which the myosin tails are the main component of a long fibre, from which the heads project outwards. The resulting thick filament is then a three-stranded right handed quasi-helical fibre, with consecutive heads at a distance of 14.5 nm, requiring nine heads for a complete turn (figure 1.8b). However, since the filament is three stranded, its periodicity is of 43 nm. Viewing the thick filament along its axis, as shown in figure 1.8b, three myosin heads project outwards every 14.5 nm, forming a crown. Each thick filament is then surrounded by six thin filaments in a hexagonal configuration, with the thick filament in the middle, allowing each thin filament to be reached by three myosins (figure 1.8c).

Myosin can be cleaved by two proteases in two different regions. Digestion with chymotrypsin divides myosin in two regions, the heavy meromyosin (HMM) and the light meromyosin (LMM), while digestion with papain removes the myosin head (or S1, figure 1.8a), keeping both of the light chains (Lowey *et al.*, 1969). The S2 portion of the thick filament rod (part of the HMM, figure 1.8a) is only loosely associated with the rest of the thick filament (McLachlan and Karn, 1982) and contains a hinge, a section of the α-helical coiled-coil which helps the myosin heads reach the actin filament and is also partly responsible for tension generation during muscle contraction (Burke *et al.*, 1973; Stewart and Roberts, 1982; Stewart and Edwards, 1984; Miller *et al.*, 2009).

The myosin-S1 structure, shown in figure 1.8a, was first solved by (Rayment, W. R. Rypniewski, *et al.*, 1993). It consists of three main subdomains, a 25 kDa domain, a 50 kDa domain and a 20 kDa domain. The 25 kDa domain most notable feature is the P-loop, to which the α- and β-phosphate of the ATP bind. The 50 kDa domain contains the actin binding sites. It is separated by a central cleft, dividing it into lower and upper 50 kDa domain. The last section of the myosin head is the lever arm, a 20 kDa domain

constituted by a α-helix coming from the myosin tail or C-terminus, consisting in the converter domain (position Phe-707 to Arg-774 (Houdusse *et al.*, 1999; Houdusse *et al.*, 2000)), and the myosin light chains binding region, the ELC and RLC.

The role of the two light chains is still a matter of discussion and differences have been seen among the various isoforms expressed in muscles (Logvinova and Levitsky, 2018). Both the RLC and ELC have been shown to have a structural role in stabilising the neck region (Rayment *et al.*, 1993), although they exert different functions on myosin binding to actin. Specifically, removing both light chains from myosin reduced the speed of actin filaments in the motility assay but without affecting actin-activated myosin ATPase (Lowey *et al.*, 1993). Later studies showed that removal of the ELC only produces a 50% decrease in the isometric force, ruling out the effect of the RLC in force production (VanBuren *et al.*, 1994), while also assigning the ELC a role in myosin strong binding to actin (Guhathakurta *et al.*, 2015; Logvinova *et al.*, 2018). However, the RLC has been shown to be important for correct folding of smooth muscle myosin (Trybus and Lowey, 1988) and lattice spacing (Colson *et al.*, 2010), while its phosphorylation is known to be important for myosin head orientation (Scruggs and Solaro, 2011; Burghardt and Sikkink, 2013; Kampourakis and Irving, 2015).

1.4 – The cross-bridge cycle

Muscle contraction is caused by the thin and thick filament sliding relative to each other, as was suggested by A. F. Huxley and H. Huxley in two separate studies

published at the same time in 1954 (Huxley and Hanson, 1954; Huxley and Niedergerke, 1954). According to the "sliding filament theory", contraction is the result of cyclical and highly regulated acto-myosin interactions that generate force, the underlying mechanism being a result of the following myosin ATPase cycle,

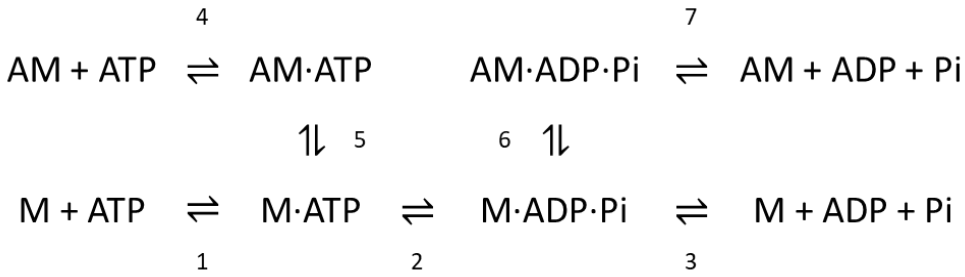

where A indicates actin and M myosin (taken from (Lymn and Taylor, 1971)). Starting from the rigor-like acto-myosin complex (AM), adding ATP (step 4, k_4 of ~1 $\mu M^{-1}s^{-1}$) results in a myosin detachment from actin (steps 5, k_5 >1000 s^{-1}). This provokes the opening of the central cleft in myosin 50 kDa domain, promoting ATP hydrolysis into ADP and Pi (step 2, k_2 of ~125 s^{-1} (Johnson and Taylor, 1978)). In this state, M·ADP·Pi is in a "cocked state" and able to bind actin again, first weakly, with the lower 50 kDa domain functioning as initial contact, then strongly (AM·ADP·Pi, step 6, k_6 of ~0.3 $\mu M^{-1}s^{-1}$), with the closing of the central cleft resulting in the upper 50 kDa domain binding to actin. Finally, the ADP and Pi are released (step 7), while the myosin lever arm swings the myosin head producing force and motion in what is called a power stroke (Huxley, 1969; Uyeda *et al.*, 1996). The length over which a myosin is able to push the thin filament has been calculated by (Kad *et al.*, 2005) to be of approximately 5 nm for the first step on regulated thin filaments and 11 nm for subsequent steps and unregulated actin. Although myosin II consists of two heavy chains and two heads, only

one head has been shown to be necessary to achieve the maximum sliding length, with the second head believed to be necessary for the orientation of the first one (Tyska *et al.*, 1999; Kad *et al.*, 2003). Moreover, in the absence of actin myosin is still capable of binding and hydrolysing ATP (steps 1 to 3) the reaction rate for the product release is much slower than in the presence of actin (k_3 of ~0.05 s^{-1} vs k_7 of ~10 s^{-1}), and the latter case is usually referred to as the actin-activated myosin ATPase (Lymn and Taylor, 1971). Recent studies have also demonstrated that myosin heads can be sequestered from actin binding, in what is called the "super relaxed state" (Hooijman *et al.*, 2011). In this configuration, associated with a folding back of the myosin head over its tail (Alamo *et al.*, 2016; Nogara *et al.*, 2016), myosin exhibits a very slow ATP turnover rate (about 30 minutes (Naber *et al.*, 2011)), thought to be necessary to limit the metabolic rate of muscle in relaxing conditions (Stewart *et al.*, 2010).

Myosin binding to actin has been later revealed to occur in two steps, first through a weak binding, with the lower 50 kDa domain functioning as initial contact, then through strong binding, with the closing of the central cleft resulting in the upper 50 kDa domain binding to actin (Coates *et al.*, 1985; Behrmann *et al.*, 2012). Particularly, this motion is calcium dependent and linked to tropomyosin position on actin, in a model called the three-state dynamic steric blocking model, by (Mckillop and Geeves, 1993).

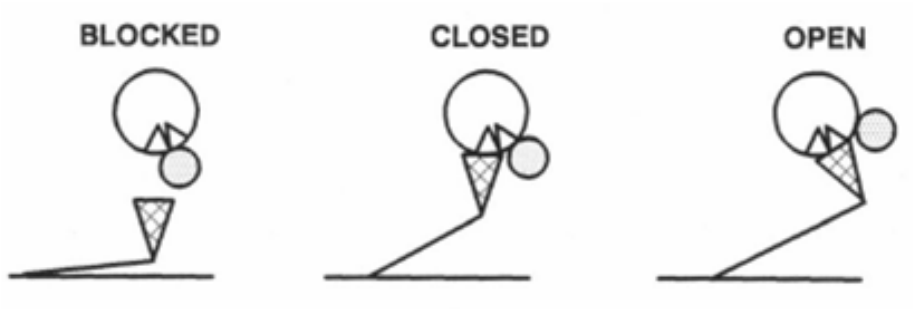

Figure 1.9: **Diagram of the three states of the thin filament.** Myosin interacting with the thin filament, highlighting the blocked, closed and open position. Taken from (Mckillop and Geeves, 1993)

This model, pictured in figure 1.9, states that tropomyosin can occupy three different positions on actin, the blocked (B), closed (C) and open (M) position, or thin-filament "states" of the opening of the myosin binding sites on actin. When the thin filament is in the blocked state, tropomyosin is derepressed by Troponin I and occupies the myosin binding sites on actin (Lehman *et al.*, 2000), sterically blocking myosin from binding to actin. In this state, tropomyosin interacts through ~30 salt bridges with actin subdomain 1 and 2, particularly with actin residues Lys326, Lys328 and Arg147, as well as with Asp25 and Arg28. In the closed state, however, tropomyosin moves towards subdomains 3 and 4, losing its interaction with actin residues Asp25 and Arg28 but approaching residues Asp311 and Lys315 (Li *et al.*, 2011; Lehman *et al.*, 2013). Here, myosin binding sites are partially available, allowing myosin to bind weakly to actin through the lower 50 kDa domain. Finally, the closure of the myosin cleft pushes tropomyosin from the closed to open position, fully uncovering other nearby myosin binding sites, resulting in cooperative activation of the thin filament (Mckillop and Geeves, 1993; Heeley *et al.*, 2006; Behrmann *et al.*, 2012). Once in the M position, tropomyosin interaction with actin is now reduced to ~11 salt bridges with actin (residue Lys315) and another 5 with myosin, particularly with Arg288 (Lehman *et al.*,

2013). There is still controversy over the precise mechanism of tropomyosin movement on actin however, several structural studies have demonstrated that the movement occurs and highlighted its different positions (Lorenz *et al.*, 1995; Poole *et al.*, 2006; von der Ecken *et al.*, 2015; Rynkiewicz *et al.*, 2016).

Since tropomyosin is bound to actin and troponin, the population of the thin-filament activation states strongly depends on calcium (Fraser and Marston, 1995; Homsher *et al.*, 1996). In the absence of Ca^{2+} about 76% of the thin-filament is in the blocked state, about 22% in the closed state and <2% in the open state. In the presence of Ca^{2+}, however, these change to <5%, 80% and 20% in the blocked, closed and open position respectively (Mckillop and Geeves, 1993). Structural studies using native thin filaments have shown that tropomyosin can switch between these three states, with a preference for the blocked and closed states (Risi *et al.*, 2017; Kiani *et al.*, 2018). However, calcium alone is not able to fully activate the thin filament and the initial binding of a myosin head is necessary for cooperative activation (Kad *et al.*, 2005; Heeley *et al.*, 2006; Desai *et al.*, 2015).

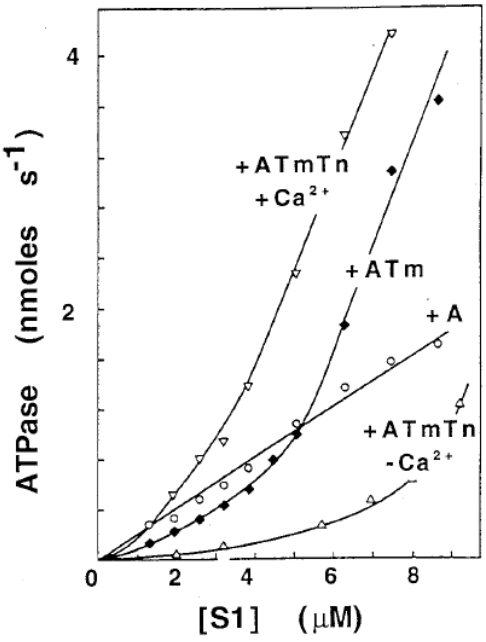

Figure 1.10: **The effect of regulatory proteins on the acto-S1 ATPase.** Graph of the actin activated ATPase of S1 at saturating ATP in the presence and absence of regulatory proteins and calcium. Taken from (Lehrer and Geeves, 1998).

Cooperative activation of the thin filament has been seen as early as (Lehrer and Morris, 1982), where the authors studied the ATPase activity dependence on the myosin-S1 concentration at saturating ATP, in the presence of actin and/or tropomyosin, troponin and Ca^{2+}. As seen in figure 1.10, in the

presence of actin only and away from V_{max}, the ATPase activity increases linearly with increasing amounts of S1, following a standard Michaelis Menten plot. The addition of Tm, Tn and calcium turns the relationship into a sigmoidal, with the cooperative activation particularly seen for actin.Tm, where the ATPase is lower than that of actin alone until about [S1] = 5 μM; the addition of troponin is seen closing the thin filament completely until calcium is added, in which case the ATPase is higher than that of actin alone (Lehrer and Morris, 1982; Lehrer and Geeves, 1998).

When considering cooperative activation, the size of the regulatory unit, (i.e. the smallest region activated by a single myosin head, also called cooperative unit) becomes important. Initial studies had looked at the extension of tropomyosin over seven actin subunits and showed the size of the cooperative unit length to be of about 40 nm. However, as mention in chapter 1.2.2, tropomyosin is a rather stiff polymer and can communicate strain to neighbouring monomers via the overlap region. In particular, the cooperative unit has been shown to vary within experiments, from the one calculated in the absence of troponin to be about 5 to 6 monomers versus 10 to 12 monomers of the full thin filament in (Geeves and Lehrer, 1994) and up to ~20 monomers (110 nm) in (Kad *et al.*, 2005).

1.5 – Myosin Binding Protein-C

Myosin Binding Protein-C (MyBP-C or C-protein in some of the older literature) is a thick filament protein and was first found as an impurity in myosin purifications (Offer

et al., 1973). Since its discovery, it has increasingly shown it is an important player in muscle contraction, as will be discussed in more details in this chapter and in chapter 5 of this thesis. MyBP-C comes in different isoforms, cardiac and slow and fast skeletal, depending on the type of muscle where it is produced (Weber *et al.*, 1993; Yasuda *et al.*, 1995). However, I will focus this sub-chapter on the cardiac isoform, which is the one that has been used in the experiments for this thesis.

Cardiac MyBP-C is composed of 11 subdomains (figure 1.11), named from C0 to C10, of which 8 are Ig-like (C0 to C5, C8 and C10) and 3 are FnIII-like domains (C6, C7 and C9) (Okagaki *et al.*, 1993).

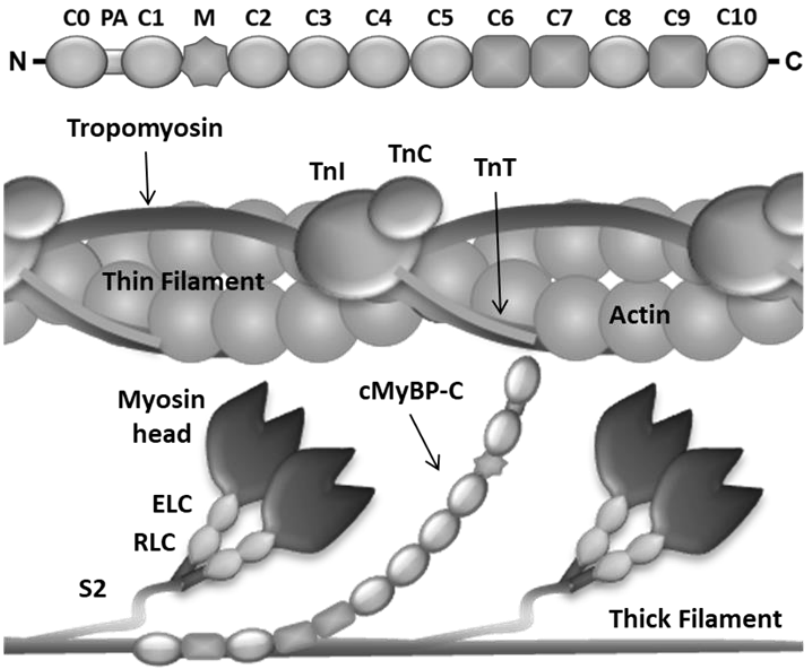

Figure 1.11: **Cardiac MyBP-C and its subdomains in relation with the thick and thin filaments**. cMyBP-C is composed of eleven subdomains, of which eight are Ig-like domains (C0 to C5, C8 and C10) and three Fn(III)-like domains (C6, C7 and C9); PA indicates the short Proline-Alanine rich domain and M the disordered M-domain. It is found in nine bands on the thick filament, in reaching distance of the thin filament.

Between domain C0 and C1, is a region rich in Proline and Alanine called the PA region and between domains C1 and C2 the M-domain is found, which is partially disordered and possess three of the four phosphorylation sites found in MyBP-C.

MyBP-C is found in seven to nine bands, spaced 43 nm apart, in each side of the A band in the sarcomere, as shown by (Luther *et al.*, 2011) (figure 1.11). Structural studies have shown that its C-terminus is bound to the thick filament and titin in particular, through domains C8-C10 (Freiburg and Gautel, 1996; Flashman *et al.*, 2004). This interaction is mainly structural, since there seem to be no other function associated with MyBP-C C-terminal domains. The N-terminus, instead, seems to have a double function in muscle contraction: it has been shown several times that it is both capable of binding actin and myosin heavy chain. For instance, the N-terminal domains can bind myosin in the S2 region (Starr and Offer, 1978; Gruen and Gautel, 1999) and to its regulatory light chain (Lu et al., 2011; Ratti et al., 2011). Studies performed by (McNamara *et al.*, 2016) suggest that these interactions serves to stabilise myosin's super-relaxed state, since mice lacking MyBP-C have shown increased ATP turnover. Other studies have been focused on the binding properties of the N-terminus to actin and on its function as a modulator of cross bridges formation, showing that there are several actin binding sites between subdomains C0 and C2. In *in vitro* motility experiments, different N-terminal fragments have been seen exerting different effects on thin filaments speed and fraction moving (Razumova *et al.*, 2006). In particular, increasing amounts of C0C2 are capable of increasing thin-filament speed at low calcium, effectively activating motility, while inhibiting speed at high calcium. A shorter fragment, C0C1, has not shown these capabilities while, when using subdomains C2 to C4 only, the activation effect at low calcium disappears. Structural studies (Harris et al.,

2016; Mun et al., 2014; Mun et al., 2011) have later shown that MyBP-C can directly push tropomyosin away from its blocked position, suggesting that the activation effect seen at low calcium might be caused by an increase in amount of available myosin sites on the thin filament; at the same time, they provided evidence that MyBP-C shares some of its binding sites on actin with myosin, possibly explaining the inhibition effect seen at high calcium with a direct competition for binding.

It is worth taking into account the possibility that some of these effects could be inherent to the assay used and not be present *in vivo*. For instance, (Walcott *et al.*, 2015) have shown that direct competition alone does not fully explain thin filament behaviour in the presence of MyBP-C N-terminal fragments at high calcium. Hence, to fully model the system, we must take into account the viscous drag produced by transient interactions between MyBP-C, actin and the surface of the coverslip.

Similar results have been obtained using laser tweezers by (Weith *et al.*, 2012), where they report MyBP-C binding to actin transiently and with two specific lifetimes: a short one, of about 20 ms and a long one, greater than 200 ms. In addition, they also show the importance of the first 17 amino acids after C1 for actin binding, providing an explanation for the behaviour observed by fragments that do not possess the M-domain. In a following study, Previs et al. were able to measure changes in the speed of native thin filaments moving along isolated thick filaments, showing a decrease in average speed within the MyBP-C containing C-zone (Previs *et al.*, 2012), further supporting the viscous load model.

Another study reporting activating and inhibitory effects has been performed by (Belknap et al., 2014), looking at changes in actin-activated myosin steady-state ATPase with increasing amounts of human MyBP-C, as shown in figure 1.12.

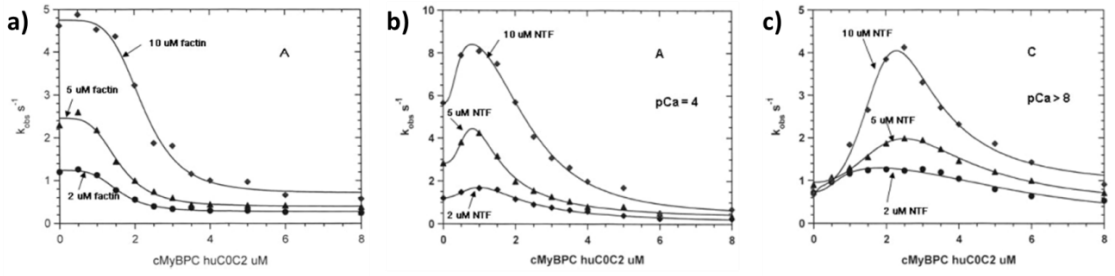

Figure 1.12: **The effects of C0C2 on myosin ATPase.** S1 ATPase activity at increasing concentration of C0C2 and a) naked actin, b) thin filaments at pCa 4 and c) thin filaments at pCa 8, adapted from (Belknap et al., 2014).

In their study, they also suggest that MyBP-C cooperatively binds to actin, as evidenced by the lag phase seen at low [C0C2] in figure 1.12a and by the Hill coefficients greater than 1 calculated from fitting the data in figure 1.12b and c. In addition, they also reported intra-species behavioural differences when studying myosin ATPase with native thin filaments and C0C1 at low calcium, which they attribute arising from the poor amino acids sequence similarities in the PA region between mouse and human MyBP-C (Belknap et al., 2014), but could also be caused by an 8-amino acids N-terminal extension known to interfere with RLC binding (Bunch *et al.*, 2018).

So far, the properties of the N-terminus as a whole have been discussed; however, a particular mention is needed for the M-domain, as it has interestingly different structural features compared with the rest of the protein. It is known to be largely disordered, with the exception of three compact α-helices at its C-terminal. The last helix in particular shares similarities with other actin binding domains found in other proteins (Howarth *et al.*, 2012). Upon phosphorylation, MyBP-C N-terminal fragment C0C3 has been seen closing in, suggesting the presence of a hinge within the M-

domain (Colson *et al.*, 2016; Previs *et al.*, 2016). Force-extension curves obtained using the atomic force microscope have also found this domain to be extensible at very low forces (Karsai *et al.*, 2011, 2013). This could be important when considering MyBP-C tether to the thick filament, suggesting that the M-domain might partially extend when domains C0 and C1 are bound to the thin filament (Luther and Craig, 2011).

To date, the physiological role of MyBP-C is still not very well understood but there is a clear consensus on it working as a modulator of muscle contraction. The studies so far suggest that MyBP-C could alternate between binding to myosin, stabilising its position on the thick filament in the super-relaxed state, and actin, activating the thin filament when necessary (Kulikovskaya *et al.*, 2003).

1.6 – Hypertrophic Cardiomyopathy

1.6.1 – Physiological effects

Hypertrophic Cardiomyopathy (HCM) is a genetic disease that affects 1:200 individuals (Semsarian *et al.*, 2015) and is the leading cause of sudden cardiac death in young adults. It was first reported by (Teare, 1958), which noted several cases of asymmetrical hypertrophy linked to sudden death of patients, and soon after found to be a genetic condition (Hollman et al., 1959).

When compared to a healthy heart, a HCM affected heart is characterised by an increase in thickness of the left ventricular wall and the interventricular septum, as shown in figure 1.13a.

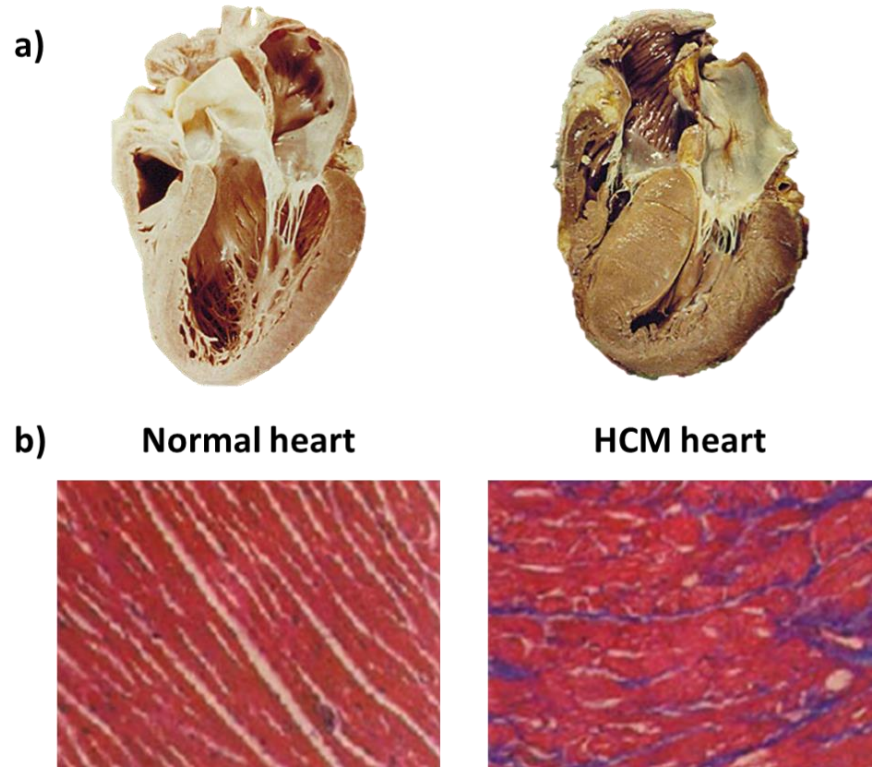

Figure 1.13: **The effects of hypertrophic cardiomyopathy on the heart.** Comparison between a) the section of a normal heart versus one affected by HCM and b) the arrangement of the myocytes in healthy versus hypertrophic tissue. Adapted from (Chung *et al.*, 2003).

Beside hypertrophy of the heart walls, HCM is also characterised by myocyte disarray and an increase in interstitial fibrosis between them (figure 1.13b). To date, however, it is still not clear whether this is a cause of HCM or a consequence of the disease. Patients affected with HCM have shown an increase in force production during systole and an impaired relaxation during diastole (B. J. Maron et al., 2012; M. S. Maron et al., 2009). It is mostly asymptomatic but patients can show atrial fibrillation and chest pain caused by imbalances of blood supply and demand. Today, the annual mortality rate for patients affected by HCM is ~ 1% (Houston and Stevens, 2015).

There is some variability in the symptoms and effects of HCM within different age groups (Arad et al., 2002). For instance, young adults have lower chances of showing a

genotype, compared to older patients; however, in both cases, about 20% of the patients experienced HCM morbidity or mortality (Loar et al., 2015). Furthermore, Coppini et al. studied the incidence of thin filament vs. thick filament mutations, showing that the former are related to milder hypertrophy but higher prevalence of systolic dysfunction and same rates of sudden cardiac death (Coppini *et al.*, 2014). It has also been noted that, although HCM affects men and women at the same rate, deaths in young athletes are more common in males (Van Camp et al., 1995).

1.6.2 – Notable mutations and where to find them

To date, more than 1400 mutations have been associated with HCM, spanning more than 11 genes (Maron *et al.*, 2012). Within these, about 40% are found in the MYH7 gene, which encodes for β-cardiac myosin II, about 33% in the MBPC3 gene, which encodes for MyBP-C, and the remaining are found in all the other genes associated to most of the proteins found within the sarcomere, in 1-5% each, including troponin and tropomyosin (Maron *et al.*, 2012; Marsiglia and Pereira, 2014). However, with the advances in genetic screening, more are found every day (Liu *et al.*, 2015; Lopes *et al.*, 2015). The majority of hypertrophic cardiomyopathy causing mutations are missense, except for the MYBPC3 gene, for which truncations or deletions are more common, as extensively reviewed in (Marian and Braunwald, 2017). Each of these mutations affect acto-myosin interactions in a different way, with some leading to a more severe clinical phenotype than others. However, it has been argued that there is a general trend with the effect of HCM mutations on muscle contractility, where they usually linked with an increase in calcium sensitivity and impediment of a complete muscle relaxation at low calcium, as evidenced from figure 1.14 (Marston, 2011). Furthermore, having multiple

different mutations highly increases the chances of a severe phenotype and early onset (Kelly and Semsarian, 2009).

Gene	Mutation	System	Ca^{2+}-sensitivity, ΔpCa_{50}	Switch-off at pCa9	Max turnover rate
ACTC	E99K	TG mouse tissue, motility	+0.39	Normal	Normal
		Human tissue, motility	+0.12	Normal	Normal
		TG mouse tissue, force	+0.11	Normal	
		Baculovirus, motility	+0.05	Normal	
MYBPC3	IVS17+4A>T truncated at 868	Human tissue, skinned cells	+0.1		
	c.2864_2865delCT truncated at 860	Human tissue, skinned cells	+0.06		
MYL2	R58Q	Recombinant exchange, force	+0.11		
	D166V	TG mouse tissue, force	+0.25		Reduced
MYH7	R403Q	Human tissue, motility			Increased
		Recombinant, motility			Increased
		TG mouse tissue, force	+0.15	Normal	
	R453C	TG mouse tissue, force	+0.30	Normal	
	R719Q	Recombinant, motility			Normal
	R719W	Recombinant, motility			Normal
	D778G	Recombinant, motility			Increased
	L908V	Human tissue, motility			Increased
TNNI3	R145G	Recombinant, ATPase	+0.56	None	
		Recombinant, ATPase	+0.32	Incomplete	Increased
		Recombinant exchange, force	+0.16		
	R145Q	Recombinant, ATPase	+0.23	Incomplete	Increased
		Recombinant exchange, force	+0.10		
	R162W	Recombinant, ATPase	+0.11	Incomplete	Normal
		Recombinant exchange, force	+0.06		
		Recombinant, ATPase	+0.13	Incomplete	
	ΔK182	Recombinant, ATPase	+0.18	Normal	Normal
		Recombinant exchange, force	+0.1		
	K206Q	Recombinant, ATPase	+0.18	Normal	
		Recombinant exchange, force	+0.04		
	G203S	Recombinant, ATPase	+0.10	Normal	
		Recombinant exchange, force	+0.02		
TNNT2	Exon 16/17del (truncated at 267)	Recombinant, ATPase	+0.43	None	Normal
	R92Q	Recombinant, ATPase	+0.24	Incomplete	
		Recombinant exchange, force	+0.18		
	I79N	Recombinant exchange, force	+0.15	Incomplete	
	R94L	Recombinant exchange, force	+0.11		
	F110I	Recombinant exchange, force	+0.37	Incomplete	Decreased
	ΔE160	Recombinant exchange, force	+0.15		
	E163K	Recombinant exchange, force	+0.07	Incomplete	Increased
	R278C	Recombinant exchange, force	+0.34	Incomplete	Increased
TPM1	A63V	Recombinant, ATPase, motility	+0.30		
	K70T	Recombinant, ATPase, motility	+0.33		
	D175N	Recombinant, motility	+0.082	Normal	Normal
		Human tissue (skeletal), force	+0.09	Normal	Normal
		TG mouse tissue, force	+0.10		
	E180G	Recombinant, motility	+0.115	Normal	Normal

Figure 1.14: **HCM mutations and their effect.** List of the most known HCM mutations with their associated effect on contraction mechanism. Adapted from (Marston, 2011).

One of the most extensively studied mutations is R403Q, the first to be discovered in myosin, notable for its severe phenotype (Epstein et al., 1992). It is located in close proximity of the actin binding site on myosin head and has been subject of controversy since different groups have found contrasting results. In particular, working with full mouse myosin and performing both single molecule and in-vitro motility experiments, (Tyska *et al.*, 2000) reported that mutation R403Q causes a two-fold increase in average force production but not at the single molecule level in laser trap assay (Palmiter *et al.*, 2000; Tyska *et al.*, 2000). In contrast, recent experiments performed by (Nag *et al.*, 2015) have showed an overall decreased activity in the mutated myosin and especially in the actin-activated ATPase activity in the presence of reconstituted thin filaments. These differences have been associated with the genetic differences between mouse and human β-cardiac myosin and with the use of the recombinant truncated versions over the full protein.

In recent years, the existence of a conserved region in the myosin head (called “mesa”) has been highlighted, where a high number of HCM mutations are located (Spudich, 2015). Evidence suggests that this region of the myosin head is responsible for the turning off of the thick filament, which occurs when the myosin head bends backwards binding to the S2 region of myosin (Nag *et al.*, 2017; Robert-Paganing *et al.*, 2018). HCM mutations in this regions, such as R249Q, R453C and H251N have been linked to a weakening of this interaction, which could lead to an increase in myosin heads available for binding to the thin filament and account for the increase in ATPase activity and force produced during muscle contraction (Adhikari *et al.*, 2016; Nag *et al.*, 2017; Trivedi *et al.*, 2017).

Other mutations have been found throughout the whole myosin heavy chain and most of them seem to affect the ATPase activity and increase calcium sensitivity, such as the R719W (Kohler *et al.*, 2002; Kirschner *et al.*, 2005) and D778G (Miller *et al.*, 2003), as reviewed in (Marston, 2011) and (Moore et al., 2012).

Mutations in MyBP-C are somewhat different from the ones found in myosin. Overall, its mutations are found to have a mostly mild phenotype and are generally related to late onset HCM. However, only one third of all the mutations found seem to be caused by a change in a single amino acid (found throughout the whole protein with the exception of the Pro-Ala region), while another third are caused by frame shifts, with the remaining being truncations, insertion or deletions, mostly affecting the C-terminal end of the protein (Harris *et al.*, 2011). Furthermore, like in myosin, patients affected by more than one mutation at once experience a more severe phenotype (Van Driest *et al.*, 2004).

Mutations in MyBP-C have been shown to provoke HCM through haploinsufficiency (a reduction in the level of expressed functional protein to 50% of the normal amount in a cell, resulting in loss of function) (Glazier *et al.*, 2018). Marston et al, studying nine different truncation and missense mutations in the MBPC3 gene found that the amount of MyBP-C expressed in the sarcomere was 24% lower than the wildtype, which they linked to the hypertrophy in the samples (Marston et al., 2009). However, they found no specific truncated protein in muscle homogenates, similarly to what others reported for different truncating mutations. This would suggest that the expressed truncated proteins are quickly degraded either by ubiquitin-proteasome system (UPS) or nonsense-mediated mRNA decay (NMD) and do not affect sarcomere function per se (Rottbauer *et al.*, 1997; Moolman *et al.*, 2000; Van Dijk *et al.*, 2009;

Marston *et al.*, 2012; Leary *et al.*, 2019). On the contrary, missense mutation A31P found in subdomain C0 has been reported to alter the subdomain structure and alter myocyte function through a poison peptide mechanism (Van Dijk *et al.*, 2016).

Several studies have used mouse models to reproduce HCM mutations in MyBP-C. Among all, (Yang et al., 1998) have reported that the truncation of the C-terminal end, containing the binding domains for the thick filament, causes hypertrophy of the heart and disarray of the myocytes. Another study by (van Dijk et al., 2015) has shown that mice lacking the PA region and subdomain C1 did not produce over-contractility. These findings are consistent with what reported in a similar study by (Witt *et al.*, 2001), where the same mutation was found to not cause an overall increase in force produced, although increasing Ca^{2+} sensitivity. Phosphorylation of MyBP-C also plays a role in hypertrophic cardiomyopathy. In their paper, (Jacques *et al.*, 2008) have found that failing hypertrophic human heart muscles showed a 40% decrease in phosphorylation compared to normal hearts. However, this change was not dependent on whether the failing heart possessed a mutation in MBPC3 gene, since they studied mutations that cause a truncation of the protein.

Tropomyosin mutations are found in about 5% of the patients affected by HCM, indicating its importance in regulating the accessibility of the thin filament for myosin, since any mutation most likely impacts survivability. Hence, they can give useful insights into how tropomyosin regulates acto-myosin interactions and to study the cooperative unit size on actin. HCM mutations on tropomyosin have been found in large part in the region in close proximity of Cys190, a very conserved residue important for Tm-actin interactions (Bai *et al.*, 2013), which is oxidised in failing heart, crosslinking the two coils together (Koubassova *et al.*, 2018).

Studies have focused on two main aspects of these tropomyosin mutations: their effect on its binding to actin and their importance on tropomyosin flexibility. Mutants D175N, E180G and L185R fall within both categories but are known to have different effects, despite their close position, with E180G having the stronger phenotype. For instance, D175N and E180G weaken Tm affinity to actin, while L185R increases it (Golitsina *et al.*, 1997; Kremneva *et al.*, 2004; Zheng *et al.*, 2016). Furthermore, using circular dichroism (Kremneva *et al.*, 2004) found that the E180G thermal stability is reduced both in the absence and presence of actin, meaning that Tm-Tm and Tm-actin interactions are weakened, while D175N did not appear different from the control. In particular, the E180G thermal denaturation occurred at temperatures closer to normal or resting body condition, as also reported by (Wang *et al.*, 2011). E180G and D175N have also shown to reduce cooperativity (reduction in the Hill coefficient) in *in vitro* motility assays, while E180G and L185R also increases calcium sensitivity, and ATPase activity (Bottinelli *et al.*, 1998; Chang *et al.*, 2005, 2014; Boussouf *et al.*, 2007; Wang *et al.*, 2011). Through molecular dynamics simulations and atomic force microscopy studies, these changes have been correlated with an increased flexibility of the polymer (Li *et al.*, 2012; Loong *et al.*, 2012; Sewanan *et al.*, 2016), thought to be caused by a local disruption of coil-coil interactions and actin-Tm interactions (Mathur *et al.*, 2011; Ly and Lehrer, 2012; Matyushenko *et al.*, 2017). Furthermore, (Bai *et al.*, 2011) studied the effects of E180G and D175N on tension produced in reconstituted myocardia, showing an increase in low calcium tension for both and stiffness, greater calcium sensitivity but reduced cooperativity for E180G. These changes can be related to a higher number of cross bridges formation at low calcium, leading to residual force and an impaired relaxation during diastole, one of the main causes of Hypertrophic

Cardiomyopathy (Mandinov *et al.*, 2000). We must also consider that most of these studies have been performed using mutated homodimers, meaning dimers of Tm both possessing the mutation. This might arise issues when studying in-vivo cases where the mutant isoform is expressed alongside the wild-type in different amounts. In a paper by (Janco *et al.*, 2012), differences between homodimers and heterodimers were reported. In particular, the E180G heterodimer did not show a significant increase in calcium sensitivity and melting curves suggest that it might be less stable than both the homodimer mutant and the wild-type.

Other notable mutations in the tropomyosin chain are V95A, known to increase calcium sensitivity and tension while being associated to a mild phenotype contrasted by an overall poor prognosis (Karibe *et al.*, 2001; Bai *et al.*, 2011), E41K, associated with the inhibition of the on/off state transition (Ochala *et al.*, 2008; Avrova *et al.*, 2018), E62Q, responsible for an increase in calcium sensitivity and velocity in in-vitro motility assay (Farman *et al.*, 2018) and an increase in myosin ATPase activity at high calcium (Chang *et al.*, 2014), A63V and K70T, both responsible to increase calcium sensitivity by altering the stability of the N-terminal region, as found using circular dichroism (Yamauchi-Takihara *et al.*, 1996; Michele *et al.*, 2002; Heller *et al.*, 2003; Zheng *et al.*, 2016).

Several HCM mutations have also been found on the troponin subunits, particularly in TnI and TnT, while only few found on TnC (reviewed in (Lu *et al.*, 2013)). Troponin I mutations R145G, R145Q, R162W, ΔK183 and K206Q have been seen increase the calcium sensitivity of skinned muscle fibres, although being found in different regions of the subcomplex (Takahashi-yanaga *et al.*, 2001; Deng *et al.*, 2003). Specifically, both mutations R145G and R145Q are found in the inhibitory region and are responsible for

a decrease in the inhibitory effect, although the overall TnI affinity for actin remains unchanged, while R145G only causes a decrease in the maximum force contraction produced and an overall slower relaxation time, thought to be caused by the stabilisation of calcium coordinated interactions (Kruger *et al.*, 2005; Lindert *et al.*, 2015). Mutations R162W and ΔK183 are instead found in the troponin C binding region and have been shown to have the opposite effect than the first two, lowering TnI affinity for actin without affecting its inhibitory effect, while R162W alone increases TnI-TnC interactions in the presence of Ca^{2+} (Elliott *et al.*, 2000; Iorga *et al.*, 2008).

Of the mutations found in troponin T, Δ14, ΔE160, S179F, I79N, R92Q, F110I, E244D, R278C and K273E are all known to produce an increase in calcium sensitivity (Yanaga *et al.*, 1999; Knollmann and Potter, 2001; Messer *et al.*, 2016), despite being found in different regions. Mutations I79N and R92Q are located in the tropomyosin binding region and are known to increase force activation and force relaxation as well as cross bridge detachment rate (Sirenko *et al.*, 2006), while inhibiting both TnI and Tm function, ultimately leading to slower relaxation rate and increased tension during diastole (Miller *et al.*, 2001; Javadpour *et al.*, 2003; Sommese *et al.*, 2013; Ferrantini *et al.*, 2017; Wang *et al.*, 2018). However, mutation F110I, found in the same region, increase the maximum ATPase while not affecting calcium sensitivity (Nakaura *et al.*, 1999). A similar effect is associated with mutations E244D and R278C, despite these two being located in the TnT and TnC binding region, while also being responsible for a reduction in the maximum force produced in transgenic mice and impaired diastolic relaxation (Hernandez *et al.*, 2005; Sirenko *et al.*, 2006). In particular, (Brunet *et al.*, 2014) have shown how R278C, when coupled with mutation R145G of TnI, is capable of rescuing the latter's phenotype, albeit exacerbating the overall loss of function.

1.7 – Experimental techniques used for the study of muscle

Muscle contraction has been a subject of study in modern science for more than 80 years, and the field has seen a huge variety of biophysical and biochemical experimental techniques being used throughout the time to address increasingly specific questions. The highly ordered array of muscle fibres enabled scientists to use X-ray diffraction and electron microscopy to understand muscle contraction, leading to the sliding filament theory (Huxley and Hanson, 1954), to the understanding of the lever arm motion of myosin, through which ATP hydrolysis is converted into mechanical force (Huxley, 1969), and to Å resolution structures of all the proteins involved in the process (Kabsch *et al.*, 1990; Rayment *et al.*, 1993; Houdusse *et al.*, 1997; Behrmann *et al.*, 2012; von der Ecken *et al.*, 2015), as mentioned in the previous sections. Structural techniques, however, suffer from high costs of deployment and need high amounts of particularly pure proteins to give reliable results, and might not be the best choice for proteins that do not form ordered structures or difficult to crystallise. Solution experiments are more easily accessible and have been widely used from the very beginning to determine the kinetic properties of myosin, culminating with the description of its ATPase cycle (Lymn and Taylor, 1971; Bagshaw and Trentham, 1973) and its interactions with the actin filament and its regulatory proteins in the three states model (Mckillop and Geeves, 1993). At the same time, different *in-vitro* assays started being developed to study acto-myosin interactions in an easy and reproducible fashion. One of the most successful is the motility or gliding assay, developed by (Kron and Spudich, 1986), where myosin molecules are adhered to the

surface of a coverslip assembled in a microfluidic chamber (figure 1.15a). Fluorescently labelled actin or thin filaments are then imaged moving over the myosin molecules as they go through their working strokes, provided the right conditions for [ATP] and [Ca^{2+}] are met (figure 1.15b, see chapter 2 for technical details).

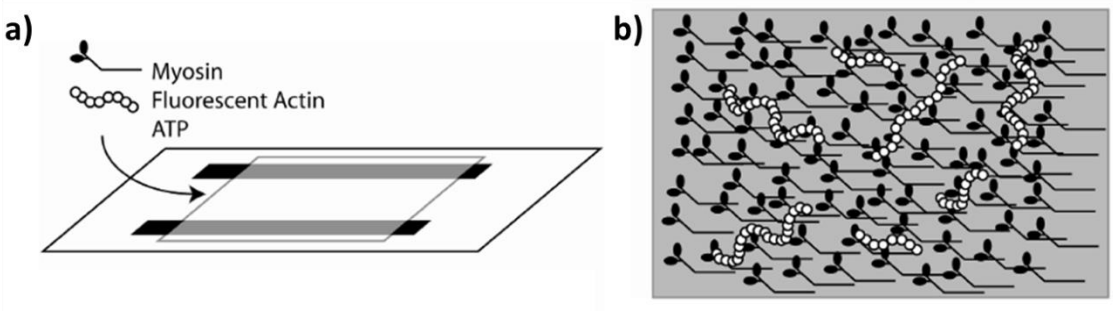

Figure 1.15: **The motility assay.** a) representation of the microfluidic chamber used in the motility assay and b) of its surface, where actin/thin filaments are seen moving over the myosin bed. Adapted from (Batters *et al.*, 2014).

This relatively simple assay allowed for a better general understanding of myosin properties such as its low duty ratio (Harris and Warshaws, 1993), the approximate size and force of a working stroke (Uyeda *et al.*, 1990; Bing *et al.*, 2000) and myosin cooperativity (Vanburen *et al.*, 1999), as well as highlighting the crucial role of troponin and tropomyosin in turning off the thin filament, with the milestone experiments of (Fraser and Marston, 1995), the importance of calcium in the contraction mechanism (Homsher *et al.*, 1996; Gorga *et al.*, 2003), and the collective behaviour of actin filaments (Butt *et al.*, 2010; Hussain *et al.*, 2013). The motility assay ease of use also favoured the study of mutations that lead to cardiomyopathies (as mentioned in the previous section and reviewed in (Marston, 2003) and (Marston, 2011)), as well as being adapted for the characterisation of other proteins of the myosin superfamily and

processive motors linked to the cytoskeleton of cells (Holzbaur and Goldman, 2010; Toepfer and Sellers, 2014).

The motility assay, however, is still in all effects an ensemble assay, i.e. the characteristic and properties measured are the result of collective motion/behaviour of hundreds of molecules at the same time, leading to an averaged result. Single molecule assays try to circumvent this limitation by having a process occur at very low protein concentrations, making it possible to discern between single molecules and characterise them individually, trying to then scale up the new knowledge and put it in context with the ensemble experiments. The downsides of these methods is that they are not as easy to perform and, as they are often combined with microscopy techniques, they require more advanced and expensive equipment, as well as the necessity to label the sample, which could impact the experimental results altogether. One of such assays, particularly used in the study of muscle, is the three beads assay, which consists in using optical tweezers to study the forces involved in muscle contraction. In this assay, as depicted in figure 1.16, a single actin filament is suspended between two trapped beads and subsequently lowered onto a pedestal (a third bead adhered to the surface), which has been functionalised with a very low myosin concentration, allowing the interaction of as low as one myosin per filament. As the acto-myosin interactions take place, the position of the two trapped beads are recorded at high positional (sub-nanometer) and temporal (sub-millisecond) resolution.

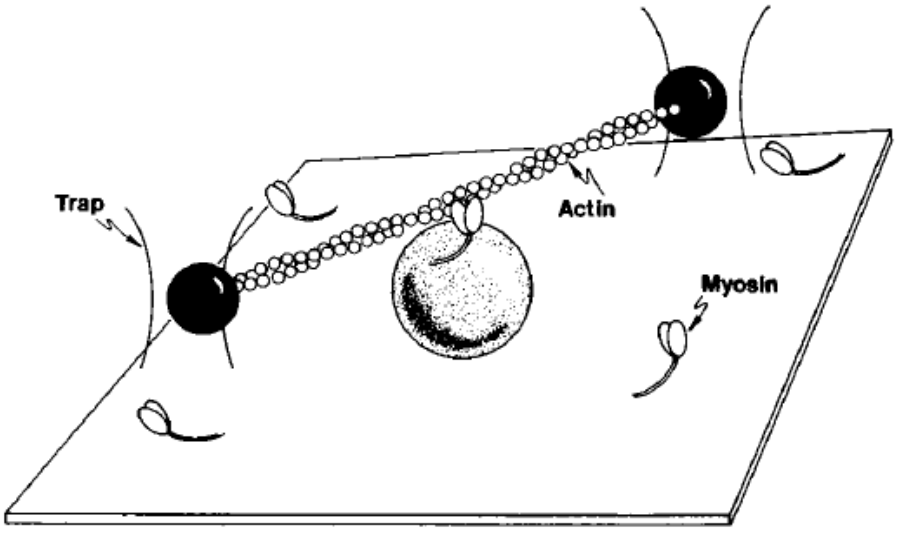

Figure 1.16: **The three beads assay.** Representation of the three beads assay, where an actin/thin filament is captured by two optically trapped beads and lowered onto a third bead functionalised with myosin, allowing the measure of forces. Taken from (Guilford *et al.*, 1997).

This assay has led to the discovery that myosin interacts with actin transiently (Molloy *et al.*, 1995), and to accurately measure the force (Rüegg *et al.*, 2002; Takagi *et al.*, 2006) and the displacement produced by a single myosin head (Veigel *et al.*, 1998; Molloy *et al.*, 2000; Kad *et al.*, 2003, 2005), as already mentioned in section 1.4. Moreover, optical trapping allows the study of myosin kinetics under load, for example as seen in (Veigel *et al.*, 2003), where the attached lifetime of smooth muscle myosin on actin has been shown to increase under high load and decrease at low load, followed by a later study by (Kad *et al.*, 2007), where the ADP release kinetics were shown to be dependent upon the direction of the applied load.

For the experiments presented in this thesis a new single molecule approach has been used, called the tightropes assay. Initially used for the direct visualisation of proteins involved in DNA repair (Kad *et al.*, 2010), this assay takes inspiration from the three beads assay but, instead of using optical tweezers to study forces, it exploits oblique

angle fluorescence microscopy (OAFM) to visualise the direct binding and release of fluorescent proteins to a suspended single actin or thin filament. However, unlike with optical trapping, an array of filaments is readily available in the experimental chamber at the start of each experiment, thereby improving the collection of data. The array of suspended filaments is obtained by flowing an actin or thin filaments solution in a flow chamber where poly-L-lysine coated silica beads have been previously adhered to the coverslip surface. Using fluorescently labelled myosin (or any other sarcomeric protein of interest), it is possible to image its interactions with the filaments in real time and with high temporal resolution, as pictured in figure 1.17. In addition, by having the filaments raised high above the coverslip surface, there will be no possible interaction between the regulatory proteins tropomyosin and troponin and the bottom of the flow chamber, at the same time granting the fluorescent proteins full 3D accessibility to each suspended filament.

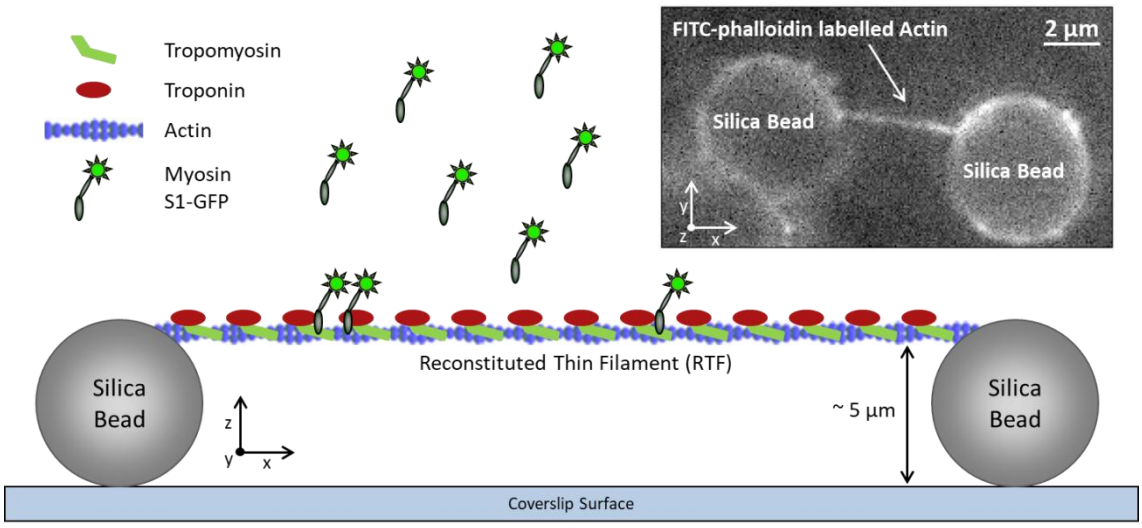

Figure 1.17: **The tightropes assay.** Diagram of the tightrope assay, where an actin/reconstituted thin filament is suspended between two silica beads, allowing the visualisation of direct interaction with fluorescently labelled sarcomeric proteins in real time.

The tightrope can be used to quantify thin filament activation and myosin cooperativity in a variety of conditions. By imaging fluorescently labelled myosin-S1 molecules binding and releasing from suspended thin filaments in a variety of conditions, (Desai *et al.*, 2015) were able to relate the fluorescence intensity to the amount of myosin bound to each filament at a specific point in time and space, as reported in the histograms in figure 1.18.

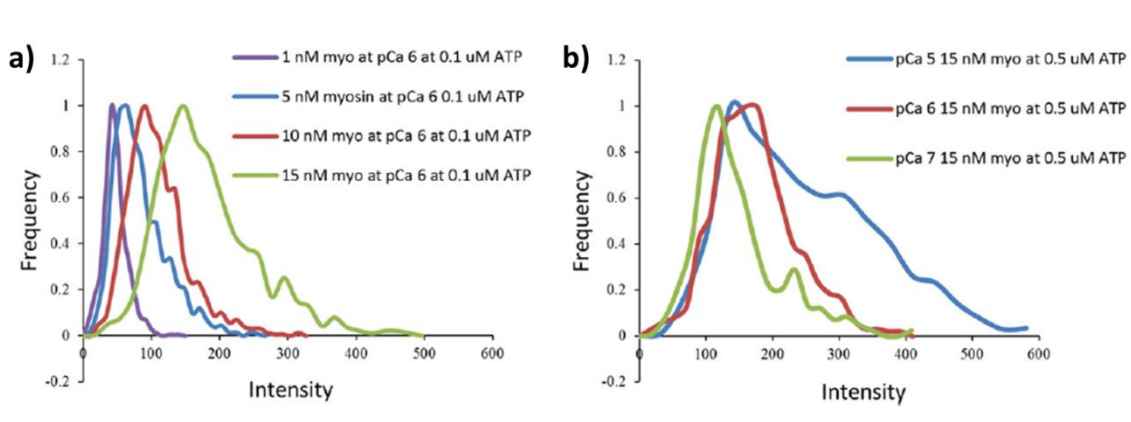

Figure 1.18: **Analysing myosin cooperativity through fluorescence intensity histograms.** Histograms of the fluorescence intensity of myosin bound to suspended thin filaments obtained with increasing a) myosin concentration and b) calcium concentration, as found in (Desai *et al.*, 2015).

By imaging at different [S1] and [Ca^{2+}] concentration they were able to establish that to an increase in myosin concentration corresponds an increase in the occupancy level of the thin filament (right shift of the main peak of the intensity histogram) while to increases in calcium concentration (figure 1.18b) corresponds not only a right shift of the intensity distribution but also its broadening, following the activation of the thin filament. By fitting these histograms to a model that takes into account the three positions of tropomyosin on actin and the duty cycle of myosin, Desai et al. directly

quantified the cooperativity of myosin, stating that at least two myosin heads are necessary for thin filament activation and measured the cooperative unit size as ~11 actin monomers (Desai *et al.*, 2015).

The tightropes assay is certainly a powerful technique but is certainly not exempt from drawbacks; for instance, the assay takes a long time to set up, with more than 40 minutes to assemble a fully functional flow chamber ready to be imaged, much longer than the 10 minutes usually necessary to set up a motility assay, to name one. Furthermore, there is some variability in the number of useful tightropes per chamber and imaging sessions can last up to two hours each, either because it is hard to find useful tightropes or because there are too many, increasing the amount of time spent imaging. Further details on this assay will be given in section 2.9 of chapter 2.

1.8 – Project objectives

As mentioned in the previous section, Hypertrophic Cardiomyopathy has been the topic of many physiological studies, aimed at understanding the role the different mutations have on heart function and on developing possible therapies. However most of these studies have been done in ensemble experiments or on mouse models and none, so far, have been able to explicitly point at a molecular cause for the disorganisation seen in the myocytes and how the mutations lead to the known physiological effects is still not clearly understood. In this thesis, we study acto-myosin interactions at the molecular level, following on the study of (Desai *et al.*, 2015). Using

the thin filament tightropes assay we first tackle the role of the E180G tropomyosin mutation and its effect on acto-myosin interactions. We show an overall equilibrium shift of the thin filament towards the closed state at the expense of both the blocked and open state and a reduction of the myosin cooperative unit size, providing an explanation for the links between our results and the decrease in relaxation efficiency witnessed in hearts affected by HCM.

Following on, we address the role of tropomyosin in regulating cross bridges: is its role entirely passive, hindering the attachment of myosin to actin, or also an active one, regulating the detachment rate of cross bridges? Through our results, we report an increase in the detachment probability of highly concentrated clusters of myosin, suggesting tropomyosin might be more actively involved in sarcomere relaxation.

Finally, we address the role of Myosin Binding Protein-C in thin-filament activation, in order to further the understanding of the second most important protein responsible for mutations leading to HCM, revealing the nature behind thin filament activation by MyBP-C and its dynamic molecular mechanism of binding to actin.

Further work will need to be done to bridge the gap between molecular and physiological studies, but we hope that the results obtained in this thesis will help shed more light into the underlying mechanism of cardiomyopathies and muscle contraction at the molecular level, hoping to bring the field a little closer in bridging molecular and physiological experiments understanding.

CHAPTER 2

EXPERIMENTAL METHODS

2.1 – Myosin purification

2.1.1 – Extraction of myosin from chicken pectoralis

Myosin was purified from chicken pectoralis. Approximately 200 g of pectoralis tissue was extracted from a freshly euthanized chicken; excess tendons and fat were removed and the tissue rinsed in 0.2 M EDTA. The tissue was then cut into pieces, passed through a meat grinder and finally stirred gently with an overhead stirrer for 12 minutes in 500 ml of Buffer A (150 mM Potassium Phosphate pH 6.7, 300 mM KCl, 20 mM EDTA, 5 mM $MgCl_2$, 5 mM DTT, 4 mM ATP), stopping the reaction by adding cold H_2O up to 2 L. The solution was then filtered through four layers of cheesecloth to remove the pulp (which was used in a later step to make acetone powder) and the myosin in solution precipitated by addition of cold H_2O up to 5 L of total volume (diluting the initial volume 10:1), which was then left to settle for 3 hours at 4°C (sample M1 in figure 2.1). The precipitate (sample M2) was then centrifuged at 10000xg for 10 minutes at 10°C in a JA-10 Beckman rotor (samples M3, corresponding to the three supernatants (out of three bottles) and M4, the pellet obtained from one of them), resuspended in Buffer B (60 mM Potassium Phosphate pH 6.7, 1 M KCl, 20 mM EDTA, 5 mM DTT) and finally dialysed overnight against 4 litres of Buffer C (25 mM

Potassium Phosphate pH 6.7, 600 mM KCl, 5 mM DTT) in 16 mm 12-14 KDa cutoff dialysis tubing at 4°C.

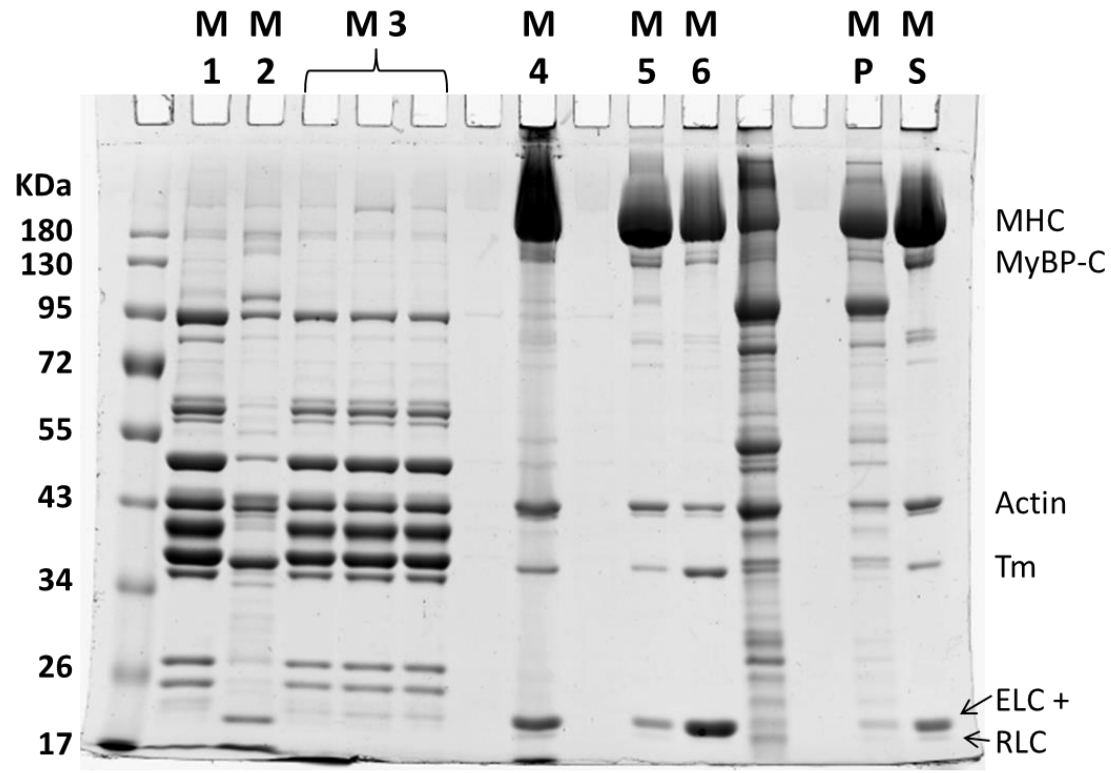

Figure 2.1: **10% SDS-PAGE gel of the myosin purification protocol.** The gel shows samples taken throughout the myosin purification protocol, where bands corresponding to the myosin heavy chain (MHC), myosin binding protein-C (MyBP-C), actin, tropomyosin (Tm) and the essential (ELC) and regulatory light chain (RLC) are seen.

The solution was then diluted 2-fold with cold H_2O and stirred gently for 30 minutes to let the actomyosin precipitate. It was then centrifuged in a JA-10 Beckman rotor as before (samples M5 and M6 being its supernatant and pellet, respectively) and the supernatant centrifuged a second time at 48000xg for 1 hour at 4°C in a JA25-50 rotor (sample M7 being its pellet). The supernatant was then subsequently diluted 8-fold with cold mqH_2O and, after 3 hours, centrifuged again for 15 minutes in a JA-10 rotor

as above. The pellet was then homogenised in 10 ml of Buffer D (50 mM Potassium Phosphate pH 6.7, 3 M KCl, 5 mM DTT) and dialysed against 2 L of Buffer E (50 mM Potassium Phosphate pH 7, 600 mM KCl, 5 mM DTT) as before. Finally, myosin was clarified by spinning it 41000xg for 2 hours at 4°C in a JA25-50 Beckman rotor (samples MP and MS for pellet and supernatant respectively) and stored at -20°C in 50% glycerol. The concentration of the final stock of myosin was determined using a Bradford Assay and its purity checked with a SDS-PAGE 10% gel, as shown in figure 2.1. Ultimately, out of an initial 200 g of tissue, about 80 ml of sample were retrieved, at a concentration of 12 mg/ml.

2.1.2 – Papain digestion of myosin head

Full-length myosin was used in the motility assay experiments while, when imaging single molecules, it was digested to obtained single myosin-S1 heads in solution. The digestion followed a modified protocol of (Margossian and Lowey, 1982), which uses Papain (from Carica Papaya, Sigma-Aldrich) to remove the S2 part of myosin heavy chain, keeping the essential and regulatory light chains. Myosin was first deglycerinated by dialysis in 200 mM ammonium acetate pH 7.2, 2 mM $MgCl_2$ and 1 mM DTT overnight at 4°C. To this solution, 70 µl of Papain solution (1 mg/ml Papain, 5 mM cysteine pH 6, 2 mM EDTA) per ml of deglycerinated myosin was added to the solution and left on a rotating mixer at room temperature for 20 minutes. This timing was chosen after doing a small scale time course digestion experiment (figure 2.2a). The reaction was stopped by the addition of Iodoacetic acid to a final concentration of 5 mM. In order to remove all the unwanted heavy chain fragments the sample underwent a few purification steps. The solution was first spun down at 8000xg in a

JA25.50 rotor for 20 min at 4°C and then dialysed in 10 mM Potassium Phosphate pH 6.5 overnight at 4°C, to let the remaining heavy chains precipitate. The solution was then centrifuged as before and the supernatant further purified using a DEAE FF (GE Healthcare) column mounted on an AKTA system, using a salt gradient from no KCl to 250 mM in 50 mM Imidazole buffer at pH 7 (figure 2.2b). The fractions were pooled together and the myosin-S1 either stored in 50% glycerol at -20°C or further used in the labelling protocol, as described in section 2.5.3.

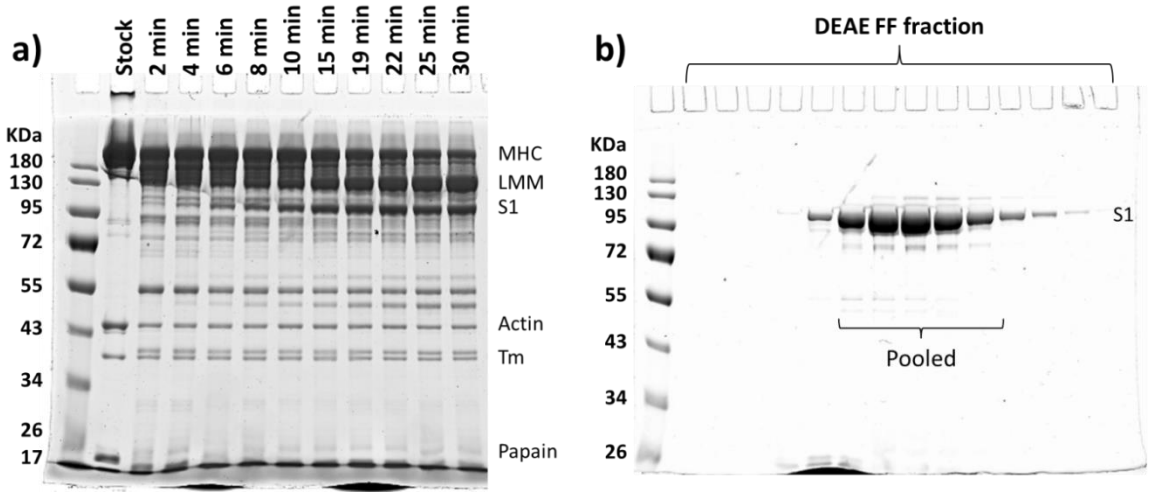

Figure 2.2: **From full-length myosin to S1, digestion and purification.** 10% SDS-PAGE gels showing a) the progression in time of the full-length myosin digestion reaction and b) of the purification of S1. In the time course, the intensity of the band corresponding to the myosin heavy chain (MHC) is seen decrease over time, while that of the bands corresponding to the light-mero-myosin (LMM) and the S1 portion are seen increase.

As mentioned above, this procedure is expected to maintain the essential and regulatory light chain bound to the S1 (Margossian and Lowey, 1982). However, the gels shown in figure 2.2 have been overrun and both light chains are not visible. Despite this, proof of their presence in the experiments will be given in section 2.5.3, in

the form of a gel of the labelled S1 used in the assay carrying both the regulatory light chain and the essential light chain.

2.2 – Acetone powder preparation and actin purification

Acetone powder is produced using a shortened version of Pardee and Spudich protocol (Pardee and Spudich, 1982). Here, the pulp and pellets obtained from the first few steps of the myosin purification were extracted with 500 ml of 50 mM $NaHCO_3$ twice, each time for 12 minutes, using an overhead stirrer. This process was then followed by a 5 minute extraction using mqH_2O and, finally, repeating the same process for three times using acetone, each time for 10 minutes. The remaining powder was left to dry overnight in a fume hood.

Actin is then purified by grinding the powder and extracting it in 20 ml of extraction buffer (2 mM Tris-Base pH 8, 0.2 mM $CaCl_2$, 1 mM DTT and 0.2 mM ATP) per gram of acetone powder. The solution is then stirred gently with an overhead stirrer for 30 minutes and centrifuged at 24000xg in a JA25.50 Beckman rotor for 20 minutes at 4°C. The extraction and centrifugation steps were repeated once more and the supernatants combined for the polymerization step, where 50 mM KCl, 2 mM $MgCl_2$ and 1 mM ATP were added to the solution, which was then left at 4°C for 2 hours. This was followed by a high salt wash (sample A1 in figure 2.3a) to loosen the bond between actin and tropomyosin, by adding KCl up to 600 mM and stirring the solution for 30 minutes at 4°C and a centrifugation at 150000xg in a type 70Ti Beckman rotor

for 1 hour at 4°C (its supernatant being sample A2). The pellet was homogenised and dialysed in extraction buffer overnight and then for 24 hours, changing dialysis buffer every 8 hours (sample A3). The solution was then clarified by spinning at 150000xg as in the previous step and the actin polymerised by adding Imidazole pH 7 up to 10mM and $MgCl_2$ to 1 mM (sample A4 corresponding to the supernatant). Finally, actin was dialysed and stored in 4 mM Imidazole pH 7, 100 mM KCl, 2 mM $MgCl_2$, 1 mM DTT and 0.5 mM ATP.

Actin concentration was determined via Bradford Assay and double checked comparing different dilutions of actin to different dilutions of an equal mass of BSA, as seen in the 10% SDS-PAGE gel in figure 2.3b. The lack of additional bands in the actin lanes indicates the success of this purification procedure.

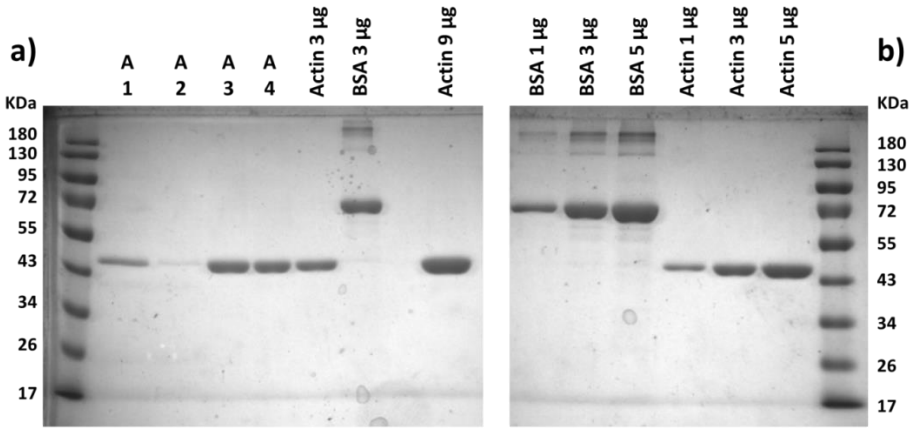

Figure 2.3: **10% SDS-PAGE gels of the actin purification protocol.** SDS-PAGE gels showing a) four samples taken throughout the purification steps, along with a comparison between the actin stock and BSA and finally an overloaded sample (last lane) to check for contaminants; b) the result of the concentration test using a standard samples of BSA. No extra protein bands are visible in both gels, highlighting the purity of the actin used for the experiments.

2.3 – Obtaining Tropomyosin and its E180G mutant

2.3.1 – Molecular biology of the plasmids

The plasmids for rabbit α-Tropomyosin was kindly donated by professor Michael A. Geeves of the University of Kent. The gene also included a N-terminal modification, consisting of the addition of an Alanine (Ala) and Serine (Ser) to mimic acetylation (Monteiro *et al.*, 1994).

The plasmid was mutated to human by substituting the Lysine in position 220 into an Arginine (K220R), according to the amino acid sequences found in the Uniprot database (P58772 and P09493 for rabbit and human respectively), following the QuickChange Site-Directed Mutagenesis protocol (Agilent Technologies, https://www.agilent.com/cs/library/usermanuals/Public/200523.pdf). This procedure consists of copying the original plasmid using polymerase chain reaction (PCR) with primers containing the desired mutation. Once copied, the mutated plasmid will not be methylated, unlike the original DNA. The solution is then digested with DpnI, removing any trace of the original methylated plasmid, and the gene carrying the correct mutation can then be transformed into *E. coli* for the expression and purification procedure. This procedure was then repeated to create the human α-Tropomyosin E180G mutation used in the experiments.

2.3.2 – Bacterial expression and purification

The plasmid carrying the gene for the human tropomyosin or its E180G mutation was transformed in *E. coli* BL21(DE3) strain. Cells were grown in LB at 37°C until their OD_{600} reached a value ranging between 0.4 and 0.6, after which they were induced with IPTG

to a final concentration of 400 µM for 3 hours. After inductions, the cells were spun down in a JA10 Beckman rotor at 4400xg and 4°C for 10 minutes and the pellets stored at -20°C overnight. The proteins were then purified according to (Kalyva *et al.*, 2012). The cell pellets were thawed and resuspended in Buffer A (5 mM Potassium Phosphate pH 7, 100 mM NaCl, 5 mM $MgCl_2$) with the addition of 1 mM PMSF, and sonicated on ice for 5 cycles of 30 seconds pulses followed by 60 seconds of waiting, to let the cells cool down. The cells were then boiled in a water bath for 10 minutes at 80°C, left on ice for 30 minutes and centrifuged at 17300xg in a JA25.50 rotor for 30 minutes at 4°C. The pH of the supernatant was then dropped to 4.8 to let tropomyosin fall out of solution (its isoelectric point being about 4.7) and subsequently centrifuged at 3000xg in a JA25.50 rotor for 10 minutes at 4°C. The pellet was then resuspended in Buffer A, its pH adjusted to 7 and then further purified using two HiTrap Q HP columns (GE Healtcare) combined serially on an AKTA system. This was set to do a salt gradient, going from 100 mM NaCl of buffer A to 1 M of buffer B (figure 2.4a). The solution was then further cycled through another series of pH drop-column-pH drop (figure 2.4b) and resuspended in Buffer C (20 mM Tris pH 7, 100 mM KCl, 5 mM $MgCl_2$). Finally, the protein was spun down at 400000xg in a TLA 110 Beckman rotor for 20 minutes at 4°C, flash frozen in liquid nitrogen and stored at -80°C. The final stock concentration was later calculated using the Bradford Assay and further checked via comparison with BSA standards on a SDS-PAGE gel (figure 2.4c).

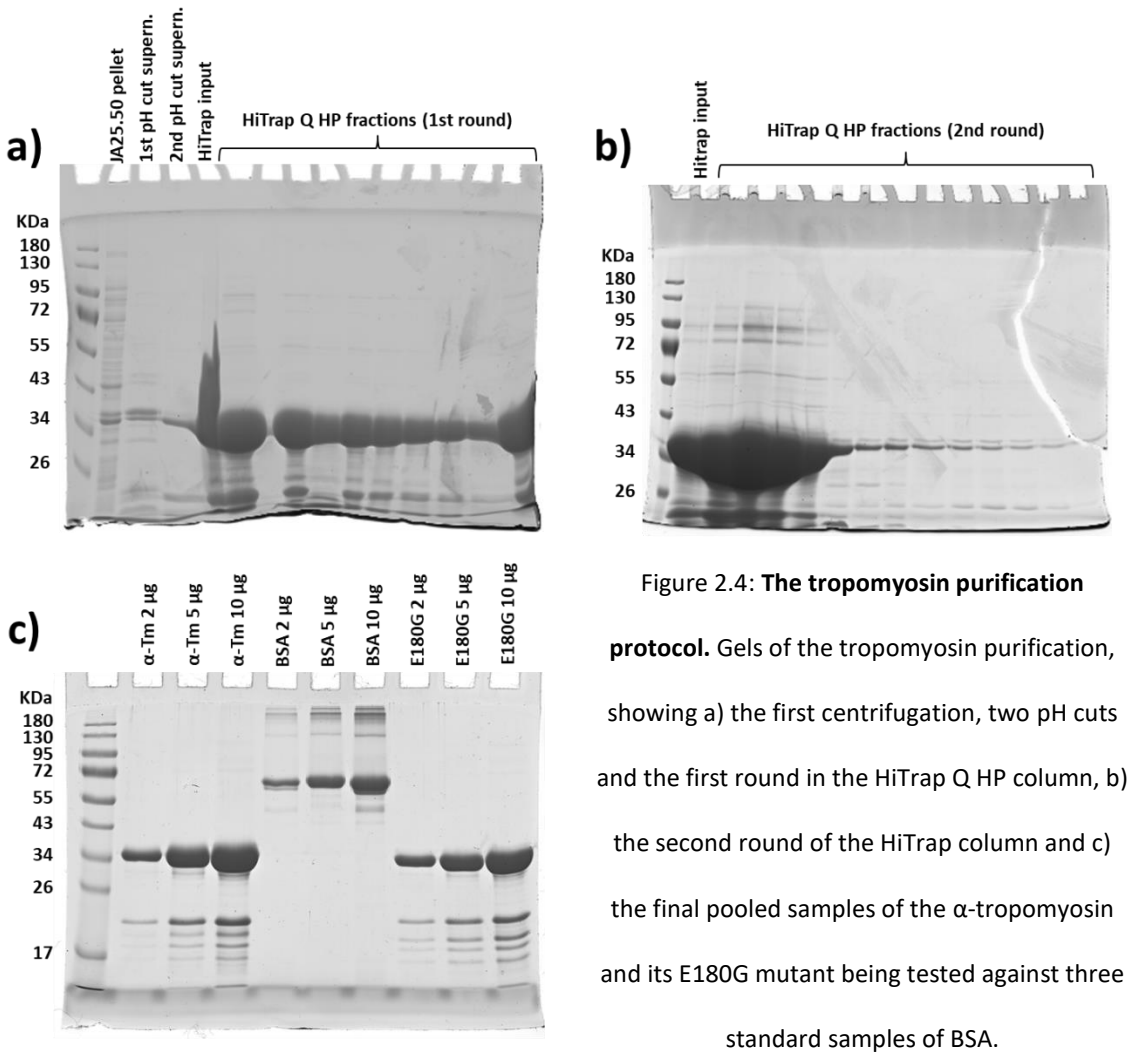

Figure 2.4: **The tropomyosin purification protocol.** Gels of the tropomyosin purification, showing a) the first centrifugation, two pH cuts and the first round in the HiTrap Q HP column, b) the second round of the HiTrap column and c) the final pooled samples of the α-tropomyosin and its E180G mutant being tested against three standard samples of BSA.

2.4 – Expression and purification of the troponin complex

The plasmids necessary to express the human cardiac troponin complex (TnI, TnC and TnT, P19429, P45379 and P63316 in the Uniprot database, respectively) were kindly donated by professor Michael A. Geeves of the University of Kent. Each component of the complex was bacterially expressed separately (as in section 2.3.2) and later purified according to (Al-Sarayreh, 2011). The cells pellets were each resuspended in 6 M Urea, 25 mM Tris pH 7, 200 mM NaCl, 1 mM EDTA, 20% sucrose and 0.1% Triton

X100 and sonicated as for the tropomyosin and finally dialysed in 2 M Urea, 10 mM Imidazole pH 7, 1 M KCl and 1 mM DTT for 5 hours. The next two steps were aimed at reducing the urea and salt concentration, allowing the proteins to refold. Hence, the solution was dialysed in 10 mM Imidazole pH 7, 0.75 M KCl, 1 mM DTT overnight and finally in 10 mM Imidazole pH 7, 0.5 M KCl, 1 mM DTT for 5 hours. The sample was then centrifuged at 17000xg in a JA25.50 for 10 minutes at 4°C and the protein in the supernatant precipitated adding 30% ammonium sulphate $(NH_4)_2SO_4$ to the solution and gently stirred at 4°C for up to one hour. It was then centrifuged at 8000xg in a JLA16.25 rotor for 30 minutes at 4°C and precipitated again bringing the ammonium sulphate concentration to 50%. After leaving it for 30 minutes on ice, the solution was centrifuged at 17000xg for 10 minutes at 4°C and its pellet resuspended in 10 mM Imidazole pH 7, 200 mM NaCl, 100 µM $CaCl_2$, 1 mM DTT and dialysed in the same buffer to remove the $(NH_4)_2SO_4$. After dialysis, the sample was spin concentrated in a 10 KDa MWCO column (Amicon Ultra) at 2360xg for 45 minutes and further purified using a Sephacryl S-300 column mounted on an AKTA system. Figure 2.5 shows a 10% SDS-PAGE gel of the fractions of the gel filtration column. The protein was then spin concentrated for the final time and 3% sucrose was added to the solution, before flash-freezing and storing it at -80°C for further use.

The troponin complex appeared difficult to purify efficiently and several bands are seen in figure 2.5b. However, the unwanted bands might not have a direct impact on the experiments, since the initial steps of the purification procedure involve the unfolding of the proteins in solution and refolding is expected only for the troponin complex. Therefore, there is a higher chance that the contaminants are not folded properly and their impact on the experiments is likely to be little to none. Evidences

that this is the case are the experiments reported in the results chapters, where in all instances the properties of thin filaments are respected and consistent with the literature, as stated in each specific case.

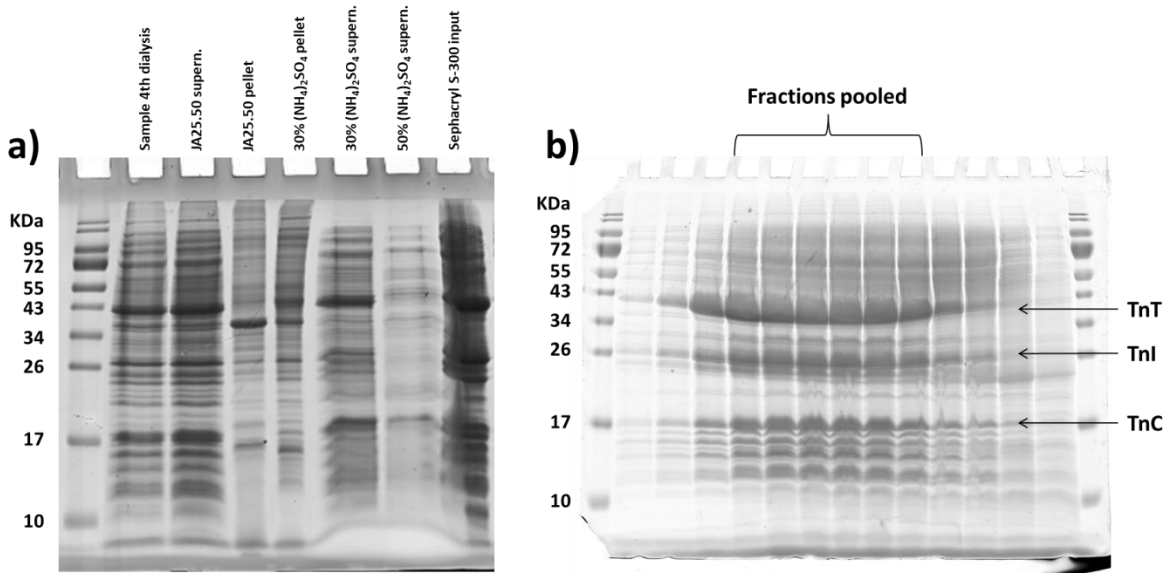

Figure 2.5: **Purification of the troponin complex.** 15% SDS-PAGE gels of a) the initial steps of the troponin purification and b) of the fractions eluted from the Sephacryl S-300 gel filtration column, highlighting the fractions pooled for the final stock. Note how the single components of the complex (TnT, TnI and TnC) are eluted at the same time.

2.5 – Fluorescent labelling of S1 with GFP

2.5.1 – Switching the 6xHis-tag from the N-terminal to the C-terminal end of the RLC-GFP

For the single molecules experiments in this thesis, myosin needs to be tagged with a fluorescent probe. To this end, our group had previously designed a regulatory light chain (expressed in *E.coli* from chicken gizzard, as section 2.3.2) tagged with an eGFP

on its C-terminus and a 6xHis-tag on its N-terminus, to allow for an easy purification. However, once expressed in E.coli and extracted from the cells, the S1 tagged with 6xHis-RLC-GFP was not pure to a good standard, despite repetitive attempts, possibly caused by the His-tag being buried within the RLC. Starting from this hypothesis, we redesigned the plasmid construct and switched the His-tag to the C-terminus of the eGFP.

The original RLC-GFP gene with a 6xHis-tag at the N-terminus was found in a pQE16b vector (sequence containing the 6xHis-RLC-GFP in the Appendix A.1). In order to switch the 6xHis-tag to the C-terminus of the GFP, we decided to extract the RLC-GFP gene from the pQE16b vector and insert it into a pET21a vector, which contains an out-of-frame 6xHis-tag at the end of the multiple cloning site (figure 2.6 gives a summary of the process). To do so, we first extracted the RLC-GFP gene from the original vector using PCR and the following forward and reverse primers

Forward primer: 5'-TCTTACATATGAGCAGCAAACGC-3'

Reverse Primer: 5'-TAGCAAAGCTTGTACAGCTCG-3'

while adding the NdeI and HindIII restriction sites, chosen to bring the 6xHis-tag in the pET21a in frame. The extracted RLC-GFP gene (insert) and the receiving vector pET21a were then digested using the NdeI and HindIII restriction enzymes and subsequently ligated. Finally, the plasmid was sent for sequencing, to check whether the 6xHis-tag switch had been successful (final sequence in the Appendix A.2).

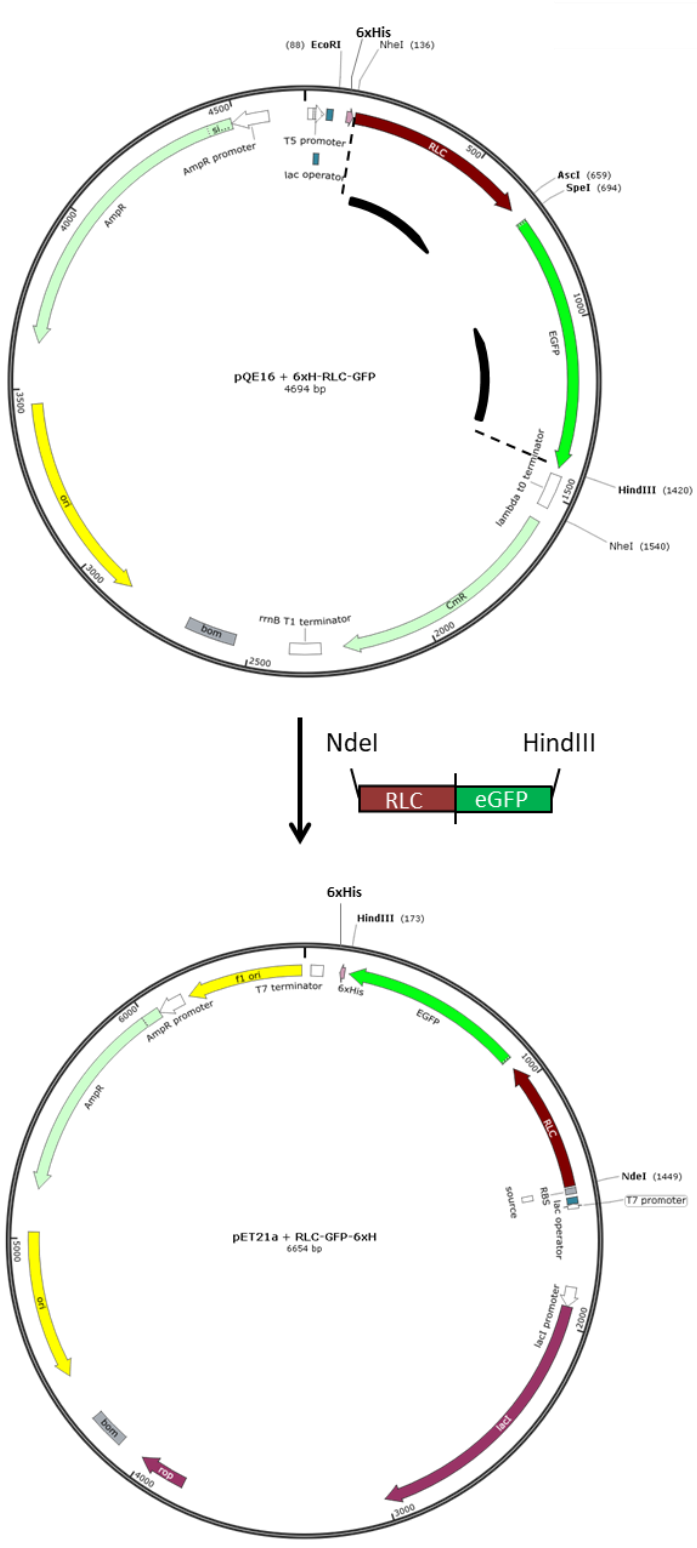

Figure 2.6: **Switching the 6xHis-tag.** Schematic of the process to switch the 6xHis-tag from the N- to the C-terminus of the eGFP, highlighting the primers' position (black arrows) on the initial vector (pQE16b), the insert and the final plasmid (pET21a backbone).

2.5.2 – Expression and purification of the RLC-GFP-6xHis

The plasmid for the RLC-GFP-6xHis was transformed in *E. coli* BL21(DE3). Cells were induced with 1 mM IPTG for 3 hours for protein expression and sonicated as detailed in section 2.3.2, with the exception of Buffer A, which consisted in 50 mM Tris pH 7.5 and 200 mM NaCl. After sonication, the cell lysate was centrifuged in a JA25.50 rotor at 24000xg for 30 minutes at 4°C, in a TLA 110 at 230000xg for 45 minutes at 4°C and finally dialysed in 50 mM NaH_2PO_4, 300 mM NaCl, 20 mM Imidazole, pH 8 for 4 hours (steps shown in the 10% SDS-PAGE gel in figure 2.7a). The solution was then further purified using a custom Ni-NTA column with a bed volume of 1.9 ml. After loading the sample, the column was washed with 3 column volumes (CV) of buffer 50 mM NaH_2PO_4, 300 mM NaCl, 20 mM Imidazole pH 8, 3 CV of same buffer with 100 mM Imidazole to elute the protein and finally with 3 CV of same buffer with 250 mM Imidazole to clean the column from any remaining contaminants. Figure 2.7b shows a 10% SDS-PAGE gel of a typical purification, where the RLC-GFP-6xHis (along with some other undetermined bands) can be found in the second elution aliquot with an expected molecular weight of 49.2kDa. However the relative amplitude of the RLC-GFP band versus the contaminants one is much higher than the contaminants and, considering that this is only an intermediate step, the purification process can be considered successful. The RLC-GFP-6xHis was finally stored in 50% glycerol at -20°C for further use in the S1 labelling protocol.

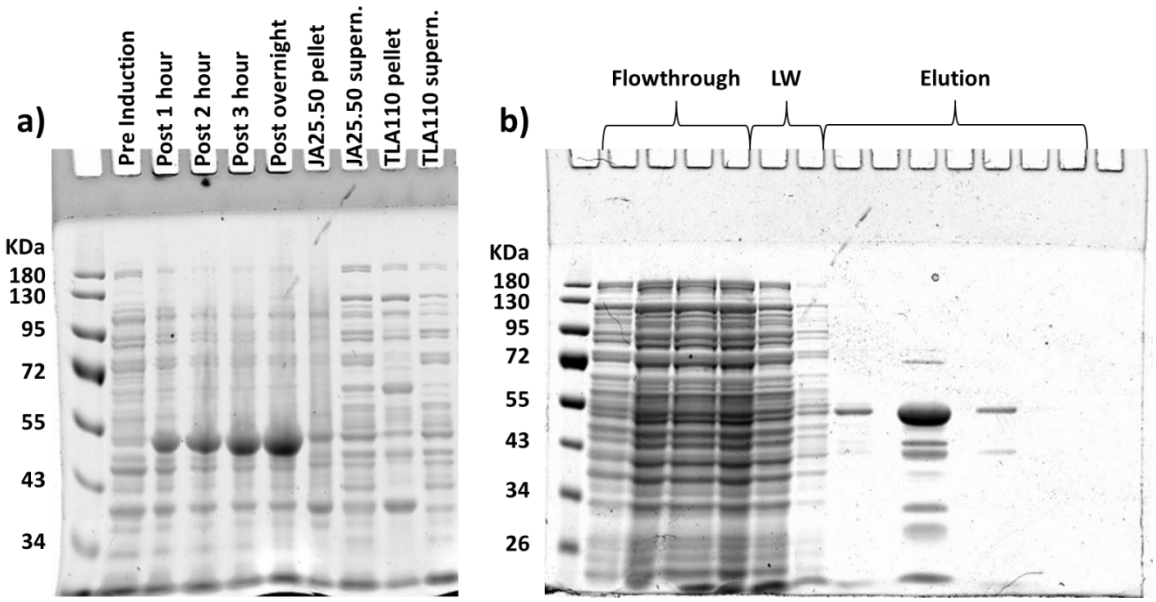

Figure 2.7: **Purification of the RLC-GFP-6xHis.** 10% SDS-PAGE gels of the RLC-GFP-6xHis a) induction (pre and post, up to overnight) and centrifuge purification steps and b) further purification using the NiNTA column, showing the lanes relative to the flowthrough of the sample in the column, the low Imidazole (20 mM) washes (LW) and the elution samples. The large band in the second elution lane is the RLC-GFP-6xHis, with an expected molecular weight of 49.2kDa.

2.5.3 – Labelling of S1 with RLC-GFP-6xHis and final purification

The labelling of S1 with the recombinant RLC-GFP-6xHis is carried out through an exchange reaction. First, both the S1 and the RLC-GFP-6xHis aliquots are separately buffer exchanged using a spin concentrator (30000 MWCO, Amicon Ultra) into exchange buffer (50 mM Potassium Phosphate pH 7, 600 mM KCl, 10 mM EDTA, 2 mM EGTA, 5 mM DTT and 2 mM ATP). After determining their concentration in a spectrophotometer, knowing the extinction coefficient of S1 at 280 nm (ε_{280}=0.83 ml·mg^{-1}cm^{-1} (Barua *et al.*, 2012)) and of GFP at 488 nm (ε_{488}=56000 M^{-1}cm^{-1} (Kaishima *et al.*, 2016)), several exchange reactions were set up independently, with S1:RLC-GFP molar ratios varying between 1:3 and 1:8, depending on the amount of sample

available. The reactions were then individually stopped with the addition of 15 mM $MgCl_2$ and pooled together.

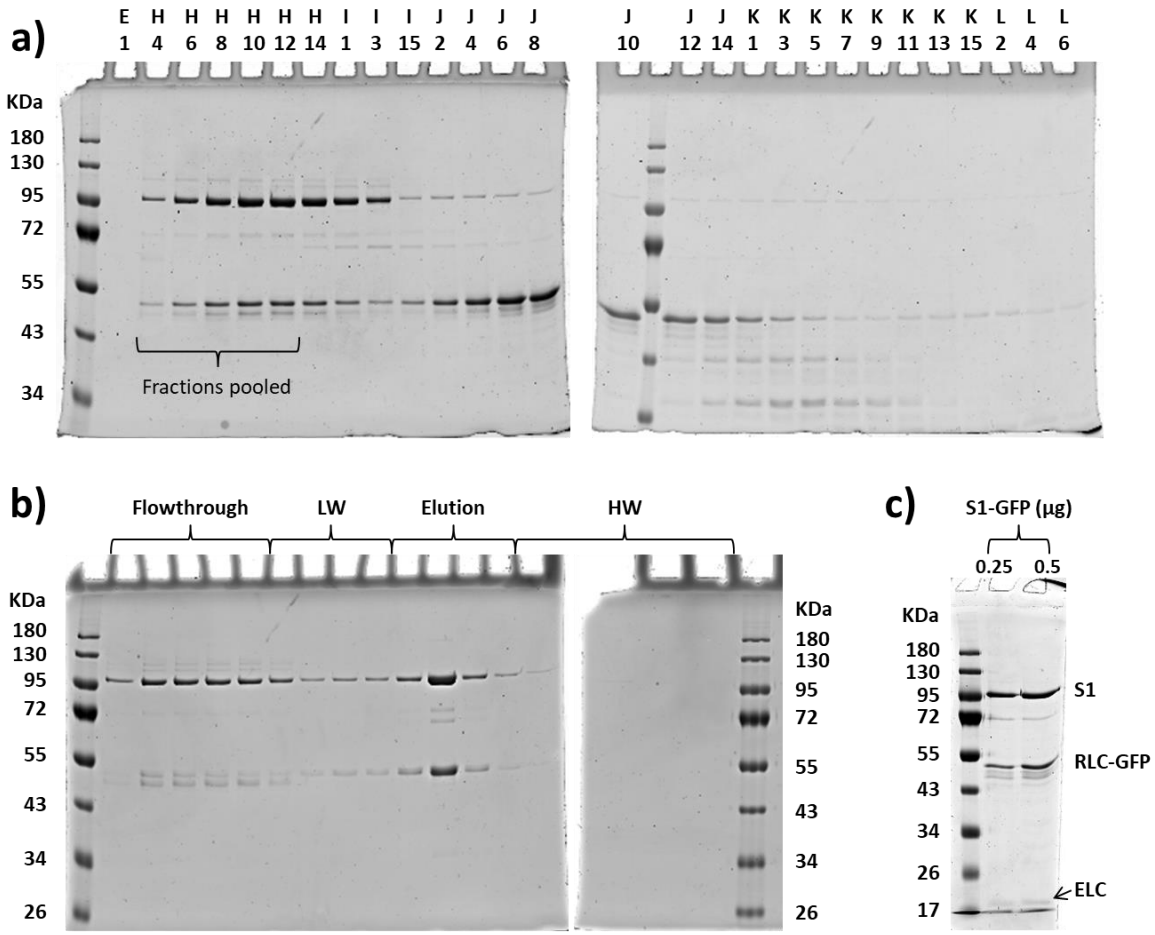

Figure 2.8: **Purification of the S1-GFP.** 10% SDS-PAGE gels of the a) Sephacryl S-200 gel filtration column fractions, b) of the NiNTA column and c) of purified S1-GFP with the essential light chain visible. Fractions H4 to H13 were pooled and moved to the next step, the NiNTA column, from which only the first three lanes of the elution were subsequently pooled and used in the experiments. LW refers to the low imidazole (20 mM) wash, while HW to the high imidazole (250 mM) wash. Sample eluted at 100 mM Imidazole, same as in the RLC-GFP-6xHis purification.

The next step consisted in injecting the sample in a Sephacryl S-200 gel filtration column (GE Healtcare), to separate the successfully labelled S1-GFP from the

unexchanged-S1 and unexchanged-RLC-GFP-6xHis, along with the other contaminants. The column was run using a low imidazole wash buffer (50 mM NaH_2PO_4, 300 mM NaCl, 20 mM Imidazole pH 8), so that the sample would be already in the right buffer for the next purification step, consisting in a final NiNTA column (performed as in section 2.5.2). This last step is necessary to make sure that there is no unlabelled S1 contamination in the final sample, which would void any experiment on myosin cooperativity. Figures 2.8a and 2.8b show the resulting 10% SDS-PAGE gels of these last two steps. Out of the elution fraction of the Ni-NTA column, only the first three were pooled together and stored in 50% glycerol and 3% sucrose at -20°C for future use. Finally, figure 2.8c shows a 10% SDS-PAGE gel of purified S1-GFP where the essential light chain is visible, proving that the papain digestion and the entire purification result in a labelled myosin-S1 with both light chains intact, and therefore fully functional.

2.6 – Myosin Binding Protein-C (MyBP-C) N-terminal fragments purification and labelling

MyBP-C N-terminal fragments C0C3, C0C1 and C0C1f (C0C1 with the addition of 17 amino acids from the following M-domain), both labelled and unlabelled used in this thesis are a kind donation of the David Warshaw and Michael Previs laboratories at the University of Vermont, Burlington, USA. The proteins were expressed in *E. coli* and purified according to (Colson *et al.*, 2016) in their laboratory and have not been altered

during the work for this thesis. All samples were shipped to our laboratory on dry ice and stored at -80°C until needed for the experiments.

In particular, the labelled fragments were all tagged with a Cy3 dye, using the same protocol as in (Colson *et al.*, 2016), on cysteine-248 on subdomain C1. Labelling efficiencies were 33% for Cy3-C0C3 and Cy3-C0C1f and 43% Cy3-C0C1. Control experiments looking at the effect of the fluorescent tag on the fragment's function were performed by Samantha Previs of the Warshaw laboratory at the University of Vermont, showing no significant differences between unlabelled and labelled samples.

2.7 – Reconstitution and labelling of actin thin filaments

Actin filaments where reconstituted by mixing actin with regulatory proteins tropomyosin and troponin with a molar ratio Actin:Tm:Tn of 2:0.5:0.25 in reconstitution buffer (4 mM Imidazole pH 7, 2 mM $MgCl_2$, 0.5 mM ATP and 1 mM DTT (Homsher *et al.*, 1996)). Following an overnight incubation, filaments were labelled with an equimolar amount of FITC-phallodin (Sigma-Aldrich), AlexaFluor633-phallodin (Invitrogen), depending on the need of the experiment.

2.8 – The *in-vitro* motility assay

2.8.1 – Experimental procedure

The motility assay is a simple but useful assay that can be used to test the activity of a freshly prepared myosin or actin stock, as well as whether the reconstitution of the actin thin filaments has been successful. It consists in laying myosin on the surface of a coverslip, followed by a solution containing the filaments; depending on the concentration of ATP and Ca^{2+} in the assay, the myosin heads will pull the actin filaments around, of which speed and percent motile can be recorded and studied.

The motility assay is carried out in a flow cell, where a glass coverslip is attached to a glass slide by two strips of bi-adhesive tape, forming a chamber of 30 to 40 µl in volume. The glass coverslip is previously coated with nitrocellulose (Sterile Collodion 2% in Amyl Acetate, Thomas Scientific), to make the surface sticky to the myosin tails (Umemoto and Sellers, 1990). To do this, the coverslips are put in a small container filled with water. Upon the addition of 50 µl of nitrocellulose solution, a thin layer forms on top of the water; removing the water from a purge hole on the bottom of the container lowers the water level, until the nitrocellulose layer is in direct contact with the coverslip. Finally, the container is placed in an incubator at 37°C for 30 minutes, to speed up the evaporation of any residual water left, at the end of which the coverslips are ready to be used in assembling the flow cell.

Before adding the myosin in the flow cell, it is spun down at 220000xg at 4°C in the presence of actin (0.3 mg/ml of myosin with 0.05 mg/ml of actin) and 1 mM ATP, to pellet any myosin incapable of releasing from actin (so called dead-heads). Finally, 2x

30 µl washes of different solutions are incubated in the flow cell, following this specific order:

1. 0.1-0.2 mg/ml myosin, 1 min/wash
2. 1 mg/ml BSA, 1 min/wash, to fill the gaps left by myosin on the coverslip
3. 1 µM unlabelled actin, 1 min/wash, vortexed for 20 seconds to break up the filaments into smaller ones
4. 1 µM ATP, no incubation time
5. Actin buffer, no incubation time; these washes, along with steps 3 and 4, are used to block any dead-head myosin by letting unlabelled actin bind to them without releasing. Any working myosin head will be freed of the actin in step 4
6. Labelled actin, 30 s/wash
7. Motility buffer, 3 washes, no incubation time

All solutions from washes 2 to 6 are made in actin buffer (25 mM Imidazole pH 7.4, 25 mM KCl, 4 mM $MgCl_2$ 1 mM EGTA and 10 mM DTT), while the myosin in wash 1 is in myosin buffer (same as actin buffer but with 300 mM KCl). The motility buffer is actin buffer with the addition of 0.5% Methylcellulose, a 1/50 dilution of oxygen scavenger mix (175 mg of Glucose, 0.98 mg of Glucose Oxidase and 1.35 mg of Catalase dissolved in 600 µl of water) and the necessary amount of ATP and Ca^{2+} required by the experiment. When working with reconstituted thin filaments the motility buffer also contained an excess of regulatory proteins tropomyosin and troponin, 100 nM each.

Videos of moving filaments were collected at 10 fps for 30 seconds or longer, using 2 mW of the 488 nm laser when using FITC-labelled filaments or, when using AF633-labelled filaments, 1 mW of the 561 nm laser or 5 mW of the 637 nm laser.

2.8.2 – Data analysis

The videos collected of moving filaments were analysed by manually collecting the instantaneous velocities of filaments using the MtrackJ plugin in ImageJ (Meijering *et al.*, 2012), of which an example is given in figure 2.9a.

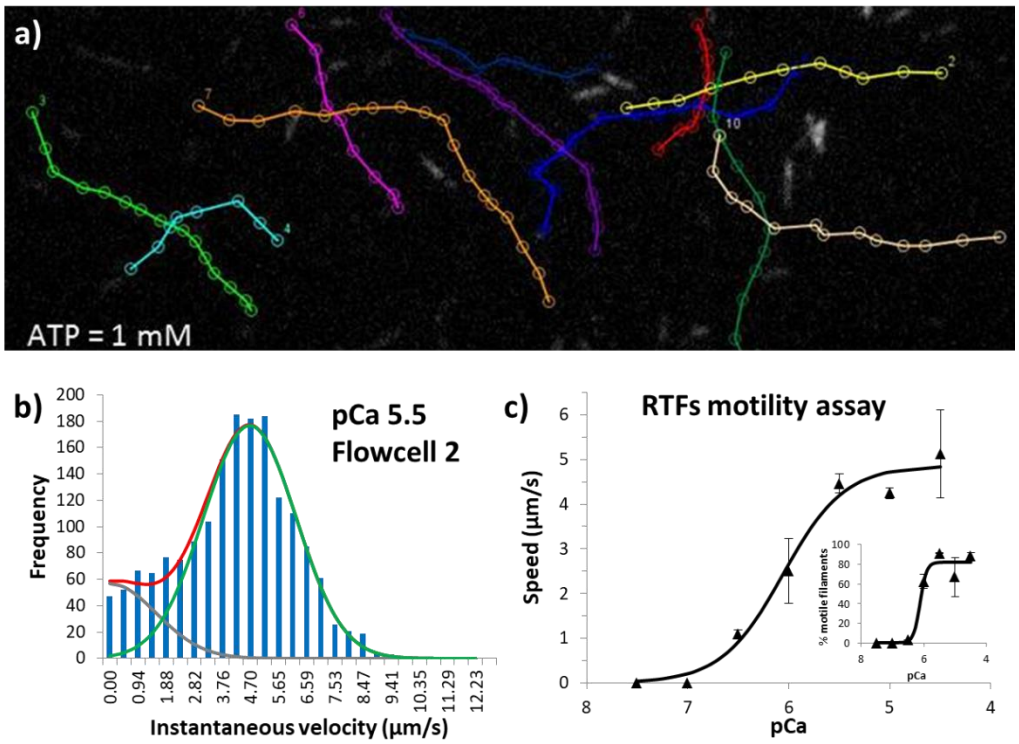

Figure 2.9: **Analysing the motility assay data.** a) Last frame of a video of the MtrackJ analysis tool for ImageJ, showing the tracked filaments (unregulated actin at 1 mM [ATP]); b) histogram of the instantaneous velocities of reconstituted thin filaments (RTFs) obtained for the second flow cell at pCa 5.5 and 1 mM ATP. Two Gaussian distributions are needed to correct for the speed obtained for stationary filaments. c) Speed-pCa relationship of RTFs obtained with the in-vitro motility assay, along with the % motile filaments-pCa relationship in the inset.

Two or more movies were acquired per flow cell in all the experiments and, after tracking the filaments, all the instantaneous velocities for each flow cell were plotted as histogram, prior to fitting to up to two Gaussian distributions (figure 2.9b), according to

$$fit(x) = \sum_{i=1}^{2} \left(A_i e^{-\frac{(x_i-\mu_i)^2}{2\sigma_i^2}} \right)$$

where A is the amplitude of the Gaussian distribution, μ its mean (i.e. the average thin filament speed within a flow cell) and σ its standard deviation. For the fitting, achieved using the Solver addin for Microsoft Excel, one of the two Gaussian distribution was forced to have a mean speed of zero μm/s, to account for stationary filaments; the mean of the second distribution is then used for data analysis, with each flow chamber being considered as an experimental replicate. Finally, plotting the speed versus the pCa, the graph in figure 2.9c is obtained, highlighting the sigmoidal relationship typical of a cooperative process. The fraction of motile filaments was collected by a simple count of the total filaments in the field of view minus the filaments that have not moved for the entirety of the movie period (between 30 seconds and 1 minute); plotting this values versus the pCa results in the graph in the inset of figure 2.9c. These data are fitted to the Hill equation, as described in details in section 3.2.1.

2.9 – The thin filament tightropes assay

2.9.1 – Experimental procedure

The thin filament tightrope assay consists of suspending fully reconstituted thin filaments (RTF) between poly-L-lysine coated silica beads, and image the association to and dissociation from actin of S1-GFP. The assay is conducted in a microfluidic flow cell, as detailed in (Springall *et al.*, 2016) and shown in figure 2.10a.

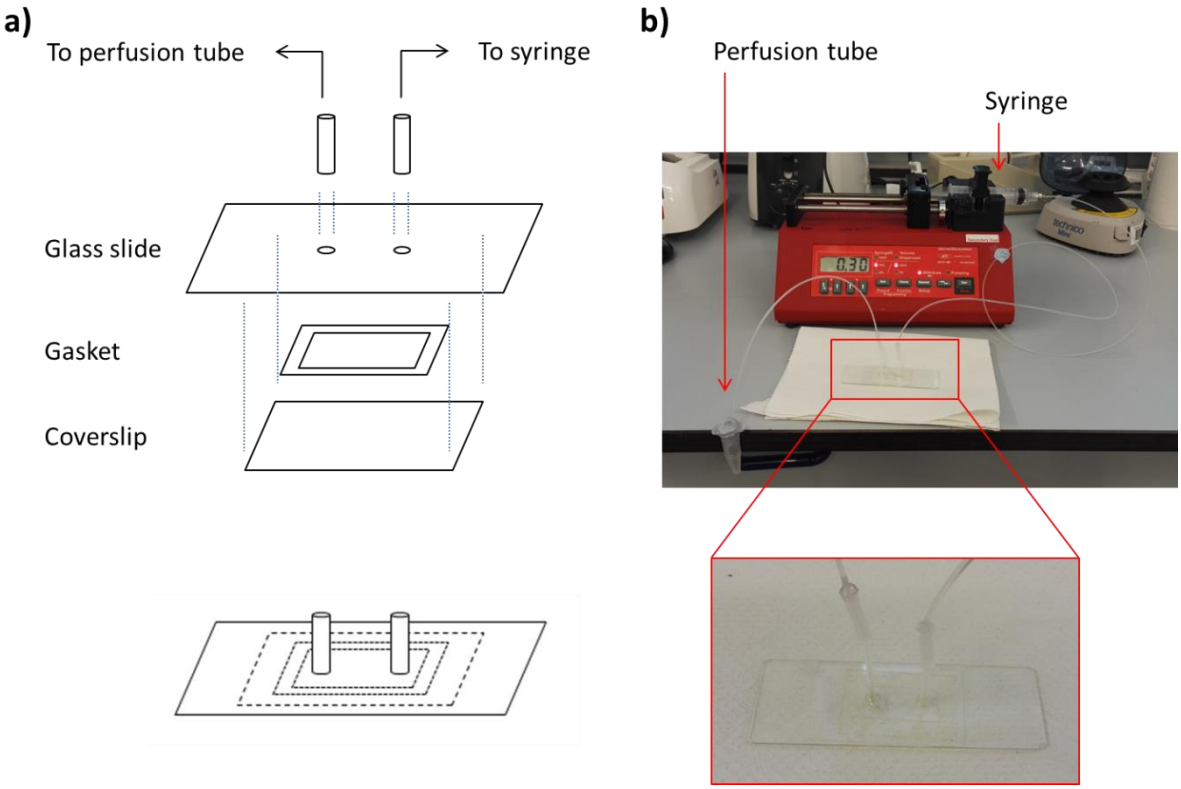

Figure 2.10: **The tightrope assay set-up.** a) schematic of the assembly of a flow cell and b) photo of flow cell connected to the perfusion tube and syringe pump.

The flow cell is constructed using a microscope coverslip (Agar Scientific, sides of 24 x 40 mm and thickness of 0.16 - 0.19 mm), a glass slide (ThermoScientific), a double sided sticky gasket as spacer (15 mm x 10 mm x 0.18 mm) and two small tubes cut to

be approximately 2 cm long as inlet and outlet. The glass slide is drilled so that it can accommodate the two tubes, resulting in a chamber with a final volume of about 20 µl, in which the experiment is conducted. Both the coverslip and the glass slide are previously treated before the assembly first by bathing in 2% Silane ((3-Aminopropyl)-triethoxysilane, Sigma-Aldrich) in Acetone, then with Methoxypolyethylene glycol 5,000 in Proprionic Acid (Sigma-Aldrich) to help prevent proteins sticking to the inside walls of the flow cell. Once assembled, the chamber is washed with 100 µl of water. The beads are then adhered to the coverslip surface by washing the flow cell with a 1/25 dilution of 5 µm silica beads (MicroSil Microspheres, Whitehouse Scientific) in water. The density of beads is critical for the formation of tightropes, since too high a density will create beads aggregates and prevent the suspension of filaments, while a too low density will create filaments suspended only on one end and thus useless, as will be explained in section 2.9.3.

Often, the density is not constant throughout the whole chamber and need to be assessed before the filaments are introduced. This is done using a basic light contrast microscope every time a flow chamber is built. A typical chamber will have a larger amount of beads near the inlet and/or outlet and a very low amount near the borders of the gasket (figure 2.11a and b respectively), caused by the geometry of the chamber itself and fluid dynamics, and an optimal density around its centre (figure 2.11c). Up to two washes (one per tube) are usually required to reach the optimal density.

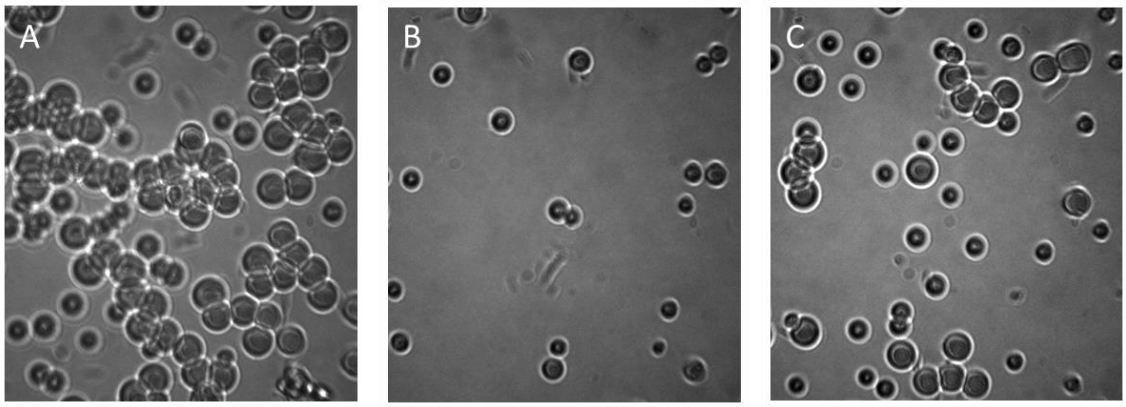

Figure 2.11: **Determining the beads density.** Images of the surface of a flow chamber showing different bead density, with a) being too high, b) too low and c) optimal for the formation of suspended filaments. Taken from (Springall *et al.*, 2016)

Once the bead density has been determined, the flow cell is washed with the appropriate buffer for the experiment (actin or calcium buffer, as above) and then connected to a bi-directional syringe pump at the outlet and a perfusion tube at the inlet, as shown in figure 2.10b, making the whole assembly air tight. A solution of 500 nM actin filaments or RTFs (in actin or calcium buffer respectively, with the addition of 100 nM of Tm/Tn when using RTFs) is then added to the flow chamber through the perfusion tube and pumped back and forth through the chamber for 30 to 90 minutes, allowing the filaments to suspend between the silica beads, forming tightropes. Finally, a solution containing the fluorescent proteins is flowed within the chamber and imaged using oblique angle fluorescent microscopy.

2.9.2 – The Oblique Angle Fluorescence microscope (OAFM)

Oblique Angle Fluorescence microscopy, also called highly inclined and laminated optical sheet (HILO) or variable angle epifluorescence microscopy (Konopka and

Bednarek, 2008; Tokunaga *et al.*, 2008; Kad *et al.*, 2010) stems as a trade-off between total internal reflection fluorescence microscopy (TIRF) and epi-illumination microscopy. It is used to image samples in solution with a better signal to noise ratio and resolution along the z-axis than epi-illumination microscopy, while using a similar principle of illuminating the sample as in TIRF. In OAFM, the laser is focused at the back focal plane of a high numerical aperture objective as in TIRF, with the difference that the angle of incidence is not critical and total internal reflection does not occur, allowing the collimated beam to exit from the objective at a steep angle. This allows fluorescent imaging deep into solution while removing part of the background fluorescence, increasing the signal to noise ratio. Figure 2.12 shows a schematic of the OAFM optical setup used for the experiments in this thesis.

In brief, the excitation path consists of four lasers, a 20 mW 488 nm DPSS (JDSU), a 561 nm (Obis) and a 633 nm laser diode (Vortran Stradus), a dichroic and several lenses to focus the laser beam off-centre at the back focal plane of a 100x 1.45 NA objective (Olympus). The fluorescence light emitted by the excited molecules in the sample is collected by the objective lens and reflected by a dichroic filter towards the Optosplit III (Cairn Research), which sorts the fluorescent light based on its wavelength, creating three separate images on a Hamamatsu Orca Flash 4.0 V2 camera.

Combining OAFM with the tightrope assay allows us to conduct multi-colour experiments and watch myosin binding to fully reconstituted thin filaments in real time and at a high temporal resolution. Furthermore, by using beads to elevate the thin filaments into solution, we can ensure that myosin has full 3D accessibility to actin and that the motion of regulatory proteins tropomyosin and troponin is not hindered by spurious interactions with the coverslip surface.

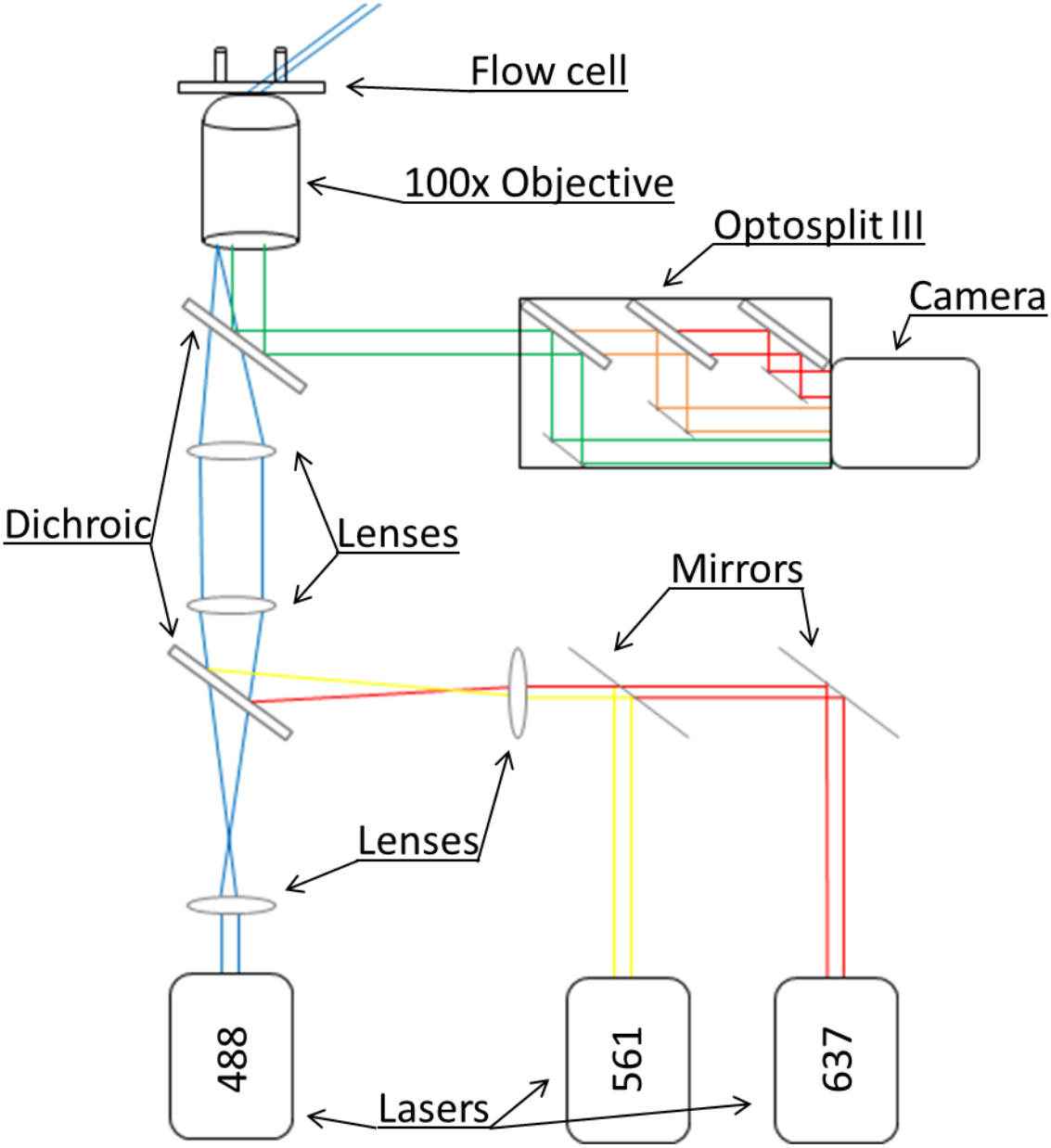

Figure 2.12: **The Oblique Angle Fluorescence Microscope set-up.** Three laser beams (488 nm, 561 nm and 633 nm) are expanded and focused off-centre at the back focal plane of a 100x objective (1.45 NA), exciting the sample at an oblique angle. The fluorescent light is then collected through the same objective and sent to the Optosplit III, where it's split into three components and collected by a camera.

2.9.3 – Imaging thin filament tightropes

Once the flow chamber is assembled and placed on the OAF microscope, the first step of every experiment consists in looking for good tightropes to image, taking care to avoid bundles and other filaments that are not suitable for data collection. The search must be as strict as possible but can only be done on a qualitative basis and is mostly down to the experience of the user to recognise good tightropes and discard the others. However, bad tightropes usually have some recognisable features and can be singled out by following a few simple criteria.

In figure 2.13 are some representative examples of good and bad tightropes. For instance, in every chamber there is a certain amount of bundled up actin or reconstituted thin filaments. Generally speaking, bundles can be recognised by the loss of a straight shape (figure 2.13a), or for forming very large aggregates (figure 2.13b), as well as by their "thicker" appearance in fluorescence, particularly closer to the beads, indicating several filaments joining together and possibly stretching to a nearby bead (figure 2.13c, right). Although bundles are easily recognised, bad tightropes do not amount to only filaments that have a specific "physical" feature, but also to ones that would not give useful data, for example those that are not parallel to the coverslip surface, hence going out partially out of focus (figure 2.13c, left), or those too short (figure 2.13d), resulting in less binding seen (due to the low number of binding sites and the beads acting as a steric encumber) and poor signal to noise ratio (caused by the high noise coming from the nearby beads). Other examples of tightropes that are discarded from data collection are those that are not bound to a bead at one end and those that are attached but fluctuating in three dimensions. Examples of good tightropes are shown in figure 2.13e and f (unregulated actin and reconstituted thin

filament, respectively), which appear straight and have a length generally comprised between 3 and 10 µm, with a calculated average of 6.98 ± 3.03 µm (mean ± SD, N = 47) and 6.41 ± 3.02 µm (N = 359) for actin and thin filaments, respectively (based on the tightropes analysed in the experiments discussed in chapter 5).

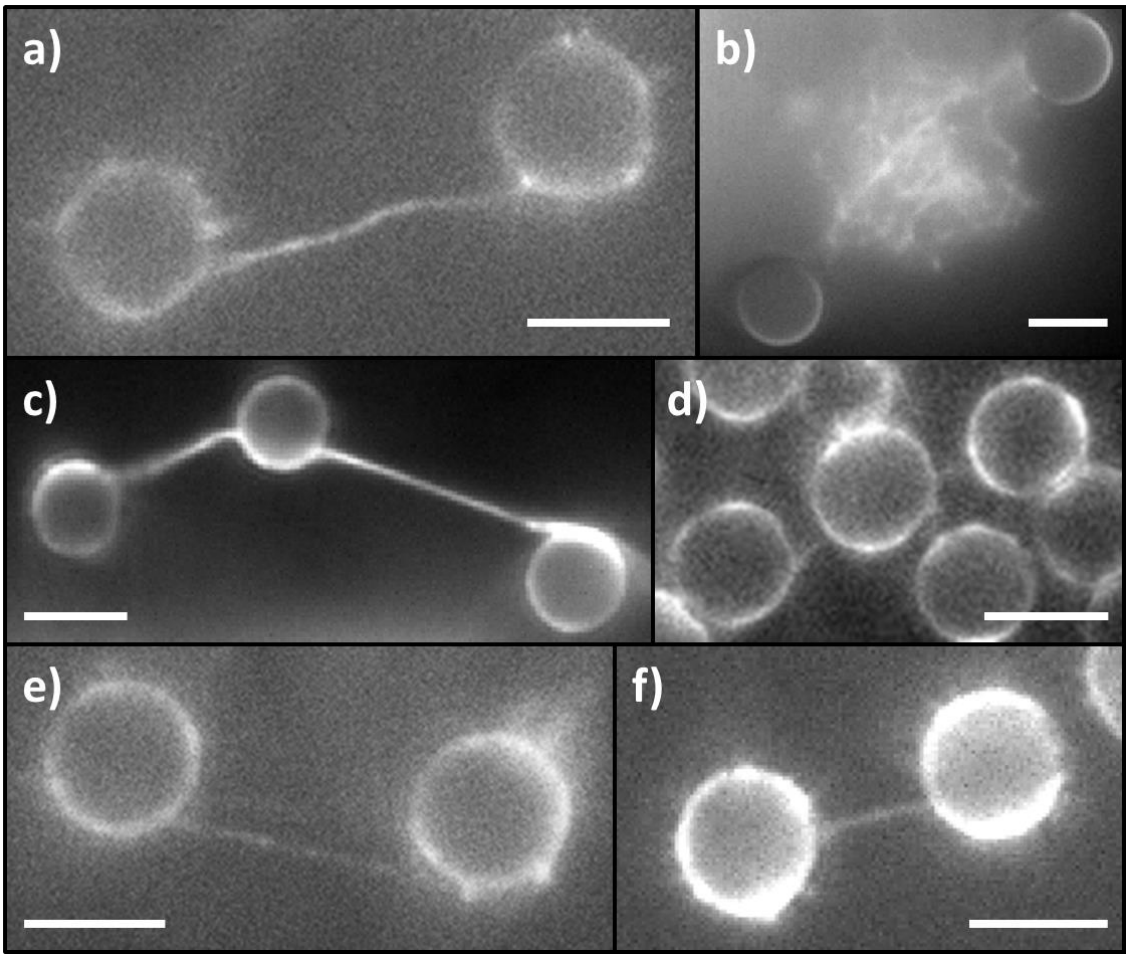

Figure 2.13: **Selecting good tightropes.** Bad tightropes can be easily recognised by a) loss of a straight shape, b) formation of large aggregates, c) high fluorescence intensity and d) very short length, compared to good tightropes of e) unregulated actin and f) reconstituted thin filaments, which are straight and have an average length of 6 µm. Scale bars are 5 µm.

All in all, the thin filament tightropes assay is a fairly reproducible technique, in which only up to one in ten flow chambers will result in no usable filaments, while there is

some variability in the number of filaments imaged per chamber, which can range from one to more than ten. Thus, each flow chamber is considered an experimental replicate and, regardless of the number of filaments found in a chamber, all data acquired in the same experimental conditions are pooled and analysed in the same way, with no difference noted between data acquired in chambers with low or high amounts of filaments found.

On average, the search for good tightropes takes about 30% of the overall time spent on a single flow chamber, which is usually imaged for about two hours since the injection of the fluorescent protein solution. This does not mean that finding good tightropes is hard, but that most of the times requires patience. The rest of the time spent per flow chamber is used in data collection, with movies that range from 30 seconds to 5 minutes long, depending on what the experiment requires; for example, when imaging S1-GFP at high calcium a lot of interactions can be recorded within a 30 seconds time window per movie, as opposed to low calcium, where interactions are scarce and movies of two minutes each are preferred. Furthermore, movies looking at diffusive properties of MyBP-C fragments are generally longer than 3 minutes, caused by the long acquisition times required to account for the low processivity of the molecules.

2.9.4 – Data analysis

Images and videos collected using the OAFM have been analysed using custom written macros in ImageJ and using Office Excel for numerical calculations. As the type of analysis performed often depends on the question asked and the information required from the experiment, details on the analysis are given in full in the results section of

each chapter. However, a common requirement in all of the analyses is knowing the pixel size of the camera field of view. This was calibrated using a graticule as a standard sample, as shown in figure 2.14.

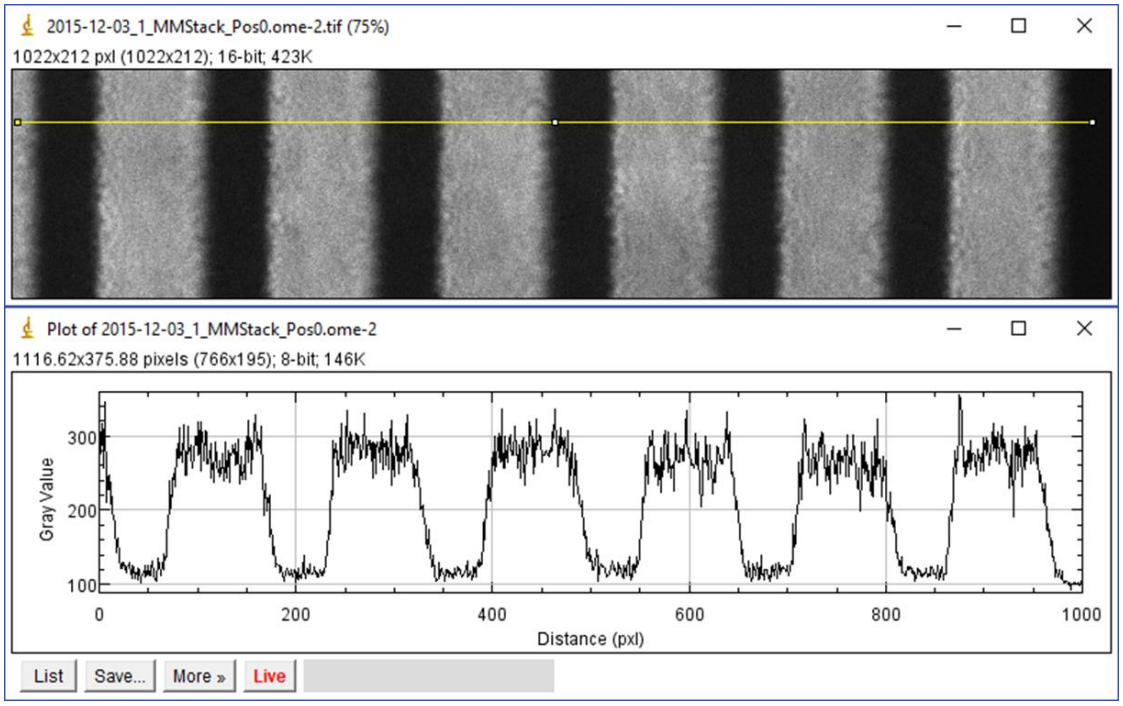

Figure 2.14: **Calibrating the pixel size of the microscope camera.** Microscope image of the calibrating graticule (top) with its respective profile (bottom). The distance between each bar corresponds to 10 µm and an average of 158.3 pixels.

By knowing the distance between each black bar is of 10 µm and calculating the average pixel distance between them (158.3 pixels), we calculated an average pixel size of 63.2 nm in the absence of camera binning.

CHAPTER 3

INVESTIGATING THE EFFECTS OF THE HYPERTROPHIC CARDIOMYOPATHY α-TROPOMYOSIN E180G MUTATION ON THIN FILAMENT ACTIVATION

3.1 – Introduction

Tropomyosin (Tm), along with the troponin complex, plays a fundamental role in muscle contraction, regulating acto-myosin interactions by sterically blocking access to myosin binding sites on actin. Hence, mutations in this protein can have important consequences on muscle functionality, as is the case with Hypertrophic Cardiomyopathy (HCM), often associated with poor prognosis. To date, several Tm mutations found all throughout its coiled coil structure have been associated with HCM. Glu180Gly (E180G) was among the first such missense mutations to be discovered (Thierfelder *et al.*, 1994). The E180G mutation removes a negative charge from the surface of tropomyosin, weakening its interaction with the positively charged groove on the actin filament, in turn leading to an overall decrease in actin-Tm affinity

(Kremneva *et al.*, 2004; Mathur *et al.*, 2011) and an increase in Tm flexibility, with its persistence length decrease ranging between 20-30% less than the wild-type (Li *et al.*, 2012; Loong *et al.*, 2012). It is also associated with an increased sensitivity of the thin filaments to calcium (Bing *et al.*, 2000; Boussouf *et al.*, 2007; Wang *et al.*, 2011; Janco *et al.*, 2012; Matyushenko *et al.*, 2017), leading to hypercontractility of the thin filaments *in vivo* and impaired relaxation (Bai *et al.*, 2011).

In this study, we investigate the effects of the E180G mutation on acto-myosin interactions at the single molecule level, highlighting the changes in thin filament activation. Looking at fluorescent myosin-S1 binding to E180G-RTFs (actin filaments reconstituted with troponin and E180G tropomyosin) across various calcium concentrations enables us to calculate the size of the actin regulatory unit. Ultimately, our results provide an explanation for a molecular mechanism of how a missing charge is responsible for impaired relaxation, potentially bridging the gap to previous physiological studies.

3.2 – Results

3.2.1 – The α-tropomyosin E180G mutation increases thin filament calcium sensitivity in the motility assay

To investigate the calcium sensitivity of the thin filaments reconstituted with the mutated α-tropomyosin we used the *in-vitro* motility assay, following the procedure described in section 2.8. Briefly, we performed the experiments at different calcium concentration ($pCa = -\log[Ca^{2+}]$) for both the wild-type tropomyosin reconstituted

thin filaments (WT-RTFs) and the E180G-tropomyosin reconstituted thin filaments (E180G-RTFs), collecting two or more movies per flow chamber (or replicate), imaging more than 20 filaments per movie. From each flow chamber we extrapolated the speed and the % of motile filaments (as detailed in section 2.8.2) and plotted the data against each respective pCa, resulting in the curves shown in figure 3.1.

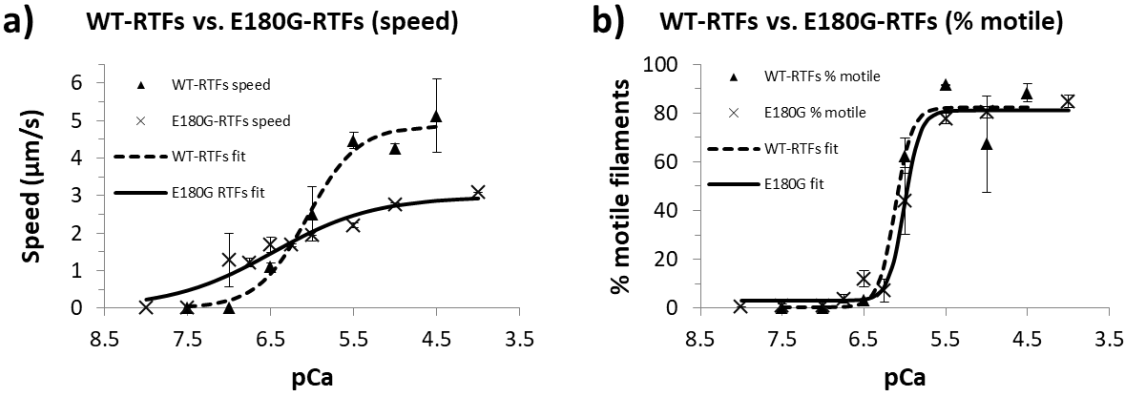

Figure 3.1: **The motility properties of E180G-RTFs.** Comparison of a) speed and b) % of motile filaments in the *in-vitro* motility assay of WT-RTFs (triangles) and E180G-RTFs (crosses), with their respective fit (dashes and full line, respectively). Errors are standard error of the mean (SEM) of the averages of speed or % of motile filaments obtained from two flow chambers. Fitting parameters are listed in table 3.1.

Each data point in the motility curves in figure 3.1 is a mean of two values obtained from two different flow chambers (experimental replicates). The data is fit to the Hill equation,

$$\theta = \frac{\theta_{max}[Ca^{2+}]^n}{K_{mot} + [Ca^{2+}]^n} + off$$

where θ corresponds to the property analysed (speed or % of motile filaments), $[Ca^{2+}]$ is the calcium concentration, n the Hill coefficient $K_{mot} = 10^{-n*pCa_{50}}$ (with pCa_{50} as the calcium concentration for which $\frac{\theta}{\theta_{max}} = \frac{1}{2}$) and off an offset. Each single experimental replicate has been fit independently and the values obtained averaged to determine the standard errors and the significance (table 3.1, distinguished between the speed or the % of motile filaments).

	WT-RTFs		**E180G-RTFs**	
	Speed	**% motile fil.**	**Speed**	**% motile fil.**
$\boldsymbol{\theta_{max}}$	4.80 ± 0.55 µm/s	88.78 ± 1.53	2.95 ± 0.13 µm/s	79.12 ± 1.04
$\boldsymbol{n}$	1.52 ± 0.07	4.07 ± 0.21	0.75 ± 0.14	3.85 ± 0.84
$\boldsymbol{pCa_{50}}$	6.05 ± 0.04	6.09 ± 0.04	6.49 ± 0.03	5.99 ± 0.09
$\boldsymbol{-Log(K_{mot})}$	9.20 ± 0.35	24.81 ± 1.13	4.86 ± 0.91	23.14 ± 5.37
$\boldsymbol{off}$	0.04 ± 0.04	0.44 ± 0.44	0.00 ± 0.00	2.70 ± 0.91

Table 3.1: Summary of the values obtained from fitting the data using the Hill equation for the WT-RTFs and E180G-RTFs, for both speed and % of the motile filaments each. Each value is an average of the fitting parameters obtained for each of the two replicates (n = 2) along with the standard error.

A comparison of the fitted parameters shows that the presence of the E180G mutation affects only the speed vs. pCa motility curve (figure 3.1a), significantly reducing the Hill coefficient of E180G-RTFs (1.52 ± 0.07 for WT-RTFs against 0.75 ± 0.14 for E180G-RTFs, with p = 0.0389) and significantly increasing their calcium sensitivity (6.05 ± 0.04 for WT-RTFs against 6.49 ± 0.03 for E180G-RTFs, with p = 0.0127). In addition, the maximum filaments speed is seen substantially decrease in the presence of the E180G mutation (4.80 ± 0.55 µm/s for WT-RTFs against 2.95 ± 0.13 µm/s for E180G-RTFs), although not significantly (p = 0.0820). Finally, the % of motile filaments in the flow

chambers seems to not be affected by the E180G mutation, with the two motility curves in figure 3.1b almost overlapping.

These results are in agreement with previous findings from the literature, with both the reduction in Hill coefficient and increase in pCa_{50} already reported in motility assay experiments performed by (Bing *et al.*, 2000; Wang *et al.*, 2011), although the E180G mutation is also seen pose an effect to the fraction of motile filaments in (Bing *et al.*, 2000), unlike here.

3.2.2 – Studying the effects of the α-tropomyosin E180G mutation on S1-GFP binding to regulated thin filaments

In order to understand what the effect of the E180G mutation is on myosin binding and its cooperativity, we collected data in our single molecule tightrope assay imaging the binding and release of S1-GFP to E180G-RTFs, varying both the [S1-GFP] and the $[Ca^{2+}]$, while keeping the [ATP] constant at 0.1 μM in all experiments. Varying the $[Ca^{2+}]$ will allow us to study the transition between the thin filament activation states, while varying the [S1-GFP] allow us to look directly at myosin cooperativity. Therefore, we collected videos of 15 nm S1-GFP binding to E180G-RTFs at pCa 7, 6, 6.5, 5 and 4, as well as videos of E180G-RTFs at pCa 4 and [S1-GFP] = 5, 10 and 15 nM. Movies were collected for at least 1 minute using an exposure time of 300 ms, imaging three or more filaments per condition, with an average of three movies (or kymographs) per filament. Our goal is to compare the data acquired with the E180G-RTFs to those found for the WT-RTFs in (Desai *et al.*, 2015) using the same experimental technique and data analysis method, based on simultaneous fitting of all the S1-GFP binding distributions.

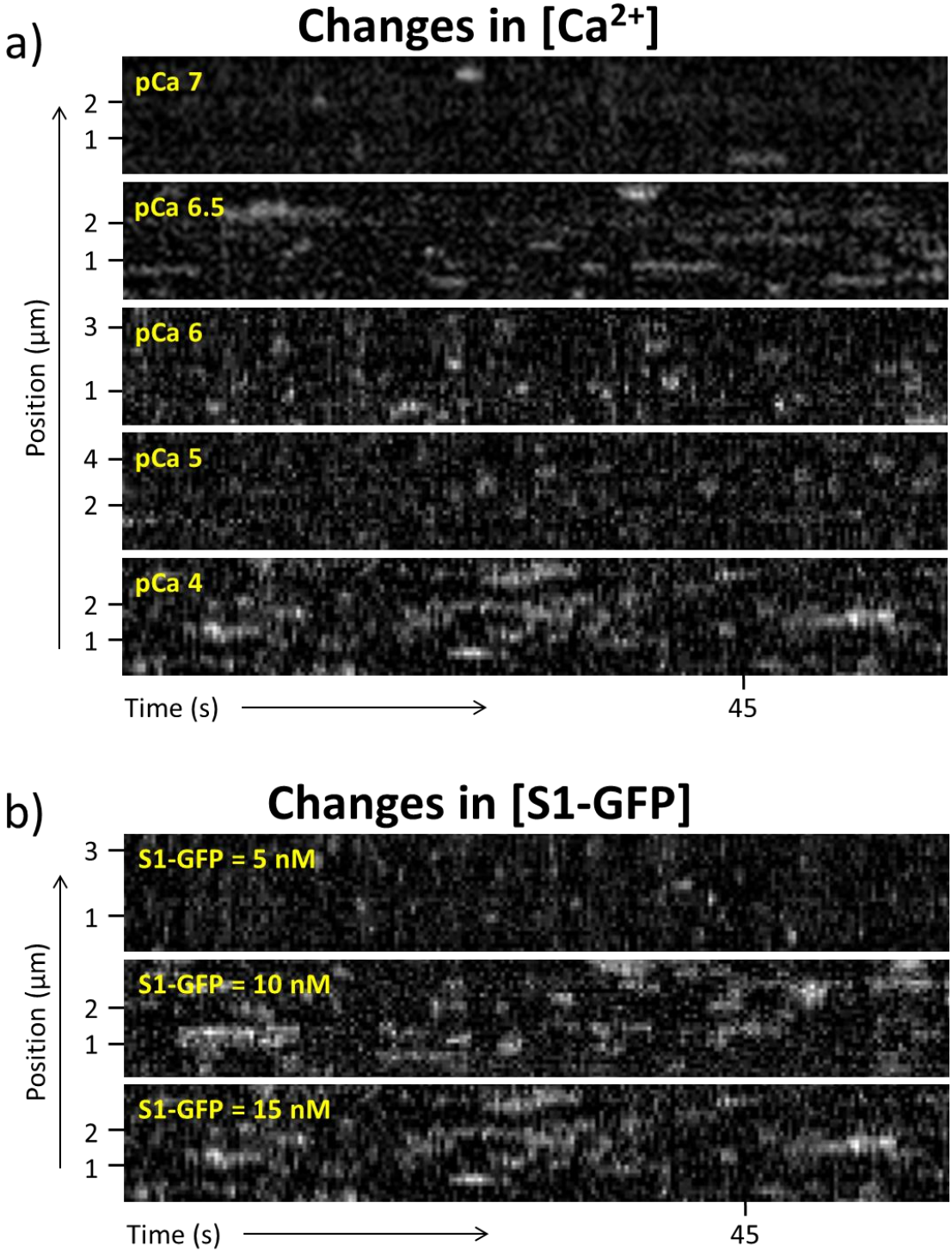

Figure 3.2: **Visualising the interactions between S1-GFP and E180G-RTFs.** Representative kymographs of tightropes imaged varying a) the [Ca^{2+}], keeping the [S1-GFP] at 15 nM, and b) varying the [S1-GFP] while keeping the calcium to pCa 4. The intensity of each kymograph was scaled to the one of pCa 4 and S1-GFP = 15 nM, to allow for better qualitative comparison.

Representative kymographs are visualised in figure 3.2a, obtained imaging 15 nM S1-GFP binding to E180G-RTFs at different [Ca^{2+}] (from pCa 7 to pCa 4, top to bottom), and 3.2b, obtained imaging 5, 10 and 15 nM S1-GFP (top to bottom) binding to E180G-RTFs at pCa 4. A qualitative assessment of these kymographs reveals the effect of calcium on myosin binding (figure 3.2a): S1-GFP is seen binding in increasing amounts from pCa 7 to pCa 4, consistent with an increased availability of actin, caused by both the increase in calcium concentration, pushing the equilibrium between the blocked and the closed state of the thin filament to the right, and by myosin cooperativity (Mckillop and Geeves, 1993; Desai *et al.*, 2015). Figure 3.2b shows the effects on S1-GFP binding caused by an increase in [S1-GFP], with frequent but short binding events at [S1-GFP] = 5 nM compared with binding events as frequent but clustered at [S1-GFP] = 10 and 15 nM.

To extrapolate the intensity of each fluorescent spot in the kymographs, we used a custom written Matlab routine (see Appendix A.3 for details), pooled all the values obtained per filament at a specific experimental condition and plot these as histograms (figure 3.3). These graphs have not been normalised to have a better understanding of the variability within each dataset; among all, the largest variation seen is relative to the amount of data acquired per filament (Fil), the extreme seen for filament # 2 at pCa 7 (figure 3.3a), but also visible in the other datasets. This variability is not only linked to the amount of S1-GFP binding at each specified condition, but also to the variability in intensity associated to each single molecule imaged, since there will always be an error linked to the measurement of each intensity value (Walcott and Kad, 2015).

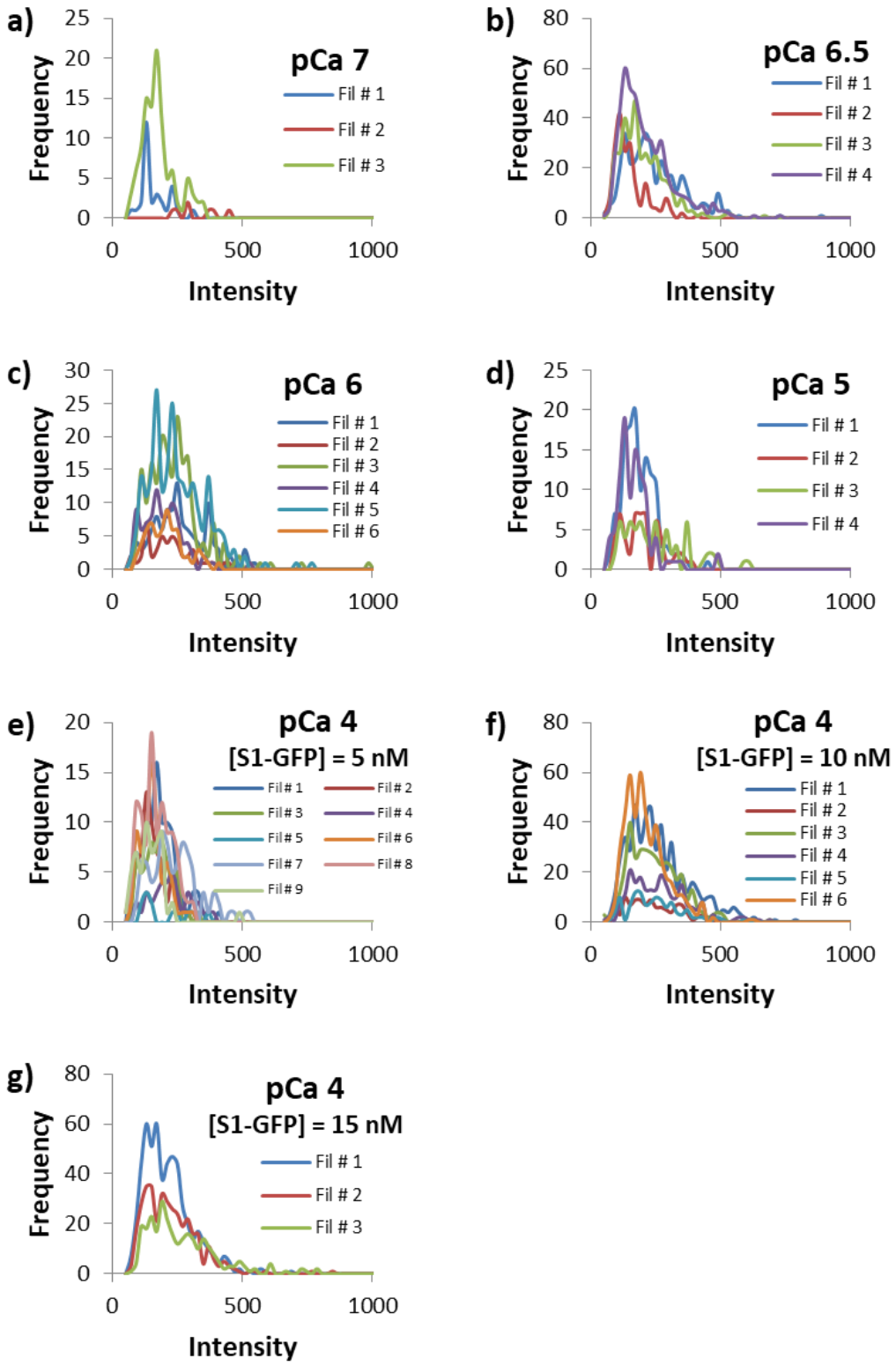

Figure 3.3: **Histograms of the extrapolated intensity values.** Histograms of the S1-GFP intensity values per each filament imaged using 15 nM S1-GFP on E180G-RTFs at a) pCa 7, b) pCa 6.5, c) pCa 6, d) pCa 5 and e) 5 nM, f) 10 nM, g) 15 nM of S1-GFP at pCa 4; ATP concentration was kept at 0.1 µM in all cases.

Considering that the overall intensity distributions in figure 3.3 show little variations within the same experimental conditions, we can pool all the data acquired into datasets (figure 3.4a and b); the resulting distributions will have, however, each be constituted by a different amount of data points, given not only by the differences discussed above, but also by the amount of filaments imaged per condition (see figure 3.3 for the # of filaments), making a direct and meaningful comparison difficult. Therefore, to account for these variations, it is necessary to normalise the distributions (figure 3.4c and d), allowing for a fair comparison of the changes in S1-GFP binding caused by the changes in [Ca^{2+}] or [S1-GFP] with the data presented in (Desai *et al.*, 2015) and shown in figure 1.18 of Chapter 1.

The normalised histograms in figure 3.4c show an increase in frequency at larger intensity values with increases in calcium concentration. The distributions obtained at pCa 6 and 5 also appear to have their maximum peak right-shifted towards higher intensity values, compared to the other distributions. A similar trend is seen in the histograms in figure 3.3d, with broader distributions and a right shift for [S1-GFP] = 10 and 15 nM compared to 5 nM. However, no clear difference is seen between the normalised intensity distributions for [S1-GFP] = 10 and 15 nM, with the two almost overlapping.

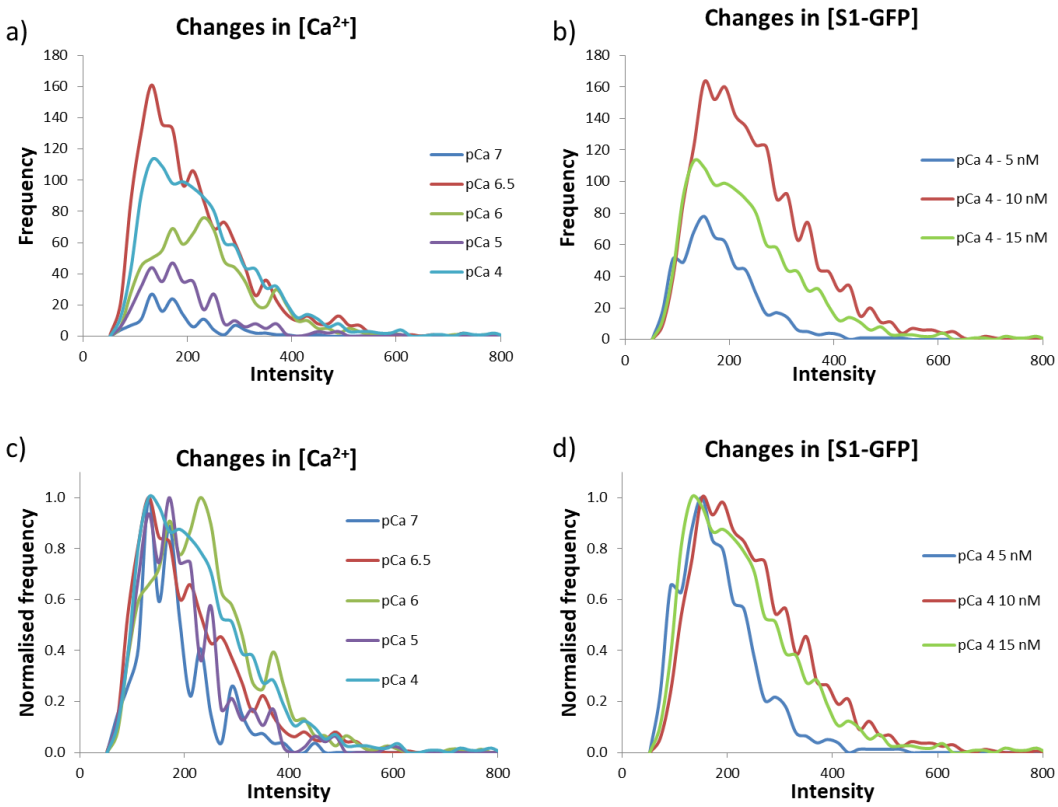

Figure 3.4: **Quantifying the binding of S1-GFP to E180G-RTFs.** Histograms of all the intensity values extrapolated from the kymographs in figure 3.2, for a) the changes in [Ca^{2+}] and b) in [S1-GFP]; c) and d) show the same plots normalised to the highest peak in the dataset, to account for the different amount of filaments imaged per condition.

Although the comparison of the intensity histograms in figure 3.4 gives us insights on the amount of S1-GFP binding to E180G-RTFs per experimental condition, a more direct way of comparing the data would be to convert the distributions in histograms of bound molecules per condition. Since throughout our experiments both the illumination power and the collection exposure time were kept constant, so that the fluorescence intensity is directly proportional to the amount of S1-GFP molecules bound within a specific region (Walcott and Kad, 2015), we can recalculate the histograms in figure 3.3 and 3.4 based on the number of myosin, using the same approach of (Desai *et al.*, 2015) and (Iino *et al.*, 2001).

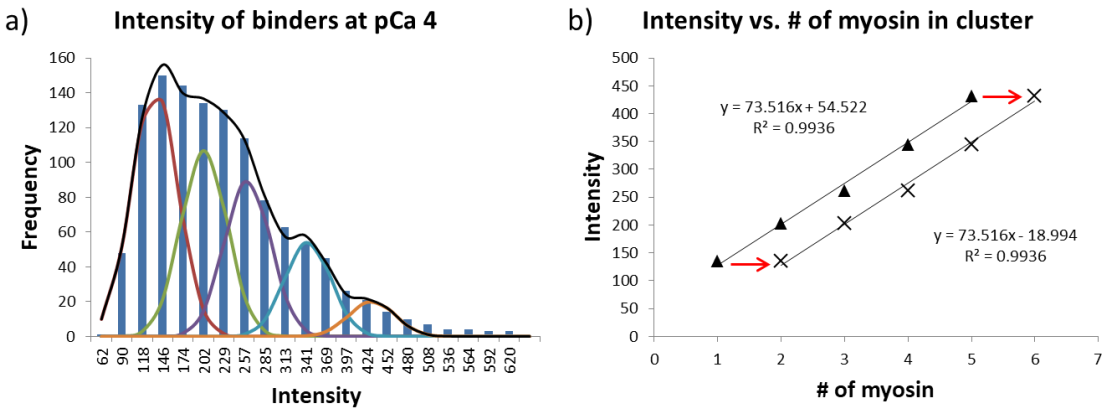

Figure 3.5: **Determination of a single S1-GFP fluorescence intensity.** a) histogram of the extrapolated intensities of 15 nM S1-GFP binding to E180G-RTFs at pCa 4 fit to five Gaussian distributions and b) plot of the mean intensity of each Gaussian distribution against the associated number of myosin, highlighting the necessity of a right shift to minimise the error on the fit.

To achieve the conversion we need to first calculate the intensity of a single binder; hence, we took the intensity distribution of binders at pCa 4 and 15 nM of S1-GFP, which gives us the highest possible number of binding events, and fit it to up to five Gaussian distributions (figure 3.5a and table 3.2). Fitting was performed using least square minimization and the Solver Add-in for Office Excel, which uses an algorithm to vary the fitting parameters until a minimum value between the data and the fit is found. The intensity and the mean of each Gaussian distribution were varied independently while their standard deviation was constrained to one value for all, to better represent the experimental distribution of intensities associated to multiple unresolvable fluorescent molecules. The values of the amplitude, mean and standard deviation (S.D.) obtained for each Gaussian distribution are listed in table 3.2.

	Gaussian 1	Gaussian 2	Gaussian 3	Gaussian 4	Gaussian 5
Amplitude	141.7	106.8	89.6	54.1	20.2
Mean	135.1	202.5	261.8	344.0	431.9
S.D.	31.53	31.53	31.53	31.53	31.53

Table 3.2: Summary of the values of amplitude, mean and standard deviation (S.D.) of each Gaussian distributions obtained from the histogram in figure 3.4a.

Plotting the mean values in table 3.2 against the expected number of bound S1-GFP results in the chart in figure 3.5b. Considering the lowest mean intensity value of 135.1 as the intensity of a single binder leads to a slope of 73.5 and an intercept equals to 54.5. However, shifting the plot to the right (considering the lowest mean intensity value as a cluster of two S1-GFP molecules) reduces the ratio between the intercept and the slope from ~74% to ~25%. A similar approach was used by (Desai *et al.*, 2015) when imaging in similar conditions, highlighting both the difficulty in detecting single molecules of S1-GFP, due to the low signal to noise ratio, and the reproducibility of the tightrope assay, where the same method can be applied to two different datasets, yielding similar conclusions.

Using the slope of the plot in figure 3.5b, which corresponds to a single S1-GFP fluorescence intensity, we can convert the histograms in figure 3.3 and 3.4 from intensity to number of myosin bound within each fluorescent spot (figure 3.6 for the changes in $[Ca^{2+}]$ and 3.7 for the changes in [S1-GFP], respectively).

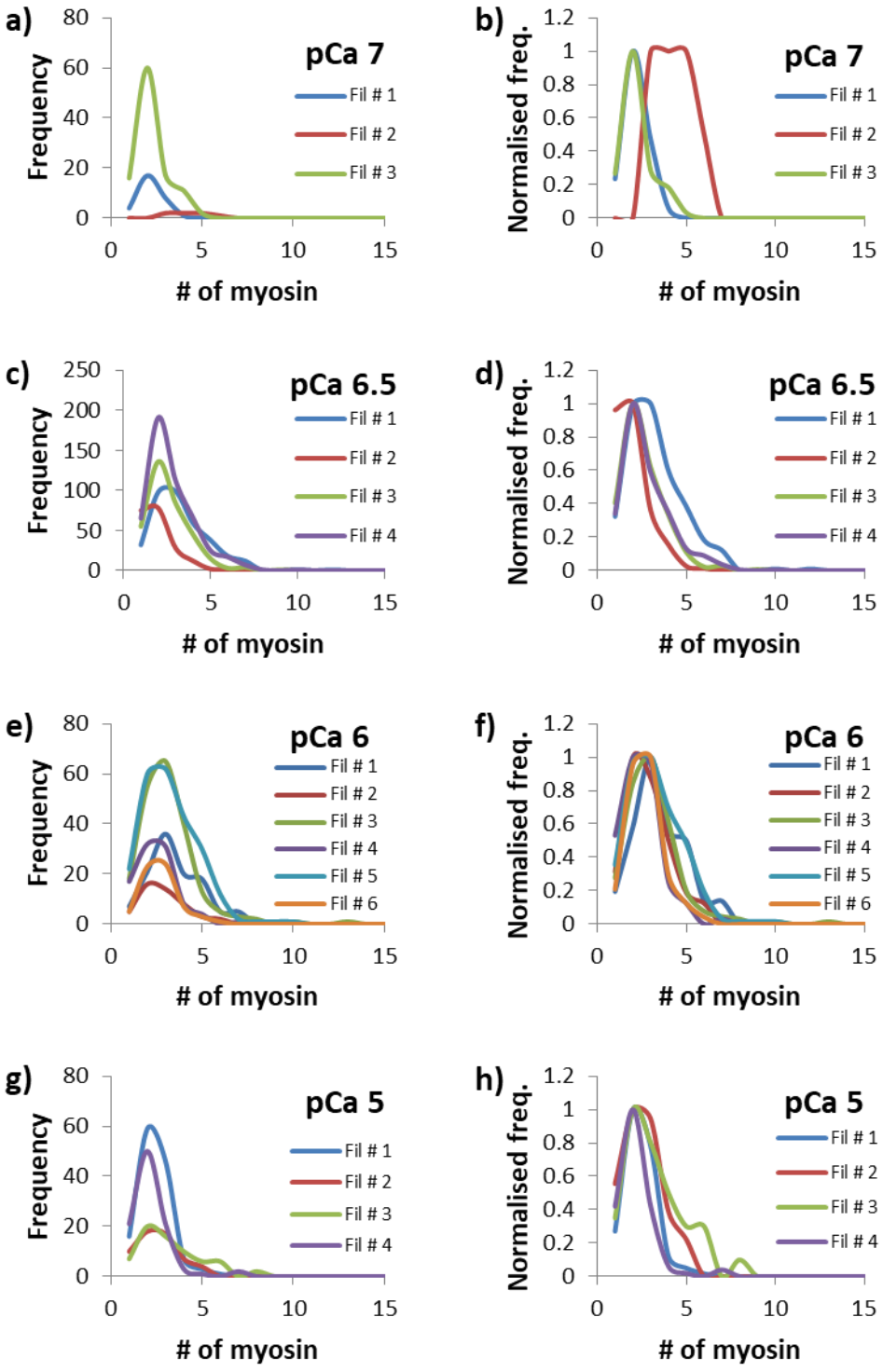

Figure 3.6: **Histograms of the # of myosin (S1-GFP) binding to E180G-RTFs at increasing [Ca^{2+}].**

Histograms of the number of S1-GFP bound per each filament imaged using 15 nM S1-GFP on E180G-RTFs at a) pCa 7, c) pCa 6.5, e) pCa 6 and g) pCa 5 with b), d), f) and h) their respective normalisation.

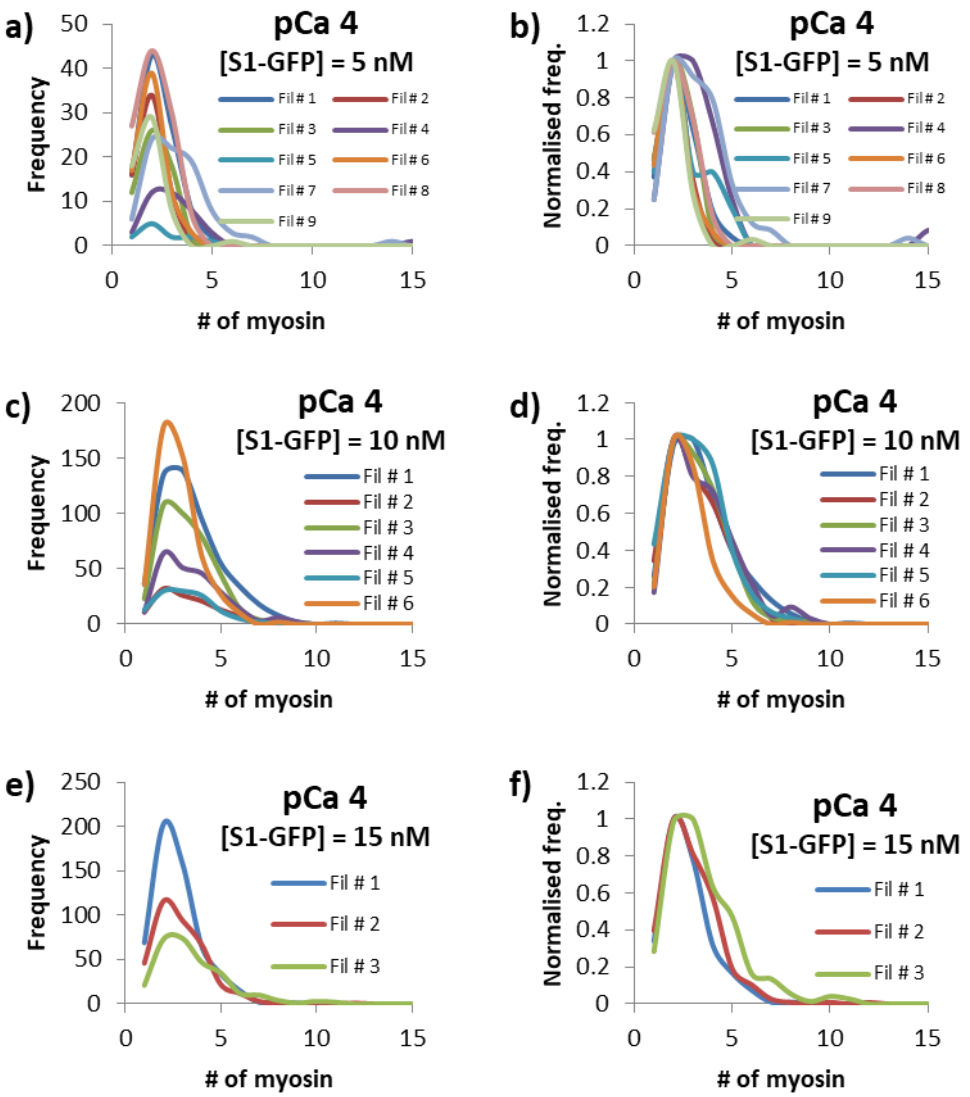

Figure 3.7: **Histograms of the # of myosin (S1-GFP) binding to E180G-RTFs at increasing [S1-GFP].** Histograms of the number of S1-GFP bound per each filament imaging E180G-RTFs at pCa 4 using a) 5 nM, c) 10 nM and e) 15 nM of S1-GFP, with b), d) and f) their respective normalisation.

The non-normalised histograms in figure 3.6 and 3.7 show the same level of variability discussed for figure 3.3, although these appear smoother because of the transition from intensity to # of molecules. Their respective normalised histogram, however, show that there is very little variability between # of molecules binding within the same experimental conditions, with most of the distributions overlapping and having a

maximum at 2 S1-GFP molecules. The only exceptions are pCa 7 (figure 3.6b), with filament # 2 being right shifted compared to the others and pCa 6.5 (figure 3.6d), with filament # 1 having a somewhat broader distribution. The former, however, does not contribute much to the overall number of datapoints acquired at pCa 7 (see figure 3.6a), while the latter can be attributed to the natural variability of data obtained by imaging at the pCa_{50} of the calcium activation curve (see Chapter 4 for the sensitivity of imaging in these conditions and how they affect S1-GFP binding).

Considering the little variability of the histograms of the # of S1-GFP bound per condition, we can pool all the data into one single histogram per experimental condition and normalise the frequency for the sum of the total events, giving us the % occurrence of having a cluster of N myosin in each of the cases explored (figure 3.8a-g). These histograms will be fit simultaneously, similarly to what has been done in (Desai *et al.*, 2015), to ensure the quantification of the kinetic parameters for our assay and, pooling the data, ensures an appropriate comparison based on the amount each number of myosin has been seen bound per condition, ultimately facilitating the simultaneous fitting of the histograms by limiting the number of distributions used.

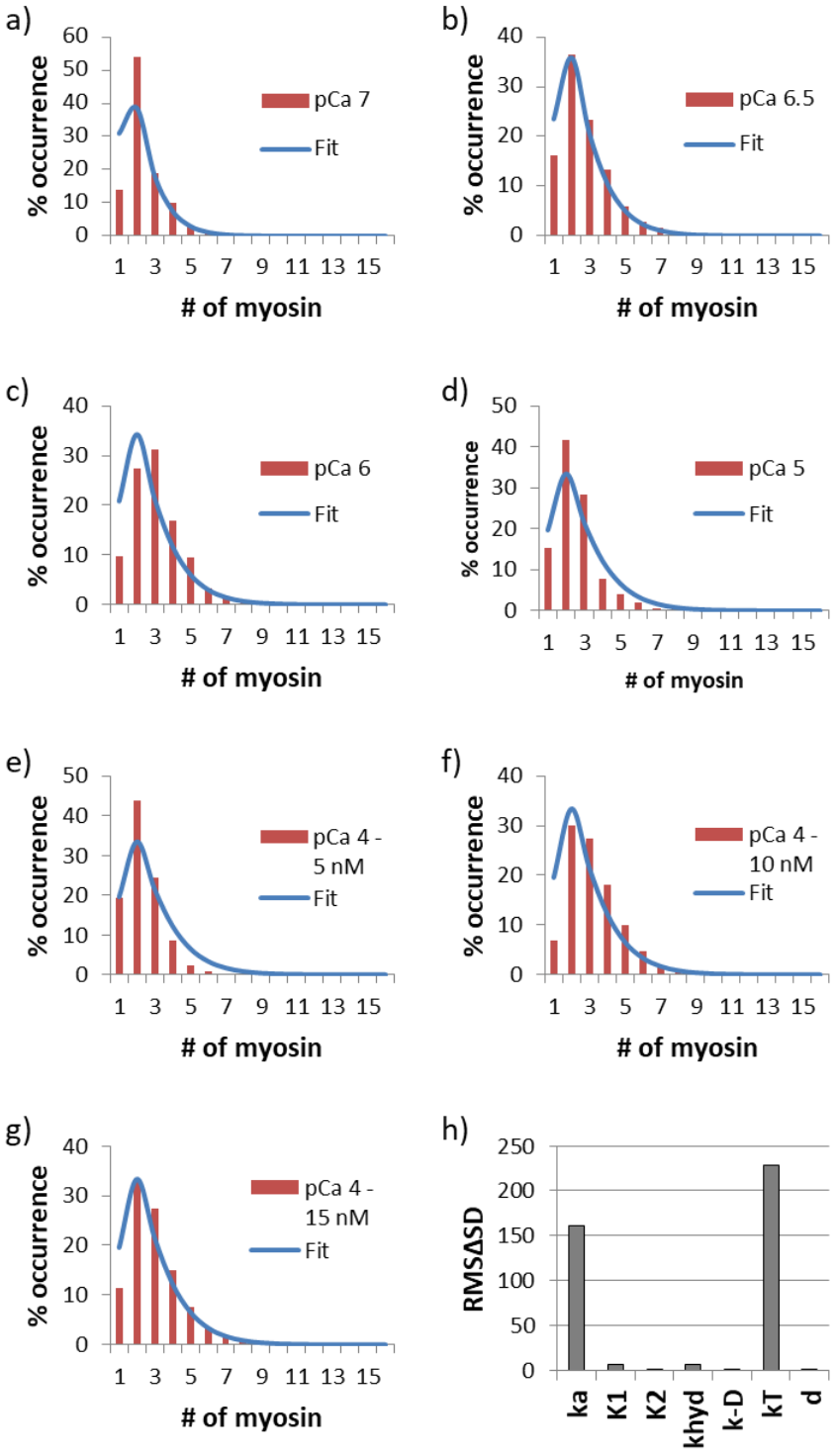

Figure 3.8: **Probability histograms of S1-GFP binding to E180G-RTFs.** Histograms of the frequency of clustered binding events (% occurrence) for 15 nM S1-GFP binding to E180G-RTFs at a) pCa 7, b) pCa 6.5, c) pCa 6, d) pCa 5 and e) 5 nM, f) 10 nM, g) 15 nM of S1-GFP at pCa 4; ATP concentration was kept at 0.1 µM in all cases. h) sensitivity plot for all the parameters used for the fitting.

Global (or simultaneous) fitting has been used in a number of occasions and has been shown to be a powerful tool to study multiple datasets and get accurate common modelling parameters (Zhang *et al.*, 2010; Herman and Ching Lee, 2012; Freiburger *et al.*, 2015; Li *et al.*, 2017). To fit the histograms in figure 3.8a-g we used the same kinetic model found in (Desai *et al.*, 2015),

$$A_B + n_{Ca}Ca^{2+} \overset{K_1}{\rightleftharpoons} A_{CL} + n_M MDP_i \overset{K_2}{\rightleftharpoons} A_M M + T$$

where T is the ATP and A_B, A_{CL} and A_M are the actin in the blocked state, in the closed state and in the open state respectively, with the restriction that myosin cannot bind to A_B. However, unlike in (Desai *et al.*, 2015), to calculate the final binding probability distributions, we used the Flory-Schulz distribution (Flory, 1936), used to predict the weight fraction of a polymer through the probability of association of its monomers, as described by the following equation:

$$W_l = l \cdot p^{(l-1)} \cdot (1-p)^2$$

where W_l is the weight fraction, p is the probability of association and l is the number of molecules in the cluster (polymer length). In this case, the probability of association or of a myosin molecule to bind the thin filament is given by the duty cycle and l is the number of myosin in a cluster. The duty cycle is calculated following:

$$duty\ cycle = \frac{\tau_{on}}{\tau_{on}+\tau_{off}} \qquad \tau_{on} = \frac{1}{k_{-D}} + \frac{1}{k_T[ATP]} \qquad \tau_{off} = \frac{1}{k_{hyd}} + \frac{1}{k_{att}}$$

where k_{-D}, k_T and k_{hyd} are the ADP dissociation, the ATP association and the ATP hydrolysis rate constants respectively, and k_{att} the second order S1-GFP attachment rate constant. Considering that myosin binds to the thin filament cooperatively, the k_{att} will have to be calculated accounting for the differences between a myosin binding to the actin closed state versus one binding to the open state. This lead to the following:

$$\tau_{off,cl} = \frac{1}{k_{hyd}} + \frac{1}{k_a A_{cl}} \qquad \tau_{off,m} = \frac{1}{k_{hyd}} + \frac{1}{k_a (A_{cl} + d A_m)}$$

where d is the size of the cooperative unit, k_a the myosin intrinsic attaching rate and A_{cl} and A_m are the relative ratio of actin available in the closed and open state respectively, given by

$$A_{cl} = \frac{A_{CL}}{A_B + A_{CL} + A_M} = \frac{[Ca^{2+}]^{n_{Ca}} K_2 [ATP]}{K_1 K_2 [ATP] + [Ca^{2+}]^{n_{Ca}} K_2 [ATP] + [M]^{n_M} [Ca^{2+}]^{n_{Ca}}}$$

$$A_m = \frac{A_M}{A_B + A_{CL} + A_M} = \frac{[Ca^{2+}]^{n_{Ca}} [M]^{n_M}}{K_1 K_2 [ATP] + [Ca^{2+}]^{n_{Ca}} K_2 [ATP] + [M]^{n_M} [Ca^{2+}]^{n_{Ca}}}$$

The full calculation to derive the ratios for A_{cl} and A_m is given in the Appendix of this thesis, section A.4.

Finally, we calculate the probability p for the Flory-Schulz distribution as the sum of the duty cycles for A_{cl} and A_m, as in

$$p = \frac{\tau_{on}}{\tau_{on} + \tau_{off,cl}} + \frac{\tau_{on}}{\tau_{on} + \tau_{off,m}}$$

and use the Flory-Schulz relationship to fit our data in figure 3.8a-g. The fits were optimised globally by calculating the sum of the sum of squared differences (SSSD) of each histogram and solving all the fits at once using the Solver Add-in for Office Excel as above. We excluded the first point of each histogram since, from figure 3.5b, we must take into account that the quality of the data of a single S1-GFP binding might be biased by the low signal to noise ratio. The analysis yielded a k_{-D} of 500 s^{-1}, k_T of 2.5 $\mu M^{-1}s^{-1}$, k_{hyd} of 100 s^{-1}, k_a of 21.8 s^{-1}, K_1 of $7.9 \cdot 10^{-8}$ M, K_2 of $5.0 \cdot 10^{-5}$ M, n_{Ca} of 1, n_M of 2.4 and a cooperative unit d of 7.3 actin subunits, comparable with the values obtained in (Desai *et al.*, 2015) (see table 3.3).

	WT-RTFs	**E180G-RTFs**
k_a **(/s)**	47	21.8
K_1 **(μm)**	$4.00 \cdot 10^{-1}$	$7.92 \cdot 10^{-2}$
K_2 **(μm)**	37.0	49.9
k_T **(μm/s)**	1.4	2.5
k_{-D} **(/s)**	500	500
k_{hyd} **(/s)**	100	100
n	1.08	1.00
d	11.6	7.3

Table 3.3: Comparison of the fitting values obtained in this work and presented in (Desai *et al.*, 2015).

Considering that the way of analysing our data already intrinsically corrects for myosin cooperativity, we used n_M only to find a better constrain for the other parameters, and

restored it to 1 once the solving algorithm converged, bringing the SSSD from 870.79 to 874.43 (a change of 0.4%). Finally, we tried to calculate the confidence intervals of the parameters according to the method published in (Kemmer and Keller, 2010); however, this resulted in a too difficult a task, since we have too many parameters compared to the published method and other ways to calculate the intervals would be too computationally demanding, while also lacking in accuracy (Spitzer *et al.*, 2006; Herman and Ching Lee, 2012). Therefore, as an alternative we calculated a sensitivity plot for each parameter by varying each value by ± 20% and recording the change in the SSSD. The square root of the sum of the squared differences between the +20% and – 20% of each parameter gives us the RMSΔSD shown in figure 3.8h, highlighting the two most sensitive parameters of the fit as k_a and k_T.

3.3 – Discussion

In this study, we elucidate the role of the E180G tropomyosin mutation in hypertrophic cardiomyopathy, particularly looking at how it affects myosin cooperativity. We first used the in vitro motility assay to look at the E180G mutation overall effects on thin filaments, finding a statistically significant left shift of the speed-pCa curve of 0.44 ± 0.05 (from 6.05 ± 0.04 of the WT-RTFs to 6.49 ± 0.03 of the E180G-RTFs, p = 0.0127) and a significant reduction in the Hill coefficient (1.52 ± 0.07 for WT-RTFs against 0.75 ± 0.14 for E180G-RTFs, p = 0.0389). These results agree well with previous *in-vitro* motility studies as well as ATPase experiments, with increases in calcium sensitivity of

up to 0.6 ΔpCa (Bing *et al.*, 2000; Boussouf *et al.*, 2007; Bai *et al.*, 2011; Wang *et al.*, 2011; Janco *et al.*, 2012; Ly and Lehrer, 2012; Matyushenko *et al.*, 2017). However, the fraction of motile filaments in our experiments did not result different from the wild-type, unlike in (Bing *et al.*, 2000) where, although small, a difference is noted, and with (Matyushenko *et al.*, 2017), where at low calcium the fraction of motile filaments significantly increased, even up to 70%. These differences are likely to be caused by the slight differences in the experimental approaches and the amount of myosin or regulatory proteins tropomyosin and troponin used in the motility buffer, known to affect the turning on of the thin filament in a concentration dependent manner (Fraser and Marston, 1995; Gorga *et al.*, 2003). It is also worth mentioning that, although the speed vs. pCa and the % of motile filaments vs. pCa curves are fit with different Hill coefficient values, this is perfectly in line with the studies published in the literature for both WT and E180G (Bing *et al.*, 2000; Matyushenko *et al.*, 2017), the fraction of motile filaments being steeper to denote how the filaments are completely turned on and off (Fraser and Marston, 1995; Homsher *et al.*, 1996; Kad *et al.*, 2005).

Having validated the mutation produced, using our *in-vitro* motility data, we used the thin filament tightrope assay to directly quantify the level of myosin binding and its cooperativity on E180G mutated thin filaments (E180G-RTFs), comparing the data obtained with those found in (Desai *et al.*, 2015) for WT-RTFs. Although this comparison might raise concerns about the lack of dedicated control experiments, the reproducibility of the thin filament tightrope assay allows for similar results to be collected even over long periods of time and different users, as can be seen by the similarities found in the results obtained in this chapter using the same approach (i.e. see figure 3.5b for the calculation of the single molecule intensity, a process that was

necessary both in (Desai *et al.*, 2015) and in this work), or by the calculation for the second order ATP binding rate constant (see Appendix A.5) among others, coming to the same conclusions and validating both the approaches used and the use of previously published data as a qualitative comparison. Further discussion on the thin filament tightrope assay reproducibility is found in Chapter 6.

When comparing the data, the level of myosin binding to WT-RTFs in (Desai *et al.*, 2015) was seen to visibly increase with the concentration of S1-GFP (see figure 1.18 in Chapter 1), leading to a marked right shift of the peak of the intensity histograms, both when changing either the [Ca^{2+}] or the [S1-GFP], along with a broadening of the whole distribution towards higher fluorescence intensities. However, our results with E180G-RTFs show a less marked right shift towards higher intensities (figure 3.4), which is then further reduced when we converted the intensity datasets into # of S1-GFP (figure 3.6 and 3.7), while the broadening of the intensity distributions is still seen (figure 3.4) for both changes in [Ca^{2+}] or [S1-GFP] (figure 3.8).

To quantify these changes we applied the same kinetic model used in (Desai *et al.*, 2015) to our data using global (or simultaneous) fitting of the experimental conditions to obtain common independent parameters. Global fitting is a method that has been in use since the 1980s (Eisenfeld and Ford, 1979; Knutson *et al.*, 1983; Beechem and Brand, 1986), initially used for the study of fluorescence decay curves; it allows the study of multiple datasets at the same time using shared fitting parameters (up to 9 in (Li *et al.*, 2017)), overall leading to an improvement of the fitting accuracy (Zhang *et al.*, 2010; Herman and Ching Lee, 2012; Freiburger *et al.*, 2015; Li *et al.*, 2017).

The model yielded similar values for most of the fundamental kinetic parameters, with the exception of K_1 ($7.9 \cdot 10^{-8}$ M, leading to a pCa_{50} of 7.1 for the blocked to closed state

transition) and the size of the cooperative unit d, which resulted in only 7 actin monomers for the E180G-RTFs versus the 11 found for the WT-RTFs (Desai *et al.*, 2015). The decrease in the cooperative unit size could be interpreted as a direct result of the increased flexibility seen in E180G-tropomyosin in atomic force microscopy or electron microscopy studies (Li *et al.*, 2012; Loong *et al.*, 2012). The decrease in d is most likely the cause for the early saturation of thin filaments by S1-GFP (as seen in the histograms in figure 3.4d) respect to WT-RTFs, reducing myosin cooperativity and impeding the formation of larger clusters (figure 3.9). These small clusters would also not be able to propagate effectively throughout the thin filament, resulting in a shift in the equilibrium between the closed and the open state of tropomyosin towards the closed state at high [Ca^{2+}]. The increase in thin filament closed to open state ratio would also explain a reduced right shift of the peak intensity of the histograms in figure 3.4c.

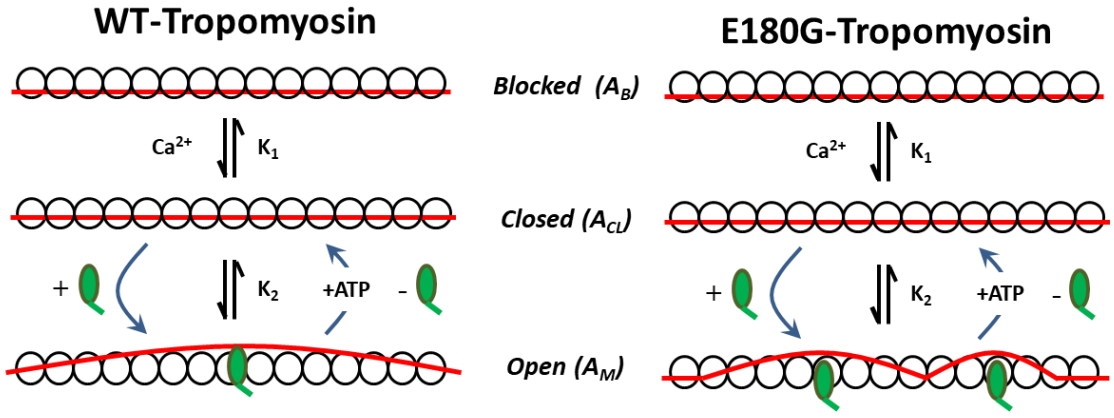

Figure 3.9: **The effect of E180G on thin filament activation.** Cartoon of the model hypothesised for the E180G mutation, where the increased tropomyosin flexibility is seen directly affect the amount of actin available to myosin and the regulatory unit size.

A similar shift towards the closed position of tropomyosin can explain the increased calcium sensitivity. Although the E180G mutation is located in the troponin T binding region of tropomyosin, it has been shown that it does not affect the TnT affinity for tropomyosin (Golitsina *et al.*, 1997, 1999), hinting that the increased calcium sensitivity might not be directly linked to calcium itself. An increase in tropomyosin flexibility would lead to myosin binding sites on actin being more accessible (i.e. increase in the closed to blocked state ratio), facilitating the activation of the thin filament at low calcium and resulting in a left shift in the pCa curve. Reinforcing this hypothesis are the simulations carried out in (Sewanan *et al.*, 2016), which also link the increased calcium sensitivity to a larger population of the thin filament being in the closed state, and those found in (Orzechowski, Fischer, *et al.*, 2014), where the E180G mutation is seen lower the energy barrier necessary for tropomyosin to transition between the different positions on actin.

Our results also highlights how the thin filament tightropes assay is capable of discerning between the thin filament blocked to closed and closed to open transitions, unlike the motility assay. This is evident when we compare the pCa_{50} obtained for the two sets of experiments, being 7.1 for the tightrope assay and 6.4 for the *in-vitro* motility assay; in particular, the relationship between the speed or the % of motile filaments is seen as a single sigmoidal curve, with the pCa_{50} representing the thin filament blocked to open transition. Hence, single molecule experiments can help characterise in more details transitions between the equilibrium state of the thin filament.

Hypertrophic Cardiomyopathy has been associated with an increase in contractile properties of the sarcomere at low calcium, leading to impaired relaxation during

diastole (Bai *et al.*, 2011; Maragiannis *et al.*, 2018; Cohn *et al.*, 2019). Our results directly link the residual contractility at low calcium to an overall increase in the probability of finding the thin filament in the closed state, thus providing a molecular mechanism for the function of the E180G mutation. Although this mutation is associated with a severe phenotype (Wernicke *et al.*, 2004) we must also take into account that our results have been obtained with a E180G-tropomyosin homodimer which, according to (Janco *et al.*, 2012) shows larger changes when compared to a heterodimer and might not be as prominent in the sarcomere in-vivo.

CHAPTER 4

THE CATASTROPHIC COLLAPSE OF ACTIVE REGIONS OF MYOSIN BOUND TO THE THIN FILAMENT AS A MECHANISM FOR MUSCLE RELAXATION

4.1 – Introduction

Muscle contraction is a process driven by the binding of myosin to the thin filament and regulated by tropomyosin and troponin. The activation of the thin filament is a cooperative process initiated by calcium, which binds to troponin and allows the movement of tropomyosin from its blocked to the closed position, partially uncovering myosin binding sites (Mckillop and Geeves, 1993; Risi *et al.*, 2017). Myosin, being now able to bind actin tightly, can then push tropomyosin further and allow more myosin molecules to bind in a cooperative fashion (Heeley *et al.*, 2006), resulting in contraction of the sarcomere. When the calcium concentration within the sarcomere drops, the thin and thick filaments slide back in the relaxed position, with tropomyosin sterically blocking myosin binding sites on actin. However, a clear molecular model of how the thin filament goes back in relaxing position is lacking, and a few questions

remain unanswered: how does tropomyosin goes back from its open to blocked position, in the presence of a high local concentration of myosin? Is tropomyosin a passive protein, waiting for myosin to complete is cycle and leave or has it an active role? Does the thin filament turn off all at the same time, in a cooperative fashion, or rather gradually?

In this chapter I describe the use of the tightrope assay to address these questions, looking at acto-myosin interactions at a calcium concentration that does not allow the thin filament to be fully turned on. Our laboratory have previously shown that under these conditions myosin binds at very high local concentration, forming clusters that can suddenly disappear (Desai *et al.*, 2015). By studying the binding and release of myosin from these regions and comparing our results with simulated data, we are able to shed light on the process of deactivation of the thin filament, showing that tropomyosin might have a more active role in relaxation than previously thought.

4.2 – Results

4.2.1 - Sub-maximal thin filament activation promotes local clusters of myosin

In order to study the process behind muscle relaxation using our single molecule tightrope assay, it is necessary to create a condition in which we have a high local concentration of myosin molecules but not a fully activated thin filament. We can achieve the latter by working close to the pCa_{50} of the thin filament, which falls around pCa 6 in our system (see figure 3.1 in chapter 3). A high local concentration of myosin

can be achieved by both increasing the S1-GFP concentration in the assay (5 to 10 nM) and by prolonging the duration of the acto-myosin complex by working at low [ATP]. Knowing that the lifetime of any given myosin molecule on actin is directly determined by the rate of ADP and Pi release and the waiting time for a new molecule of ATP to bind myosin (Gorga *et al.*, 2003; Kad *et al.*, 2005; Desai *et al.*, 2015), we used a low ATP concentration (0.1 µM) to increase the probability that a new myosin molecule would bind within an already locally activated area, preventing the complete turning on of the thin filament. By promoting the local recruitment of myosin, we can thus study S1-GFP detachment dynamics within highly concentrated active regions.

Figure 4.1a shows a representative kymograph of a thin filament in sub-maximal activating conditions, obtained by working at pCa 6, 0.1 µM ATP and S1-GFP at 5 nM. S1-GFP is seen binding to the thin filament in "patches" or locally active regions (some labelled A to E) throughout the tightrope. Although these can exist in more than one position within the same timeframe, the thin filament doesn't appear to be active throughout its full length, since regions depleted of fluorescence are clearly visible in the kymograph, demonstrating myosin preferential binding to already activated regions. The patches are also capable of shifting along the tightrope with respect to their starting position (e.g. patches C and E) with no apparent directional bias (Desai *et al.*, 2015), suggesting that the binding of a new S1-GFP to an already existing patch is an entirely stochastic process and can happen at both of its ends.

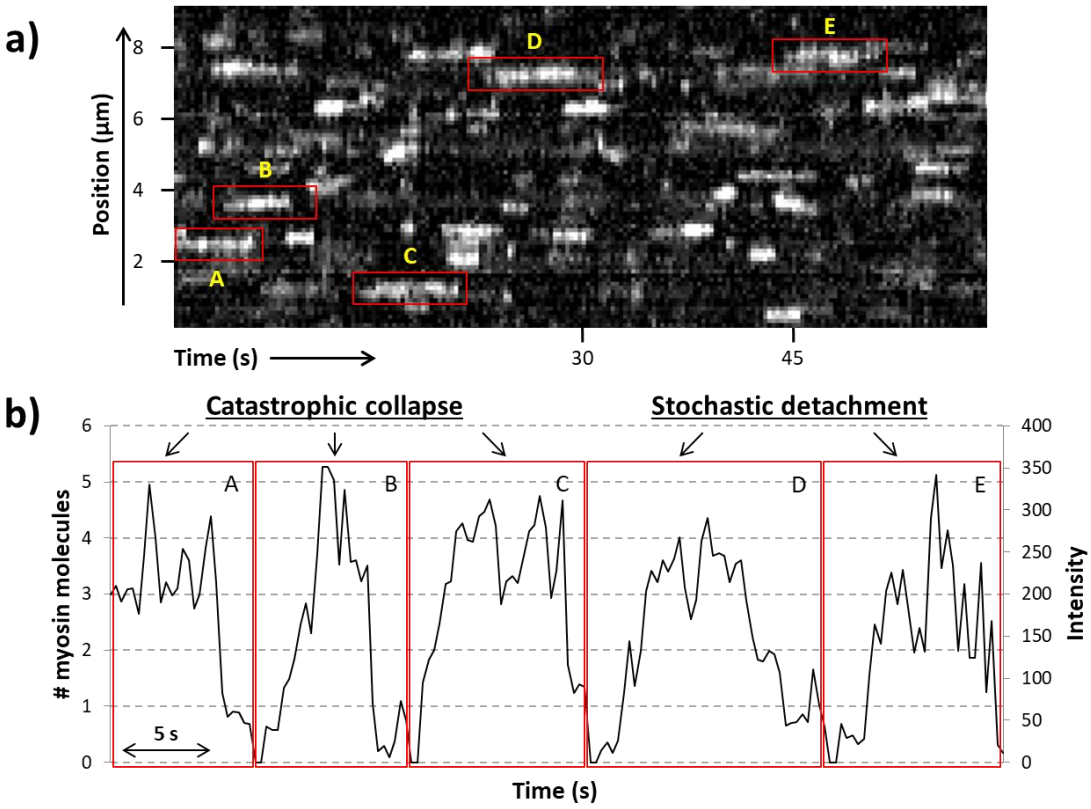

Figure 4.1: **Highlighting locally active regions in a kymograph.** a) representative kymograph of a thin filament in sub-maximal activating conditions, with some of the locally active regions highlighted by red boxes and labelled A to E and b) plot of the number of myosin molecules over time of each highlighted active region. Sudden collapse of the active region is seen in particular for area A, B and C, while regions D and E show more stochastic behaviour. Data was obtained imaging the interactions of 5 nM of S1-GFP with thin filaments at pCa 6, in the presence of 0.1 µM ATP.

We can plot the profile of the intensity vs. time for each patch and relate the intensity to the number of myosin molecules (as in figure 3.4 in chapter 3), obtaining the graph depicted in figure 4.1b. The binding of S1-GFP is seen to occur mostly in a step-wise fashion, as expected (patches B to E). The detachment of S1-GFP, however, is seen occur both via a stochastic step-wise release (patches D and E and middle part of A and C), mostly with transitions of a single myosin per event, and via a sudden collapse of up to five molecules at once (patches A, B and C), which we termed "catastrophic

collapse". Considering that the probability of a given number N of S1-GFP molecules detaching from the thin filament at the same time scales with the N-th power of the probability of each single event, the catastrophic collapse of an active region should be a highly unfavourable event; to understand the occurrence of these events in our kymographs we analysed our datasets using an unbiased statistical approach, aimed at visualising the probability of occurrence of the sudden collapse of active regions versus the stochastic detachment and step-wise release mechanism.

4.2.2 – De-convoluting kymographs into transition matrices

To study the catastrophic collapse of myosin patches and the binding or release events within each kymograph, we de-convolved the fluorescent intensity values in each pixel of a kymograph into number of myosins, using the Reversible-jump Markov Chain Monte Carlo (RJMCMC) stochastic algorithm. This particular analysis has been performed in collaboration with Dr. Hongsheng Dai and Madalina Mihailescu of the Department of Mathematical Sciences at the University of Essex, therefore is only explained in details in the Appendix (A.6). The output of the algorithm is a linear series of intensity values corresponding to the most likely intensity of a specific number of S1-GFP molecules. A kymographs is, as such, converted into number of molecules and then analysed using a script written in R (by M. Mihailescu and Dr. H. Dai), which consider the number of myosins in each pixel as a "state" of the acto-myosin system, therefore allowing us to study the binding and release of S1-GFP from the thin filament as transitions between states.

With this method, we measured the number of S1-GFP transitioning from an initial state i to a final state j after a single time frame (equivalent to a single frame or

vertical slice in a kymograph) and calculated the percentage of occurrence of each one, finally assembling the results into transition matrices shown in figure 4.2. Each table is the averaged result of three kymographs, each related to a different filament imaged at pCa 6 in the presence of 0.1 μM ATP and either 5 or 10 nM of S1-GFP (figure 4.2a and c respectively), with the number of transitions (figure 4.2b and d) being calculated as the sum of the transitions visualised in two of the three kymographs (one being unfortunately lost by our collaborators). The transition matrices have also been colour coded as a heat map to better visualise the differences in probabilities, according to the legend in figure 4.2.

The tables are read from left to right, with the first column representing the initial state i. Along each row of the following columns, we find the probability of transition to the each final state j state, $p_{i\to j}$, normalised such as $\sum_{j=0}^{n} p_{i\to j} = 1$, where n is the maximum number of myosin molecules seen in a cluster per condition (n = 8 for S1-GFP = 5 nM and n = 10 for S1-GFP = 10 nM, figure 4.2a and 4.2b respectively). This normalisation is done considering the maximum number of S1-GFP seen in a kymograph as the maximum state each active region can reach. Therefore, according to the rules of probability, the sum of each transition probability related to a given initial state (i.e. a raw) must be equal to one. The diagonal of each matrix is represented as dashes, to indicate that pauses (or missed transitions) within a time window are not noted in the calculation of the transition probabilities. Finally, the tables have been colour coded as a heat map from blue to red, blue representing the lowest values of transition probability and red the highest ones.

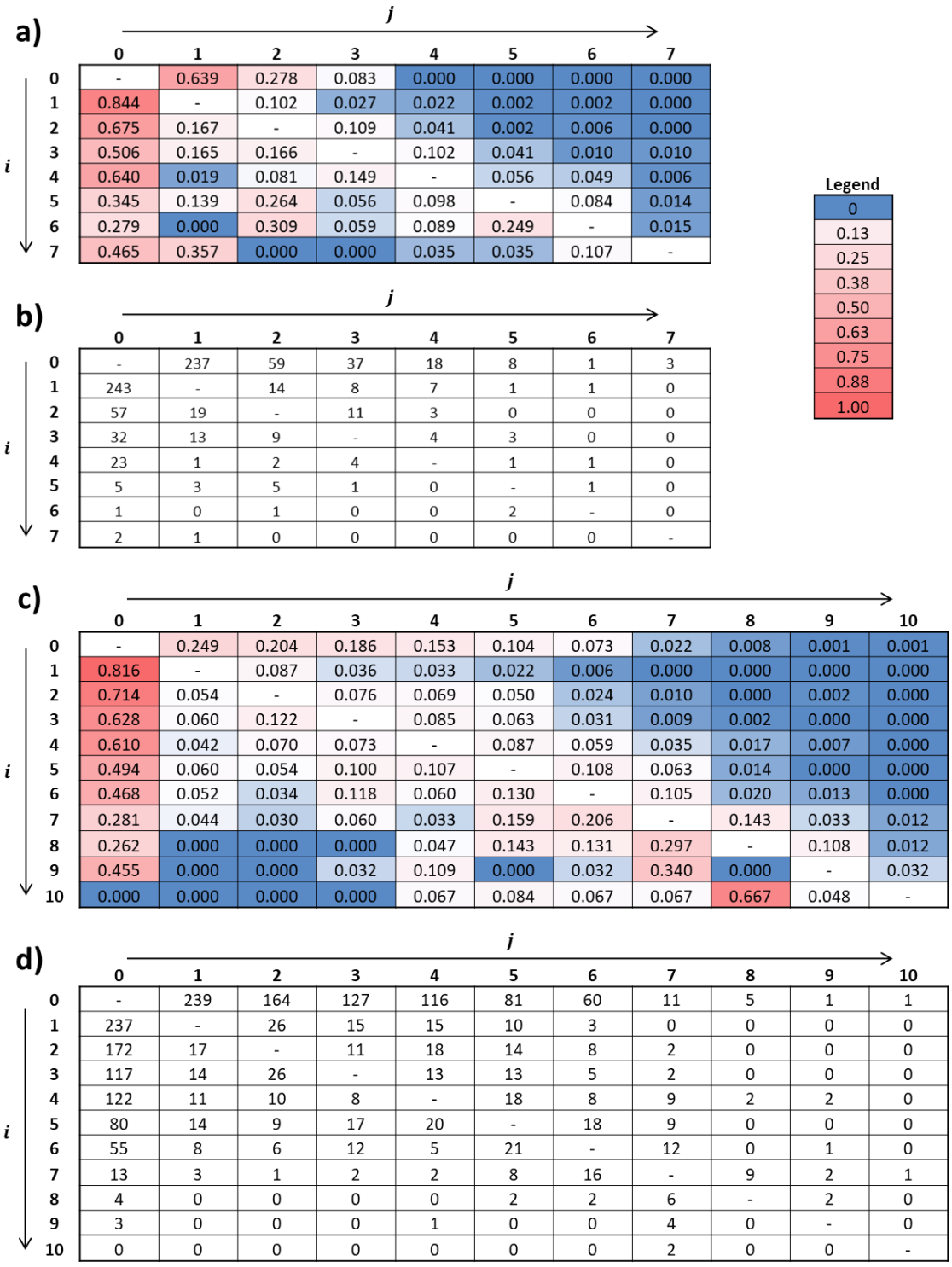

Figure 4.2: **Experimental transition matrices of myosin patches.** Probability of myosin binding and release events of thin filament at pCa 6, 0.1 µM ATP and S1-GFP equals to a) 5 nM and c) 10 nM, along with their respective number of events seen per transition b) and d). Each raw of the tables has been normalised and colour coded as detailed in the main text.

As an example, consider an active region with an initial number of S1-GFP molecules equal to 4 (i.e. i = 4); if to this region were to bind an extra two S1-GFP molecules within a frame (0.3 seconds), its final state would be equal to 6 (i.e. j = 6) and the probability of such transition would be equal to 0.049 for S1 = 5 nM and 0.059 for S1 = 10 nM (equivalent of saying that this transition occurs 4.9% and 5.9% of the times for an active region with 4 S1-GFP molecules). Conversely, if from this region one S1-GFP molecule were to release from the thin filament, its final state would be equal to 3, with the probability of such transition occurring being 0.149 and 0.073 for S1 = 5 nM and 10 nM respectively. However, if all the S1-GFP molecules were to release within 0.3 seconds, the final state of this active region would be 0, with the probability of this transition to occur being 0.64 S1 = 5 nM and 0.61 for S1 = 10 nM. Finally, if this patch was to neither acquire nor lose a S1-GFP within a frame, its final state would still be equal to 4 and thus fall on the diagonal of the matrix and its probability indicated by a dash, as it is not considered in the analysis and subsequent normalisation.

4.2.3 – Modelling the transition probability within an active region

To better understand our experimental results, we compared the tables shown in figure 4.2 with predicted transition matrices, obtained by modelling each transition as a purely stochastic process dependent on the rate of attachment and detachment of S1-GFP. Knowing that the ATP second-order binding rate constant k_T is 2.03 $\mu M^{-1}s^{-1}$ (see the appendix, A.5), the ATP concentration in our assay is 0.1 µM and the time between frames in our videos is 300 ms, therefore we calculate the probability of detachment P_d as

$$P_d = 1 - e^{-kt}$$

where $k = k_T * [ATP]$, making the term e^{-kt} the probability of an ATP molecule of binding to myosin, hence the probability of myosin staying attached to the thin filament. Since we are assuming that the detachment of multiple molecules from the thin filament is a stochastic process, the cumulative probability of detachment of n molecules in a cluster will scale with the nth power of P_d. We can write n as a difference between the initial (i) and the final (j) number of molecules $n = i - j$ (with $0 \leq j < i$ and $i > 0$) and therefore our probability of n molecules detaching $P_{d(n)}$, corresponding to a transition $i \rightarrow j$, becomes:

$$P_{d(n)} = P_d^n * \frac{i!}{j!\, n!}$$

where, the term $\frac{i!}{j!n!}$ acts as a scaling factor to account for all the possible combinations of molecules.

Likewise, the probability of a myosin joining an already active region can be calculated using the nth power of the attachment probability, P_a. Therefore, we calculated the probability of n molecules binding to a cluster, transitioning from an initial state i to a final state j, so that $0 < j > i$ and $i \geq 0$, as:

$$P_{a(n)} = \langle P_a \rangle^n$$

Considering the nature of our assay, P_a cannot be modelled reliably; we can, however, extrapolate it from the experimental data shown in figure 4.2, by simply calculating the mean of our transition rates where only one myosin is seen joining an active region, i.e. all the values directly to the right of the diagonal of the transition matrices. The mean attachment probabilities, when using either 5 nM or 10 nM of S1-GFP are found to be not statistically significantly different from each other (0.15 ± 0.03 (SEM) and 0.11 ± 0.01 (SEM) respectively, with p = 0.1853).

Figure 4.3 shows the resulting predicted matrices. As in figure 4.2, each matrix has been normalised so that the sum along each raw is equal to 1, and the diagonal is indicated by dashes since the model does not take into account missed transitions.

i \ j	0	1	2	3	4	5	6	7	8
0	-	0.842	0.133	0.021	0.003	0.001	8.34E-05	1.32E-05	2.09E-06
1	0.228	-	0.650	0.103	0.016	0.003	4.07E-04	6.44E-05	1.02E-05
2	0.010	0.367	-	0.524	0.083	0.013	0.002	3.28E-04	5.19E-05
3	4.67E-04	0.025	0.457	-	0.435	0.069	0.011	0.002	2.73E-04
4	2.19E-05	0.002	0.043	0.517	-	0.369	0.058	0.009	0.001
5	1.05E-06	9.46E-05	0.003	0.062	0.557	-	0.318	0.050	0.008
6	5.07E-08	5.49E-06	2.48E-04	0.006	0.081	0.584	-	0.278	0.044
7	2.49E-09	3.15E-07	1.70E-05	0.001	0.009	0.100	0.604	-	0.247
8	1.27E-10	1.83E-08	1.16E-06	4.18E-05	0.001	0.014	0.123	0.635	-

Legend
0
0.13
0.25
0.38
0.50
0.63
0.75
0.88
1.00

Figure 4.3: **Calculated transition matrix of S1-GFP on thin filaments.** Probability of myosin binding and release events scaled for different patches sizes. Each raw has been normalised to give a sum equal to 1. The table has been colour coded as a heat map to better visualise the differences in probabilities.

Looking at a similar cases used as examples for figures 4.2, we consider an active region with an initial number of S1-GFP molecules equal to 4; in the predicted transition matrix, the probability of this active region to gain an extra two S1-GFP molecules within a frame (0.3 seconds), thus going from an initial state i = 4 to a final

state j = 6, has a probability to occur of 0.058 (equivalent of saying that this transition can occur 5.8% of the times). Conversely, the probability of an S1-GFP molecule to release from an active region with 4 other molecules is of 0.517. However, the probability of all the S1-GFP molecules to release within 0.3 seconds would be equal to $2.19 \cdot 10^{-5}$, highlighting the difference between the experimental data and the probabilistic model.

4.3 – Discussion

The comparison of the experimental transition matrices with the calculated matrix, allows us to understand the nature of the association and dissociation of myosin to the thin filament. The modelled transition matrix show that the probability of association and dissociation decreases further away from the diagonal along each raw in an exponential fashion, as expected from a stochastic model. The same is seen in the experimental transition matrices for both concentrations of S1-GFP used, showing an inverse proportionality of the transition probability to the number of myosin molecules that leave the thin filament at once. These results indicate that the association and dissociation within an open active region is a stochastic process, dependent only on the power of the binding and release rate of a single myosin.

Furthermore, in the calculated matrix, the probability of a single myosin association is inversely proportional to the cluster size, the opposite of what is found for the detachment probability. In the experimental matrices, however, it is hard to define a

specific trend, with association and dissociation probabilities being similar all throughout. Since each experimental transition matrix is an average of only three transition matrices obtained in the same experimental conditions, we correlate this difference with the experimental error caused by the low number of data points. Furthermore, by looking at the number of times each transition has been observed throughout all experiments, it is clear that the transitions 0 to 1 and 1 to 0 (i.e. the binding and release of a single S1-GFP) are preferred against the formation of clusters, which highlights the different significance within the probabilities seen for large number of clusters and the difficulty, as well as the importance, in tuning the experimental conditions to achieve sub-maximal activating conditions.

The main difference between the experimental and calculated transition matrices is, however, seen in the first column (j = 0), in the form of a highly increased probability for the complete collapse of an active region in our experimental dataset. This behaviour is the most seen for each cluster size i (figure 4.2b and d) and is in line with the raw data seen in the kymograph in figure 4.1, where the fluorescence intensity of active regions drops suddenly, hinting at the simultaneous release of a large number of myosin molecules.

We can exclude photobleaching as a cause for the increased probability, since we know that at 0.1 μM ATP the average lifetime of a single S1-GFP on a thin filament is of 2.3 seconds (see appendix A.5), longer than our time resolution of 300 ms; moreover, photobleaching would be seen as a step-wise decay in fluorescence and would not explain the high probability of detachment seen for large myosin clusters, leaving us with the hypothesis that it is a concerted mechanism, that we term catastrophic collapse.

The only likely protein that would be capable of exerting such a critical effect is tropomyosin, meaning that the catastrophic collapse observed here could be an active way of turning off the thin filament during sarcomere relaxation. Our data also suggests that the thin filament is not turned off all at once, since in the kymographs we can still see regions of activation further away from a collapsed myosin patch (figure 4.1). Several studies have found that the regulatory unit size of the thin filament spans up to 14 actin monomers (Geeves and Lehrer, 1994; Maytum *et al.*, 1999; Kad *et al.*, 2005) and can contain up to 11 myosin molecules (Desai *et al.*, 2015). These results are consistent with our findings, since the maximum number of myosin molecules found within an active region in our experiments is 7 at [S1-GFP] = 5 nM and 10 at [S1-GFP] = 10 nM, as shown in figure 4.2a and c. This suggests that the active regions created in sub-maximal activating conditions are similar in size than a thin filament regulatory unit, a distance determined by tropomyosin shifting from the closed to the open position, caused by the binding of a first myosin, further implying that tropomyosin must be involved in the catastrophic collapse mechanism.

However, the resolution of our optical microscope is diffraction limited, and prevent us to distinguish each single myosin molecule and precisely model the relaxation mechanism. Many questions still need to be answered: how would tropomyosin provoke the instantaneous release of myosin? Is its mechanism based on elastic forces, where the more myosin molecules present, the more strain is exerted on tropomyosin, leading to a force build-up that eventually breaks down and causes tropomyosin to return to a less energetic position? Is calcium releasing from the troponin complex partly responsible, allowing direct competition between the TnI subdomain and myosin, forcing tropomyosin back in its blocked position? Is actin involved in this

process and how? Would it be possible for a large amount of myosin molecules to modify its helical structure until it is not sustainable anymore? More detailed experiments are necessary to answer all these questions, but this study could pave the way for a better understanding of the relaxation process of the sarcomere, leading to a better understanding of diseases that impair heart relaxation, such as Hypertrophic Cardiomyopathy (Maron *et al.*, 2009; Bai *et al.*, 2011; Coppini *et al.*, 2014).

CHAPTER 5

CHARACTERIZING THE CONSEQUENCES OF N-TERMINAL MYOSIN BINDING PROTEIN-C FRAGMENTS INTERACTIONS WITH ACTIN

5.1 – Introduction

Cardiac myosin binding protein-C (cMyBP-C) is a sarcomeric protein that is thought to function as a modulator of muscle contraction and is known to play an important role in Hypertrophic Cardiomyopathy (HCM) (Harris *et al.*, 2011). As mentioned in chapter 1, about 33% of HCM causing mutations are found in cMyBP-C, making it the second most important protein that leads to the genetic disease (Maron *et al.*, 2012). However, before embarking on understanding the role of these mutations in disease, we must first have a clear understanding of its role in muscle contraction. To this end, we focused our studies in understanding cMyBP-C's role in thin filament activation, working with three different murine cMyBP-C N-terminal fragments, namely C0C3, C0C1 and C0C1f (C0C1 with the addition of the next 17 amino acids from the M-domain). We explored the role of each fragment on myosin binding to thin filaments,

as well as their binding behaviour on thin filaments on their own. These studies provide evidence for the molecular mechanism of how cMyBP-C could function both as an activator and repressor of muscle contraction.

5.2 – Results

5.2.1 – Investigating the effects of cMYBP-C N-terminal fragments on myosin binding to thin filaments

The effects of C0C3, C0C1f and C0C1 on acto-myosin interactions were investigated by examining the level of 15 nM of S1-GFP binding to the thin filament in the presence and absence of 1 μM of unlabelled fragments, both at low and high calcium (pCa 7 and pCa 4 respectively), imaging ten or more tightropes across more than 3 flow cells per condition. Figure 5.1 shows examples of kymographs obtained in the experiments.

In agreement with (Desai *et al.*, 2015), the kymograph at low calcium with no fragment in figure 5.1a shows very few S1-GFP binding events, since 93% of the thin filament is in its blocked state (Desai *et al.*, 2015). However, introducing C0C3 increases the number of binding events, while the presence of C0C1 and C0C1f does not affect S1-GFP binding. The opposite is observed at high calcium or pCa 4 in the top panel of figure 5.1b where, in the absence of fragment, myosin is seen binding frequently to the thin filament, with the formation of clusters caused by myosin cooperativity. In contrast, when C0C3 is introduced in the assay at high calcium, the amount of myosin binding to the thin filament is drastically reduced. As for low calcium, the presence of C0C1 and C0C1f does not lead to any visible changes in the amount of myosin bound.

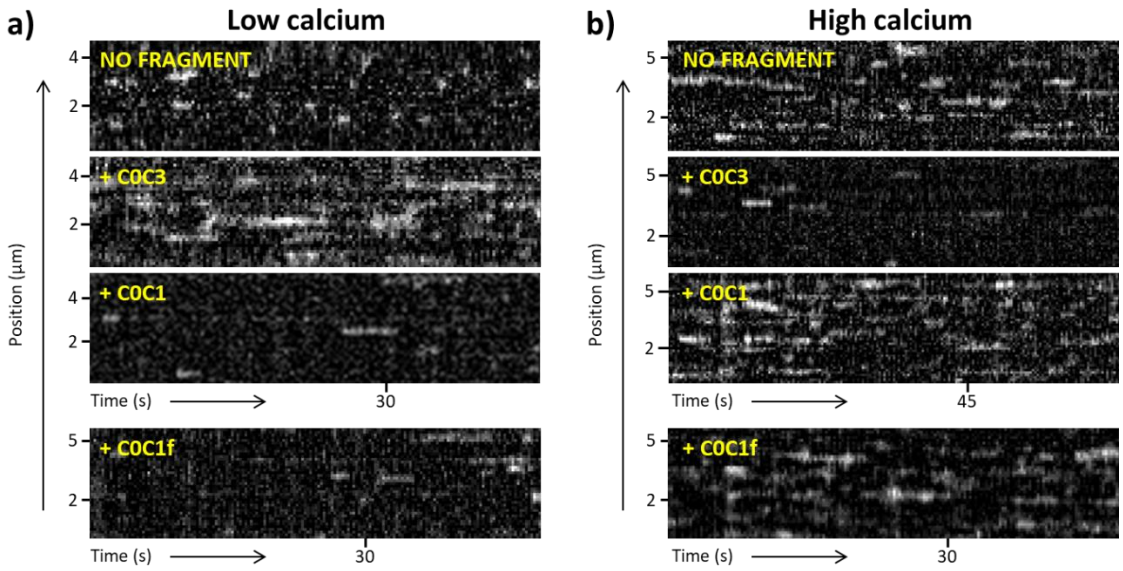

Figure 5.1: **Effects of cMyBP-C N-terminal fragments on acto-myosin interactions.** Representative kymographs of S1-GFP binding to reconstituted thin filaments in the absence and presence of cMyBP-C N-terminal fragments (from top to bottom, no fragment, C0C3, C0C1 and C0C1f) obtained at a) low calcium (pCa 7) and b) high calcium (pCa 4). Data were collected using 15 nM of S1-GFP and 1 µM of fragment, imaging more than 10 tightropes per condition throughout more than 3 flow chambers.

To quantify the changes in S1-GFP binding we calculated the average intensity per pixel for each kymograph and averaged all data collected in the same experimental conditions. Normalising the data to the binding of S1-GFP at the same calcium concentration in the absence of the construct gives us the relative change in intensity caused by the presence of the cMyBP-C fragment, as shown in the bar chart in figure 5.2 (with n being the number of filaments imaged over the number N of replicated flow chambers).

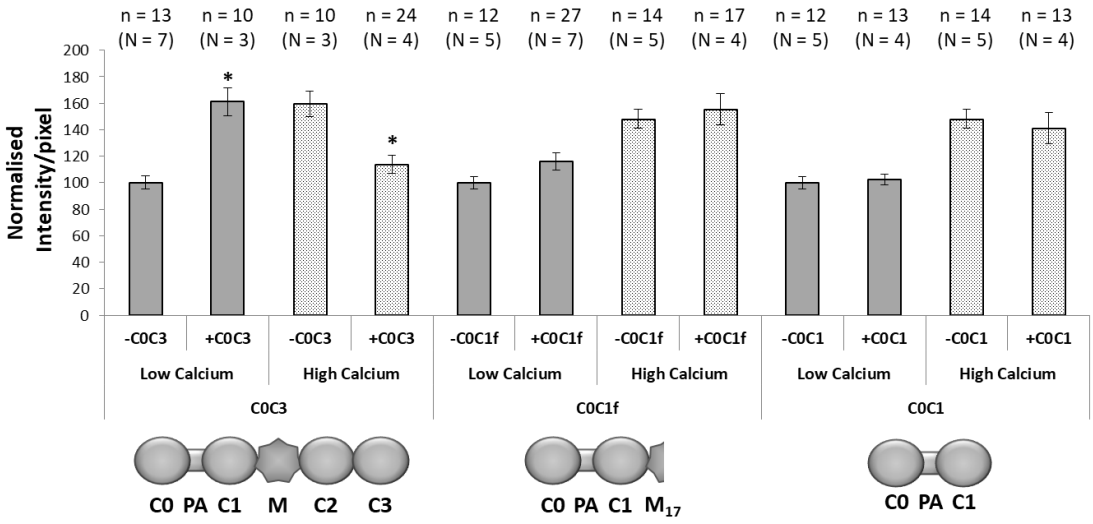

Figure 5.2: **Quantifying cMyBP-C N-terminal fragments effect on S1-GFP binding to thin filaments.** Bar chart of the average intensity/pixel ratio in the kymographs in figure 5.1 of S1-GFP binding in the absence and presence of different cMyBP-C N-terminal fragments. The values have been normalised to each respective control experiment (i.e. no fragment present at same [Ca^{2+}]). Data were collected using 15 nM S1-GFP w/ or w/o 1 µM of fragment, with n values representing the number of tightropes imaged per condition while the N in parenthesis indicate the number of flow chambers used per condition. Only results obtained in the presence of C0C3 showed a statistically significant (indicated by the *) increase (61.2% ± 11.7 (SEM), $p < 0.001$) or reduction (45.5% ± 11.9 (SEM), $p = 0.009$) in S1-GFP binding at low and high calcium, respectively.

At low calcium there is a significant ($p < 0.0001$) increase in S1-GFP binding (61.2% ± 11.7) in the presence of C0C3. Whereas at high calcium, S1-GFP binding is significantly ($p = 0.009$) reduced to 45.5% ± 11.9 with C0C3. Interestingly, no significant difference in myosin binding is seen throughout the experiments performed with the shorter fragment C0C1f (16.0% ± 8.2, $p = 0.1390$ at low calcium and 7.5% ± 13.8, $p = 0.6126$ at high calcium) and C0C1 (2.4% ± 6.2, $p = 0.7072$ at low calcium and -6.8% ± 13.7, $p = 0.6189$ at high calcium), indicating that the deleted subdomains M to C3 are necessary for the modulation of acto-myosin interactions.

5.2.2 – Visualising cMyBP-C N-terminal fragments binding to actin

Previous studies have shown that cMyBP-C N-terminus directly binds myosin in its S2 region and its regulatory light chain (Starr and Offer, 1978; Gruen and Gautel, 1999; Kunst *et al.*, 2000; Ratti *et al.*, 2011; Kampourakis *et al.*, 2014). Other groups also show that it can bind to actin through several sites found throughout its whole N-terminus (Mun *et al.*, 2011, 2014; Belknap, Harris and White, 2014; Harris *et al.*, 2016). Since in our previous experiments we are not able to determine whether the fragments are binding directly to S1-GFP, the thin filaments, or both, we cannot exclude these scenarios. Therefore, in order to have a better understanding of cMyBP-C mechanism, we fluorescently tagged the fragments with Cy3 (see section 2.6) and studied their binding properties in our tightrope assay in the absence of myosin. Data were collected by visualising 20 nM of fragment on actin filaments or on reconstituted thin filament at both low and high calcium, throughout 2 or more flow chambers, and with each tightrope being exposed for 1 sec.

Figure 5.3 shows examples of images of C0C3 bound to tightropes in different conditions. There is a striking difference between the images, where only a few molecules are seen bound on unregulated actin (figure 5.3a) and to thin filaments at low calcium (figure 5.3b), unlike at high calcium, where thin filaments appear highly decorated (figure 5.3c).

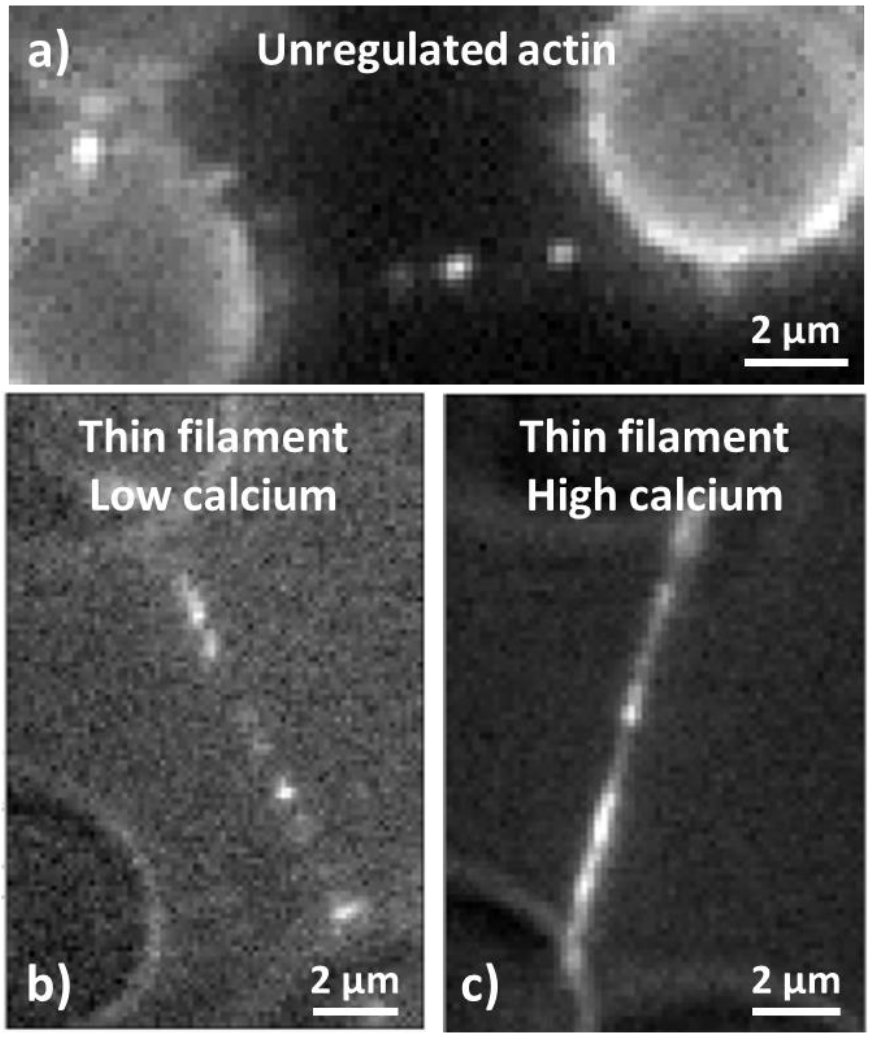

Figure 5.3: **Imaging fluorescent C0C3.** Pictures of tightropes obtained with 20 nM of Cy3-C0C3 on a) unregulated actin filaments and on thin filaments at b) low calcium (pCa 7) and c) high calcium (pCa 4), collected using an exposure time of 1 second.

On the contrary, no difference is observed in images of C0C1f and C0C1 on regulated thin filaments, as shown in figure 5.4, obtained in the same conditions as in figure 5.3.

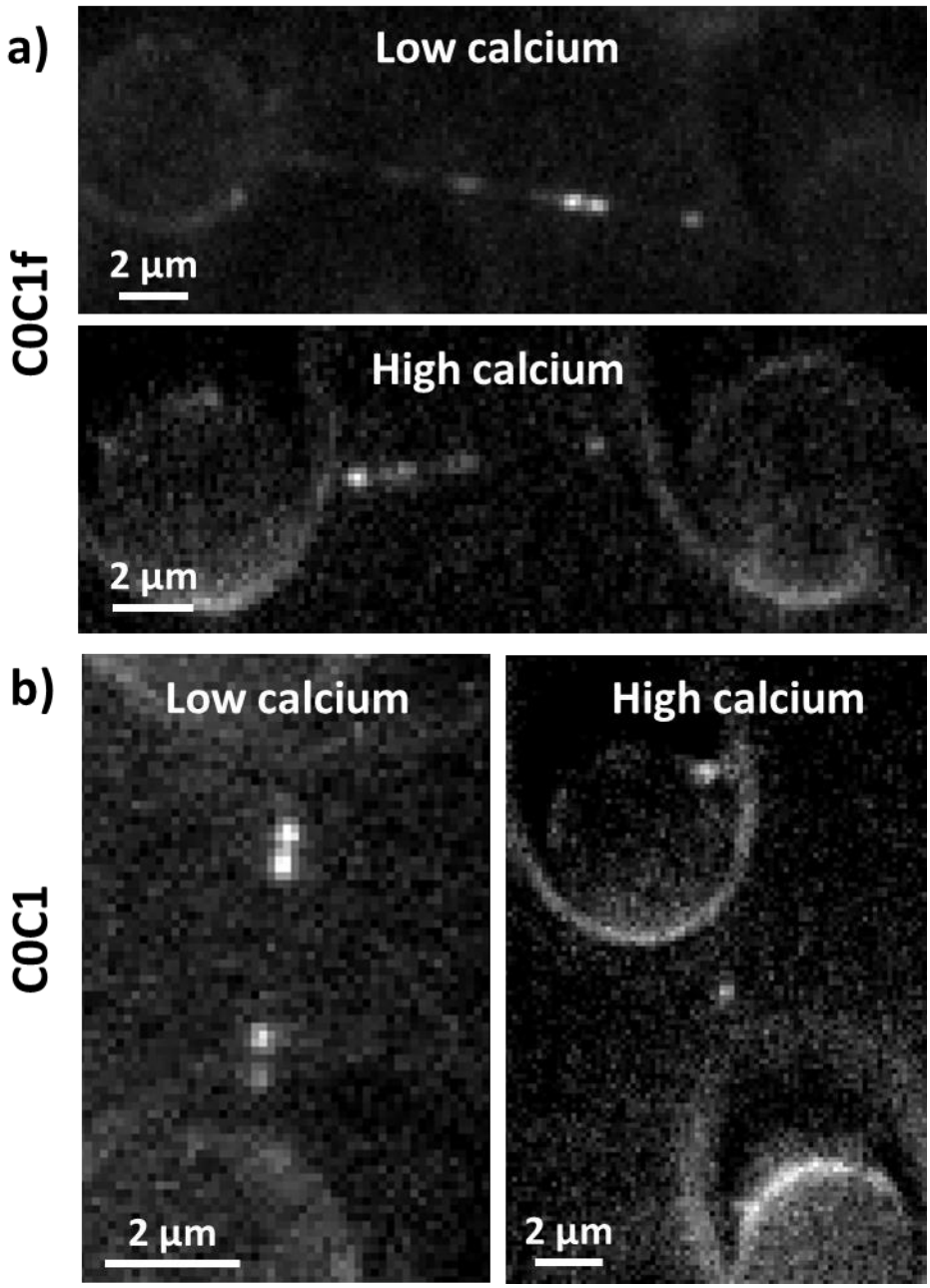

Figure 5.4: **Imaging fluorescent C0C1f and C0C1.** Pictures of 20 nM of a) Cy3-C0C1f and b) Cy3-C0C1 on thin filament tightropes at low and high calcium (pCa 7 and pCa 4 respectively), collected using an exposure time of 1 second.

We can quantify the level of decoration by calculating the average number of molecules bound per unit length of thin filament (µm). To do this, we can follow the approach used by (Desai *et al.*, 2015) and (Iino *et al.*, 2001) and fit each fluorescence

point spread function to a Gaussian distribution, the intensity of which determines how many molecules are associated within it. This requires knowing the fluorescence intensity of a single molecule bound to the thin filament, which we measured by fitting a distribution of intensity values at low calcium, where molecules are assumed to bind mostly as single entities (an example is seen in figure 5.5 for C0C3).

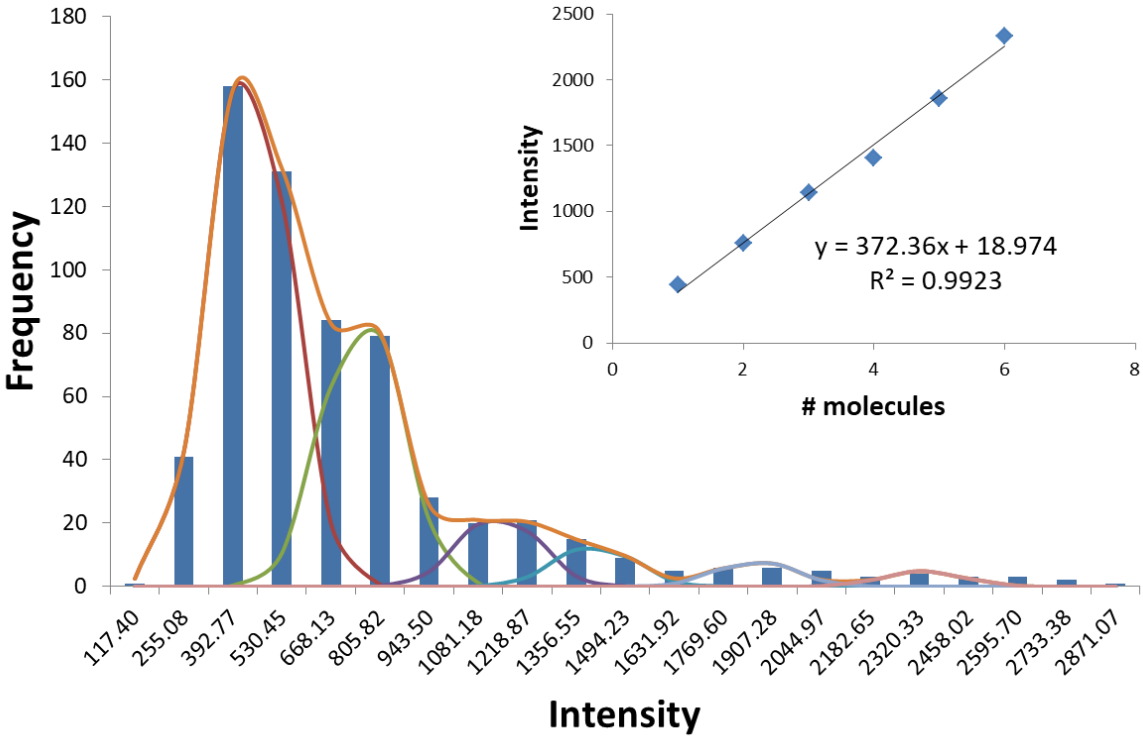

Figure 5.5: **Calculating the fluorescent intensity of a single binder.** A histogram of the intensities of the fluorescence point spread function of C0C3, collected at pCa 7. The histogram is fit to a number of Gaussian distributions, whose mean values are plot as a function of the hypothetical number of molecules associated with it and fit to a straight line, where the slope corresponds to the intensity of a single binder (inset).

Throughout these experiments we kept the frame rates constant, to ensure that the fluorophores emit approximately the same amount of light (Walcott and Kad, 2015).

The histogram in figure 5.5 was fitted to six Gaussian distributions (see Appendix A.7 for details) using the least square displacement method and the Solver Add-in for Office Excel, which uses an algorithm to vary the fitting parameters until a minimum value between the data and the fit is found. The intensity and the average of each of the six Gaussian distributions were fit independently while their standard deviation was constrained to one value for all, to better represent the experimental distribution of intensities associated to multiple unresolvable fluorescent molecules. Table 5.1 summarises the values of the amplitude, mean and standard deviation (S.D.) obtained for each Gaussian distribution.

	Gaussian 1	**Gaussian 2**	**Gaussian 3**	**Gaussian 4**	**Gaussian 5**	**Gaussian 6**
Amplitude	170.94	87.43	22.61	12.96	7.98	4.89
Mean	439.06	757.19	1139.28	1407.72	1859.92	2330.27
S.D.	110.38	110.38	110.38	110.38	110.38	110.38

Table 5.1: Summary of the values of amplitude, mean and standard deviation (S.D.) of each Gaussian distributions obtained from the histogram in figure 5.5.

Plotting the mean values of each Gaussian distribution versus the predicted number of molecules gives us the linear chart in the inset of figure 5.5, with a slope of 372.36 and an intercept of 18.97. We consider the slope as the average fluorescence intensity of a single C0C3 molecule and the intercept its associated error. Using this value we determined the level of C0C3 decoration at low and high calcium to be 1 ± 0.12 and 5.69 ± 0.55 molecules/μm respectively. These two values are found to be statistically significantly different, with a $p < 0.0001$. Remarkably, C0C3 decoration of unregulated

actin with no calcium yielded a value of 1.22 ± 0.11 molecules/µm, not statistically significant from the decoration of C0C3 seen on thin filaments at pCa 7 (p = 0.1813).

For C0C1f, no change in decoration of thin filaments was observed (figure 5.4a) between high and low calcium (1.14 ± 0.11 and 1.61 ± 0.21 molecules/µm respectively, p = 0.0523), while C0C1 (figure 5.4b) decorated thin filaments more avidly at pCa 7 (2.76 ± 0.37 molecules/µm) compared to pCa 4 (0.73 ± 0.23 molecules/µm; significantly different with p = 0.0055). Table 5.2 shows a summary of all the decoration results, along with details on the number of filaments imaged (n) and flow cells used (N).

	C0C3			**C0C1f**		**C0C1**	
	ACTIN	**THIN FILAMENTS**		**THIN FILAMENTS**		**THIN FILAMENTS**	
[Calcium]	**-**	**pCa 7**	**pCa 4**	**pCa 7**	**pCa 4**	**pCa 7**	**pCa 4**
Mean (molecules/µm)	1.22	1.00	5.69	1.14	1.61	2.76	0.73
SEM	0.11	0.12	0.55	0.11	0.21	0.37	0.23
n (filaments)	47	50	28	94	99	68	19
N (flow cells)	2	11	2	9	5	7	4

Table 5.2: Results of the decoration of unregulated actin/reconstituted thin filaments by cMyBP-C fragments, indicating the mean (molecules/µm), standard error of the mean (SEM), filaments imaged (n) and flow chambers used (N).

The number of molecules per fluorescent spot also provides information on the cooperative binding of cMyBP-C fragments. Figure 5.6 shows histograms of the number of molecules within each fluorescent spot or cluster for C0C3 and C0C1f at low and high calcium, normalised to the total number of molecules.

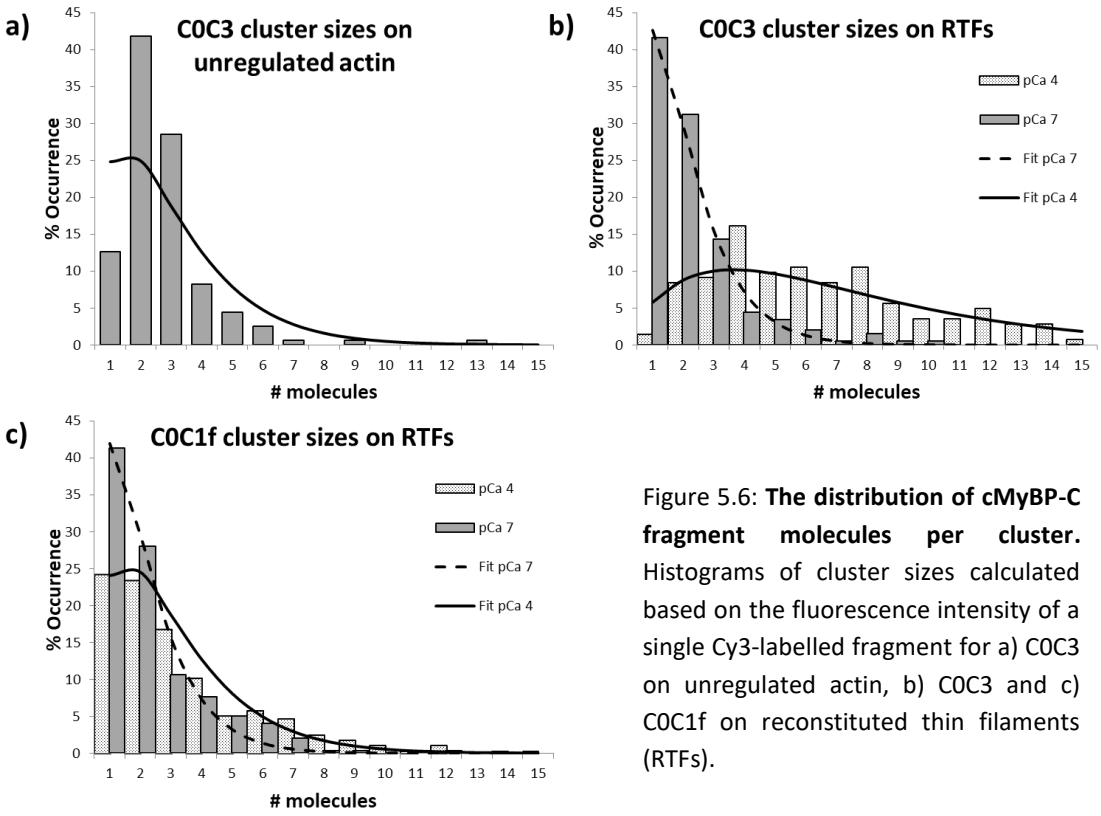

Figure 5.6: **The distribution of cMyBP-C fragment molecules per cluster.** Histograms of cluster sizes calculated based on the fluorescence intensity of a single Cy3-labelled fragment for a) C0C3 on unregulated actin, b) C0C3 and c) C0C1f on reconstituted thin filaments (RTFs).

These histograms can be fit using a Flory-Schulz distribution (Flory, 1936), which predicts the weight fraction of a polymer through the probability of association of its monomers, as described by the following equation:

$$W_l = l \cdot p^{(l-1)} \cdot (1-p)^2$$

where W_l is the weight fraction (termed % occurrence in figure 5.6), p is the probability of association and l is the number of molecules in the cluster (polymer length). The probability is calculated via a quadratic binding isotherm taking into account the cMyBP-C fragment concentration $[C]$, the available actin concentration $[A]$ and the fragment affinity for actin K_C, as described by:

$$p = \frac{([A] + [C] + K_C) - \sqrt{([A] + [C] + K_C)^2 - 4[C][A]}}{2[C]}$$

However the available actin concentration depends on the thin filament activation state and consequently on the calcium concentration $[Ca^{2+}]$. Hence, when using thin filaments, we calculated it according to:

$$[A] = \frac{[Ca^{2+}]}{k_{Ca} + [Ca^{2+}]} * \varphi$$

where K_{Ca} is the thin filament calcium affinity and φ is a scaling factor that accounts for the loss of thin filaments as they are suspended between the beads in our assay. This value was constrained to be larger than zero and lower or equal to the maximum amount of actin in the flow cell (or nominal concentration), which is the concentration of unregulated actin/reconstituted thin filaments flowed in the microfluidic chamber to suspend the filaments. When considering C0C3 binding to unregulated actin, $[A]$ was set to be equal to nominal concentration, since there is no calcium dependent mechanics that alters the availability of actin binding sites.

The K_{Ca} (affinity of calcium binding to thin filaments) was determined to be 0.3 µM (pCa_{50} of ~6.5), the C0C3 affinity for unregulated actin was determined to be 486.3 nM, while for reconstituted thin filaments (RTFs) at pCa 7 and pCa 4 was 212.8 nM and 153.1 nM respectively. Finally, C0C1f was found to have an affinity to RTFs equals to 207.7 nM and 470.1 nM at pCa 7 and pCa 4 respectively. The magnitude of the change in COC3 affinity between calcium concentrations is not substantial therefore we can state that calcium does not affect the binding of C0C3; C0C1f, however, shows a larger

change and therefore calcium may be reducing the binding affinity to thin filaments for this construct, although to no effect on the number of bound molecules, as seen in figure 5.6c. Insufficient binding of C0C1 at high calcium did not allow us to conduct the same analysis reliably.

5.2.3 – Dynamics of cMyBP-C N-terminal fragments on RTFs

So far we have discussed the effect of calcium on C0C3 binding to thin filament without taking into account its dynamics. However, upon closer inspection of the kymographs and on long timescales, some of the C0C3 molecules have been seen diffuse along the tightrope, evident as movement along the y-axis (figure 5.7a). We set out to further investigate this by collecting movies of filaments imaged at 1 frame per second (fps) for up to 5 minutes, at a concentration of 20 nM of C0C3 on unregulated actin and RTFs at pCa 7, as well as 20 nM of C0C1f or C0C1 at pCa 7; at pCa 4, to compensate for decoration levels that enable individual molecules to be distinguished, 5 nM C0C3 and C0C1f or 20 nM C0C1 was used. Figure 5.7b shows a bar chart of the % of diffusing molecules per condition, with N being the number of replicated flow chambers and n the total number of molecules imaged. To prove that diffusion is not concentration dependent and was not altered by the ratio of labelled:unlabelled molecules (see Chapter 2, section 2.6), we collected movies on thin filaments at low calcium using 20 nM of fluorescent C0C3 and 90 nM of unlabelled C0C3 (indicated as pCa 7 (+) in figure 5.7b).

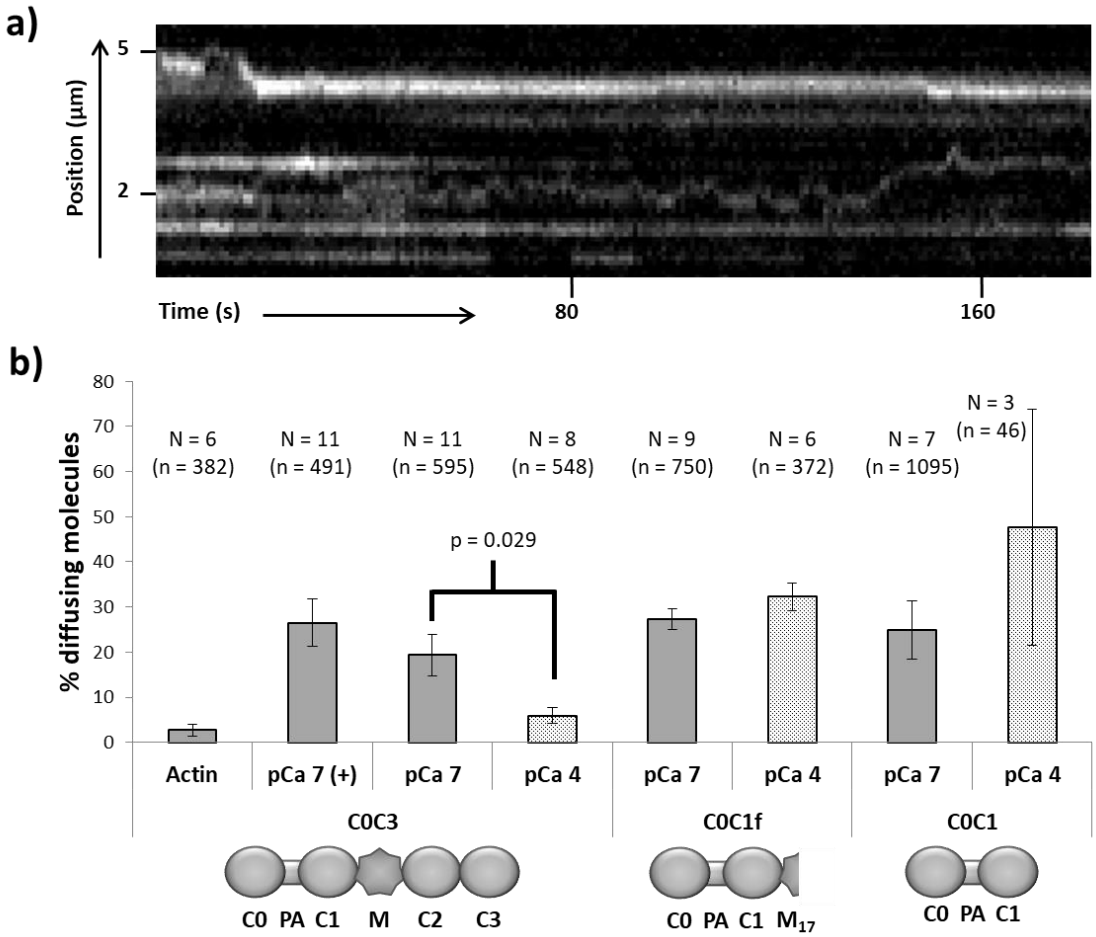

Figure 5.7: **Comparing the dynamics of cMyBP-C fragments on actin and thin filaments.** a) kymograph of molecules of C0C3 diffusing along a thin filament tightrope imaged at pCa 7, along with static ones; b) comparison of the % of diffusing molecules for C0C3 on unregulated actin and C0C3, C0C1f and C0C1 on thin filaments at low calcium (pCa 7) and high calcium (pCa 4). Values are averages of percentages calculated over N different flow cells, while (n) is the total number of molecules visualised. A control experiment was necessary to confirm that diffusion was not caused by the labelled:unlabelled ratio, therefore we collected data on thin filaments at low calcium using 20 nM of fluorescent C0C3 and 90 nM of unlabelled C0C3, indicated as pCa 7 (+).

The number of diffusing C0C3 molecules was found to be not significantly different ($p = 0.3232$) when imaging with an excess of unlabelled C0C3 (26.5 % ± 5.3 molecules diffusing at pCa 7 (+), N = 11, where N is the number of experiments performed) or

with fluorescent C0C3 only (19.4 % ± 4.6 molecules diffusing at pCa 7, N = 11). However, this amount decreased significantly (p = 0.029) to 6.0 % ± 1.8 (N = 8) at high calcium. The value obtained at high calcium is, however, not significantly different (p = 0.1882) than the one found when using unregulated actin, with only 2.7 % ± 1.3 (N = 6) molecules diffusing. This last result in particular also proves that diffusion is not caused by aggregation of molecules in solution and that the difference in C0C3 concentration used between pCa 7 and pCa 4 does not alter diffusional properties.

In comparison, C0C1f showed no significant difference (p = 0.2025) in diffusive behaviour at both low and high calcium, 27.3 % ± 2.2 (N = 9) and 32.3 % ± 3.1 (N = 6) respectively. Similarly, C0C1 also showed no change in the level of diffusion with calcium, with about 24.5 % ± 6.4 (N = 7) of the molecules diffusing at pCa 7 versus 47.7 % ± 26.2 (N = 3) at pCa 4 (p = 0.2542).

Throughout all the conditions explored, about 60% of the diffusing molecules where diffusing individually, while the rest diffused in clusters of 2 or more molecules; the only exception we found was C0C1 at low calcium, where only 35% of the molecules were diffusing individually. Using only the molecules diffusing individually, we calculated the diffusion constants and alpha coefficient using the mean squared displacement MSD:

$$MSD = \frac{1}{n}\sum_{i=1}^{n}\left(x_i(t) - x_i(0)\right)^2 = 2Dt^{\alpha}$$

where D is the diffusion constant of the molecule, t is the time between each diffusional step x_i respect to its reference position $x_i(0)$ and α is a coefficient that

denotes the nature of the diffusion, being it driven by a force ($\alpha > 1$), random ($\alpha = 1$) or constrained by other mechanisms ($\alpha < 1$). Applying this analysis to our data, results in the values of D and α listed in table 5.3.

	C0C3						**C0C1f**				**C0C1***	
	pCa 7 (+)		**pCa 7**		**pCa 4**		**pCa 7**		**pCa 4**		**pCa 7**	
	D	**α**	**D**	**α**	**D**	**α**	**D**	**α**	**D**	**α**	**D**	**α**
Mean	4.23 $\cdot 10^{-3}$	1.05	6.28 $\cdot 10^{-3}$	0.98	6.81 $\cdot 10^{-4}$	1.36	4.06 $\cdot 10^{-3}$	1.00	2.95 $\cdot 10^{-3}$	0.88	1.13 $\cdot 10^{-3}$	0.71
SEM	8.91 $\cdot 10^{-4}$	0.06	1.24 $\cdot 10^{-4}$	0.07	2.13 $\cdot 10^{-4}$	0.16	8.99 $\cdot 10^{-4}$	0.07	1.15 $\cdot 10^{-3}$	0.08	3.96 $\cdot 10^{-4}$	0.09
n	37	39	32	33	5	6	39	39	15	15	9	12

Table 5.3: Values of the mean diffusion constant (in $\mu m^2/s$) and coefficient alpha in the different conditions explored, along with the standard error of the mean (SEM) and the number of molecules (n) used in the calculation. *Due to insufficient binding, diffusion data was not acquired for C0C1 at pCa4.

These results indicate that the fragments are diffusing randomly along the thin filament. We can check the statistical differences between the diffusion constant values in logarithmic space (since the MSD depends on the α power of D), resulting in no difference between the diffusion at low calcium of C0C3 and C0C1f and a statistically significant difference when compared to C0C1 ($p = 0.1516$ and $p < 0.0001$ respectively). In addition, the diffusion of C0C3 at low calcium is found to be statistically significantly lower than that at high calcium ($p < 0.0001$), although the same cannot be said for C0C1f ($p = 0.4569$). The addition of extra unlabelled fragment is also seen to not produce any effect on the diffusive characteristics of C0C3, with no statistically significance seen between the two diffusion constants ($p = 0.1822$).

Diffusion along a lattice can be described as multiple discrete steps, allowing us to calculate the average step size of the fragments on the thin filament, provided the lifetime of each one on actin is known. Laser trap studies (Weith *et al.*, 2012) indicated that C0C3, C0C1f and C0C1 can bind to actin with two different lifetime populations, a very short one of less than 30 ms and one longer than 200 ms. Considering that the reported longer events were ~60 times less frequent in their experiments (Weith *et al.*, 2012), we used the short attached lifetime to calculate the step size for each fragment at low calcium, according to the following equations (Kad *et al.*, 2010):

$$\frac{steps}{s} = \frac{1}{\tau} = \frac{2D}{l^2} \qquad\qquad l = \sqrt{2D\tau}$$

where τ is the attached lifetime, D is the diffusion constant and l is the average step size. This provides in an average step size of 16.63 ± 2.80 nm (SD) for C0C3, 12.42 ± 1.69 nm (SD) for C0C1f and 6.88 ± 1.32 nm for C0C1.

5.3 – Discussion

5.3.1 – The whole N-terminus of cMyBP-C is responsible for thin filament activation

Truncation constructs of cMyBP-C enabled us to isolate which fragments have the capability to modulate thin filament activity. Only the full N-terminal fragment C0C3 was found to be able of both activating and inhibiting myosin attachment to thin filaments. The activation observed at low calcium was seen to be caused by a direct

increase in myosin binding to the thin filament, whereas inhibition was caused by a substantial decrease in the amount of myosin binding at high calcium. This implies that the modulation of velocity observed in vitro motility assays experiments (Razumova *et al.*, 2006; Weith *et al.*, 2012) derives from the availability of myosin for motion generation. In agreement with the ATPase data in (Belknap *et al.*, 2014), removing of the M- along with the C2 and C3 subdomains produced fragments that neither activated nor inhibited myosin binding. However, restoration of the first 17 residues of the M-domain (C0C1f), previously known to inhibit in vitro motility velocity (Weith *et al.*, 2012), did not affect myosin association significantly in our thin filament tightropes assay (Figure 5.1). Although our results agree with previous studies in terms of these shorter fragments being unable to activate thin filaments, the disagreement in the thin filament inhibition characteristic of C0C1f suggests that, in the in vitro motility assay, inhibition occurs through a different mechanism. Previous studies have suggested that cMyBP-C can function as a viscous load, slowing thin filament speed (Previs *et al.*, 2012), or increasing force production in hearts lacking cMyBP-C (Korte *et al.*, 2003), suggesting that both competition and viscous load must be taken into account to fully explain inhibition by cMyBP-C (Walcott *et al.*, 2015). However, force or load do not play a role in our assay and the only possible mechanism we can detect is direct competition or inhibition; therefore, we can assert that the discrepancy seen with C0C1f must be caused by its viscous interactions with the actin and/or the surface in the motility assay (Weith *et al.*, 2012).

As with our studies without the M-domain, the myosin ATPase was seen to be unaffected by C0C1 at low and high calcium (Belknap *et al.*, 2014). This highlights the importance of a complete M-domain for the stimulation and inhibition of thin

filament-myosin interactions. Taken together with previous studies (Weith *et al.*, 2012; Belknap *et al.*, 2014; Mun *et al.*, 2014), this suggests the presence of multiple sites in the M-domain with alternate activities, likely modulated by phosphorylation (Stelzer *et al.*, 2006; Shaffer *et al.*, 2009; Previs *et al.*, 2016).

5.3.2 – cMyBP-C possesses a weak binding state to actin

The N-terminal domains C0 and C1 have been known to possess actin binding properties (Lu *et al.*, 2011; Mun *et al.*, 2011; Orlova *et al.*, 2011; Harris *et al.*, 2016), while the M-domain is known to possess the ability to modulate actin binding (Bezold *et al.*, 2013; Mun *et al.*, 2014; Previs *et al.*, 2016). These properties have also been shown in our data, where all the fragments showed thin filaments binding capabilities with only C0C3 being capable of increasing myosin binding to the thin filaments. However, our results highlight a new mode of actin binding for the N-terminal region of cMyBP-C. Figure 5.7 shows that at low calcium for C0C3 and regardless of calcium for C0C1f and C0C1, about 20-30% of the molecules observed diffuse along the thin filament. From the diffusional characteristics we were able to define this as an unbiased random walk, as would be expected from cMyBP-C, since it is not a motor protein. Using data from (Weith *et al.*, 2012) we were able to calculate that the fragments' diffusing step size ranges between ~7 and ~15 nm, consistent with 1 to 3 actin monomers, although the optical resolution in our microscope set-up does not allow us to visualise individual steps. The fact that the diffusion constant and amount of molecules diffusing are the same for all fragments at low calcium, suggests that diffusion is a general mechanism and that it is linked to the thin filament activation state. However, our data also suggest that the interaction of subdomains C0 and C1 is

not enough for thin filament activation (figure 5.1), whereas the whole N-terminal region is required to increase/decrease myosin binding to the thin filament. Hence, the interactions of subdomains M to C3 could lead to a further shift in position of Tm, exposing more binding sites at high calcium, leading to a significant shift towards all static binding. Knowing that tropomyosin moves across the face of actin (Mckillop and Geeves, 1993; Poole *et al.*, 2006) and that these structural positions are in thermal flux (Schaertl *et al.*, 1995; Moore *et al.*, 2016), it is possible that cMyBP-C association is facilitated at high calcium, as indicated by our decoration data for C0C3 at pCa 4 (figure 5.3). Once cMyBP-C binds to the thin filament, it would hold the Tm in the closed position (Mckillop and Geeves, 1993; Mun *et al.*, 2014) permitting myosin binding and activation of the thin filament, at the same time potentiating its own binding capability. This is also demonstrated by the C0C3 significant decrease in diffusion constant at high calcium compared to low calcium, indicating that not only the number of molecules diffusing decreases with the opening up of the thin filament, but that their motility also slows down.

The observation that 70-80 % of the molecules are not diffusing does not mean that the majority of cMyBP-C fragments are strongly associated. At equilibrium there will be molecules free in solution, therefore the true determinant of association is the relative numbers of free versus bound molecules. Although it would be interesting to have a better understanding of the kinetic mechanism behind the diffusion-to-static transition, the thin filament tightropes assay can only measure attached molecules, thus preventing a more in depth analysis on that front. Other experiments are necessary to cover that aspect of the mechanism, possibly performed through concentration dependency studies of the amount of cMyBP-C bound. Therefore, the

most likely scenario based on our current knowledge and experiments is that the high percentage of static versus motile molecules actually represents the outcomes of successful diffusional searches, with unsuccessful searches eventually leading to detachment of the cMyBP-C N-terminal fragment.

In muscles tissue, cMyBP-C is C-terminally anchored to the thick filament in the C-zone of the sarcomere (Freiburg and Gautel, 1996; Flashman *et al.*, 2004), raising doubts over whether diffusion would happen in vivo at all. Knowing that N-terminal fragments have been shown to modulate thin filament sliding in a calcium concentration dependence in in vitro motility assay (Razumova *et al.*, 2006, 2008; Mun *et al.*, 2014) and that it has been thought to function as a viscous load (Walcott *et al.*, 2015), it is difficult to rule out that our in vitro observations on cMyBP-C diffusion do not have a physiological role. In this scenario, diffusion might be a response mechanism to the shortening of the sarcomere, where cMyBP-C binding would switch from a static position on the thin filament to a dynamic attachment/detachment mechanism during muscle contraction, with the C-terminus fixed on the thick filament and the N-terminus transiently binding to the thin filament, which would be seen as a viscous load in motility assay experiments, or as diffusive motion in our thin filament tightrope assay. This hypothesis however, does not fit well with the results shown here, since the amount of C0C3 diffusing molecules is drastically reduced for thin filaments at high calcium and unregulated actin (figure 5.3 and table 5.1) and, knowing that the thin filament tightropes assay does not allow us to measure load or study cMyBP-C tension dependence binding to the thin filament, it is impossible to draw a meaningful conclusion on this mechanism.

Another possibility is that the diffusion we observed in our experiments represents a weak interaction of the cMyBP-C N-terminus with actin and tropomyosin. Indeed, such an interactions could depend on the calcium concentration or the thin filament activation state, where multiple cMyBP-C binding sites becoming more accessible as tropomyosin shifts its position on actin, as discussed above. Therefore, our experiments points strongly towards a two binding states working model for the N-terminus of cMyBP-C in the sarcomere: a first weak binding interaction (diffusive), in which the C0 and C1 domains interact with the thin filament, binding and releasing quickly, and a subsequent strong and stable binding, characterised by a higher affinity for the thin filament, in which subdomains M to C3 also contribute to actin binding, facilitating the movement of tropomyosin from the blocked to the closed state as well as myosin binding, finally resulting in the activation of the whole thin filament.

5.3.3 – Inhibition of myosin binding is due to cooperative proximal binding of cMyBP-C to thin filaments

The distribution of single molecules bound to thin filaments provides insight into the spatial coordination of cMyBP-C binding and its dependence on calcium. C0C3 clearly shows a significant increase in thin filament binding at pCa 4. Detailed examination of the binding indicates C0C3 forms clusters (Figure 5.3c and 5.6b), indicating that C0C3 is increasing its own binding proximally, hence binding cooperatively. Interestingly, comparing these results with unregulated actin highlights how this binding is not caused by a larger amount of actin exposed at high calcium, indicating rather that the regulatory proteins themselves play a role in clustering cMyBP-C. Using a polymer

growth model we are able to estimate the affinity of cMyBP-C fragments for thin filaments as ~200 nM. However, this value is tighter than the affinity we found for unregulated actin (486.3 nM, figure 5.6a) and considerably tighter than ~2 μM reported elsewhere (Belknap *et al.*, 2014). Our value for the binding constant derives from directly imaging cooperative binding and therefore is likely to represent monomer binding affinity. This k_C however, is not a simple value in the context of cooperative binding, since it is still not clear how this could inhibit myosin ATPase or thin filament speed in the motility assay (Razumova *et al.*, 2006).

Within the sarcomere, cMyBP-C is fixed in position along the thick filament lattice, through its C-terminus, at an enforced spacing of ~43 nm, which would preclude clustering. However, considering that each thin filament in a muscle lattice is surrounded by three thick filaments, our observations suggest that these could bind in the near vicinity to one another and cluster, although at a lower density level to what seen in our experiments. This may explain the reduced force response seen in stretch activation as a result of cMyBP-C interactions (Stelzer *et al.*, 2006).

CHAPTER 6

DISCUSSION

In this thesis work I used a single molecule approach to study how tropomyosin, its E180G mutation and myosin binding protein-C regulate and modulate acto-myosin interactions and cross bridge formation, in order to expand our understanding of how errors in the molecular mechanism of muscle contraction can lead to hypertrophic cardiomyopathy.

To understand how the E180G tropomyosin mutation leads to hypertrophic cardiomyopathy, we looked at how it affects myosin binding and cooperativity, while comparing our results with data obtained in (Desai *et al.*, 2015) for the wild-type tropomyosin. Through *in-vitro* motility assay experiments, we found that thin filaments possessing the E180G tropomyosin homodimer mutation have increased sensitivity to calcium, ($\Delta pCa = 0.44 \pm 0.05$) and exhibit reduced cooperativity (highlighted by the reduced Hill coefficient), confirming the results shown in (Bing *et al.*, 2000) and (Matyushenko *et al.*, 2017), among others. Using our thin filament tightropes assay, we confirmed the increase in calcium sensitivity ($\Delta pCa > 0.5$) and linked the reduced cooperativity found in the motility experiments to a reduction in the myosin cooperative unit, from 11 actin subunits found for wild-type tropomyosin to 7 for the E180G mutation. These findings are also supported by other studies found in the

literature, with the increased calcium sensitivity visible not only in motility assay experiments, but also in ATPase assays and tension vs. pCa curves (Bing *et al.*, 2000; Boussouf *et al.*, 2007; Bai *et al.*, 2011; Wang *et al.*, 2011; Janco *et al.*, 2012; Ly and Lehrer, 2012; Matyushenko *et al.*, 2017), while the increase in flexibility of the tropomyosin chain was observed both using electron microscopy and Atomic Force Microscopy (despite these studies disagreeing in the flexibility measurements by a 2-fold factor) (Li *et al.*, 2012; Loong *et al.*, 2012).

Our experiments, however, are the first to be conducted using a single molecule assay, which allowed to directly quantify myosin binding to actin and study how its cooperativity is affected by the E180G mutation. The results showed that increases in [Ca^{2+}] did not lead to a significant shift towards the formation of larger clusters of myosin molecules bound to the thin filament, unlike what has been shown from the wild-type measurements performed in (Desai *et al.*, 2015). The same is seen for changes in [S1-GFP] concentration, where the amount of S1 bound at 10 and 15 nM were indistinguishable. Both of these results suggest a shift in the activation state of the thin filament towards the closed state at the expense of both the blocked and the open states.

In the context of hypertrophic cardiomyopathy these findings would imply that hyper-contractility is a result of myosin binding to the thin filament at low calcium, which is translated in an apparent increase in calcium sensitivity. Since calcium does not directly bind to tropomyosin, but instead affects tropomyosin position indirectly through troponin, it is unlikely that a mutation in the tropomyosin chain would affect the affinity of TnC to calcium. The E180G mutation is positioned within the TnT binding region and (Golitsina *et al.*, 1997, 1999) have showed that, although the overall Tn

affinity to Tm is weaker in the presence of the E180G mutation, the TnT affinity did not change and the stoichiometry was always close to 1:1 Tn:Tm or TnT:Tm. However, (Dong *et al.*, 2003) have reported that the troponin complex acts as a cooperative unit during thin filament deactivation which, when coupled to tropomyosin, leads to regional stress build-up within the polymeric chain that propagate (releasing the accumulated stress) to neighbouring monomers through Ca^{2+} binding to troponin (Robinson *et al.*, 2004). Therefore, it is possible that the removal of a negative charge that occurs in the E180G mutation from tropomyosin chain would impair its binding to actin, reducing the overall polymer chain cooperativity through its ability to propagate stress/forces via head to tail interactions. This is further supported by the simulations carried out in (Orzechowski, Fischer, *et al.*, 2014) and (Orzechowski, Moore, *et al.*, 2014), where tropomyosin mutations that lead to Hypertrophic Cardiomyopathy have shown causing a reduction of the difference in energy necessary to switch between binding states on actin, lowering the energy barrier necessary to shift from the blocked to the closed position, facilitating myosin binding to actin, as indicated by our results obtained in the thin filament tightropes assay. As suggested by (Bai *et al.*, 2011) this would ultimately translate into an increase in the force generated at low calcium, impairing relaxation during diastole (Huelnhagen *et al.*, 2018; Maragiannis *et al.*, 2018; Wu *et al.*, 2019).

To better understand the relaxation process, we also looked at whether tropomyosin role in regulating acto-myosin interactions is only passive, working as a steric block for myosin binding sites on actin, or if it also actively limits the number of myosin bound within a regulatory unit. Imaging myosin binding to the thin filament in sub-maximal activating conditions ([ATP] = 0.1 μM, [S1-GFP] = 5 and 10 nM and $[Ca^{2+}] = 10^{-6}$ M)

allowed us to study the release process of myosin molecules from clusters in locally active regions. We were able to related the intensity of the bound S1-GFP molecules at each given time through our collaboration with Dr. Hongsheng Dai and Madalina Mihailescu of the Department of Mathematical Sciences at the University of Essex who, using a Reversible-Jump Markov Chain Monte Carlo (RJMCMC) approach helped us determine the transition probabilities of myosin detachment from the thin filament. A further comparison with a purely stochastic model based on the probability of random detachment/attachment of multiple S1-GFP within a set timeframe (300 ms) revealed an increased probability for multiple myosin molecules detaching at the same instant, resulting in the catastrophic collapse of the locally active region. Considering that these results cannot be explained simply by fluorophore photobleaching or stochastic release, we suggested an active role for tropomyosin in suppressing myosin cross bridges during relaxation. Such a concerted relaxation mechanism could be based on tropomyosin rigidity and, as mentioned above, would be supported by the studies on the energy landscapes of tropomyosin binding to actin performed by (Orzechowski, Moore, *et al.*, 2014), which imply that tropomyosin could be capable of "slinging" back to the blocked position (where its energy is at the minimum) during muscle relaxation (Moore *et al.*, 2016). This mechanism would have further implications in cardiomyopathies and tie with the results presented in Chapter 3, since an increase in tropomyosin flexibility caused by the E180G mutation would mean a decrease in the elastic force exerted by tropomyosin during the open to blocked transition, overall reducing its capability to actively regulate myosin release from actin and lead to an increased tension during diastole (Bai *et al.*, 2011; Cohn *et al.*, 2019).

Following on, to better understand the molecular mechanism behind cardiomyopathy, it would be interesting to look at how different mutations lead to disease using our single molecule assay and the methodologies used in this thesis. For instance, carrying out the catastrophic collapse experiments in the presence of the E180G mutation would be an obvious follow up to both the experiments presented in Chapter 3 and 4, to understand whether the collapse mechanism can be disrupted or enhanced by mutations. Other interesting mutations could be D175N (Asp175Asn) and L185R (Leu185Arg) which, although being found in close proximity of E180G, have been shown to have different effects and overall severity (Thierfelder *et al.*, 1994; Golitsina *et al.*, 1997; Chang *et al.*, 2014) and, understanding how they affect myosin binding at the single molecule level or the catastrophic collapse of myosin active regions could help shed light on the overall molecular implications of cardiomyopathies for muscle relaxation. To this end, than is no real restriction posed by our single molecule assay itself and potentially any mutation in any protein of the sarcomere can be studied following the same methodologies shown in this thesis.

I also studied three cardiac myosin binding protein-C (cMyBP-C) N-terminal fragments (C0C3, C0C1f and C0C1) to elucidate their role in acto-myosin interactions and thin filament activation. The results show that only the full N-terminal domain (C0C3) is capable of activating the thin filament at low calcium and affect myosin binding at high calcium, highlighting the presence of one or more actin binding sites further away from the C1 subdomain. These results are partly in line with what has been seen in the literature for N-terminal fragments using the *in-vitro* motility assay (Razumova *et al.*, 2006; Mun *et al.*, 2014), with the activation at low calcium seen for C0C3 and the modulation at high calcium seen for both C0C3 and C0C1f. Thus, the controversy lies

with the shorter fragment C0C1f, with C0C3 being thought to cause the activation of the thin filament through subdomains C1 and/or M (depending whether the protein is from human or mouse (Belknap *et al.*, 2014)) directly interacting with tropomyosin, stabilising the closed position (Mun *et al.*, 2014; Risi *et al.*, 2018). Using our tightropes assay, we are the first to show that the activation mechanism seen at low calcium is caused by C0C3 directly increasing myosin binding to the thin filament, while the modulation effect seen at high calcium for both fragments in motility experiments is most likely a combination of direct competition and viscous drag (Walcott *et al.*, 2015) and C0C3 direct competition in ours, meaning that C0C1f lacks the necessary subdomains to provide a significant steric encumbrance to myosin.

We also looked at fluorescent constructs of the same cMyBP-C N-terminal fragments to establish the mechanism behind thin filament activation. Imaging at both low and high calcium, we have seen how C0C3 binding to the thin filament is calcium dependent and cooperative, unlike C0C1f and C0C1. Fitting our data also revealed an increased affinity of C0C3 for thin filaments, in contrast with the affinity values reported previously in the literature (Belknap *et al.*, 2014). Further dynamic studies of the fragments binding properties to the thin filament revealed that ~25% of the imaged molecules randomly diffused, with only C0C3 diffusion being reduced significantly at high calcium and for unregulated actin. Taking all our data into consideration, we were able to define a two-step model for MyBP-C binding to the thin filament, in which the first step consist in a weak association of the C0 and C1 subdomains to actin, characterised by rapid binding and release seen as diffusion in our assay, with the follow-up step characterised by the binding of the further sub-

domains to actin, displacing tropomyosin from the blocked to its closed position and facilitating further binding of either cMyBP-C or myosin.

An essential follow-up to these results would be performing dual colour experiments, where both S1 and cMyBP-C N-terminal fragments are labelled, in an effort to answer whether S1 binding to the thin filament is driven by the fragment, working as a direct recruiter (Starr and Offer, 1978; Kunst *et al.*, 2000; Ratti *et al.*, 2011; Nag *et al.*, 2017), or as a two steps mechanism (S1 binding upon thin filament activation by cMyBP-C fragment). It would be also of interest to perform concentration dependence studies of C0C3, to accurately characterise its cooperativity and understand the kinetics behind its diffusive behaviour. Furthermore, knowing the ability of cMyBP-C to change its conformation upon phosphorylation (Colson *et al.*, 2016; Previs *et al.*, 2016), it would be interesting to study how phosphorylation of C0C3 affects its thin filament binding, activation, cooperativity and diffusion capabilities.

A final theme arising in all the experiments performed in this thesis is the ability of the thin filament tightrope assay and, more generally, single molecule experiments to be able to pinpoint the independent mechanistic roles of calcium and myosin. As pointed out earlier for the E180G results, we were able to see the different effects that calcium and myosin have on thin filament activation separately, by looking at how calcium affects myosin binding and how myosin concentration affects its cooperativity. A similar picture is seen when looking at the binding characteristics of fluorescent C0C3 on thin filaments, where we can distinguish between its calcium induced cooperative binding and its role in promoting myosin binding. In contrast, using ensemble experiments such as the *in-vitro* motility assay only results in a partial understanding of the mechanism of action, seen both for our data with the E180G (figure 3.1) and with

the known literature on cMyBP-C (Razumova *et al.*, 2006). This is because in the motility assay, both the calcium and myosin cooperativity dependence of thin filaments motion is described by a single sigmoidal, thus making it harder to pinpoint molecular mechanism of action.

The results in this thesis demonstrate the capabilities of single molecule approaches and highlight their importance as a powerful addition to ensemble experiments (Månsson *et al.*, 2018). However, these approaches are not exempt from drawbacks and the thin filament tightrope assay is no exception. For instance, as mentioned in Chapter 1 and 2, the assay can take a long time to set-up and master compared to other techniques. Furthermore, there are inherent difficulties that stem from the helical shape of actin and the three dimensional structure of our assay, meaning that myosin can bind to both sides of the filament independently and there is currently no easy way to distinguish the two cases, which needs to be kept in mind when discussing clustering and cooperativity. In addition to this, using a diffraction limited microscope, which limits the spatial resolution of our microscope to about 200 nm, makes it so that data analysis usually requires more advanced analytical and computational methods to identify the single molecules, some of which might be time consuming and could lead to difficult to interpret results; examples of these can be the simultaneous fitting of the binding data discussed in Chapter 3 which, despite its advantages, takes time to optimise and implement, the deconvolution of intensity datasets into transition matrices shown in Chapter 4, only applicable because of the high amount of data each kymographs inherently possesses, and the application of the Flory-Shulz distribution to fit the cMyBP-C fragments binding data in Chapter 5.

However, despite the challenges, the thin filament tightrope is still a viable alternative to other single molecule techniques available and its reproducibility is highlighted by some of the experiments carried out here. For instance, the calculation of the second order ATP binding rate constant provided in the Appendix A.5 is consistent with what has been found previously by other users using the same assay and methodology (2.03 $\mu M^{-1}s^{-1}$ vs. the 1.88 $\mu M^{-1}s^{-1}$ declared in (Desai *et al.*, 2015), as well as the correction necessary to calculate the single S1-GFP intensity, leading to a right shift of the linear plot in figure 3.5b, showing as the same assays leads to similar conclusions over time and with different users (Desai *et al.*, 2015). Furthermore, the collapse of myosin active regions discussed in Chapter 4 has also been achieved in similar conditions to what had been reported in their paper.

Concluding, there are still questions that remain unanswered in the field of muscle contraction towards reaching a better understanding of cardiomyopathies and how they affect acto-myosin interactions and, although there is still much work to be done in that regard, I hope that the results and methodologies reported in this thesis will provide a step in the right direction.

APPENDIX

A.1 – Sequencing results of the 6xHis-RlC-GFP

```
  1   K  I  Y  L  L  C  E  R  I  T  I  I  I  D  S  I  V  S  G  *
  1  K  N  L  F  A  L  *  A  D  N  N  Y  N  R  F  N  C  E  R  I
  1 *  K  F  I  C  F  V  S  G  *  Q  L  *  *  I  Q  L  *  A  D
  1 TAAAAATTTATTTGCTTTGTGAGCGGATAACAATTATAATAGATTCAATTGTGAGCGGAT
  1          10        20        30        40        50
  1 ATTTTTAAATAAACGAAACACTCGCCTATTGTTAATATTATCTAAGTTAACACTCGCCTA
 21   Q  F  H  T  E  F  I  K  E  E  K  L  S  M  H  H  H  H  H  H
 21  T  I  S  H  R  I  H  *  R  G  E  I  K  H  A  P  S  P  S  P
 21 N  N  F  T  Q  N  S  L  K  R  R  N  *  A  C  T  I  T  I  T
 61 AACAATTTCACACAGAATTCATTAAAGAGGAGAAATTAAGCATGCACCATCACCATCACC
 61          70        80        90        100       110
 61 TTGTTAAAGTGTGTCTTAAGTAATTTCTCCTCTTTAATTCGTACGTGGTAGTGGTAGTGG
 41   A  S  M  S  S  K  R  A  K  A  K  T  T  K  K  R  P  Q  R  A
 41  C  *  H  E  Q  Q  T  R  E  S  E  N  H  Q  K  T  P  A  A  R
 41 M  L  A  *  A  A  N  A  R  K  R  K  P  P  K  N  A  R  S  A
121 ATGCTAGCATGAGCAGCAAACGCGCGAAAGCGAAAACCACCAAAAAACGCCCGCAGCGCG
121          130       140       150       160       170
121 TACGATCGTACTCGTCGTTTGCGCGCTTTCGCTTTTGGTGGTTTTTTGCGGGCGTCGCGC
 61   T  S  N  V  F  A  M  F  D  Q  S  Q  I  Q  E  F  K  E  A  F
 61  D  Q  Q  R  V  C  D  V  *  S  E  P  D  S  G  I  *  R  S  V
 61 R  P  A  T  C  L  R  C  L  I  R  A  R  F  R  N  L  K  K  R
181 CGACCAGCAACGTGTTTGCGATGTTTGATCAGAGCCAGATTCAGGAATTTAAAGAAGCGT
181          190       200       210       220       230
181 GCTGGTCGTTGCACAAACGCTACAAACTAGTCTCGGTCTAAGTCCTTAAATTTCTTCGCA
 81   N  M  I  D  Q  N  R  D  G  F  I  D  K  E  D  L  H  D  M  L
 81  *  H  D  *  S  E  P  R  W  L  Y  *  *  R  R  S  A  *  Y  A
 81 L  T  *  L  I  R  T  A  M  A  L  L  I  K  K  I  C  M  I  C
241 TTAACATGATTGATCAGAACCGCGATGGCTTTATTGATAAAGAAGATCTGCATGATATGC
241          250       260       270       280       290
241 AATTGTACTAACTAGTCTTGGCGCTACCGAAATAACTATTTCTTCTAGACGTACTATACG
101   A  S  M  G  K  N  P  T  D  E  Y  L  E  G  M  M  S  E  A  P
101  G  E  H  G  Q  K  P  D  R  *  I  S  G  R  H  D  E  R  S  A
101 W  R  A  W  A  K  T  R  P  M  N  I  W  K  A  *  *  A  K  R
301 TGGCGAGCATGGGCAAAAACCCGACCGATGAATATCTGGAAGGCATGATGAGCGAAGCGC
301          310       320       330       340       350
301 ACCGCTCGTACCCGTTTTTGGGCTGGCTACTTATAGACCTTCCGTACTACTCGCTTCGCG
121   G  P  I  N  F  T  M  F  L  T  M  F  G  E  K  L  N  G  T  D
121  G  P  D  *  L  Y  H  V  S  D  H  V  W  R  K  T  E  R  H  R
121 R  A  R  L  T  L  P  C  F  *  P  C  L  A  K  N  *  T  A  P
361 CGGGCCCGATTAACTTTACCATGTTTCTGACCATGTTTGGCGAAAAACTGAACGGCACCG
361          370       380       390       400       410
361 GCCCGGGCTAATTGAAATGGTACAAAGACTGGTACAAACCGCTTTTTGACTTGCCGTGGC
```

```
141   P  E  D  V  I  R  N  A  F  A  C  F  D  E  E  A  S  G  F  I
141  S  G  R  C  D  S  Q  R  V  C  V  L  *  *  R  S  E  R  L  Y
141 I  R  K  M  *  F  A  T  R  L  R  A  L  M  K  K  R  A  A  L
421 ATCCGGAAGATGTGATTCGCAACGCGTTTGCGTGCTTTGATGAAGAAGCGAGCGGCTTTA
421          430       440       450       460       470
421 TAGGCCTTCTACACTAAGCGTTGCGCAAACGCACGAAACTACTTCTTCGCTCGCCGAAAT
161   H  E  D  H  L  R  E  L  L  T  T  M  G  D  R  F  T  D  E  E
161  S  *  R  S  S  A  R  T  A  D  H  H  G  R  S  L  Y  R  *  R
161 F  M  K  I  I  C  A  N  C  *  P  P  W  A  I  A  L  P  M  K
481 TTCATGAAGATCATCTGCGCGAACTGCTGACCACCATGGGCGATCGCTTTACCGATGAAG
481          490       500       510       520       530
481 AAGTACTTCTAGTAGACGCGCTTGACGACTGGTGGTACCCGCTAGCGAAATGGCTACTTC
181   V  D  E  M  Y  R  E  A  P  I  D  K  K  G  N  F  N  Y  V  E
181  S  G  *  N  V  S  R  S  A  D  *  *  K  R  Q  L  *  L  C  G
181 K  W  M  K  C  I  A  K  R  R  L  I  K  K  A  T  L  T  M  W
541 AAGTGGATGAAATGTATCGCGAAGCGCCGATTGATAAAAAAGGCAACTTTAACTATGTGG
541          550       560       570       580       590
541 TTCACCTACTTTACATAGCGCTTCGCGGCTAACTATTTTTTCCGTTGAAATTGATACACC
201   F  T  R  I  L  K  H  G  A  K  D  K  D  D  G  A  P  S  G  S
201  I  Y  P  H  S  E  T  W  R  E  R  *  R  *  W  R  A  F  R  *
201 N  L  P  A  F  *  N  M  A  R  K  I  K  M  M  A  R  L  Q  V
601 AATTTACCCGCATTCTGAAACATGGCGCGAAAGATAAAGATGATGGCGCGCCTTCAGGTA
601          610       620       630       640       650
601 TTAAATGGGCGTAAGACTTTGTACCGCGCTTTCTATTTCTACTACCGCGCGGAAGTCCAT
221   S  G  T  S  S  G  T  S  M  V  S  K  G  E  E  L  F  T  G  V
221  L  W  H  F  K  R  Y  *  Y  G  E  Q  G  R  G  A  V  H  R  G
221 A  L  A  L  Q  A  V  L  V  W  *  A  R  A  R  S  C  S  P  G
661 GCTCTGGCACTTCAAGCGGTACTAGTATGGTGAGCAAGGGCGAGGAGCTGTTCACCGGGG
661          670       680       690       700       710
661 CGAGACCGTGAAGTTCGCCATGATCATACCACTCGTTCCCGCTCCTCGACAAGTGGCCCC
241   V  P  I  L  V  E  L  D  G  D  V  N  G  H  K  F  S  V  S  G
241  G  A  H  P  G  R  A  G  R  R  R  K  R  P  Q  V  Q  R  V  R
241 W  C  P  S  W  S  S  W  T  A  T  *  T  A  T  S  S  A  C  P
721 TGGTGCCCATCCTGGTCGAGCTGGACGGCGACGTAAACGGCCACAAGTTCAGCGTGTCCG
721          730       740       750       760       770
721 ACCACGGGTAGGACCAGCTCGACCTGCCGCTGCATTTGCCGGTGTTCAAGTCGCACAGGC
261   E  G  E  G  D  A  T  Y  G  K  L  T  L  K  F  I  C  T  T  G
261  R  G  R  G  R  C  H  L  R  Q  A  D  P  E  V  H  L  H  H  R
261 A  R  A  R  A  M  P  P  T  A  S  *  P  *  S  S  S  A  P  P
781 GCGAGGGCGAGGGCGATGCCACCTACGGCAAGCTGACCCTGAAGTTCATCTGCACCACCG
781          790       800       810       820       830
781 CGCTCCCGCTCCCGCTACGGTGGATGCCGTTCGACTGGGACTTCAAGTAGACGTGGTGGC
281   K  L  P  V  P  W  P  T  L  V  T  T  L  T  Y  G  V  Q  C  F
281  Q  A  A  R  A  L  A  H  P  R  D  H  P  D  L  R  R  A  V  L
281 A  S  C  P  C  P  G  P  P  S  *  P  P  *  P  T  A  C  S  A
841 GCAAGCTGCCCGTGCCCTGGCCCACCCTCGTGACCACCCTGACCTACGGCGTGCAGTGCT
841          850       860       870       880       890
841 CGTTCGACGGGCACGGGACCGGGTGGGAGCACTGGTGGGACTGGATGCCGCACGTCACGA
301   S  R  Y  P  D  H  M  K  Q  H  D  F  F  K  S  A  M  P  E  G
301  Q  P  L  P  R  P  H  E  A  A  R  L  L  Q  V  R  H  A  R  R
301 S  A  A  T  P  T  T  *  S  S  T  T  S  S  S  P  P  C  P  K
901 TCAGCCGCTACCCCGACCACATGAAGCAGCACGACTTCTTCAAGTCCGCCATGCCCGAAG
901          910       920       930       940       950
901 AGTCGGCGATGGGGCTGGTGTACTTCGTCGTGCTGAAGAAGTTCAGGCGGTACGGGCTTC
321   Y  V  Q  E  R  T  I  F  F  K  D  D  G  N  Y  K  T  R  A  E
321  L  R  P  G  A  H  H  L  L  Q  G  R  R  Q  L  Q  D  P  R  R
321 A  T  S  R  S  A  P  S  S  S  R  T  T  A  T  T  R  P  A  P
961 GCTACGTCCAGGAGCGCACCATCTTCTTCAAGGACGACGGCAACTACAAGACCCGCGCCG
961          970       980       990       1000      1010
961 CGATGCAGGTCCTCGCGTGGTAGAAGAAGTTCCTGCTGCCGTTGATGTTCTGGGCGCGGC
```

```
 341   V  K  F  E  G  D  T  L  V  N  R  I  E  L  K  G  I  D  F  K
 341   G  E  V  R  G  R  H  P  G  E  P  H  R  A  E  G  H  R  L  Q
 341 R  *  S  S  R  A  T  P  W  *  T  A  S  S  *  R  A  S  T  S
1021 AGGTGAAGTTCGAGGGCGACACCCTGGTGAACCGCATCGAGCTGAAGGGCATCGACTTCA
1021          1030      1040      1050      1060      1070
1021 TCCACTTCAAGCTCCCGCTGTGGGACCACTTGGCGTAGCTCGACTTCCCGTAGCTGAAGT
 361   E  D  G  N  I  L  G  H  K  L  E  Y  N  Y  N  S  H  N  V  Y
 361   G  G  R  Q  H  P  G  A  Q  A  G  V  Q  L  Q  Q  P  Q  R  L
 361 R  R  T  A  T  S  W  G  T  S  W  S  T  T  T  T  A  T  T  S
1081 AGGAGGACGGCAACATCCTGGGGCACAAGCTGGAGTACAACTACAACAGCCACAACGTCT
1081          1090      1100      1110      1120      1130
1081 TCCTCCTGCCGTTGTAGGACCCCGTGTTCGACCTCATGTTGATGTTGTCGGTGTTGCAGA
 381   I  M  A  D  K  Q  K  N  G  I  K  V  N  F  K  I  R  H  N  I
 381   Y  H  G  R  Q  A  E  E  R  H  Q  G  E  L  Q  D  P  P  Q  H
 381 I  S  W  P  T  S  R  R  T  A  S  R  *  T  S  R  S  A  T  T
1141 ATATCATGGCCGACAAGCAGAAGAACGGCATCAAGGTGAACTTCAAGATCCGCCACAACA
1141          1150      1160      1170      1180      1190
1141 TATAGTACCGGCTGTTCGTCTTCTTGCCGTAGTTCCACTTGAAGTTCTAGGCGGTGTTGT
 401   E  D  G  S  V  Q  L  A  D  H  Y  Q  Q  N  T  P  I  G  D  G
 401   R  G  R  Q  R  A  A  R  R  P  L  P  A  E  H  P  H  R  R  R
 401 S  R  T  A  A  C  S  S  P  T  T  T  S  R  T  P  P  S  A  T
1201 TCGAGGACGGCAGCGTGCAGCTCGCCGACCACTACCAGCAGAACACCCCCATCGGCGACG
1201          1210      1220      1230      1240      1250
1201 AGCTCCTGCCGTCGCACGTCGAGCGGCTGGTGATGGTCGTCTTGTGGGGGTAGCCGCTGC
 421   P  V  L  L  P  D  N  H  Y  L  S  T  Q  S  A  L  S  K  D  P
 421   P  R  A  A  A  R  Q  P  L  P  E  H  P  V  R  P  E  Q  R  P
 421 A  P  C  C  C  P  T  T  T  T  *  A  P  S  P  P  *  A  K  T
1261 GCCCCGTGCTGCTGCCCGACAACCACTACCTGAGCACCCAGTCCGCCCTGAGCAAAGACC
1261          1270      1280      1290      1300      1310
1261 CGGGGCACGACGACGGGCTGTTGGTGATGGACTCGTGGGTCAGGCGGGACTCGTTTCTGG
 441   N  E  K  R  D  H  M  V  L  L  E  F  V  T  A  A  G  I  T  L
 441   Q  R  E  A  R  S  H  G  P  A  G  V  R  D  R  R  R  D  H  S
 441 P  T  R  S  A  I  T  W  S  C  W  S  S  *  P  P  P  G  S  L
1321 CCAACGAGAAGCGCGATCACATGGTCCTGCTGGAGTTCGTGACCGCCGCCGGGATCACTC
1321          1330      1340      1350      1360      1370
1321 GGTTGCTCTTCGCGCTAGTGTACCAGGACGACCTCAAGCACTGGCGGCGGCCCTAGTGAG
 461   G  M  D  E  L  Y  K  *  E
 461   R  H  G  R  A  V  Q  V  R  K
 461 S  A  W  T  S  C  T  S  K  K
1381 TCGGCATGGACGAGCTGTACAAGTAAGAAAG
1381          1390      1400      1410
1381 AGCCGTACCTGCTCGACATGTTCATTCTTTC
```

A.2 – Sequencing results of the RlC-GFP-6xHis

```
  1   Y  F  V  Y  F  K  K  E  I  Y  I  *  A  A  N  A  R  K  R  K
  1   I  F  C  L  L  *  E  G  D  I  H  M  S  S  K  R  A  K  A  K
  1 D  I  L  F  T  L  R  R  R  Y  T  Y  E  Q  Q  T  R  E  S  E
  1 GATATTTTGTTTACTTTAAGAAGGAGATATACATATGAGCAGCAAACGCGCGAAAGCGAA
  1          10        20        30        40        50
  1 CTATAAAACAAATGAAATTCTTCCTCTATATGTATACTCGTCGTTTGCGCGCTTTCGCTT
 21   P  P  K  N  A  R  S  A  R  P  A  T  C  L  R  C  L  I  R  A
 21  T  T  K  K  R  P  Q  R  A  T  S  N  V  F  A  M  F  D  Q  S
 21 N  H  Q  K  T  P  A  A  R  D  Q  Q  R  V  C  D  V  *  S  E
 61 AACCACCAAAAAACGCCCGCAGCGCGCGACCAGCAACGTGTTTGCGATGTTTGATCAGAG
 61          70        80        90        100       110
 61 TTGGTGGTTTTTTGCGGGCGTCGCGCGCTGGTCGTTGCACAAACGCTACAAACTAGTCTC
 41   R  F  R  N  L  K  K  R  L  T  *  L  I  R  T  A  M  A  L  L
 41  Q  I  Q  E  F  K  E  A  F  N  M  I  D  Q  N  R  D  G  F  I
 41 P  D  S  G  I  *  R  S  V  *  H  D  *  S  E  P  R  W  L  Y
121 CCAGATTCAGGAATTTAAAGAAGCGTTTAACATGATTGATCAGAACCGCGATGGCTTTAT
121          130       140       150       160       170
121 GGTCTAAGTCCTTAAATTTCTTCGCAAATTGTACTAACTAGTCTTGGCGCTACCGAAATA
 61   I  K  K  I  C  M  I  C  W  R  A  W  A  K  T  R  P  M  N  I
 61  D  K  E  D  L  H  D  M  L  A  S  M  G  K  N  P  T  D  E  Y
 61 *  *  R  R  S  A  *  Y  A  G  E  H  G  Q  K  P  D  R  *  I
181 TGATAAAGAAGATCTGCATGATATGCTGGCGAGCATGGGCAAAAACCCGACCGATGAATA
181          190       200       210       220       230
181 ACTATTTCTTCTAGACGTACTATACGACCGCTCGTACCCGTTTTTGGGCTGGCTACTTAT
 81   W  K  A  *  *  A  K  R  R  A  R  L  T  L  P  C  F  *  P  C
 81  L  E  G  M  M  S  E  A  P  G  P  I  N  F  T  M  F  L  T  M
 81 S  G  R  H  D  E  R  S  A  G  P  D  *  L  Y  H  V  S  D  H
241 TCTGGAAGGCATGATGAGCGAAGCGCCGGGCCCGATTAACTTTACCATGTTTCTGACCAT
241          250       260       270       280       290
241 AGACCTTCCGTACTACTCGCTTCGCGGCCCGGGCTAATTGAAATGGTACAAAGACTGGTA
101   L  A  K  N  *  T  A  P  I  R  K  M  *  F  A  T  R  L  R  A
101  F  G  E  K  L  N  G  T  D  P  E  D  V  I  R  N  A  F  A  C
101 V  W  R  K  T  E  R  H  R  S  G  R  C  D  S  Q  R  V  C  V
301 GTTTGGCGAAAAACTGAACGGCACCGATCCGGAAGATGTGATTCGCAACGCGTTTGCGTG
301          310       320       330       340       350
301 CAAACCGCTTTTTGACTTGCCGTGGCTAGGCCTTCTACACTAAGCGTTGCGCAAACGCAC
121   L  M  K  K  R  A  A  L  F  M  K  I  I  C  A  N  C  *  P  P
121  F  D  E  E  A  S  G  F  I  H  E  D  H  L  R  E  L  L  T  T
121 L  *  *  R  S  E  R  L  Y  S  *  R  S  S  A  R  T  A  D  H
361 CTTTGATGAAGAAGCGAGCGGCTTTATTCATGAAGATCATCTGCGCGAACTGCTGACCAC
361          370       380       390       400       410
361 GAAACTACTTCTTCGCTCGCCGAAATAAGTACTTCTAGTAGACGCGCTTGACGACTGGTG
141   W  A  I  A  L  P  M  K  K  W  M  K  C  I  A  K  R  R  L  I
141  M  G  D  R  F  T  D  E  E  V  D  E  M  Y  R  E  A  P  I  D
141 H  G  R  S  L  Y  R  *  R  S  G  *  N  V  S  R  S  A  D  *
421 CATGGGCGATCGCTTTACCGATGAAGAAGTGGATGAAATGTATCGCGAAGCGCCGATTGA
421          430       440       450       460       470
421 GTACCCGCTAGCGAAATGGCTACTTCTTCACCTACTTTACATAGCGCTTCGCGGCTAACT
161   K  K  A  T  L  T  M  W  N  L  P  A  F  *  N  M  A  R  K  I
161  K  K  G  N  F  N  Y  V  E  F  T  R  I  L  K  H  G  A  K  D
161 *  K  R  Q  L  *  L  C  G  I  Y  P  H  S  E  T  W  R  E  R
481 TAAAAAAGGCAACTTTAACTATGTGGAATTTACCCGCATTCTGAAACATGGCGCGAAAGA
481          490       500       510       520       530
481 ATTTTTTCCGTTGAAATTGATACACCTTAAATGGGCGTAAGACTTTGTACCGCGCTTTCT
```

```
181   K  M  M  A  R  L  Q  V  A  L  A  L  Q  A  V  L  V  W  *  A
181  K  D  D  G  A  P  S  G  S  S  G  T  S  S  G  T  S  M  V  S
181 *  R  *  W  R  A  F  R  *  L  W  H  F  K  R  Y  *  Y  G  E
541 TAAAGATGATGGCGCGCCTTCAGGTAGCTCTGGCACTTCAAGCGGTACTAGTATGGTGAG
541          550       560       570       580       590
541 ATTTCTACTACCGCGCGGAAGTCCATCGAGACCGTGAAGTTCGCCATGATCATACCACTC
201   R  A  R  S  C  S  P  G  W  C  P  S  W  S  S  W  T  A  T  *
201  K  G  E  E  L  F  T  G  V  V  P  I  L  V  E  L  D  G  D  V
201 Q  G  R  G  A  V  H  R  G  G  A  H  P  G  R  A  G  R  R  R
601 CAAGGGCGAGGAGCTGTTCACCGGGGTGGTGCCCATCCTGGTCGAGCTGGACGGCGACGT
601          610       620       630       640       650
601 GTTCCCGCTCCTCGACAAGTGGCCCCACCACGGGTAGGACCAGCTCGACCTGCCGCTGCA
221   T  A  T  S  S  A  C  P  A  R  A  R  A  M  P  P  T  A  S  *
221  N  G  H  K  F  S  V  S  G  E  G  E  G  D  A  T  Y  G  K  L
221 K  R  P  Q  V  Q  R  V  R  R  G  R  G  R  C  H  L  R  Q  A
661 AAACGGCCACAAGTTCAGCGTGTCCGGCGAGGGCGAGGGCGATGCCACCTACGGCAAGCT
661          670       680       690       700       710
661 TTTGCCGGTGTTCAAGTCGCACAGGCCGCTCCCGCTCCCGCTACGGTGGATGCCGTTCGA
241   P  *  S  S  S  A  P  P  A  S  C  P  C  P  G  P  P  S  *  P
241  T  L  K  F  I  C  T  T  G  K  L  P  V  P  W  P  T  L  V  T
241 D  P  E  V  H  L  H  H  R  Q  A  A  R  A  L  A  H  P  R  D
721 GACCCTGAAGTTCATCTGCACCACCGGCAAGCTGCCCGTGCCCTGGCCCACCCTCGTGAC
721          730       740       750       760       770
721 CTGGGACTTCAAGTAGACGTGGTGGCCGTTCGACGGGCACGGGACCGGGTGGGAGCACTG
261   P  *  P  T  A  C  S  A  S  A  A  T  P  T  T  *  S  S  T  T
261  T  L  T  Y  G  V  Q  C  F  S  R  Y  P  D  H  M  K  Q  H  D
261 H  P  D  L  R  R  A  V  L  Q  P  L  P  R  P  H  E  A  A  R
781 CACCCTGACCTACGGCGTGCAGTGCTTCAGCCGCTACCCCGACCACATGAAGCAGCACGA
781          790       800       810       820       830
781 GTGGGACTGGATGCCGCACGTCACGAAGTCGGCGATGGGGCTGGTGTACTTCGTCGTGCT
281   S  S  S  P  P  C  P  K  A  T  S  R  S  A  P  S  S  S  R  T
281  F  F  K  S  A  M  P  E  G  Y  V  Q  E  R  T  I  F  F  K  D
281 L  L  Q  V  R  H  A  R  R  L  R  P  G  A  H  H  L  L  Q  G
841 CTTCTTCAAGTCCGCCATGCCCGAAGGCTACGTCCAGGAGCGCACCATCTTCTTCAAGGA
841          850       860       870       880       890
841 GAAGAAGTTCAGGCGGTACGGGCTTCCGATGCAGGTCCTCGCGTGGTAGAAGAAGTTCCT
301   T  A  T  T  R  P  A  P  R  *  S  S  R  A  T  P  W  *  T  A
301  D  G  N  Y  K  T  R  A  E  V  K  F  E  G  D  T  L  V  N  R
301 R  R  Q  L  Q  D  P  R  R  G  E  V  R  G  R  H  P  G  E  P
901 CGACGGCAACTACAAGACCCGCGCCGAGGTGAAGTTCGAGGGCGACACCCTGGTGAACCG
901          910       920       930       940       950
901 GCTGCCGTTGATGTTCTGGGCGCGGCTCCACTTCAAGCTCCCGCTGTGGGACCACTTGGC
321   S  S  *  R  A  S  T  S  R  R  T  A  T  S  W  G  T  S  W  S
321  I  E  L  K  G  I  D  F  K  E  D  G  N  I  L  G  H  K  L  E
321 H  R  A  E  G  H  R  L  Q  G  G  R  Q  H  P  G  A  Q  A  G
961 CATCGAGCTGAAGGGCATCGACTTCAAGGAGGACGGCAACATCCTGGGGCACAAGCTGGA
961          970       980       990       1000      1010
961 GTAGCTCGACTTCCCGTAGCTGAAGTTCCTCCTGCCGTTGTAGGACCCCGTGTTCGACCT
341   T  T  T  T  A  T  T  S  I  S  W  P  T  S  R  R  T  A  S  R
341  Y  N  Y  N  S  H  N  V  Y  I  M  A  D  K  Q  K  N  G  I  K
341 V  Q  L  Q  Q  P  Q  R  L  Y  H  G  R  Q  A  E  E  R  H  Q
1021 GTACAACTACAACAGCCACAACGTCTATATCATGGCCGACAAGCAGAAGAACGGCATCAA
1021         1030      1040      1050      1060      1070
1021 CATGTTGATGTTGTCGGTGTTGCAGATATAGTACCGGCTGTTCGTCTTCTTGCCGTAGTT
361   *  T  S  R  S  A  T  T  S  R  T  A  A  C  S  S  P  T  T  T
361  V  N  F  K  I  R  H  N  I  E  D  G  S  V  Q  L  A  D  H  Y
361 G  E  L  Q  D  P  P  Q  H  R  G  R  Q  R  A  A  R  R  P  L
1081 GGTGAACTTCAAGATCCGCCACAACATCGAGGACGGCAGCGTGCAGCTCGCCGACCACTA
1081         1090      1100      1110      1120      1130
1081 CCACTTGAAGTTCTAGGCGGTGTTGTAGCTCCTGCCGTCGCACGTCGAGCGGCTGGTGAT
```

```
 381   S  R  T  P  P  S  A  T  A  P  C  C  C  P  T  T  T  T  *  A
 381  Q  Q  N  T  P  I  G  D  G  P  V  L  L  P  D  N  H  Y  L  S
 381 P  A  E  H  P  H  R  R  R  P  R  A  A  A  R  Q  P  L  P  E
1141 CCAGCAGAACACCCCCATCGGCGACGGCCCCGTGCTGCTGCCCGACAACCACTACCTGAG
1141          1150      1160      1170      1180      1190
1141 GGTCGTCTTGTGGGGGTAGCCGCTGCCGGGGCACGACGACGGGCTGTTGGTGATGGACTC
 401   P  S  P  P  *  A  K  T  P  T  R  S  A  I  T  W  S  C  W  S
 401  T  Q  S  A  L  S  K  D  P  N  E  K  R  D  H  M  V  L  L  E
 401 H  P  V  R  P  E  Q  R  P  Q  R  E  A  R  S  H  G  P  A  G
1201 CACCCAGTCCGCCCTGAGCAAAGACCCCAACGAGAAGCGCGATCACATGGTCCTGCTGGA
1201          1210      1220      1230      1240      1250
1201 GTGGGTCAGGCGGGACTCGTTTCTGGGGTTGCTCTTCGCGCTAGTGTACCAGGACGACCT
 421   S  *  P  P  P  G  S  L  S  A  W  T  S  C  T  S  L  R  P  H
 421  F  V  T  A  A  G  I  T  L  G  M  D  E  L  Y  K  L  A  A  A
 421 V  R  D  R  R  R  D  H  S  R  H  G  R  A  V  Q  A  C  G  R
1261 GTTCGTGACCGCCGCCGGGATCACTCTCGGCATGGACGAGCTGTACAAGCTTGCGGCCGC
1261          1270      1280      1290      1300      1310
1261 CAAGCACTGGCGGCGGCCCTAGTGAGAGCCGTACCTGCTCGACATGTTCGAACGCCGGCG
 441   S  S  T  T  T  T  T  T  E  I  R
 441  L  E  H  H  H  H  H  H  *  D  P  A
 441 T  R  A  P  P  P  P  P  L  R  S  G
1321 ACTCGAGCACCACCACCACCACCACTGAGATCCGGCT
1321          1330      1340      1350
1321 TGAGCTCGTGGTGGTGGTGGTGGTGACTCTAGGCCGA
```

A.3 – Matlab script for the extraction of intensity data

To extract the intensity data from each of the kymographs used in chapters 3 and 4 we used a custom written Matlab script, of which a representative picture of its interface is shown in figure A.1.

This routine takes every vertical slice of a kymograph (equal to a single frame in a movie) and, based on a previously assigned threshold, finds the regions where the fluorescence intensity is greater than the sum of the assigned threshold and the minimum value of intensity and the minimum intensity value averaged through all the frames of the kymograph. The intensity values for each slice of the middle panel are then fitted to up to eight Gaussian distributions, identifying their mean position, amplitude (intensity of the fluorophore), standard deviation and an offset

(corresponding to the noise level). Finally, the data are manually screened, based on the original kymograph, to separate the fluorescence intensity values from random background noise that has not been filtered out by the threshold.

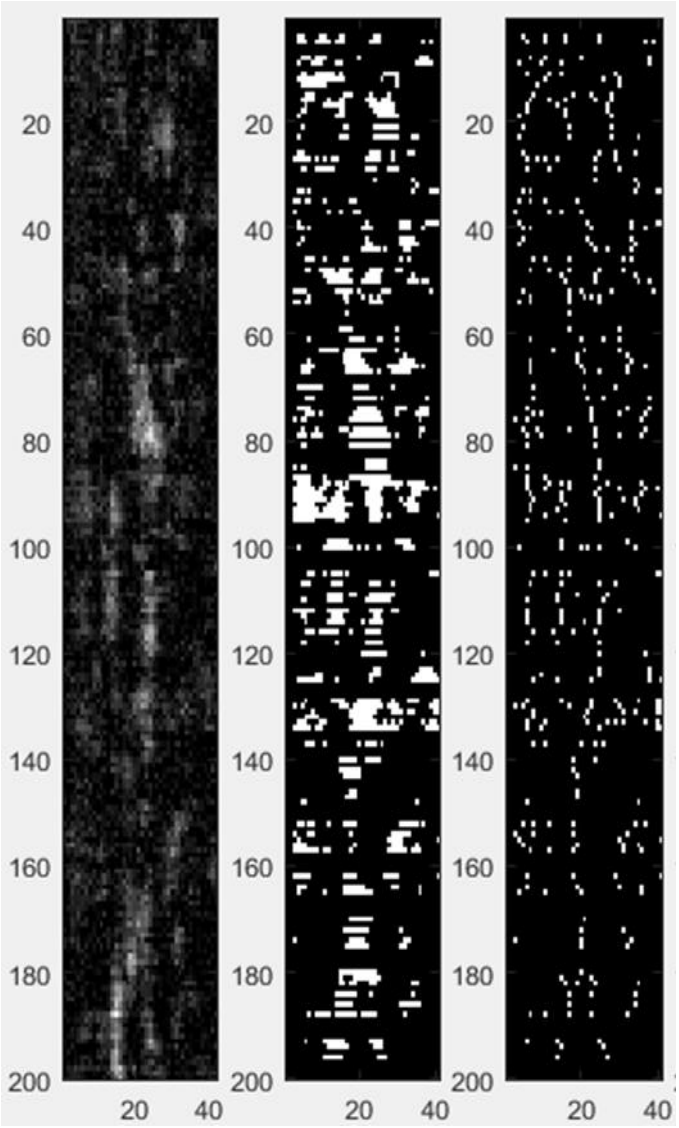

Figure A.1: **Extracting the fluorescence intensity from a kymograph.** Representative picture of the output of the Matlab script sued to determine the intensity of each fluorescent spot in a kymograph. In the left panel is the original kymograph, in the middle panel is a representation of all the pixels that pass a set threshold and in the right panel a binary plot of the Gaussian peaks position found by the script.

A.4 – Calculating the relative ratios of A_{CL} and A_M used in the kinetic model

$$A_B + n_{Ca}Ca^{2+} \overset{K_1}{\rightleftharpoons} A_{CL} + n_M MDP_i \overset{K_2}{\rightleftharpoons} A_M M + T$$

$$K_1 = \frac{A_B[Ca^{2+}]^{n_{Ca}}}{A_{CL}} \qquad K_2 = \frac{A_{CL}[M]^{n_M}}{A_M[ATP]}$$

$$\frac{A_B}{A_{CL}} = \frac{K_1}{[Ca^{2+}]^{n_{Ca}}} \qquad \frac{A_M}{A_{CL}} = \frac{[M]^{n_M}}{K_2[ATP]} \qquad \frac{A_B}{A_M} = \frac{K_1K_2[ATP]}{[Ca^{2+}]^{n_{Ca}}[M]^{n_M}}$$

$$A_{cl} = \frac{A_{CL}}{A_B + A_{CL} + A_M} = \frac{1}{\frac{A_B}{A_{CL}} + 1 + \frac{A_M}{A_{CL}}}$$

$$= \frac{[Ca^{2+}]^{n_{Ca}}K_2[ATP]}{K_1K_2[ATP] + [Ca^{2+}]^{n_{Ca}}K_2[ATP] + [M]^{n_M}[Ca^{2+}]^{n_{Ca}}}$$

$$A_m = \frac{A_M}{A_B + A_{CL} + A_M} = \frac{1}{\frac{A_B}{A_M} + \frac{A_{CL}}{A_M} + 1}$$

$$= \frac{[Ca^{2+}]^{n_{Ca}}[M]^{n_M}}{K_1K_2[ATP] + [Ca^{2+}]^{n_{Ca}}K_2[ATP] + [M]^{n_M}[Ca^{2+}]^{n_{Ca}}}$$

A.5 – Calculating the second order ATP binding rate constant

The second order ATP binding rate constant of myosin was calculated using the thin filament tightrope assay, looking at the binding of 5 nM S1-GFP on unregulated actin thin filaments in the same imaging experimental conditions used in the results chapters (300 ms exposure time, 5 mW of 488 nm laser power).

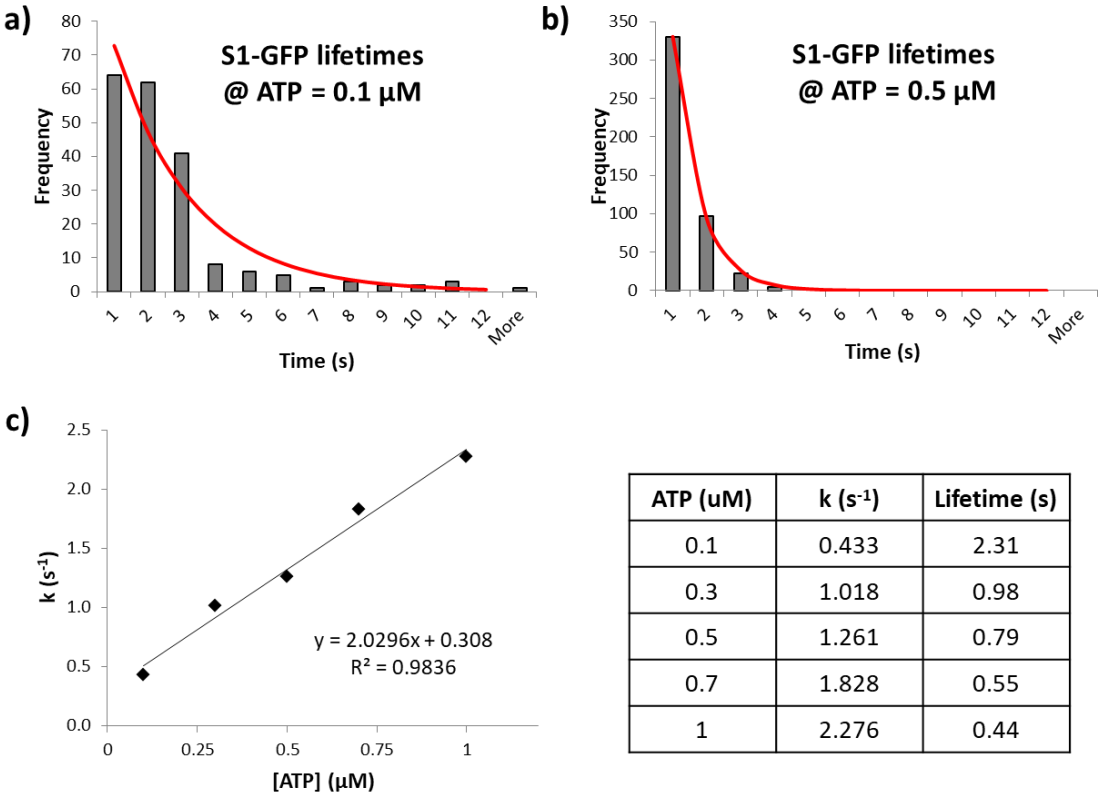

ATP (uM)	k (s^{-1})	Lifetime (s)
0.1	0.433	2.31
0.3	1.018	0.98
0.5	1.261	0.79
0.7	1.828	0.55
1	2.276	0.44

Figure A.2: **Calculating the second order ATP binding rate constant.** a) and b) are histograms of the lifetimes of the S1-GFP on unregulated actin concentration at the stated ATP concentration; c) plotting a graph of the S1-GFP binding frequency vs. the ATP concentration resulted in a linear relationship having a slope equals to the second order ATP binding rate constant, 2.03 $\mu M^{-1}s^{-1}$. All the data acquired are listed in the table.

We looked at the time spent by S1-GFP on the actin filaments (lifetime) and plot all the values in histograms (figure A.2a and b). Fitting these histograms to a decaying exponential distribution, yielded the myosin binding frequency. A plot of the myosin binding frequency at different [ATP] yielded a linear relationship with a slope being the second order ATP binding rate constant of 2.03 $\mu M^{-1}s^{-1}$, consistent with the value found by (Lymn and Taylor, 1971) and (Desai *et al.*, 2015).

A.6 – The Reversible Jump Markov-Chain Monte Carlo (RJMCMC) and generation of transition matrices

The RJMCMC algorithm is a statistical analysis that allow the modelling of stochastics transitions based only on the present state, without knowledge of past transitions. The algorithm models the data in a series of iterations, reaching convergence and outputting the probability of each transition in a kymograph.

Four independent Markov chains were generated for a kymograph, in order to calculate the average mean and variance value for each population of binders, where the mean corresponds to the predicted intensity values for a defined number of binders. The number of components (maximum number of binders) used in the RJMCMC algorithm was constrained so that the intensity would have a linear dependence with the number of binders. Table A1 shows the average of four simulated RJMCMC chains with two different numbers of components is shown in. For both 7 components (equivalent to background plus 6 binders) and 9 components

(equivalent to background plus 8 binders) clear increments between binders are seen. However the 9 component simulation provides a better linear relationship and was used as the basis for further analysis. Further confirmation of the choice of component number derives from the weighting or relative abundance of these binders. For 9 components the predominant population is between 1 and 5 molecules per bound cluster, few components are seen for 6 to 8.

	Total of 6 Binders (7 components)			**Total of 8 Binders (9 components)**		
	Mean	**Variance**	**Weight**	**Mean**	**Variance**	**Weight**
No Binders	57.17	34.73	0.12	24.52	35.58	0.10
1 Binder	150.75	42.07	0.21	138.57	41.54	0.15
2 Binders	198.26	50.68	0.20	173.87	46.04	0.16
3 Binders	254.73	60.71	0.15	210.90	51.35	0.16
4 Binders	314.23	69.58	0.14	264.22	55.51	0.14
5 Binders	401.37	85.73	0.11	322.20	62.04	0.11
6 Binders	551.86	111.40	0.07	382.67	80.58	0.08
7 Binders				490.73	72.01	0.05
8 Binders				652.38	91.13	0.04

Table A1: **Summary results of the average of four RJMCMC chains.** The values of mean, variance and weight resulted from the RJMCMC of a kymograph, to test the model for a total of either 6 or 8 myosin molecules, and find the fluorescence intensity ranges of myosin clusters, used in the analysis of the experimental data.

The midpoint between successive means for the 9 component simulation was used as the cut-off pixel intensity value for that population of binders (calculated as the mean between two subsequent binders intensity), in order to discern between different

clusters of myosin. Table A2 provides a breakdown of all the values used for these cut-offs. These mean and cut-off values were carried forward into the analysis of all subsequent kymographs to generate datasets of number of bound myosin molecules within a cluster, and finally derive the transition matrices.

	Lower Bound	**Upper Bound**
Range of values for 0 binders	0	81.54
Range of values for 1 binder	81.55	156.21
Range of values for 2 binders	156.22	192.38
Range of values for 3 binders	192.39	237.55
Range of values for 4 binders	237.56	293.20
Range of values for 5 binders	293.21	352.43
Range of values for 6 binders	352.44	436.69
Range of values for 7 binders	436.70	571.55
Range of values for 8 binders	571.56	641.55
Range of values for 9 binders	641.56	711.55
Range of values for 10 binders	711.56	781.55
Range of values for 11 binders	781.56	>781.56

Table A2: **Range of intensity values for each cluster of myosin molecules.** These values have been used to transform the raw kymograph into a transition matrix.

A.7 – Determination of the number of Gaussian distributions for the fitting of the C0C3 intensity histogram

To determine average number of cMyBP-C molecules bound per unit length of thin filament (µm) we need to calculate fluorescence intensity value associated with a single molecule. Using the same approach of (Desai *et al.*, 2015) and (Iino *et al.*, 2001), we pooled into a histograms all the fluorescence point spread function intensity values obtained imaging 20 nM Cy3-C0C3 on thin filaments at pCa 7 and then fitted it to a number of Gaussian distribution, as described in section 5.2.2. The mean intensity of each distribution would then follow a linear relationship with their associated number of molecules, leading us to the intensity of a single Cy3 fluorophore. This linear relationship can also be used to evaluate the right number of Gaussian distributions chosen for the fitting. Figure A.3 shows an example of this procedure.

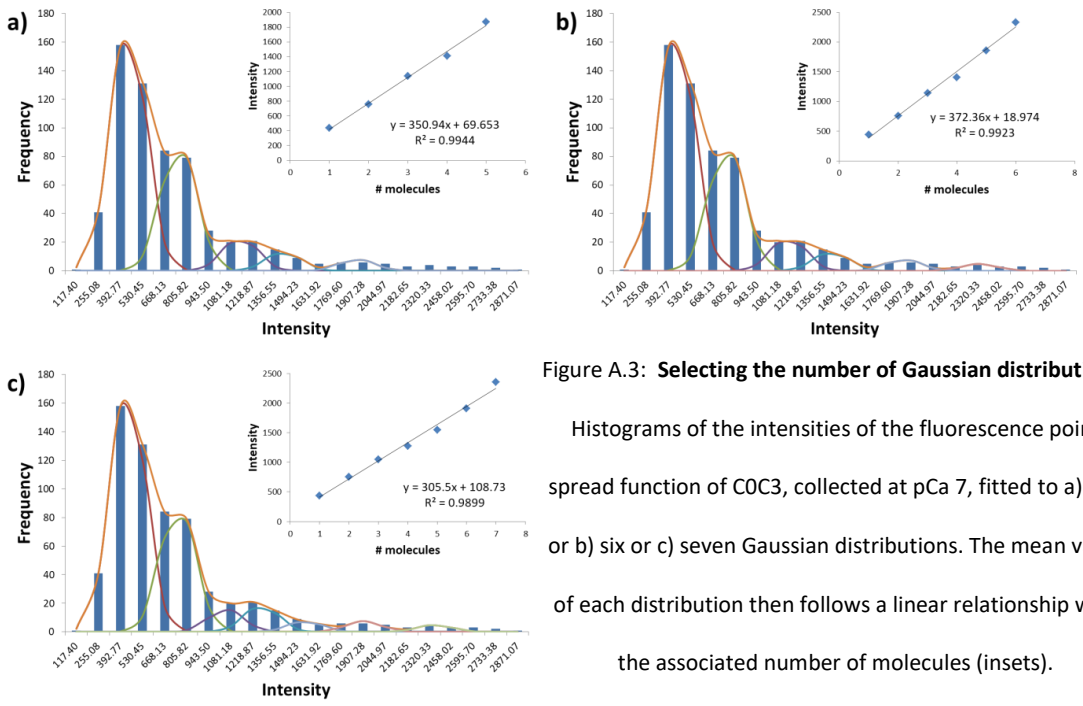

Figure A.3: **Selecting the number of Gaussian distributions.** Histograms of the intensities of the fluorescence point spread function of C0C3, collected at pCa 7, fitted to a) five or b) six or c) seven Gaussian distributions. The mean value of each distribution then follows a linear relationship with the associated number of molecules (insets).

Although the intensity histogram can be fit adequately with up to seven Gaussian distributions (figure A.3), each resulting linear relationship yield different values of slope and intercept. In particular, fitting the Cy3 intensity histogram using five Gaussian distributions (figure A.3a) produces a slope (single molecule intensity) of 350.9 and an intercept (single molecule intensity associated error) of 69.7, with an R^2 of 0.994, while using seven Gaussian distributions (figure A.3c) brings the slope down to 305.5 and the intercept up to 108.7, with an R^2 of 0.990. Considering that using six Gaussian distributions (figure A.3b) results in an in-between value of R^2 (0.992), a lower intercept (19.0) and a similar value of slope to figure A.3 a, we chose six as the optimal number of Gaussian distributions to fit out intensity histogram and proceeded to use its linear relationship for the quantification of the single molecules in the subsequent analysis.

BIBLIOGRAPHY

Adhikari, A. S. *et al.* (2016) 'Mutations Significantly Increase the Velocity, Force, and Actin-Activated ATPase Activity of Human beta-Cardiac Myosin', *CellReports*, 17(11), pp. 2857–2864.

Al-Khayat, H. A. (2013) 'Three-dimensional structure of the human myosin thick filament: Clinical implications', *Global Cardiology Science and Practice*, 2013(3), p. 36.

Al-Sarayreh, S. A. (2011) *Effect of hypertrophic and dilated cardiomyopathies associated mutations in troponin I on cardiac thin filament dynamics.* - Department of Biochemistry, College of Medicine, Biological Sciences and Psychology - University of Leicester.

Alamo, L. *et al.* (2016) 'Conserved Intramolecular Interactions Maintain Myosin Interacting-Heads Motifs Explaining Tarantula Muscle Super-Relaxed State Structural Basis', *Journal of Molecular Biology*. 428(6), pp. 1142–1164.

Arad, M. *et al.* (2002) 'Phenotypic diversity in hypertrophic cardiomyopathy.', *Human molecular genetics*, 11(20), pp. 2499–506.

Avrova, S. V *et al.* (2018) 'The reason for the low Ca2+-sensitivity of thin filaments associated with the Glu41Lys mutation in the TPM2 gene is " freezing " of tropomyosin near the outer domain of actin and inhibition of actin monomer switching off during the ATPase cycle', *Biochemical and Biophysical Research Communications*. 502(2), pp. 209–214.

Badr, M. A. *et al.* (2016) 'Fluorescent protein-based Ca^{2+} sensor reveals global, divalent cation-dependent conformational changes in cardiac troponin C', *PLoS ONE*, 11(10), pp.

1–27.

Bagshaw, C. R. and Trentham, D. R. (1973) 'The reversibility of adenosine triphosphate cleavage by myosin', *The Biochemical journal*, 133(2), pp. 323–328.

Bai, F. *et al.* (2011) 'Enhanced active cross-bridges during diastole: Molecular pathogenesis of tropomyosin's HCM mutations', *Biophysical Journal*, 100(4), pp. 1014–1023.

Bai, F. *et al.* (2013) 'A study of tropomyosin's role in cardiac function and disease using thin-filament reconstituted myocardium', *Journal of Muscle Research and Cell Motility*, 34(1), pp. 295–310.

Barua, B. *et al.* (2012) 'Regulation of actin-myosin interaction by conserved periodic sites of tropomyosin', *Proceedings of the National Academy of Sciences*, 109(45), pp. 18425–18430.

Batters, C. *et al.* (2014) 'To understand muscle you must take it apart', *Frontiers in Physiology*, 5, pp. 1–14.

Beechem, M. and Brand, L. (1986) 'Global Analysis of Fluorescence Decay: Applications to Some Unusual Experimental and Theoretical Studies', *Photochemistry and Photobiology*, 44(3), pp. 323–329.

Behrmann, E. *et al.* (2012) 'Structure of the Rigor Actin-Tropomyosin-Myosin Complex', *Cell*, 150(2), pp. 327–338.

Belknap, B. *et al.* (2014) 'Modulation of thin filament activation of myosin ATP hydrolysis by N-terminal domains of cardiac myosin binding protein-C', *Biochemistry*, 53(42), pp. 6717–24.

Bezold, K. L. *et al.* (2013) 'A gain-of-function mutation in the M-domain of cardiac myosin-binding protein-C increases binding to actin', *Journal of Biological Chemistry*,

288(30), pp. 21496–21505.

Bing, W. *et al.* (2000) 'Effect of hypertrophic cardiomyopathy mutations in human cardiac muscle α-tropomyosin (Asp175Asn and Glu180Gly) on the regulatory properties of human cardiac troponin determined by in vitro motility assay', *Journal of Molecular and Cellular Cardiology*, 32(8), pp. 1489–1498.

Bing, W. *et al.* (2000) 'A simple method for measuring the relative force exerted by myosin on actin filaments in the in vitro motility assay: evidence that tropomyosin and troponin increase force in single thin filaments.', *The Biochemical journal*, 350 Pt 3, pp. 693–699.

Bottinelli, R. *et al.* (1998) 'A mutant tropomyosin that causes hypertrophic cardiomyopathy is expressed in vivo and associated with an increased calcium sensitivity', *Circulation Research*, 82(1), pp. 106–115.

Boussouf, S. E. *et al.* (2007) 'Role of tropomyosin isoforms in the calcium sensitivity of striated muscle thin filaments', *Journal of muscle research and cell motility*, 28(1), pp. 49–58.

Brunet, N. M. *et al.* (2014) 'Ca^{2+}-regulatory function of the inhibitory peptide region of cardiac troponin I is aided by the C-terminus of cardiac troponin T : Effects of familial hypertrophic cardiomyopathy mutations cTnI R145G and cTnT R278C, alone and in combination, on filament sliding', *Arch Biochem Biophys*, 552–553, pp. 11–20.

Bunch, T. A. *et al.* (2018) 'N-terminal extension in cardiac myosin-binding protein C regulates myofilament binding', *Journal of Molecular and Cellular Cardiology*, 125, pp. 140–148.

Burghardt, T. P. and Sikkink, L. A. (2013) 'Regulatory Light Chain Mutants Linked to Heart Disease Modify the Cardiac Myosin Lever Arm', *Biochemistry*, 52, pp. 1249–1259.

Burke, M. *et al.* (1973) 'Studies on the "Hinge" Region of Myosin', *Biochemistry*, 12(4), pp. 701–710.

Butt, T. *et al.* (2010) 'Myosin Motors Drive Long Range Alignment of Actin Filaments', *Journal of Biological Chemistry*, 285(7), pp. 4964–4974.

Van Camp, S. *et al.* (1995) 'Nontraumatic sports death in high school and college athletes', *Medicine and Science in Sports and Exercise*, 27, pp. 641–647.

Carlier, M.-F. *et al.* (1986) 'The effects of Mg^{2+} at the high affinity and low affinity sites on the polymerization of actin and associated ATP hydrolysis', *Journal of Biological Chemistry*, 261(23), pp. 10785–10792.

Carlier, M. *et al.* (1997) 'Actin Depolymerizing Factor (ADF/Cofilin) Enhances the Rate of Filament Turnover: Implication in Actin-based Motility', *The Journal of cell biology*, 136(6), pp. 1307–1323.

Carlier, M. F. *et al.* (1984) 'Evidence for an ATP cap at the ends of actin filaments and its regulation of the F-actin steady state', *Journal of Biological Chemistry*, 259(16), pp. 9983–9986.

Casellas, J. F. and Torres, A. (1994) 'Interaction of Cap Z with Actin', *Journal of Biological Chemistry*, 269(9), pp. 6992–6998.

Chang, A. N. *et al.* (2005) 'Functional Consequences of Hypertrophic and Dilated Cardiomyopathy-causing Mutations in alpha-Tropomyosin', *Journal of Biological Chemistry*, 280(40), pp. 34343–34349.

Chang, A. N. *et al.* (2014) 'Structural and protein interaction effects of hypertrophic and dilated cardiomyopathic mutations in alpha-tropomyosin.', *Frontiers in physiology*, 5, p. 460.

Chong, P. C. S. and Hodges, R. S. (1982) 'Photochemical cross-linking between rabbit

skeletal troponin and a-tropomyosin', *Journal of Biological Chemistry*, 257(15), pp. 9152–9160.

Chung, M.-W. *et al.* (2003) 'Hypertrophic cardiomyopathy: From gene defect to clinical disease', *Cell Research*, 13(1), pp. 9–20.

Coates, J. H., Criddle, A. H. and Geeves, M. A. (1985) 'Pressure-relaxation studies of pyrene-labelled actin and myosin subfragment 1 from rabbit skeletal muscle. Evidence for two states of acto-subfragment 1.', *The Biochemical journal*, 232(2), pp. 351–6.

Cohn, R. *et al.* (2019) 'A Contraction Stress Model of Hypertrophic Cardiomyopathy due to Sarcomere Mutations Rachel', *Stem Cell Reports*, 12, pp. 1–13.

Colson, B. A. *et al.* (2010) 'Differential roles of regulatory light chain and myosin binding protein-C phosphorylations in the modulation of cardiac force development', *The Journal of physiology*, 588(6), pp. 981–993.

Colson, B. A. *et al.* (2016) 'Site-directed spectroscopy of cardiac myosin-binding protein C reveals effects of phosphorylation on protein structural dynamics.', *Proceedings of the National Academy of Sciences of the United States of America*, 113(12), pp. 3233–3238.

Cooke, R. (1975) 'The Role of the Bound Nucleotide in the Polymerization of Actin', *Biochemistry*, 14(14), pp. 3250–3256.

Coppini, R. *et al.* (2014) 'Clinical phenotype and outcome of hypertrophic cardiomyopathy associated with thin-filament gene mutations', *Journal of the American College of Cardiology*, 64(24), pp. 2589–2600.

Cutts, A. (1988) 'The range of sarcomere lengths in the muscles of the human lower limb', *Journal of anatomy*, 160, pp. 79–88.

Dahiya, R. *et al.* (1994) 'Equilibrium linkage analysis of cardiac thin filament assembly.

Implications for the regulation of muscle contraction', *Journal of Biological Chemistry*, 269(47), pp. 29457–29461.

Deng, Y. *et al.* (2003) 'Phosphorylation of human cardiac troponin I G203S and K206Q linked to familial hypertrophic cardiomyopathy affects actomyosin interaction in different ways', *Journal of Molecular and Cellular Cardiology*, 35, pp. 1365–1374.

Desai, R. *et al.* (2015) 'Using fluorescent myosin to directly visualize cooperative activation of thin filaments', *Journal of Biological Chemistry*, 290(4), pp. 1915–1925.

Van Dijk, S. J. *et al.* (2009) 'Cardiac myosin-binding protein C mutations and hypertrophic ardiomyopathy haploinsufficiency, deranged phosphorylation, and cardiomyocyte dysfunction', *Circulation*, 119(11), pp. 1473–1483.

Van Dijk, S. J. *et al.* (2016) 'The A31P missense mutation in cardiac myosin binding protein C alters protein structure but does not cause haploinsufficiency', *Archives of Biochemistry and Biophysics*. Elsevier Inc, 601, pp. 133–140.

Van Dijk, S. J. *et al.* (2015) 'Normal cardiac contraction in mice lacking the proline-alanine rich region and C1 domain of cardiac myosin binding protein C', *Journal of Molecular and Cellular Cardiology*, 88, pp. 124–132.

Dominguez, R. and Holmes, K. C. (2011) 'Actin Structure and Function', *Annual Review of Biophysics*, 40(1), pp. 169–186.

Dong, W. *et al.* (2003) 'Kinetics of Conformational Transitions in Cardiac Troponin Induced by Ca^{2+} Dissociation Determined by Forster Resonance Energy Transfer', *Journal of Biological Chemistry*, 278(43), pp. 42394–42402.

Van Driest, S. L. *et al.* (2004) 'Myosin binding protein C mutations and compound heterozygosity in hypertrophic cardiomyopathy', *Journal of the American College of Cardiology*, 44(9), pp. 1903–1910.

von der Ecken, J. *et al.* (2015) 'Structure of the F-actin–tropomyosin complex', *Nature*, 519(7541), pp. 114–117.

van Eerd, J.-P. and Takahashi, K. (1975) 'The amino acid sequence of bovine cardiac troponin-C. Comparison with rabbit skeletal troponin-C', *Biochemical and Biophysical Research Communications*, 64(1), pp. 122–127.

Eisenfeld, J. and Ford, C. C. (1979) 'A Systems-Theory Approach to the Analysis of Multiexponential Fluorescence Decay', *Biophysical Journal*, 26(1), pp. 73–84.

Elliott, K., Watkins, H. and Redwood, C. S. (2000) 'Altered Regulatory Properties of Human Cardiac Troponin I Mutants That Cause Hypertrophic Cardiomyopathy', *Journal of Biological Chemistry*, 275(29), pp. 22069–22074.

Epstein, N. D. *et al.* (1992) 'Differences in clinical expression of hypertrophic cardiomyopathy associated with two distinct mutations in the beta-myosin heavy chain gene. A $908^{Leu->Val}$ mutation and a $403^{Arg->Gln}$ mutation', *Circulation*, 86(2), pp. 345–352.

Estes, J. E. *et al.* (1981) 'Mechanism of Action of Phalloidin on the Polymerization of Muscle Actin', *Biochemistry*, 20(4), pp. 708–712.

Farman, G. P. *et al.* (2018) 'HCM and DCM cardiomyopathy-linked α-tropomyosin mutations influence off-state stability and crossbridge interaction on thin filaments', *Archives of Biochemistry and Biophysics*.

Fenix, A. M. *et al.* (2018) 'Muscle-specific stress fibers give rise to sarcomeres in cardiomyocytes', *eLife*, 7(e42144), pp. 1–33.

Ferrantini, C. *et al.* (2017) 'Pathogenesis of hypertrophic cardiomyopathy is mutation rather than disease specific: A comparison of the cardiac troponin T E163R and R92Q mouse models', *Journal of the American Heart Association*, 6(7), pp. 1–20.

Flashman, E. *et al.* (2004) 'Cardiac myosin binding protein C: Its role in physiology and disease', *Circulation Research*, 94(10), pp. 1279–1289.

Flory, P. J. (1936) 'Molecular Size Distribution in Linear Condensation Polymers', *Journal of the American Chemical Society*, 58(10), pp. 1877–1885.

Franklin, A. J. *et al.* (2012) 'The C-terminus of troponin T is essential for maintaining the inactive state of regulated actin', *Biophysical Journal*, 102(11), pp. 2536–2544.

Fraser, I. D. C. and Marston, S. B. (1995) 'In vitro motility analysis of actin-tropomyosin regulation by troponin and calcium. The thin filament is switched as a single cooperative unit', *Journal of Biological Chemistry*, pp. 7836–7841.

Freiburg, A. and Gautel, M. (1996) 'A molecular map of the interactions between titin and myosin-binding protein C: implications for sarcomeric assembly in familial hypertrophic cardiomyopathy', *European Journl of Biochemistry*, 235, pp. 317–323.

Freiburger, L. *et al.* (2015) 'Global ITC fitting methods in studies of protein allostery', *Methods*, 76, pp. 149–161.

Frye, J. *et al.* (2010) 'Structure of the tropomyosin overlap complex from chicken smooth muscle: Insight into the diversity of N-terminal recognition', *Biochemistry*, 49(23), pp. 4908–4920.

Fujii, T. *et al.* (2010) 'Direct visualization of secondary structures of F-actin by electron cryomicroscopy', *Nature*, 467(7316), pp. 724–728.

Gautel, M. (2011) 'Cytoskeletal protein kinases: Titin and its relations in mechanosensing', *Pflugers Archiv European Journal of Physiology*, 462(1), pp. 119–134.

Geeves, M. A. and Lehrer, S. S. (1994) 'Dynamics of the muscle thin filament regulatory switch: the size of the cooperative unit', *Biophysical Journal*, 67(1), pp. 273–282.

Glazier, A. A. *et al.* (2018) 'Allelic imbalance and haploinsufficiency in MYBPC3-linked

hypertrophic cardiomyopathy', *Pflugers Archiv European Journal of Physiology*.

Gokhin, D. S. *et al.* (2015) 'Tropomodulin 1 directly controls thin filament length in both wild-type and tropomodulin 4-deficient skeletal muscle', *The Company of Biologists*, 142, pp. 4351–4362.

Golitsina, N. *et al.* (1997) 'Effects of two familial hypertrophic cardiomyopathy-causing mutations on alpha-tropomyosin structure and function', *Biochemistry*, 36(15), pp. 4637–4642.

Golitsina, N. *et al.* (1999) 'Erratum: Effects of Two Familial Hypertrophic Cardiomyopathy- Causing Mutations on alpha-Tropomyosin Structure and Function', *Biochemistry*, 38, p. 3850.

Goode, B. L. and Eck, M. J. (2007) 'Mechanism and Function of Formins in the Control of Actin Assembly', *Annual Review of Biochemistry*, 76, pp. 593–627.

Gordon, A. M. *et al.* (1966) 'The variation in isometric tension with sarcomere length in vertebrate muscle fibres', *The Journal of Physiology*, 184(1), pp. 170–192.

Gorga, J. A. *et al.* (2003) 'Activation of the calcium-regulated thin filament by myosin strong binding', *Biophysical Journal*, 85(4), pp. 2484–2491.

Greenfield, N. J. *et al.* (2006) 'Solution NMR Structure of the Junction between Tropomyosin Molecules : Implications for Actin Binding and Regulation', *Journal of molecular biology*, 364, pp. 80–96.

Gruen, M. and Gautel, M. (1999) 'Mutations in beta-myosin S2 that cause familial hypertrophic cardiomyopathy (FHC) abolish the interaction with the regulatory domain of myosin-binding protein-C', *Journal of molecular biology*, 286(3), pp. 933–49.

Guhathakurta, P. *et al.* (2015) 'Amplitude of the actomyosin power stroke depends strongly on the isoform of the myosin essential light chain', *PNAS*, 112(15), pp. 4660–

4665.

Guilford, W. H. *et al.* (1997) 'Smooth Muscle and Skeletal Muscle Myosins Produce Similar Unitary Forces and Displacements in the Laser Trap', *Biophysical Journal*, 72(3), pp. 1006–1021.

Hanson, J. and Huxley, H. E. (1953) 'Structural basis of the cross-striations in muscle', *Nature*, 172(4377), pp. 530–532.

Harris, D. E. and Warshaws, D. M. (1993) 'Smooth and Skeletal Muscle Myosin Both Exhibit Low Duty Cycles at Zero Load in Vitro', *Journal of Biological Chemistry*, 268(20), pp. 14764–14768.

Harris, S. P. *et al.* (2016) 'C0 and C1 N-terminal Ig domains of myosin binding protein C exert different effects on thin filament activation', *Proceedings of the National Academy of Sciences of the United States of America*, 113(6), pp. 1558–63.

Harris, S. P. *et al.* (2011) 'In the thick of it: HCM-causing mutations in myosin binding proteins of the thick filament', *Circulation Research*, 108(6), pp. 751–764.

Heeley, D. H. *et al.* (2006) 'Maximal activation of skeletal muscle thin filaments requires both rigor myosin S1 and calcium', *Journal of Biological Chemistry*, 281(1), pp. 668–676.

Heller, M. J. *et al.* (2003) 'Cardiomyopathic Tropomyosin Mutations that Increase Thin Filament Ca^{2+}-sensitivity and Tropomyosin N-domain Flexibility', *Journal of Biological Chemistry*, 278(43), pp. 41742–41748.

Herman, P. and Ching Lee, J. (2012) 'The advantage of Global Fitting of Data Involving Complex Linked Reactions', *Methods in Molecular Biology*.

Hernandez, O. M. *et al.* (2005) 'F110I and R278C Troponin T Mutations That Cause Familial Hypertrophic Cardiomyopathy Affect Muscle Contraction in Transgenic Mice

and Reconstituted Human Cardiac Fibers', *Journal of Biological Chemistry*, 280(44), pp. 37183–37194.

Hitchcock-DeGregori, S. E. and Heald, R. W. (1987) 'Altered actin and troponin binding of amino-terminal variants of chicken striated muscle alpha-tropomyosin expressed in Escherichia coli.', *Journal of Biological Chemistry*, 262(20), pp. 9730–9735.

Hollman, A. *et al.* (1959) 'A Family with Obstructive Cardiomyopathy (Asymmetrical Hypertrophy)', pp. 449–456.

Holmes, K. C. *et al.* (1990) 'Atomic model of the actin filament.', *Nature*, pp. 44–49.

Holzbaur, E. L. F. and Goldman, Y. E. (2010) 'Coordination of molecular motors : from in vitro assays to intracellular dynamics', *Current Opinion in Cell Biology*, 22(1), pp. 4–13.

Homsher, E. *et al.* (1996) 'Calcium regulation of thin filament movement in an in vitro motility assay', *Biophysical journal*, 70, pp. 1881–1892.

Hooijman, P., Stewart, M. A. and Cooke, R. (2011) 'A new state of cardiac myosin with very slow ATP turnover: A potential cardioprotective mechanism in the heart', *Biophysical Journal*, 100(8), pp. 1969–1976.

Houdusse, a *et al.* (1997) 'Structures of four Ca^{2+}-bound troponin C at 2.0 A resolution: further insights into the Ca^{2+}-switch in the calmodulin superfamily', *Structure (London, England: 1993)*, 5, pp. 1695–1711.

Houdusse, A. *et al.* (1999) 'Atomic Structure of Scallop Myosin Subfragment S1 Complexed with MgADP : A Novel Conformation of the Myosin Head', *Cell*, 97, pp. 459–470.

Houdusse, A., Szent-Györgyi, A. G. and Cohen, C. (2000) 'Three conformational states of scallop myosin S1', *Proceedings of the National Academy of Sciences of the United States of America*, 97(21), pp. 11238–11243.

Houston, B. A. and Stevens, G. R. (2015) 'Hypertrophic cardiomyopathy: A review', *Clinical Medicine Insights: Cardiology*, 8, pp. 53–65.

Howarth, J. W. *et al.* (2007) 'Phosphorylation-dependent Conformational Transition of the Cardiac Specific N-Extension of Troponin I in Cardiac Troponin', *Journal of Molecular Biology*, 373(3), pp. 706–722.

Howarth, J. W. *et al.* (2012) 'Structural insight into unique cardiac myosin-binding protein-C motif: A partially folded domain', *Journal of Biological Chemistry*, 287(11), pp. 8254–8262.

Huelnhagen, T. *et al.* (2018) 'Myocardial Effective Transverse Relaxation Time T2* is Elevated in Hypertrophic Cardiomyopathy: A 7.0 T Magnetic Resonance Imaging Study', *Scientific Reports*, (November 2017), pp. 1–9.

Hussain, S. *et al.* (2013) 'Spatiotemporal Dynamics of Actomyosin Networks Analytical measures', *Biophysical Journal*, 105(6), pp. 1456–1465.

Huxley, A. F. and Niedergerke, R. (1954) 'Structural changes in muscle during contraction: Interference microscopy of living muscle fibres', *Nature*, 173(4412), pp. 971–973.

Huxley, H. E. (1969) 'The Mechanism of Muscular Contraction', *Science*, 164(3886), pp. 1356–1366.

Huxley, H. and Hanson, J. (1954) 'Changes in the Cross-Striations of Muscle during Contraction and Stretch and their Structural Interpretation', *Nature*, 173(4412), pp. 973–976.

Ichetovkin, I. *et al.* (2000) 'Actin Filaments Are Severed by Both Native and Recombinant Dictyostelium Cofilin But to Different Extents', *Cell Motility and the Cytoskeleton*, 306, pp. 293–306.

Iino, R., Koyama, I. and Kusumi, A. (2001) 'Single Molecule Imaging of Green Fluorescent Proteins in Living Cells: E-Cadherin Forms Oligomers on the Free Cell Surface', *Biophysical Journal*, 80(6), pp. 2667–2677.

Ingraham, R. H. and Swenson, C. A. (1984) 'Binary interaction of troponin subunits', *Journal of Biological Chemistry*, 259(15), pp. 9544–9548.

Iorga, B. *et al.* (2008) 'Lys184 deletion in troponin I impairs relaxation kinetics and induces hypercontractility in murine cardiac myofibrils', *Cardiovascular Research*, 77, pp. 676–686.

Isambert, H. *et al.* (1995) 'Flexibility of Actin Filaments from Thermal Fluctuations', *The Journal of biological chemistry*, 270(19), pp. 11437–11444.

Iskratsch, T. and Ehler, E. (2011) 'Formin-g muscle cytoarchitecture', *Bioarchitecture*, 1(2), pp. 66–68.

Iwasa, M. *et al.* (2008) 'Dual roles of Gln137 of actin revealed by recombinant human cardiac muscle α-actin mutants', *Journal of Biological Chemistry*, 283(30), pp. 21045–21053.

Jacques, A. M. *et al.* (2008) 'Myosin binding protein C phosphorylation in normal, hypertrophic and failing human heart muscle', *Journal of Molecular and Cellular Cardiology*, 45(2), pp. 209–216.

Janco, M. *et al.* (2012) 'alpha-Tropomyosin with a D175N or E180G mutation in only one chain differs from tropomyosin with mutations in both chains', *Biochemistry*, 51(49), pp. 9880–9890.

Javadpour, M. M. *et al.* (2003) 'Decreased energetics in murine hearts bearing the R92Q mutation in cardiac troponin T', *Journal of Clinical Investigation*, 112(5), pp. 768–775.

Jayasundar, J. J. *et al.* (2014) 'Molecular Dynamics Simulations of the Cardiac Troponin Complex Performed with FRET Distances as Restraints', *PLoS ONE*, 9(2), p. e87135.

Johnson, K. A. and Taylor, E. W. (1978) 'Intermediate States of Subfragment 1 and Actosubfragment 1 ATPase: Reevaluation of the Mechanism', *Biochemistry*, 17(17), pp. 3432–3442.

Kabsch, W. *et al.* (1990) 'Atomic structure of the actin:DNase I complex', *Nature*, pp. 37–44.

Kad, N. M. *et al.* (2003) 'A mutant heterodimeric myosin with one inactive head generates maximal displacement', *Journal of Cell Biology*, 162(3), pp. 481–488.

Kad, N. M. *et al.* (2005) 'Single-myosin crossbridge interactions with actin filaments regulated by troponin-tropomyosin.', *Proceedings of the National Academy of Sciences of the United States of America*, 102(47), pp. 16990–16995.

Kad, N. M. *et al.* (2007) 'Mutation of a Conserved Glycine in the SH1-SH2 Helix Affects the Load-Dependent Kinetics of Myosin', *Biophysical Journal*, 92(5), pp. 1623–1631.

Kad, N. M. *et al.* (2010) 'Collaborative Dynamic DNA Scanning by Nucleotide Excision Repair Proteins Investigated by Single- Molecule Imaging of Quantum-Dot-Labeled Proteins', *Molecular Cell*, 37(5), pp. 702–713.

Kaishima, M. *et al.* (2016) 'Expression of varied GFPs in Saccharomyces cerevisiae: Codon optimization yields stronger than expected expression and fluorescence intensity', *Scientific Reports*, 6(October), pp. 1–15.

Kalyva, A. *et al.* (2012) 'In vitro formation and characterization of the skeletal muscle alpha-tropomyosin heterodimers', *Biochemistry*, 51(32), pp. 6388–6399.

Kampourakis, T. *et al.* (2014) 'Myosin binding protein-C activates thin filaments and inhibits thick filaments in heart muscle cells', *Proceedings of the National Academy of*

Sciences of the United States of America, 111(52), pp. 18763–18768.

Kampourakis, T. and Irving, M. (2015) 'Phosphorylation of myosin regulatory light chain controls myosin head conformation in cardiac muscle', *Journal of Molecular and Cellular Cardiology*, 85, pp. 199–206.

Karibe, A. *et al.* (2001) 'Hypertrophic cardiomyopathy caused by a novel alpha-tropomyosin mutation (V95A) is associated with mild cardiac phenotype, abnormal calcium binding to troponin, abnormal myosin cycling, and poor prognosis', *Circulation*, 103, pp. 65–71.

Karsai, Á. *et al.* (2011) 'Mechanical unfolding of cardiac myosin binding protein-C by atomic force microscopy', *Biophysical Journal*, 101(8), pp. 1968–1977.

Karsai, Á. *et al.* (2013) 'Cross-species mechanical fingerprinting of cardiac myosin binding protein-C', *Biophysical Journal*, 104(11), pp. 2465–2475.

Kelly, M. and Semsarian, C. (2009) 'Advances in genetics, proteomics, and metabolomics multiple mutations in genetic cardiovascular disease a marker of disease severity?', *Circulation: Cardiovascular Genetics*, 2(2), pp. 182–190.

Kemmer, G. and Keller, S. (2010) 'Nonlinear least-squares data fitting in Excel spreadsheets', *Nature Protocols*, 5(2), pp. 267–281.

Khaitlina, S., Tsaplina, O. and Hinssen, H. (2017) 'Cooperative effects of tropomyosin on the dynamics of the actin filament', *FEBS Letters*, 591, pp. 1884–1891.

Kiani, F. A. *et al.* (2018) 'Spontaneous transitions of actin-bound tropomyosin toward blocked and closed states', *Journal of General Physiology*, pp. 1–5.

Kirschner, S. E. *et al.* (2005) 'Hypertrophic cardiomyopathy-related beta-myosin mutations cause highly variable calcium sensitivity with functional imbalances among individual muscle cells', *American Journal of Physiology and Heart Circulation*

Physiology, 288, pp. H1242–H1251.

Knollmann, B. C. and Potter, J. D. (2001) 'Altered Regulation of Cardiac Muscle Contraction by Troponin T Mutations that Cause Familial Hypertrophic Cardiomyopathy', *Trends in Cardiovascular Medicine*, 11(5), pp. 206–212.

Knutson, J. R. *et al.* (1983) 'Simultaneous Analysis of Multiple Fluorescence Decay Curves: A Global Approach', *Chemical Physics Letters*, 102(6), pp. 501–507.

Kobirumaki-Shimozawa, F. *et al.* (2012) 'Sarcomere imaging by quantum dots for the study of cardiac muscle physiology', *Journal of Biomedicine and Biotechnology*, 2012(i).

Kohler, J. *et al.* (2002) 'Mutation of the myosin converter domain alters cross-bridge elasticity', *Proceedings of the National Academy of Sciences of the United States of America*, 99(6), pp. 3557–3562.

Kojima, H. *et al.* (1994) 'Direct measurement of stiffness of single actin filaments with and without tropomyosin by in vitro nanomanipulation', *Proceedings of the National Academy of Sciences of the United States of America,* 91, pp. 12962–12966.

Konopka, C. A. and Bednarek, S. Y. (2008) 'Variable-angle epifluorescence microscopy: A new way to look at protein dynamics in the plant cell cortex', *Plant Journal*, 53(1), pp. 186–196.

Korte, F. S. *et al.* (2003) 'Loaded Shortening, Power Output, and Rate of Force Redevelopment Are Increased With Knockout of Cardiac Myosin Binding Protein-C', *Circulation Research*, 93(8), pp. 752–758.

Koubassova, N. A. *et al.* (2018) 'Effects of an Interchain Disulfide Bond on Tropomyosin Structure : A Molecular Dynamics Study', *International Journal of Molecular Sciences*, 19(3376), pp. 1–10.

Kremneva, E. *et al.* (2004) 'Effects of two familial hypertrophic cardiomyopathy

mutations in alpha-tropomyosin, Asp175Asn and Glu180Gly, on the thermal unfolding of actin-bound tropomyosin', *Biophysical Journal*, 87(6), pp. 3922–3933.

Krishnan, K. and Moens, P. D. J. (2009) 'Structure and functions of profilins', *Biophysical Reviewss*, 1, pp. 71–81.

Kron, S. J. and Spudich, J. A. (1986) 'Fluorescent actin filaments move on myosin fixed to a glass surface', *Proceedings of the National Academy of Sciences of the United States of America*, 83, pp. 6272–6276.

Kruger, M. *et al.* (2005) 'Effects of the mutation R145G in human cardiac troponin I on the kinetics of the contraction – relaxation cycle in isolated cardiac myofibrils', *Journal of Physiology*, 564(2), pp. 347–357.

Kulikovskaya, I. *et al.* (2003) 'Effect of MyBP-C Binding to Actin on Contractility in Heart Muscle', *The Journal of General Physiology*, 122(6), pp. 761–774.

Kunst, G. *et al.* (2000) 'Myosin binding protein C, a phosphorylation-dependent force regulator in muscle that controls the attachment of myosin heads by its interaction with myosin S2', *Circulation Research*, 86(1), pp. 51–58.

De La Cruz, E. M. and Pollard, T. D. (1994) 'Transient Kinetic Analysis of Rhodamine Phalloidin Binding to Actin Filaments', *Biochemistry*, 33(48), pp. 14387–14392.

Leary, T. S. O. *et al.* (2019) 'MYBPC3 truncation mutations enhance actomyosin contractile mechanics in human hypertrophic cardiomyopathy', *Journal of Molecular and Cellular Cardiology*. Elsevier Ltd, 127, pp. 165–173.

Lehman, W. *et al.* (2000) 'Tropomyosin and actin isoforms modulate the localization of tropomyosin strands on actin filaments.', *Journal of molecular biology*, 302(3), pp. 593–606.

Lehman, W. *et al.* (2013) 'Gestalt-Binding of tropomyosin on actin during thin filament

activation', *Journal of Muscle Research and Cell Motility*, 34(3–4), pp. 155–163.

Lehrer, S. S. and Geeves, M. A. (1998) 'The Muscle Thin Filament as a Classical Cooperative/Allosteric Regulatory System', *Journal of Molecular Biology*, 277, pp. 1081–1089.

Lehrer, S. S. and Morris, P. (1982) 'Dual Effects of Tropomyosin and Troponin-Tropomyosin on Actomyosin Subfragment 1 ATPase', *Journal of Biological Chemistry*, 257(14), pp. 8073–8080.

Lehrer, S. S. and Qian, Y. (1990) 'Unfolding/Refolding Studies of Smooth Muscle Tropomyosin', *Journal of Biological Chemistry*, 2, pp. 1134–1138.

Li, A., Ziehr, J. L. and Johnson, K. A. (2017) 'A new general method for simultaneous fitting of temperature and concentration dependence of reaction rates yields kinetic and thermodynamic parameters for HIV reverse transcriptase specificity', *Journal of Biological Chemistry*, 292(16), pp. 6695–6702.

Li, X. *et al.* (2011) 'Tropomyosin position on F-actin revealed by EM reconstruction and computational chemistry', *Biophysical Journal*, 100(4), pp. 1005–1013.

Li, X. E. *et al.* (2012) 'The flexibility of two tropomyosin mutants, D175N and E180G, that cause hypertrophic cardiomyopathy', *Biochemical and Biophysical Research Communications*, 424(3), pp. 493–496.

Li, Y. *et al.* (2002) 'The crystal structure of the C-terminal fragment of striated-muscle alpha-tropomyosin reveals a key troponin T recognition site', *Proceedings of the National Academy of Sciences of the United States of America*, 99(11), pp. 7378–7383.

Lin, Y.-H. *et al.* (2013) 'CapZ and actin capping dynamics increase in myocytes after a bout of exercise and abates in hours after stimulation ends', *Journal of Applied Physiology*, 114(6), pp. 1603–1609.

Lin, Y.-H. *et al.* (2016) 'Myofibril growth during cardiac hypertrophy is regulated through dual phosphorylation and acetylation of the actin capping protein CapZ', *Cellular Signalling*, 28(8), pp. 1015–1024.

Lindert, S. *et al.* (2015) 'Article Effects of HCM cTnI Mutation R145G on Troponin Structure and Modulation by PKA Phosphorylation Elucidated by Molecular Dynamics Simulations', *Biophysical journal*, 108(2), pp. 395–407.

Littlefield, R. *et al.* (2001) 'Actin dynamics at pointed ends regulates thin filament length in striated muscle', *Nature Cell Biology*, 3, pp. 544–551.

Liu, X. *et al.* (2015) 'Screening mutations of MYBPC3 in 114 unrelated patients with hypertrophic cardiomyopathy by targeted capture and next-generation sequencing', *Scientific Reports*, 5(June), pp. 1–8.

Loar, R. W. *et al.* (2015) 'Genotype-phenotype Correlations of Hypertrophic Cardiomyopathy When Diagnosed in Children, Adolescents, and Young Adults', *Congenital Heart Diseases*, pp. 8–10.

Logvinova, D. S. *et al.* (2018) 'Transient interaction between the N-terminal extension of the essential light chain-1 and motor domain of the myosin head during the ATPase cycle', *Biochemical and Biophysical Research Communications*, 495(1), pp. 163–167.

Logvinova, D. S. and Levitsky, D. I. (2018) 'Essential Light Chains of Myosin and Their Role in Functioning of the Myosin Motor', *Biochemistry*, 83(8), pp. 944–960.

Loong, C. K. P. *et al.* (2012) 'Familial hypertrophic cardiomyopathy related E180G mutation increases flexibility of human cardiac alpha-tropomyosin', *FEBS Letters,* 586(19), pp. 3503–3507.

Loong, C. K. P. *et al.* (2012) 'Persistence length of human cardiac alpha-tropomyosin measured by single molecule direct probe microscopy', *PLoS ONE*, 7(6), pp. 1–11.

Lopes, L. R. *et al.* (2015) 'Novel genotype–phenotype associations demonstrated by high-throughput sequencing in patients with hypertrophic cardiomyopathy', *Heart*, 101(4), pp. 294–301.

Lorenz, M. *et al.* (1995) 'An atomic model of the unregulated thin filament obtained by X-ray fiber diffraction on oriented actin-tropomyosin gels', *Journal of Molecular Biology*, 246(6), pp. 108–119.

Lorenz, M. *et al.* (1993) 'Refinement of the F-Actin Model against X-ray Fiber Diffraction Data by the Use of a Directed Mutation Algorithm', *Journal of Molecular Biology*, 234, pp. 826–836.

Lowey, S. *et al.* (1969) 'Substructure of the myosin molecule: I. Subfragments of myosin by enzymic degradation', *Journal of Molecular Biology*. Academic Press, 42(1), pp. 1–29.

Lowey, S., Waller, G. S. and Trybus, K. M. (1993) 'Function of skeletal muscle myosin heavy and light chain isoforms by an in vitro motility assay', *The Journal of biological chemistry*, 268(27), pp. 20414–20418.

Lu, Q., Wu, X. and Morimoto, S. (2013) 'Inherited cardiomyopathies caused by troponin mutations', *Journal of Geriatric Cardiology*, 10, pp. 91–101.

Lu, Y. *et al.* (2011) 'The C0C1 fragment of human cardiac myosin binding protein C has common binding determinants for both actin and myosin', *Journal of Molecular Biology*, 413(5), pp. 908–913.

Luther, P. K. (2009) 'The vertebrate muscle Z-disc : sarcomere anchor for structure and signalling', *Journal of Muscle Research and Cell Motility*, 30, pp. 171–185.

Luther, P. K. *et al.* (2011) 'Direct visualization of myosin-binding protein C bridging myosin and actin filaments in intact muscle', *Proceedings of the National Academy of*

Sciences, 108(28), pp. 11423–11428.

Luther, P. K. and Craig, R. (2011) 'Modulation of striated muscle contraction by binding of myosin binding protein C to actin', *BioArchitecture*, 1(November), pp. 277–283.

Ly, S. and Lehrer, S. S. (2012) 'Long-range effects of familial hypertrophic cardiomyopathy mutations E180G and D175N on the properties of tropomyosin', *Biochemistry*, 51(32), pp. 6413–6420.

Lymn, R. W. and Taylor, E. W. (1971) 'Mechanism of Adenosine Triphosphate Hydrolysis by Actomyosin', *Biochemistry*, 10(25), pp. 4617–4624.

Mandinov, L. *et al.* (2000) 'Diastolic Heart Failure', *Cardiovascular Research*, 45(4), pp. 813–825.

Månsson, A. *et al.* (2018) 'Do Actomyosin Single-Molecule Mechanics Data Predict Mechanics of Contracting Muscle?', *International Journal of Molecular Sciences*, 19(1863), pp. 1–37.

Maragiannis, D. *et al.* (2018) 'Left ventricular function in patients with hypertrophic cardiomyopathy and its relation to myocardial fibrosis and exercise tolerance', *The International Journal of Cardiovascular Imaging*. Springer Netherlands, 34(1), pp. 121–129.

Margossian, S. S. and Lowey, S. (1982) 'Preparation of myosin and its subfragments from rabbit skeletal muscle', *Methods in Enzymology*. Academic Press, 85, pp. 55–71.

Marian, A. J. and Braunwald, E. (2017) 'Hypertrophic cardiomyopathy: Genetics, pathogenesis, clinical manifestations, diagnosis, and therapy', *Circulation Research*, 121(7), pp. 749–770.

Maron, B. J., Maron, M. S. and Semsarian, C. (2012) 'Genetics of Hypertrophic Cardiomyopathy After 20 Years', *Journal of the American College of Cardiology*, 60(8),

pp. 705–715.

Maron, M. S. *et al.* (2009) 'Hypertrophic Cardiomyopathy Phenotype Revisited After 50 Years With Cardiovascular Magnetic Resonance', *Journal of the American College of Cardiology*. American College of Cardiology Foundation, 54(3), pp. 220–228.

Marsiglia, J. D. C. and Pereira, A. C. (2014) 'Hypertrophic cardiomyopathy: how do mutations lead to disease?', *Arquivos brasileiros de cardiologia*, 102(3), pp. 295–304.

Marston, S. (2003) 'Random walks with thin filaments: application of in vitro motility assay to the study of actomyosin regulation', *Journal of Muscle Research and Cell Motility*, 24, pp. 149–156.

Marston, S. *et al.* (2009) 'Evidence from human myectomy samples that MYBPC3 mutations cause hypertrophic cardiomyopathy through haploinsufficiency', *Circulation Research*, 105(3), pp. 219–222.

Marston, S. *et al.* (2012) 'How do MYBPC3 mutations cause hypertrophic cardiomyopathy?', *Journal of Muscle Research and Cell Motility*, 33(1), pp. 75–80.

Marston, S. B. (2011) 'How Do Mutations in Contractile Proteins Cause the Primary Familial Cardiomyopathies?', *Journal of Cardiovascular Translational Research*, 4(3), pp. 245–255.

Mathur, M. C., Chase, P. B. and Chalovich, J. M. (2011) 'Several cardiomyopathy causing mutations on tropomyosin either destabilize the active state of actomyosin or alter the binding properties of tropomyosin', *Biochemical and Biophysical Research Communications*, 406(1), pp. 74–78.

Matyushenko, A. M. *et al.* (2017) 'Structural and Functional Effects of Cardiomyopathy-Causing Mutations in the Troponin T-Binding Region of Cardiac Tropomyosin', *Biochemistry*, 56(1), pp. 250–259.

Maytum, R., Lehrer, S. S. and Geeves, M. A. (1999) 'Cooperativity and switching within the three-state model of muscle regulation', *Biochemistry*, 38(3), pp. 1102–1110.

Mckillop, D. F. A. and Geeves, M. A. (1993) 'Regulation of the Interaction between Actin and Myosin Subfragment 1: Evidence for Three States of the Thin Filament', *Biophysical Journal*, 65(August), pp. 693–701.

McLachlan, A. D. and Karn, J. (1982) 'Periodic features in the amino acid sequence of nematode myosin rod', *Journal of Molecular Biology*, 299, pp. 226–231.

McLachlan, A. D. and Stewart, M. (1976) 'The 14-fold periodicity in α-tropomyosin and the interaction with actin', *Journal of Molecular Biology*. Academic Press, 103(2), pp. 271–298.

McLaughlin, P. J. *et al.* (1993) 'Structure of gelsolin segment 1-actin complex and the mechanism of filament severing', *Nature*, 364, pp. 685–692.

McNamara, J. W. *et al.* (2016) 'Ablation of cardiac myosin binding protein-C disrupts the super-relaxed state of myosin in murine cardiomyocytes', *Journal of Molecular and Cellular Cardiology*, 94, pp. 65–71.

Meijering, E., Dzyubachyk, O. and Smal, I. (2012) 'Methods for cell and particle tracking', *Methods Enzymol*, 504(9), pp. 183–200.

Messer, A. E. *et al.* (2016) 'Mutations in troponin T associated with Hypertrophic Cardiomyopathy increase Ca^{2+}-sensitivity and suppress the modulation of Ca^{2+}-sensitivity by troponin I phosphorylation', *Archives of Biochemistry and Biophysics*, 601, pp. 113–120.

Michele, D. E. *et al.* (2002) 'Cardiac Dysfunction in Hypertrophic Cardiomyopathy Mutant Tropomyosin Mice Is Transgene-Dependent, Hypertrophy-Independent, and Improved by beta-Blockade', *Circulation Research*, pp. 255–262.

Mijailovich, S. M. *et al.* (2016) 'Three-dimensional stochastic model of actin – myosin binding in the sarcomere lattice', *The Journal of General Physiology*, 148(6), pp. 459–488.

Miller, G. *et al.* (2003) 'Heterologous expression of wild-type and mutant b -cardiac myosin changes the contractile kinetics of cultured mouse myotubes', *J Physiol*, 548.1, pp. 167–174.

Miller, M. S. *et al.* (2009) 'Alternative S2 hinge regions of the myosin rod affect myofibrillar structure and myosin kinetics', *Biophysical Journal*. Biophysical Society, 96(10), pp. 4132–4143.

Miller, T. *et al.* (2001) 'Abnormal Contractile Function in Transgenic Mice Expressing a Familial Hypertrophic Cardiomyopathy-linked Troponin T (I79N) Mutation', *Journal of Biological Chemistry*, 276(6), pp. 3743–3755.

Miyamoto, Y. *et al.* (1986) 'Stoichiometry the Toxin of Actin and Phalloidin Binding: One Molecule of Dominates Two Actin Subunits', 100(6), pp. 1677–1680.

Molloy, J. E. *et al.* (1995) 'Single-Molecule Mechanics of Heavy Meromyosin and S1 Interacting with Rabbit or Drosophila Actins Using Optical Tweezers', *Biophysical Journal*, 68, pp. 298–303.

Molloy, J. E. *et al.* (2000) 'An unexpectedly large working stroke from chymotryptic fragments of myosin II', *FEBS Letters*, 480, pp. 293–297.

Monteiro, P. B. *et al.* (1994) 'Functional alpha-tropomyosin produced in Escherichia coli. A dipeptide extension can substitute the amino-terminal acetyl group', *Journal of Biological Chemistry*, 269(14), pp. 10461–10466.

Moolman, J. a *et al.* (2000) 'A newly created splice donor site in exon 25 of the MyBP-C gene is responsible for inherited hypertrophic cardiomyopathy with incomplete

disease penetrance', *Circulation*, 101(12), pp. 1396–1402.

Moore, J. R. *et al.* (2016) 'Structural determinants of muscle thin filament cooperativity', *Archives of Biochemistry and Biophysics*, 594, pp. 8–17.

Moore, J. R. *et al.* (2012) 'Understanding cardiomyopathy phenotypes based on the functional impact of mutations in the myosin motor', *Circulation Research*, 111(3), pp. 375–385.

Morris, E. P. and Lehrer, S. S. (1984) 'Troponin-Tropomyosin Interactions. Fluorescence Studies of the Binding of Troponin, Troponin T, and Chymotryptic Troponin T Fragments to Specifically Labeled Tropomyosin', *Biochemistry*, 23(10), pp. 2214–2220.

Mun, J. Y. *et al.* (2011) 'Electron microscopy and 3D reconstruction of F-actin decorated with cardiac myosin-binding protein C (cMyBP-C)', *Journal of Molecular Biology*, 410(2), pp. 214–225.

Mun, J. Y. *et al.* (2014) 'Myosin-binding protein C displaces tropomyosin to activate cardiac thin filaments and governs their speed by an independent mechanism', *Proceedings of the National Academy of Sciences of the United States of America*, 111(6), pp. 2170–2175.

Murakami, K. *et al.* (2008) 'Structural basis for tropomyosin overlap in thin (actin) filaments and the generation of a molecular swivel by troponin-T', *Proceedings of the National Academy of Sciences of the United States of America*, 105(20), pp. 7200–7205.

Naber, N. *et al.* (2011) 'Slow Myosin ATP Turnover in the Super-Relaxed State in Tarantula Muscle', *Journal of Molecular Biology*. Elsevier Ltd, 411(5), pp. 943–950.

Nag, S. *et al.* (2015) 'Contractility parameters of human beta-cardiac myosin with the hypertrophic cardiomyopathy mutation R403Q show loss of motor function', *Science Advances*, 1(9), p. e1500511

Nag, S. *et al.* (2017) 'The myosin mesa and the basis of hypercontractility caused by hypertrophic cardiomyopathy mutations', *Nature*, 24(6), pp. 525–533.

Nakaura, H. *et al.* (1999) 'Effects of Missense Mutations Phe110Ile and Glu244Asp in Human Cardiac Troponin T on Force Generation in Skinned Cardiac Muscle Fibers', *Journal of Biochemistry*, 126(3), pp. 457–460.

Nogara, L. *et al.* (2016) 'Spectroscopic Studies of the Super Relaxed State of Skeletal Muscle', *PLoS ONE*, 11(8), pp. 1–24.

Ochala, J. *et al.* (2008) 'Defective regulation of contractile function in muscle fibres carrying an E41K β -tropomyosin mutation', *Journal of Physiology*, 586(12), pp. 2993–3004.

Oda, T. *et al.* (2009) 'The nature of the globular- to fibrous-actin transition', *Nature*, 457(7228), pp. 441–445.

Offer, G. *et al.* (1973) 'A new protein of the thick filaments of vertebrate skeletal myofibrils. Extraction, purification and characterization', *Journal of Molecular Biology*. Academic Press, 74(4), pp. 653–676.

Okagaki, T. *et al.* (1993) 'The Major Myosin-Binding Domain of Skeletal Muscle MyBP-C (C-Protein) Resides in the COOH-Terminal, Immunoglobulin-C2 Motif', *Journal of Cell Biology*, 123(3), pp. 619–626.

De Oliveira, G. A. P. *et al.* (2013) 'Insights into the intramolecular coupling between the N- and C-domains of troponin C derived from high-pressure, fluorescence, nuclear magnetic resonance, and small-angle X-ray scattering studies', *Biochemistry*, 52(1), pp. 28–40.

Orlova, A. *et al.* (2011) 'The N-terminal domains of myosin binding protein C can bind polymorphically to F-actin', *Journal of Molecular Biology*, 412(3), pp. 379–386.

Orzechowski, M., Fischer, S., *et al.* (2014) 'Energy landscapes reveal the myopathic effects of tropomyosin mutations', *Archives of Biochemistry and Biophysics*, 564, pp. 89–99.

Orzechowski, M., Moore, J. R., *et al.* (2014) 'Tropomyosin movement on F-actin during muscle activation explained by energy landscapes', *Archives of Biochemistry and Biophysics*, 545, pp. 63–68.

Otterbein, L. *et al.* (2001) 'The CrystaL Structure of Uncomplexed Actin in the ADP State', 293, pp. 708–711.

Palm, T. *et al.* (2003) 'Tropomyosin Ends Determine the Stability and Functionality of Overlap and Troponin T Complexes', *Biophysical journal*. Elsevier, 84(5), pp. 3181–3189.

Palmiter, K. A. *et al.* (2000) 'R403Q and L908V mutant beta-cardiac myosin from patients with familial hypertrophic cardiomyopathy exhibit enhanced mechanical performance at the single molecule level', *Journal of Muscle Research and Cell Motility*, 21, pp. 609–620.

Pardee, J. D. and Spudich, J. A. (1982) *Methods in Cell Biology - Purification of Muscle Actin*.

Pearlstone, J. R. and Smillie, L. B. (1982) 'Binding of troponin-T fragments to several types of tropomyosin. Sensitivity to Ca^{2+} in the presence of troponin-C', *Journal of Biological Chemistry*, 257(18), pp. 10587–10592.

Perry, S. V. (2001) 'Vertebrate tropomyosin: Distribution, properties and function', *Journal of Muscle Research and Cell Motility*, 22(1), pp. 5–49.

Pollard, T. D. and Mooseker, M. S. (1981) 'Direct Measurement of Actin Polymerization Rate Constants by Electron-Microscopy of Actin-Filaments Nucleated by Isolated Microvillus Cores', *Journal of Cell Biology*, 88(3), pp. 654–659.

Poole, K. J. V. *et al.* (2006) 'A comparison of muscle thin filament models obtained from electron microscopy reconstructions and low-angle X-ray fibre diagrams from non-overlap muscle', *Journal of Structural Biology*, 155(2), pp. 273–284.

Potter, J. D. and Gergely, J. (1974) 'Troponin, tripomyosin, and actin interactions in the Ca2+ ion regulation of muscle contraction', *Biochemistry*, 13(13), pp. 2697–2703.

Previs, M. J. *et al.* (2012) 'Molecular Mechanics of Cardiac Myosin-Binding Protein C in Native Thick Filaments', *Science*, 337(6099), pp. 1215–1218.

Previs, M. J. *et al.* (2016) 'Phosphorylation and calcium antagonistically tune myosin-binding protein C's structure and function', *Proceedings of the National Academy of Sciences of the United States of America*, 2(19), pp. 2–7.

Rao, J. N. *et al.* (2014) 'Mechanism of actin filament pointed-end capping by tropomodulin', *Science*, 345(6195), pp. 463–468.

Ratti, J. *et al.* (2011) 'Structure and interactions of myosin-binding protein C domain C0: Cardiac-specific regulation of myosin at its neck?', *Journal of Biological Chemistry*, 286(14), pp. 12650–12658.

Rayment, I., Rypniewski, W. R., *et al.* (1993) 'Three-Dimensional Structure of Myosin Subfragment-1 : A Molecular Motor Published by : American Association for the Advancement of Science Three-Dimensional Structure of Myosin Subfragment-1 : A Molecular Motor', 261(5117), pp. 50–58.

Rayment, I., Rypniewski, W., *et al.* (1993) 'Three-Dimensional Structure of Myosin Subfragment-1: A molecular', *Science*, 261, pp. 50–58.

Razumova, M. V. *et al.* (2006) 'Effects of the N-terminal domains of myosin binding protein-C in an in vitro motility assay: Evidence for long-lived cross-bridges', *Journal of Biological Chemistry*, 281(47), pp. 35846–35854.

Razumova, M. V *et al.* (2008) 'Contribution of the myosin binding protein C motif to functional effects in permeabilized rat trabeculae.', *The Journal of general physiology*, 132(5), pp. 575–85.

Ribeiro, E. D. A. *et al.* (2014) 'The structure and regulation of human muscle α-Actinin', *Cell*, 159(6), pp. 1447–1460.

Risi, C. *et al.* (2017) 'Ca^{2+}-induced movement of tropomyosin on native cardiac thin filaments revealed by cryoelectron microscopy', *Proceedings of the National Academy of Sciences*, 114(26), p. 201700868.

Risi, C. *et al.* (2018) 'N-Terminal Domains of Cardiac Myosin Binding Protein C Cooperatively Activate the Thin Filament Article N-Terminal Domains of Cardiac Myosin Binding Protein-C Cooperatively Activate the Thin Filament', pp. 1604–1611.

Robert-Paganing, J. *et al.* (2018) 'Hypertrophic cardiomyopathy disease results from disparate impairments of cardiac myosin function and auto-inhibition', *Nature Communications*, 9(4019), pp. 1–13.

Robinson, J. M. *et al.* (2004) 'Switching of Troponin I : Ca^{2+} and Myosin-induced Activation of Heart Muscle', *Journal of Molecular Biology*, 340, pp. 295–305.

Rottbauer, W. *et al.* (1997) 'Myosin Binding Protein-C Mutation Novel Splice Donor Site Mutation in the Cardiac Myosin-binding Protein-C Gene in Familial Hypertrophic Cardiomyopathy Characterization of Cardiac Transcript and Protein', *Journal of Clinical Investigation*, 100(2), pp. 475–482.

Rüegg, C. *et al.* (2002) 'Molecular Motors : Force and Movement Generated by Single Myosin II Molecules', *News in Physiological Sciences*, 17, pp. 213–218.

Rynkiewicz, M. J. *et al.* (2016) 'The propensity for tropomyosin twisting in the presence and absence of F-actin', *Archives of Biochemistry and Biophysics*, 609, pp. 51–58.

Schaertl, S. *et al.* (1995) 'Separation and Characterization of the Two Functional Regions of Troponin Involved in Muscle Thin Filament Regulation', *Biochemistry*, 34(49), pp. 15890–15894.

Schutt, C. E. *et al.* (1993) 'The structure of crystalline profilin-beta-actin', *Nature*, 365, pp. 810–816.

Scruggs, S. B. and Solaro, R. J. (2011) 'The significance of regulatory light chain phosphorylation in cardiac physiology', *Archives of Biochemistry and Biophysics*, 510(2), pp. 129–134.

Semsarian, C. *et al.* (2015) 'New perspectives on the prevalence of hypertrophic cardiomyopathy', *Journal of the American College of Cardiology*, 65(12), pp. 1249–1254.

Sewanan, L. R. *et al.* (2016) 'Predicting effects of tropomyosin mutations on cardiac muscle contraction through myofilament modeling', *Frontiers in Physiology*, 7(OCT), pp. 1–13.

Shaffer, J. F. *et al.* (2009) 'The myosin-binding protein C motif binds to F-actin in a phosphorylation-sensitive manner', *Journal of Biological Chemistry*, 284(18), pp. 12318–12327.

Sherer, L. A. *et al.* (2018) 'Dissection of two parallel pathways for formin-mediated actin filament elongation', *Journal of Biological Chemistry*, 293(46), pp. 17917–17928.

Sirenko, S. G. *et al.* (2006) 'Differential effect of troponin T mutations on the inotropic responsiveness of mouse hearts – role of myofilament Ca^{2+} sensitivity increase', *Journal of Physiology*, 575(1), pp. 201–213.

Sjöblom, B. *et al.* (2008) 'α-Actinin structure and regulation', *Cellular and Molecular Life Sciences*, 65(17), pp. 2688–2701.

Sommese, R. F. *et al.* (2013) 'Effects of Troponin T Cardiomyopathy Mutations on the Calcium Sensitivity of the Regulated Thin Filament and the Actomyosin Cross-Bridge Kinetics of Human b -Cardiac Myosin', *PLoS ONE*, 8(12), p. e83403.

Spitzer, P. *et al.* (2006) 'Algorithm for multi-curve-fitting with shared parameters and a possible application in evoked compound action potential measurements', *Biomedical Engineering OnLine*, 5(13), pp. 1–8.

Springall, L. *et al.* (2016) 'DNA–Protein Interactions Studied Directly Using Single Molecule Fluorescence Imaging of Quantum Dot Tagged Proteins Moving on DNA Tightropes', in Humana Press, New York, NY, pp. 141–150.

Spudich, J. A. (2015) 'The myosin mesa and a possible unifying hypothesis for the molecular basis of human hypertrophic cardiomyopathy', *Biochemical Society Transactions*, 43(1), pp. 64–72.

Squire, J. M. (2009) 'Muscle myosin filaments: Cores, crowns and couplings', *Biophysical Reviews*, 1(3), pp. 149–160.

Starr, R. and Offer, G. (1978) 'The interaction of C-protein with heavy meromyosin and subfragment-2', *The Biochemical journal*, 171(3), pp. 813–6.

Stefancsik, R. *et al.* (1998) 'Identification and mutagenesis of a highly conserved domain in troponin T responsible for troponin I binding: potential role for coiled coil interaction', *Proceedings of the National Academy of Sciences of the United States of America*, 95(February), pp. 957–962.

Stelzer, J. E. *et al.* (2006) 'Ablation of cardiac myosin-binding protein-C accelerates stretch activation in murine skinned myocardium', *Circulation Research*, 98(9), pp. 1212–1218.

Stewart, M. A. *et al.* (2010) 'Myosin ATP turnover rate is a mechanism involved in

thermogenesis in resting skeletal muscle fibers', *Proceedings of the National Academy of Sciences of the United States of America*, 107(1), pp. 430–5.

Stewart, M. and Edwards, P. (1984) 'Length of myosin rod and its proteolytic fragments determined by electron microscopy', *FEBS Letters*, 168(1), pp. 75–78.

Stewart, M. and Roberts, G. C. K. (1982) '1H NMR study of long and short myosin S2 fragments', 146(2), pp. 293–296.

Straub, F. B. (1943) *Actin*, *Studies from the Institute of Medical Chemistry University Szeged Vol. III*. Edited by A. G. Szent-Györgyi. S. Karger.

Syska, H. *et al.* (1976) 'The relationship between biological activity and primary structure of troponin I from white skeletal muscle of the rabbit', *Biochemical Journal*, 153, pp. 375–387.

Szent-Györgyi, A. G. (2004) 'The Early History of the Biochemistry of Muscle Contraction', *The Journal of General Physiology*, 123(6), pp. 631–641.

Takagi, Y. *et al.* (2006) 'Force Generation in Single Conventional Actomyosin Complexes under High Dynamic Load', *Biophysical Journal*, 90(4), pp. 1295–1307.

Takahashi-yanaga, F. *et al.* (2001) 'Functional Consequences of the Mutations in Human Cardiac Troponin I Gene Found in Familial Hypertrophic Cardiomyopathy', *Journal of Molecular and Cellular Cardiology*, 33, pp. 2095–2107.

Takeda, S. *et al.* (2003) 'Structure of the core domain of human cardiac troponin in the Ca2+-saturated form', *Nature*, 424(6944), pp. 35–41.

Teare, D. (1958) 'Asymmetrical Hypertrophy of the Heart in Young Adults', *Heart*, 20(1), pp. 1–8.

Thierfelder, L. *et al.* (1994) 'α-tropomyosin and cardiac troponin T mutations cause familial hypertrophic cardiomyopathy: A disease of the sarcomere', *Cell*, 77(5), pp.

701–712.

Tobacman, L. S. (1996) ‘Thin Filament-mediated regulation of cardiac contraction’, *Annual Review of Physiology*, 7(58), pp. 447–481.

Toepfer, C. and Sellers, J. R. (2014) *Use of Fluorescent Techniques to Study the In Vitro Movement of Myosins*, *Fluorescent Methods for Molecular Motors*, pp. 193-210.

Tokunaga, M. *et al.* (2008) ‘Highly inclined thin illumination enables clear single-molecule imaging in cells’, *Nature Methods*, 5(2), pp. 159–161.

Trivedi, D. V. *et al.* (2017) ‘Hypertrophic cardiomyopathy and the myosin mesa: viewing an old disease in a new light’, *Biophysical Reviews*. Biophysical Reviews, 10(1).

Trybus, K. M. and Lowey, S. (1988) ‘The regulatory light chain is required for folding of smooth muscle myosin’, *Journal of Biological Chemistry*, 263(31), pp. 16485–16492.

Tyska, M. J. *et al.* (1999) ‘Two heads of myosin are better than one for generating force and motion’, *Proceedings of the National Academy of Sciences of the United States of America*, 96(8), pp. 4402–4407.

Tyska, M. J. *et al.* (2000) ‘Single-molecule mechanics of R403Q cardiac myosin isolated from the mouse model of familial hypertrophic cardiomyopathy’, *Circulation research*, 86(7), pp. 737–744.

Umemoto, S. and Sellers, J. R. (1990) ‘Characterization of in vitro motility assays using smooth muscle and cytoplasmic myosins’, *Journal of Biological Chemistry*, 265(25), pp. 14864–14869.

Urbancikova, M. and Hitchcock-DeGregori, S. E. (1994) ‘Requirement of amino-terminal modification for striated muscle alpha-tropomyosin function’, *Journal of Biological Chemistry*, 269(39), pp. 24310–24315.

Uyeda, T. Q., Abramson, P. D. and Spudich, J. a (1996) ‘The neck region of the myosin

motor domain acts as a lever arm to generate movement.', *Proceedings of the National Academy of Sciences of the United States of America*, 93(April), pp. 4459–4464.

Uyeda, T. Q. *et al.* (1990) 'Myosin Step Size Estimation From Slow Sliding Movement of Actin Over Low Densities of Heavy Meromyosin', *Journal of Molecular Biology*, 214, pp. 699–710.

VanBuren, P. *et al.* (1994) 'The essential light chain is required for full force production by skeletal muscle myosin', *Proceedings of the National Academy of Sciences of the United States of America*, 91(26), pp. 12403–12407.

VanBuren, P. *et al.* (1998) 'Fluorescent Phalloidin Enables Visualization of Actin Without Effects on Myosin ' s Actin Filament Sliding Velocity and Hydrolytic Properties in vitro', *Journal of Molecular & Cellular Cardiology*, 30, pp. 2777–2783.

Vanburen, P. *et al.* (1999) 'Tropomyosin directly modulates actomyosin mechanical performance at the level of a single actin filament', *PNAS*, 96(22), pp. 12488–12493.

Vandekerckhove, J. *et al.* (1985) 'The phalloidin binding site of F-actin.', *The EMBO Journal*, 4(7), pp. 2815–2818.

Veigel, C. *et al.* (1998) 'The Stiffness of Rabbit Skeletal Actomyosin Cross-Bridges Determined with an Optical Tweezers Transducer', *Biophysical Journal*, 75(3), pp. 1424–1438.

Veigel, C. *et al.* (2003) 'Load-dependent kinetics of force production by smooth muscle myosin measured with optical tweezers', *Nature Cell Biology*, 5(11), pp. 980–986.

Vinogradova, M. V *et al.* (2005) 'Ca^{2+}-regulated structural changes in troponin', *Proceedings of the National Academy of Sciences of the United States of America*, 102(14), pp. 5038–43.

Walcott, S. *et al.* (2015) 'Effects of cardiac Myosin binding protein-C on actin motility

are explained with a drag-activation-competition model', *Biophysical Journal*, 108(1), pp. 10–3.

Walcott, S. and Kad, N. M. (2015) 'Direct Measurements of Local Coupling between Myosin Molecules Are Consistent with a Model of Muscle Activation', *PLoS Computational Biology*, 11(11), pp. 1–20.

Walker, S. M. and Schrodt, G. R. (1974) 'I segment lengths and thin filament periods in skeletal muscle fibers of the rhesus monkey and the human', *The Anatomical Record*, 178(1), pp. 63–81.

Wang, F. *et al.* (2011) 'Facilitated cross-bridge interactions with thin filaments by familial hypertrophic cardiomyopathy mutations in α-tropomyosin', *Journal of Biomedicine and Biotechnology*, 2011.

Wang, H. *et al.* (2010) 'The structure of native G-actin', *Cytoskeleton*, 67(7), pp. 456–465.

Wang, L. *et al.* (2018) 'Journal of Molecular and Cellular Cardiology Hypertrophic cardiomyopathy-linked mutation in troponin T causes myo fi brillar disarray and pro-arrhythmic action potential changes in human iPSC cardiomyocytes', *Journal of Molecular and Cellular Cardiology*, 114, pp. 320–327.

Wear, M. A. *et al.* (2003) 'How Capping Protein Binds the Barbed End of the Actin Filament', *Current Biology*, 13, pp. 1531–1537.

Weber, F. E. *et al.* (1993) 'Complete sequence of human fast-type and slow-type muscle myosin-binding-protein C (MyBP-C): Differential expression, conserved domain structure and chromosome assignment', *European Journal of Biochemistry*, 216(2), pp. 661–669.

Wegner, A. and Isenbergt, G. (1983) '12-Fold difference between the critical monomer

concentrations of the two ends of actin filaments in physiological salt conditions', *Biochemistry*, 80(August), pp. 4922–4925.

Weith, A. *et al.* (2012) 'Unique single molecule binding of cardiac myosin binding protein-C to actin and phosphorylation-dependent inhibition of actomyosin motility requires 17 amino acids of the motif domain', *Journal of Molecular and Cellular Cardiology*. Elsevier Ltd, 52(1), pp. 219–227.

Wernicke, D. *et al.* (2004) 'alpha-Tropomyosin mutations Asp175Asn and Glu180Gly affect cardiac function in transgenic rats in different ways', *American Journal of Physiology - Regulatory, Integrative and Comparative Physiology*, 287, pp. 685–695.

Wieland, T. and Heinz, F. (1995) 'Amatoxins, Phallotoxins, Phallolysin, and Antamanide: the Biologically Active Components of Poisonous Amanita Mushrooms', *Food Reviews International*, 11(1), pp. 83–107.

Witt, C. C. *et al.* (2001) 'Hypercontractile properties of cardiac muscle fibers in a knock-in mouse model of cardiac myosin-binding protein-C', *The Journal of biological chemistry*, 276(7), pp. 5353–9.

Wu, X.-P. *et al.* (2019) 'Impaired left ventricular mechanics and functional reserve are associated with reduced exercise capacity in patients with hypertrophic cardiomyopathy', *Echocardiography*, pp. 1–10.

Yamashiro, S. *et al.* (2012) 'Tropomodulins: Pointed-End Capping Proteins That Regulate Actin Filament Architecture in Diverse Cell Types', *Cytoskeleton*, 69, pp. 337–370.

Yamashita, A. *et al.* (2003) 'Crystal structure of CapZ : structural basis for actin filament barbed end capping', *The EMBO journal*, 22(7), pp. 1529–1538.

Yamauchi-takihara, K. *et al.* (1996) 'Clinical implications of hypertrophic

cardiomyopathy associated with mutations in the alpha-tropomyosin gene', *Heart*, 76, pp. 63–65.

Yanaga, F. *et al.* (1999) 'Calcium Sensitization and Potentiation of the Maximum Level of Myofibrillar ATPase Activity Caused by Mutations of Troponin T Found in Familial Hypertrophic Cardiomyopathy', *Journal of Biological Chemistry*, 274(13), pp. 8806–8812.

Yang, F. H. and Pyle, W. G. (2011) 'Cardiac Actin Capping Protein Reduction and Protein Kinase C Inhibition Maintain Myofilament Function During Cardioplegic Arrest', *Cellular Physiology and Biochemistry*, 27, pp. 263–272.

Yang, Q. *et al.* (1998) 'A Mouse Model of Myosin Binding Protein C Human Familial Hypertrophic Cardiomyopathy', *Journal of Clinical Investigation*, 102(7), pp. 1292–1300.

Yang, S. *et al.* (2014) 'Three-dimensional organization of troponin on cardiac muscle thin filaments in the relaxed state', *Biophysical Journal*. Biophysical Society, 106(4), pp. 855–864.

Yasuda, M. *et al.* (1995) 'Complete primary structure of chicken cardiac C-protein (MyBP-C) and its expression in developing striated muscles', *Journal of Molecular & Cellular Cardiology*, 27(10), pp. 2275–2286.

Zhang, S. *et al.* (2010) 'A fast mathematical programming procedure for simultaneous fitting of assembly components into cryoEM density maps', *Bioinformatics*, 26, pp. 261–268.

Zheng, W. *et al.* (2016) 'Investigating the effects of tropomyosin mutations on its flexibility and interactions with filamentous actin using molecular dynamics simulation', *Journal of Muscle Research and Cell Motility*, 37(4), pp. 131–147.

Zot, H. and Potter, J. D. (1982) 'A Structural Role for the Ca2+-Mg2+ Sites on Troponin

C in the Regulation of Muscle Contraction', *Journal of Biological Chemistry*, 257(13), pp. 7678–7683.

ACKNOWLEDGEMENTS

Call me Alessio. Some years ago - never mind how long precisely - having little or no money in my purse, and nothing particular to interest me on the continent, I thought I would come to England and start working in the field of single molecule microscopy. Having finished my time, I now have to move on, but not without thanking all the people I met throughout this project.

First of all I would like to thank my supervisor Dr. Neil Kad, for allowing me to work in his lab (and talk a lot) and for his constant help and support, as well as for not banning me from knocking on his office door every 5 minutes; without his presence and all his efforts I would not have enjoyed this project so much.

Special thanks go to the Kad lab members with whom I shared most of this experience, Luke, Jamie and JingYu, for not driving me completely crazy and for all the helpful discussions (not only about science) and Alex and Rob, who joined in my final months and were lucky enough to not spend a long time with me; it has been great fun being around all of them and I can't thank them enough for being there whenever I needed help or a drink.

I am also grateful to the past members of the lab, Svetlana, Michelle and Harish, for all the help they gave me at the beginning and for not forgetting about me after I left the university of Essex, but particularly to Rama, for the incredible and selfless support I received from her throughout my PhD project.

A special mention goes to Prof. Dave Warshaw, Dr. Mike Previs and Sam Previs of the University of Vermont, for giving me the opportunity to work on MyBP-C, which I have

been fascinated to from the very beginning and for all their help and support throughout the experiments.

I would also like to thank Prof. Mike Geeves and Dr. Dan Mulvihill for being constant sources of knowledge and their past and present lab members, particularly Cassie, Sam, Alice, Jenny, Zoltan, Johnny, Holly and Karen, for welcoming me in Kent and in their lab for small non-work-related chats. A big thank you goes also to all the other friends I met from the department, especially Alex, Diego and Sara.

Finally, my gratitude goes to all my family for their constant love and support and to my friends Fabio and Giuseppe for helping me de-stress, but most importantly to my wife Yuhan, for her unconditional love and for taking care of me whenever I most needed it.